Zurich Lectures on Multiphase Flow
Series Editors:
George Yadigaroglu · Sanjoy Banerjee · Geoffrey F. Hewitt

George Yadigaroglu
Geoffrey F. Hewitt *Editors*

Introduction to Multiphase Flow

Basic Concepts, Applications and Modelling

Springer

Zurich Lectures on Multiphase Flow

The series tracks critical research and engineering practice imparted through the Zurich Short Courses on Multiphase Flows. Multiphase flows occur in very many situations of industrial importance, including conventional or nuclear power plants, the oil and gas industry, chemical processing plants; as well as in biomedical applications. Understanding the basic laws governing the behavior of multiphase flows—such as flows of air and water, steam and water, oil and natural gas—, and producing methods, tools, codes, and best practices capable of predicting their behavior are crucial to engineering in these areas. The Zurich Lectures on Multiphase Flows brings together concise volumes that cover the field starting from the very fundamentals, such as void fraction, pressure drop, and heat transfer in multiphase flows; governing equations, closure laws, phenomenological modeling, correlations, experimental techniques, to the more advanced and specialized topics including non-equilibrium flows, instabilities, numerical methods for multiphase flows, applications to multiphase flows in nuclear power plants, in the oil-and-gas industry, and related technologies. The monographs appearing in the Zurich Lecture Series comprise a critical knowledge base particularly relevant to a range of engineering and scientific problems in industrial/commercial R&D, facility operation/optimization, product quality assurance, as well as in academic/biomedical research settings.

More information about this series at http://www.springer.com/series/15392

George Yadigaroglu · Geoffrey F. Hewitt
Editors

Introduction to Multiphase Flow

Basic Concepts, Applications and Modelling

Springer

Editors
George Yadigaroglu
ETH Zurich
Zurich
Switzerland

Geoffrey F. Hewitt
Department of Chemical Engineering
Imperial College London
London
UK

Zurich Lectures on Multiphase Flow
ISBN 978-3-319-58717-2 ISBN 978-3-319-58718-9 (eBook)
DOI 10.1007/978-3-319-58718-9

Library of Congress Control Number: 2017939918

Printed on acid-free paper

This Springer imprint is published by Springer Nature
The registered company is Springer International Publishing AG
The registered company address is: Gewerbestrasse 11, 6330 Cham, Switzerland

Preface

Sometime in 1983 four of us, Sanjoy Banerjee, Gad Hetsroni, Geoff Hewitt and George Yadigaroglu met and decided to organize a Short Course on multiphase flows, following the model that had been successfully tested at Stanford University previously (1979–1983). George Yadigaroglu was appointed the local organizer in Zurich. This was the beginning of a great "enterprise" that is still going on. The first Zurich Short Course took place in March 1984 and an unexpectedly large number of persons participated. Zurich turned out to be an excellent venue and we are grateful to ETH Zurich for hosting the course in its excellent facilities. The audiences kept growing and over 2000 participants took part in the Zurich courses until now. The courses that are still offered—obviously with new material and some new lecturers—became an initiation rite for the junior staff of the research and engineering departments of large companies, national laboratories, university laboratories, etc. Beginners, doctoral students, as well as their professors, young and older scientists, and engineers attended.

In March 2015, Gad Hetsroni died after a short illness. He had a very protective love for the Short Courses and had been the main organizer of the earlier sessions in California. He was involved as a Course Director and Lecturer up to 2015 and material from his lectures is included in these published Zurich notes. We wish to place on record our sincere appreciation of the crucial role he had played.

The Zurich Short Courses not only offered the opportunity to the participants to meet and interact with outstanding lecturers, but also with colleagues working worldwide on similar topics but in different industries. An aim of the courses was to promote interdisciplinary information exchanges between various industries and areas where multiphase flows are important but communications poor. For the lecturers also, the annual meetings became excellent opportunities to meet and interact.

The courses started with the four founders mentioned above, but soon the number of lecturers was expanded: we tried to attract not only the best specialists in their areas but also good communicators and teachers. In 1989, two parallel sessions were offered and the course became modular. The first three days were devoted to Basics while on Thursday and Friday the participants could choose

between two options. Part A was always the "nuclear" one, as many participants came from nuclear industries, even when their particular research interests were not necessarily in the narrower nuclear area. Part B, in response to the increasing interest in computational modelling and computational multi-fluid dynamics, was fully devoted to these topics. In fact, the computational aspects became gradually more important *throughout* the course, reflecting on-going changes and progress. From 2005 on, the course was enriched by bringing in the practical experience of the commercial code developers. By then the number of lecturers was expanded from the initial four to over a dozen.

Today the courses are organized in this modular form as an intensive introduction for persons having basic knowledge of fluid mechanics, heat transfer and numerical techniques and also serve as advanced courses for specialists wishing to obtain the latest information in the field; this series of books has the same goal. In 2007 introductory tutorials were used for the first time; they were mailed to the participants before the course to introduce the very basic concepts, fill any gaps in their basic background and prepare them for the tough week of lectures to come: four to five hour-and-a-half lectures per day. Tutorials are also appended to the volumes now.

The four principals met after each course to organize the next one: Geoff Hewitt always wrote the next outline. Obviously the lectures have evolved over the years, older material had to be shed to make place for new knowledge. The emphasis on the various topics also changed. After some 35 years of Short Courses, an impressive amount of material had accumulated. We finally decided to print the notes in book form, also allowing use of the new electronic means of disseminating the information. We are grateful to Springer that was interested in publishing this material as a series. We are assembling the lecture notes in thematic volumes: basics, conservation equations and closures, phenomenological modelling, boiling heat transfer, two-phase flow dynamics, multiphase flows in the nuclear industry, computational multi-fluid dynamics, etc. The present volume is the first of the series. We expect our volumes to be of interest to scientists and engineers working in the great variety of industries, thermal, chemical, nuclear, petrochemical, food, pharmaceutical, oil-and-gas, etc. where multiphase flows are ubiquitous.

The chapters of the volumes, although initially reflecting the state of the art at the time they were originally written, have been continuously updated over the years and fully updated again for this publication. Although most of the material can be found in the notes distributed to the participants over the years, it has been rearranged to better fit the format of a book. The final result approaches the form of a handbook or a series of textbooks; the pedagogical aspects remain very present. The best parts of lectures (often given by different persons) were re-assembled in the newly updated chapters that continue representing the state of the art.

The reader should not be surprised if a lot of original, old, seminal work is referenced: we prefer to cite the original author and work rather than its latest mention or presentation in a recent paper or textbook; this may make some of the references look "old" but they have been included only if their value has passed the test of time. Throughout the chapters, we insist on understanding of the physics and

on mechanistic modelling while not ignoring the empirical, well-established methods as well as the numerical applications. Our approach is to start from the basic principles and ideas and to progress gradually, ending up with the state of the art and occasionally looking beyond. A special effort is made to remain as educational as possible.

A few words about the present volume on *Introduction to Multiphase Flow* and Basics: After introducing the reader to multiphase and in particular two-phase flows, the basic concepts, variables, notions and tools necessary for the following chapters are introduced in Chap. 1. Chapter 2 discusses the various alternatives available for *modelling* and studying analytically or numerically two-phase flows. The more advanced alternatives are simply surveyed in this chapter as they need more in-depth and formal treatment in other volumes. Chapter 3 is an introduction to the *interfacial instabilities* that govern a multitude of two-phase flow phenomena; the early introduction of this material will help the following presentations. A long Chap. 4 covers in depth the *flow regimes*, a special characteristic of two-phase flows that governs their mechanistic modelling; consequently this chapter gives an excellent opportunity to introduce the reader to phenomenological modelling. Finally, Chaps. 5 and 6 cover *void fraction* and *pressure drop* in two-phase flow, two topics that are of particular concern to any designer or analyst of two-phase equipment and systems.

Zurich, Switzerland — George Yadigaroglu
London, UK — Geoffrey F. Hewitt
January 2017

Contents

Chapter 1
Nature of Multiphase Flows and Basic Concepts

George Yadigaroglu and Gad Hetsroni

1.1 The Nature of Multiphase Flows

Multiphase flows and heat transfer with phase change are one specialized discipline among many others in the much more general area combining thermodynamics, fluid mechanics and heat transfer; often this area is referred to as *thermal-hydraulics*. The study of multiphase flows requires basic knowledge in these three areas. Appendix I of this volume, a tutorial, provides some of the indispensable minimal background from these three areas for the reader that may need it.

The adjective *multiphase* characterizes situations where several different phases —liquids, gases, solids—are flowing simultaneously. In the case of liquids, the two flowing media can also be two chemically different ones, e.g. oil and water. *Two-phase flows* take place when only two phases are present, most often liquid and gas.

Another categorization of flows is according to the presence or absence of heat transfer: we speak of *adiabatic* or *diabatic* multiphase flows. In diabatic multiphase flows, we can have phase change: *vaporization* or *condensation*. Phase change can also take place, however, in adiabatic flows due to pressure changes; such vaporization is referred as *flashing*.

Another important distinction is according to the flow direction: *vertical, horizontal, or inclined*. Flow direction is more important in multiphase flows when gravity plays a more important role in presence of large differences in the density of

Gad Hetsroni—Deceased Author.

G. Yadigaroglu (✉)
ETH-Zurich, Zurich, Switzerland
e-mail: yadi@ethz.ch

G. Hetsroni
Technion - Israel Institute of Technology, Haifa, Israel

G. Yadigaroglu and G.F. Hewitt (eds.), *Introduction to Multiphase Flow*,
Zurich Lectures on Multiphase Flow, DOI 10.1007/978-3-319-58718-9_1

the phases; such differences can easily be of the order of 1000 (e.g. air–water flow at atmospheric pressure).

Finally, we speak of *parallel or co-current flow* when the two-phases flow in the same direction, and of *counter-current flow* when they flow in opposite directions (e.g. falling liquid and rising gas).

Multiphase flows are present in everyday life, in nature, in industrial processes, in power plants, in the oil and gas industry, etc. All phase-change processes such as boiling and condensation produce two-phase flows; these heat and mass transfer processes are "core" considerations in the multiphase flow area where many applications involve phase change or at least interactions between phases. Water boils in power plants to produce steam. In processing plants, different phases are mixed to react or are the products of chemical reactions. Thus, heat transfer with phase change (e.g. boiling or condensation) is intimately linked to two-phase flows.

After some reminders and formal definitions in Sect. 1.2, we will consider in Sect. 1.3 a few examples where the nature of multiphase flows is dominant, and controls the behaviour, the response and the operation of the whole system. In particular, we note that some peculiarities of multiphase flow produce unique responses that may have a profound effect on the dynamics and safe operation of the system; we touch here only two such phenomena: the Critical Heat Flux (CHF) phenomenon and a particular type of flow instability.

We will deal mainly with *one-dimensional* flows in ducts. In fluid mechanics, the notion of one-dimensional flow is applied in a broader sense. For example, the flow in a complex system of pipes that may have bends, enlargements, curved sections, etc., such as the one shown in Fig. 1.1 is, strictly speaking, certainly not one dimensional. However, as long as the three-dimensional details of the velocity and temperature distributions do not interest us and we deal only with the average velocity and the mass flux-weighted average fluid temperature, such systems can still be treated as "one dimensional". Indeed, we are dealing in this volume mainly with one-dimensional two-phase flow, very much like in the excellent book by G.B. Wallis that has exactly this title (Wallis 1969).

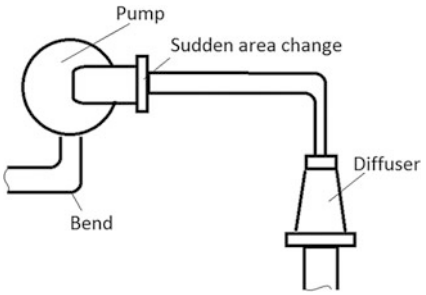

Fig. 1.1 A complex circuit with bends, enlargements, fittings, a pump, etc. that can be still considered as one dimensional when only cross-sectional-average variables are of interest

1.2 Phases, Components, Fields

A *phase* is a thermodynamic definition for the state of the matter, which can be either solid, liquid or gas; these can co-exist in a conduit. Examples of multiphase flows are abundant, e.g. when oil is produced, one normally gets oil, water, gas and sand flowing in the pipelines (three-phase flow). Normally, by two-phase (or by extension multiphase) flow we mean a mixture of two (or more) phases which is not extremely dilute and the phases have a distinguishable size. Thus, though clean city tap water is, strictly speaking, a two- (water–air) or three- (water–air–microscopic solids) phase mixture, for practical purposes, it is considered a single phase. However, city water carrying sand should, for filtration purposes at least, be considered a two-phase mixture.

The term *mixture* is most of the time used to denote the two (or more) phases flowing together and does not necessarily imply that these are intimately *mixed*. For example, in the case of annular flow that we will introduce below, we may still refer to the flow as *the two-phase mixture* in spite of the fact that the liquid film on the wall and the gaseous core are not at all "mixed". The term "separated flow" is often used loosely to denote two-phase flows where the two phases have different average velocities. This distinguishes such flows from the *homogeneous* ones, where the phases have the same average velocity; again, such flows may strictly speaking not be homogeneous at all. For example, bubbly flow with fairly large bubbles can be considered as *homogeneous*.

A *component*, is a chemical species. So, the term two-component is used to describe the flow of two chemical species. A water–steam mixture is two-phase, one-component, while a water–air mixture is two-phase, two-component flow; a water–oil mixture is one-phase, two-component, etc. The approach in modelling of the two alternative two-phase configurations—with one or two components—is often the same or very similar, though the physical behaviour of different mixtures may be quite different.

The term *field* is used to denote a topologically distinct or clearly identifiable fraction of a phase. For example, in the so-called annular flow, the liquid can be present as either a film on the wall or as droplets in the core where the gas flows; the droplets and the film can be considered as different fields. In a closed vessel such as a pressure cooker containing boiling water, we may define a field of steam bubbles in the liquid and a field of steam in the space above the liquid surface as separate fields.

For simplicity of presentation, the approaches and various methods that will be covered here will be presented mainly for two-phase flows. However, their extension to multiphase and multi-field flows is most often possible, although such applications are less frequently encountered in practice.

In this volume, we mainly deal with liquid-gas mixtures. There are many other two-phase flows, e.g. gas-solid flows such as fluidized beds, conveying of granular materials by gas; liquid-solid flows where sedimentation and filtration may be phenomena of interest, etc. Such flows will not be treated in this volume and in this

series of books which are mostly directed to two-phase gas-liquid flows of industrial interest: steam-water flows, oil and gas flows, two- or multiphase flows in processing plants, etc. There are other texts which deal with the other types of multiphase flows, namely the Handbook by Hetsroni (1982) and monographs such as Fan and Zhu (1998) for gas-solid flows and Brown and Heywood (1991) for liquid-solid flows (slurries).

1.3 Multiphase Flow Phenomena

We give examples in the following section of situations where peculiarities of multiphase flow produce unique responses not found in single-phase flows. The Critical Heat Flux (CHF) phenomenon and a particular type of flow instability will be briefly introduced. In Sect. 1.3.2, we discuss phenomena that are not unique to multiphase flows but become much more complex in the presence of several phases.

1.3.1 Phenomena Unique to Multiphase Flows

The *critical heat flux (CHF)* phenomenon is a situation that may take place in heat transfer with boiling. To illustrate the situation, we consider a very simple experiment conducted with a heated tube immersed in a pool of liquid, Fig. 1.2. This is the situation referred to as *pool boiling*. The heat flux from the wall is plotted in the graph of Fig. 1.2 against the excess wall temperature (i.e. the wall temperature T_w minus the saturation temperature T_{sat} of the fluid in the pool). The heat flux is gradually increased; one can observe that once a certain heat flux is reached, the

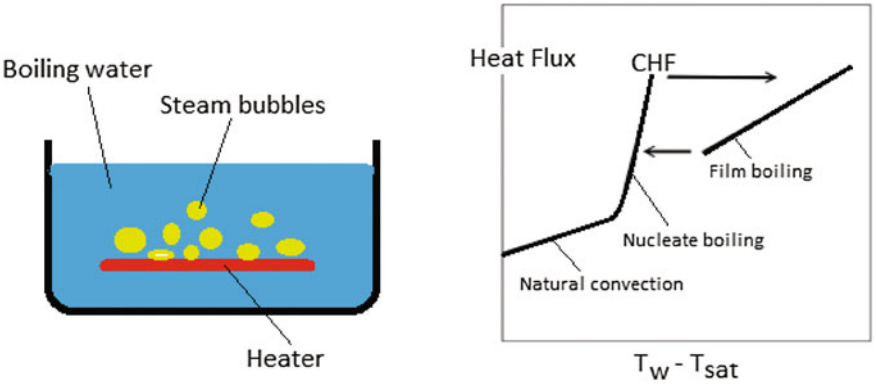

Fig. 1.2 A pool boiling experiment (*left*). The boiling curve (*right*)

CHF, a dramatic change takes place and a further increase in heat flux will cause a very large, sudden rise in wall temperature, resulting most likely in the failure of the tube. When the CHF is reached, the liquid can no longer wet the heater surface and cooling takes place through a vapour film surrounding the heater rather than by boiling of the liquid in contact with the wall. As the vapour has much reduced thermal conductivity and density, heat transfer deteriorates markedly and leads to the temperature excursion. This subject is of utmost practical importance and will be further treated in other volumes. It is a phenomenon taking place only in heat transfer with phase change.

We also note here that as the heat flux is *reduced*, the operating point stays on the film boiling characteristic curve rather than going back at CHF to the nucleate-boiling curve. It appears that the film surrounding the heater is stable, keeping film boiling going on; it will take a further reduction of the heat flux to produce another jump back to the nucleate-boiling curve. This particular hysteresis behaviour during pool boiling was studied by Nukiyama (1934) who published the *boiling curve*.

Another example which is typical to two-phase flow is a flow excursion which can occur in a two-phase loop having certain flow characteristics. The situation is illustrated in Fig. 1.3. If the two-phase section of the loop has a negative slope in its pressure drop—flow-rate characteristic $(\dot{M}, \Delta p)$, i.e. if $\partial p/\partial \dot{M} < 0$ something that happens often in two-phase flow (and cannot happen in single-phase flow), a flow excursion will occur. This situation was described first by Ledinegg (1938). Ledinegg instabilities can be of great practical importance regarding the stability of two-phase equipment such as steam generators. Flow instabilities will be dealt with in another volume; some additional information is included in the following section.

1.3.2 Phenomena Complicated by the Presence of Many Phases

A number of single-phase flow phenomena take also place in single-phase flows, but the presence of two or more phases complicates greatly the situation.

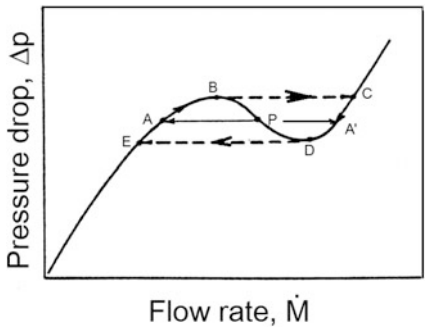

Fig. 1.3 The flow-rate versus pressure-drop characteristic of a boiling channel. The Ledinegg instability occurs if the slope of the characteristic is locally negative, as in the segment BD. Point P is unstable and the operating point will migrate to either A or A'

For example, the *pressure drop* is a factor of importance in the design of any hydraulic system. Its estimation is rather straightforward in single-phase systems, but it becomes much more difficult—and inaccurate in fact—in two-phase flows. Figure 1.4 shows the pressure drop—flow rate characteristic of a heated pipe. The all-liquid and all-vapour characteristics are nearly parabolic, but, in between the heated pipe exhibits a much more complex behaviour in the presence of two-phase flow. As the heat flux increases, a negative-slope part of the characteristic emerges; it is such behaviour that is responsible for the Ledinegg instability just mentioned.

Critical flows are another case where the multiphase nature of the problem greatly complicates the situation. We will use this phenomenon to show the importance of non-equilibria in two- or multiphase flows. In the simpler case of

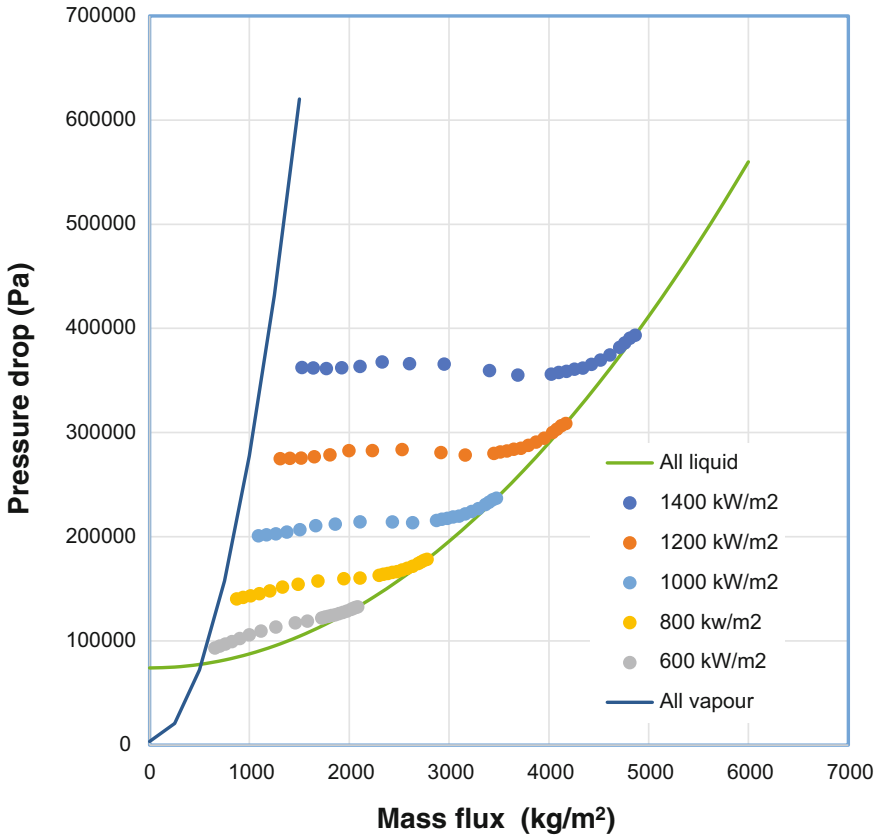

Fig. 1.4 The flow rate—pressure drop characteristics of a heated pipe at different heat fluxes and with all-liquid and all-vapour flow (with no heat addition). Pipe length $L = 10$ m, diameter $D = 0.02$ m, friction factor $f = 0.005$. Pressure $p = 69$ bar. Inlet non-dimensional subcooling $\Delta h_{in}/h_{LG} = 0.45$. The computations were performed with Thom's charts given as an Appendix to Chap. 6

two-phase flow, the gas and the liquid may have different average velocities and temperatures; this is what we denote as *non-equilibrium*.

In the case of single-phase flow, the flow becomes chocked as the critical flow condition is reached when, essentially, the flow velocity reaches the sonic velocity of the fluid; the latter is determined as a thermodynamic fluid property depending only on temperature and pressure (e.g. Shapiro 1953). The assumption is made that the properties of the fluid are given along its thermodynamic path by its state equation. The same approach can be taken for two-fluid mixtures but difficulties appear: the state equation of the mixture depends now on whether the gas and liquid velocities and temperatures are equal or not. As such equilibria are subject to all sorts of flow conditions and on the history of the fluid upstream of the choking point, there is no simple answer to this problem and the critical flow of a two-phase mixture depends on assumptions made about the state of the mixture.

1.4 Flow Regimes

One of the major difficulties in multiphase or two-phase flows is that the phases are distributed in the duct in particular ways; the various typical (topological) configurations that result are called *flow regimes*.

The boundaries between phases area called *interfaces*. The topology of the flow, i.e. the geometry of the interfaces, is not known and cannot be determined a priori, but is rather a part of the solution. In contrast, for example, in single-phase flow of a fluid in a tube, knowing the geometry we can determine, either experimentally or analytically, the velocity distributions, the shear stress distribution, the pressure drop, etc. When two phases flow in a conduit, we cannot tell a priori how the phases are going to distribute themselves: whether bubbles will be distributed uniformly throughout the liquid (we call this situation *bubbly* flow) or whether the bubbles will coalesce and gas will flow in the centre of the pipe, while the liquid will form a film on the wall (this is called *annular* flow). *Flow regime determination* is needed to answer such questions; this is treated in Chap. 4.

The cross-sectional distribution of the phases in the pipe determines other parameters such as heat transfer, pressure drop and, without knowing this phase distribution, we cannot calculate these. Furthermore, it is not likely that the two phases will flow with the same average velocity. On the contrary, most likely, the gas will flow at a higher average axial velocity than the liquid, which will cause a change of the *void fraction* or *volume fraction* of the gas phase in the channel (i.e. the fraction of area occupied by gas in the cross section). Often, until we have a way to determine the flow regime, there is really no way we can accurately model and

calculate other parameters of engineering significance. Therefore, one of the first problems we will address in this volume is the study and determination of *flow patterns* or *flow regimes*. The reader should be aware that flow patterns depend on many parameters, such as the inclination of the conduit, the geometry, pressure, type of fluid, etc.

1.5 Some Important Multiphase Flow Systems

We site now some examples where multiphase flows play a dominant effect in the design and operation of very large engineering systems.

Offshore production has been important for the extraction of hydrocarbons since the 1950s. It usually involves a drilling platform which operates a number of wells to produce crude oil. The oil comes out of the ground usually as a mixture of crude oil, sea water, sand and gas—a multi-component, multiphase mixture which needs to be handled carefully because of various hazards and because of the extremely costly equipment involved. Figure 1.5 shows production wells, drilling platforms, and a floating production, storage and offloading vessel.

Electric power production from oil, coal or gas: A majority of power plants use a steam cycle where water is the working fluid. Figure 1.6 shows the steam cycle of a modern plant; water gets vaporized in the high-pressure steam generator section and the low-pressure steam exiting from the turbine gets condensed in the condenser. Again, two-phase flows and phase change processes are present throughout the steam plant.

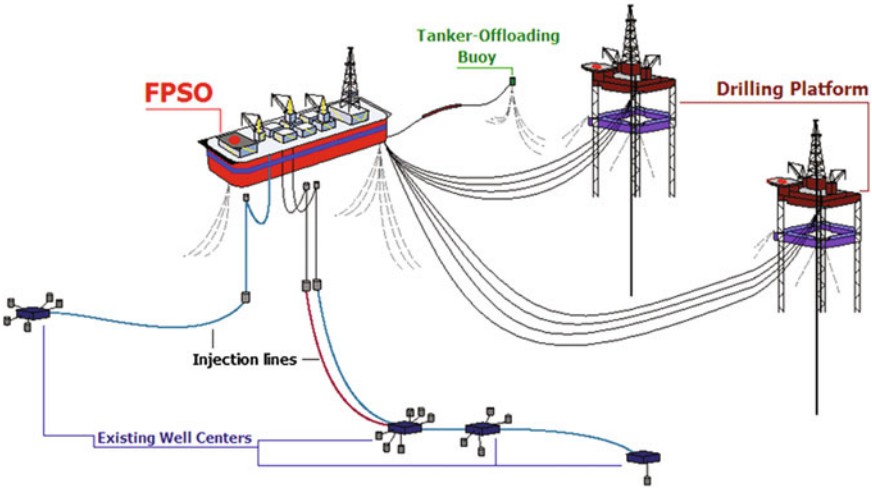

Fig. 1.5 FPSO, floating, production, storage and offloading for offshore production of oil

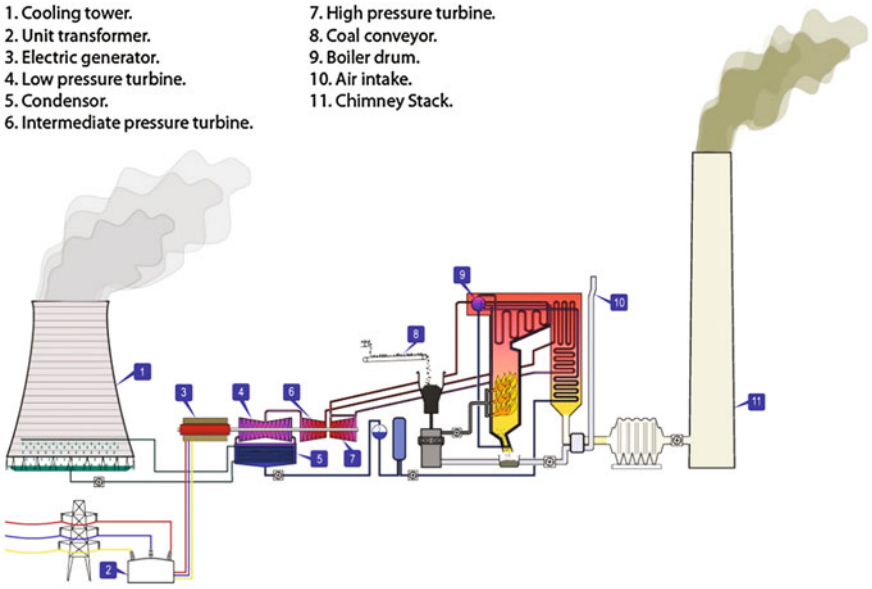

Fig. 1.6 A modern steam power plant. Boiling and two-phase flows take place in the steam generator while evaporation of droplets in the cooling tower (from http://www.zeroco2.no)

In a nuclear power plant (NPP), the *nuclear steam supply system* (NSSS or "en-triple-ess") is the part of the plant where water at high pressure is heated in the reactor vessel by the nuclear chain reaction taking place in the fuel rods. Steam is then produced (either in the reactor vessel, as in a boiling water reactor, Fig. 1.7 (bottom), or in a steam generator, as in a pressurized water reactor, Fig. 1.7 (top), and used in the turbine-generator to produce electric power. The multiphase flow of water and steam takes place in very costly equipment. To operate the system safely and efficiently for the lifetime of the equipment, one needs detailed knowledge of multiphase flow and heat transfer. Understanding two-phase flow situations and phenomena and being able to predict the outcomes becomes even more important in case of an accident in a NPP when unusual situations are encountered. In fact, the disciplines of two-phase flow and heat transfer with phase change progressed tremendously the last three or four decades of the twentieth century driven by the need to fully understand, model and simulate the complex phenomena taking place during thermal-hydraulic accidents in NPPs. Other books in this series will be devoted to two-phase flows in nuclear power plants.

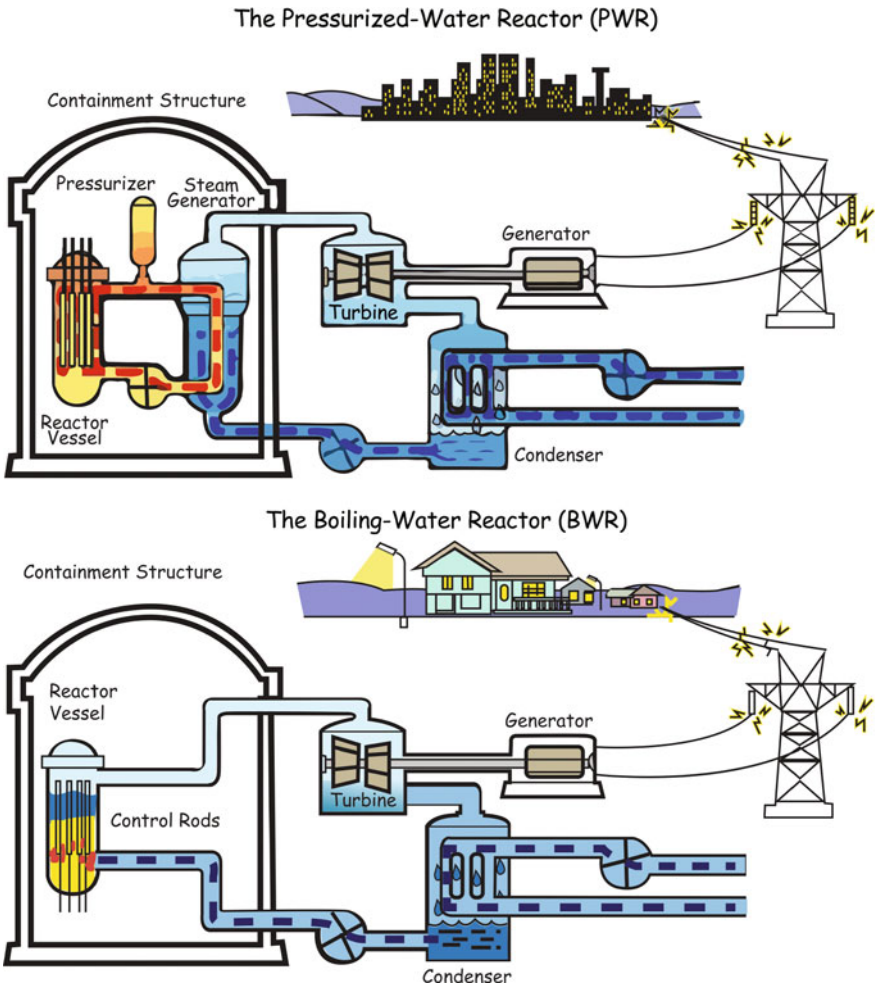

Fig. 1.7 Pressurized Water Reactor (*top*) and Boling Water Reactor (*bottom*). Figures from www.nrc.gov. The conventional power production systems of these two main types on NPPs are quite similar and operate under very similar thermodynamic conditions. In the BWR, direct steam generation takes place in the reactor core while, in the PWR, it takes place in the intermediate steam generator

1.6 Averaging in Two-Phase Flows

It is often necessary to perform averaging in multiphase flows and in particular averaging over the flow cross section in one-dimensional, two-phase flows. This is in particular necessary when dealing with the conservation equations where one starts with instantaneous local equations that must be integrated in time and space to arrive at usable forms.

Averaging will be applied either to two-phase *mixture* variables (variables for both the liquid and the gas flowing together) or to each phase separately. We will use averages of *mixture* properties such as the mixture density as well as averages of *phase* variables such as the channel-cross-sectional-average liquid or gas velocity. This section briefly introduces the concepts.

Generally, we will add the subscript k, (k = L,G), where L denotes the liquid and G the gas, to the phase variables to differentiate them from mixture variables that are usually written without a subscript. Thus, f_k is a local instantaneous variable pertaining to phase k, e.g. the local, instantaneous velocity or enthalpy, u_k or h_k.

1.6.1 Space Averaging

We consider space averages of generally instantaneous values. The following averages can be defined:
Cross-sectional average of any variable f

$$<f> = \frac{1}{A}\int_A f\, dA, \tag{1.6.1}$$

where the angle brackets operator $<\cdot>$ denotes the cross-sectional averaging over the flow area A.
Phase cross-sectional average of a *phase* variable f_k

$$<f_k>_k = \frac{1}{A_k}\int_{A_k} f_k dA, \quad k = L, G \tag{1.6.2}$$

where the integration is now performed only over the area of the channel A_k occupied by phase k at a given moment. The second subscript outside the angle brackets in $<f_k>_k$ reminds us that the cross-sectional average of the local phase property f_k was performed over the area of the channel occupied by phase k *only*: $<\cdot>_k$.

1.6.2 Time Averaging

The time or statistical average of any variable f is

$$\overline{f} = \frac{1}{T}\int_{[T]} f\, dt. \tag{1.6.3}$$

The integration interval [T] must be chosen such that, for example, high frequency perturbations such as those created by turbulence are averaged out while the transient nature of the process is still well represented.

The *phase* time or statistical average of a *phase* variable f_k is

$$\overline{f}_k^k = \frac{1}{T_k} \int_{[T_k]} f_k dt, \tag{1.6.4}$$

where $[T_k]$ is the subset of residence time intervals where phase k is present at a given point and T_k is the sum of the presence times of phase k at that given point. T is the total averaging time interval. The rather heavy notation for the interval $[T_k]$ is necessary to remind us that it is discontinuous, Fig. 1.8.

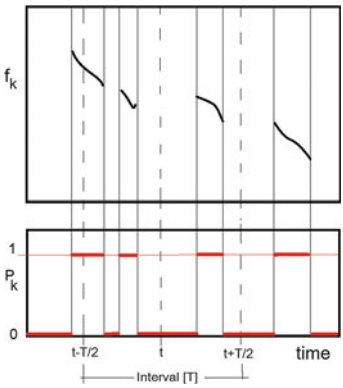

Fig. 1.8 Measurements of a piecewise continuous variable f_k, such as phase velocity, pertaining to phase k (*above*) and phase indicator function P_k (*below*). Such signals could be actually measured, e.g. by a hot-wire anemometer (phase velocity); the signal of the anemometer could be treated to detected the phase present

1.7 Void Fractions and Their Measurement

The term *void fraction* (denoted in general by $\varepsilon_{G,}$ where the subscript G denotes the gas, dimensionless) generically describes in space or time the fraction occupied by the gas phase. The notion is specialized as needed below. For each definition of the void fraction, an experimental method that may produce such a measurement is indicated; some additional information on void fraction measurements is given in Chap. 5.

1.7.1 The Local Void Fraction

The *local void fraction* is defined as the fraction of time in which the gas phase occupies a given point in space **r**. We may characterize the presence (or absence) of

phase k (k = G, L) at a given point **r** and at a given time t by the unit or zero value of the *phase density* or *phase presence* function $P_k(\mathbf{r}, t)$

$$P_k(\mathbf{r},t) = \left\{ \begin{array}{l} 1 \; if \; \mathbf{r} \text{ is in phase } k \\ 0 \; if \; \mathbf{r} \text{ is in the other phase} \end{array} \right\}.$$

The instantaneous value is usually integrated over a time period T to give a time-averaged value. Thus the *time-averaged local k-phase fraction* is the time-averaged phase density function

$$\bar{\varepsilon}_K(\mathbf{r},t) = \frac{1}{T}\int_T P_k(\mathbf{r},t)\, dt = \overline{P_k(\mathbf{r},t)} \tag{1.7.1}$$

according to the definition of the time-averaging operator. In the case of gas, k = G, this becomes the *local statistical or time-average* void fraction:

$$\bar{\varepsilon}_G(\mathbf{r},t) = \frac{1}{T}\int_T P_G(\mathbf{r},t)\, dt = \overline{P_G(\mathbf{r},t)}.$$

Alternatively, we can define the local statistical or time-average void fraction as the fractional presence time of the gas phase at a given point:

$$\bar{\varepsilon}_G \equiv \frac{T_G}{T} \quad \text{and also} \quad 1 - \bar{\varepsilon}_G \equiv \bar{\varepsilon}_L \equiv \frac{T_L}{T} \tag{1.7.2}$$

where T_k (k = L,G) is the summation of all the times during which phase k was present at the measuring point, and T is the total period of observation. The bar over ε denotes time or statistical averaging. The overbar will be dropped for simplicity of notation when it is implicit that we are dealing with time-average values. Also, if no subscript is added to ε, it is assumed that the meaning is ε_G and the liquid local time-averaged fraction becomes $1\text{-}\varepsilon = \varepsilon_L$. Clearly, $\varepsilon_G + \varepsilon_L = 1$.

The local void fraction can be measured by a miniature resistive probe, a U-shaped fibre-optical sensor or a hot-wire anemometer. All these devices detect the presence of a phase at their sensing tip.

An optical probe is sensitive to the change in the refractive index of the surrounding medium enabling measurements of local void fraction. It can also record interfacial passages and interface passage frequencies. Optical probes can operate in conducting or non-conducting liquids. The tiny optical probe, which is frequently used, Fig. 1.9, consists, e.g. of a single optical fibre, 40 μm in diameter, which may be bent in a U shape. A light shines from a source through one arm of the U bend. This light, according to Snell's law, is either refracted (if the surrounding medium is liquid) or reflected to the other side of the U bend (if the surrounding fluid is gas), Fig. 1.9a. By analysing the signal of the phototransistor, one can infer the *local* void fraction, Fig. 1.9d.

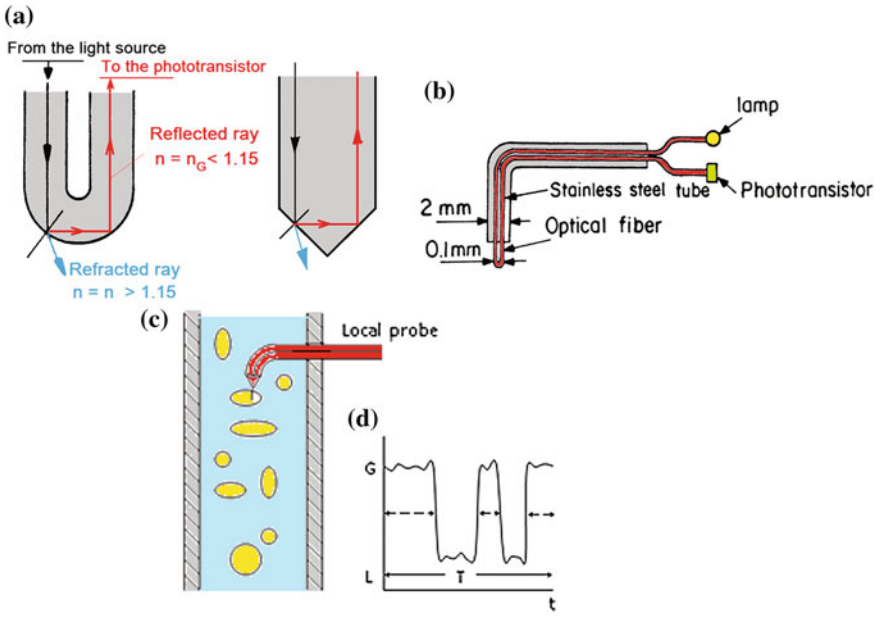

Fig. 1.9 **a** Active parts of fibre-optical sensors showing the refraction or reflection of the light. **b** U-shaped fibre-optical sensor assembly (Danel and Delhaye 1971). **c** Optical probe positioned inside the channel in bubbly flow. **d** Probe signal indicating the presence of gas or liquid

1.7.2 The Chordal Void Fraction

The *chordal void fraction* is defined as the fraction of a chord or ray occupied at a given instant by gas:

$$\varepsilon_{G1} = \frac{L_G}{L_L + L_G},$$

where L_k, k = L,G is the instantaneous cumulative length on the chord occupied by phase k. This is best illustrated in Fig. 1.10 where $L_G = L_1 + L_2$.

The chordal-average void fraction is typically measured by means of radiation absorption methods. These methods use γ or X-ray beams which are attenuated by the material through which they pass. The intensity after absorption of a collimated beam of initial intensity I_0 (photons/m^{2}s) is given by

$$I = I_0 e^{-\mu z},$$

where μ is the linear absorption coefficient, which is a property of the absorbing material and the type of radiation and z is the distance travelled through a

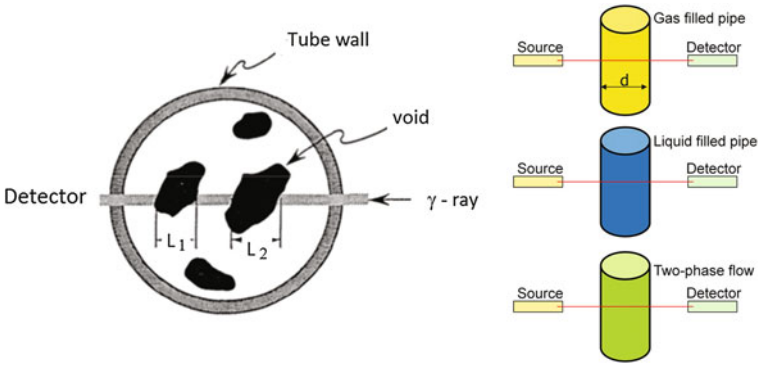

Fig. 1.10 Chordal void fraction. *Left* The sum of the segments L_1 and L_2 over the diameter define the chordal void fraction. *Right* Calibration method

homogeneous absorbing medium. In applying this technique to the measurement of void fraction, a collimated beam is passed through the channel walls and through the two-phase mixture to a detector. First one measures the intensity of the beam at the detector when the channel is full of liquid, I_L and then full of gas, I_G. The void fraction is then related to the intensity I measured during two-phase flow by

$$\varepsilon_{G1} = \ln\left(\frac{I}{I_L}\right) / \ln\left(\frac{I_G}{I_L}\right).$$

The chordal void fraction can be averaged in time if necessary. An arrangement to measure chordal-average void fractions is depicted in Fig. 1.11.

1.7.3 The Cross-Sectional Void Fraction

The *cross-sectional-average instantaneous void fraction* is the fraction of the cross section occupied at a given instant by the gas:

$$R_G \equiv \frac{A_G}{A}, \tag{1.7.3}$$

where A_G is the sum of the areas which are occupied by voids in the cross section (the white areas in Fig. 1.12), A_L is the sum of the areas which are occupied by the liquid, and A is the total cross-sectional area. Similarly, for the liquid:

$$R_L \equiv \frac{A_L}{A} = 1 - R_G.$$

In terms of the *phase presence* function $P_k(\mathbf{r}, t)$, we can write

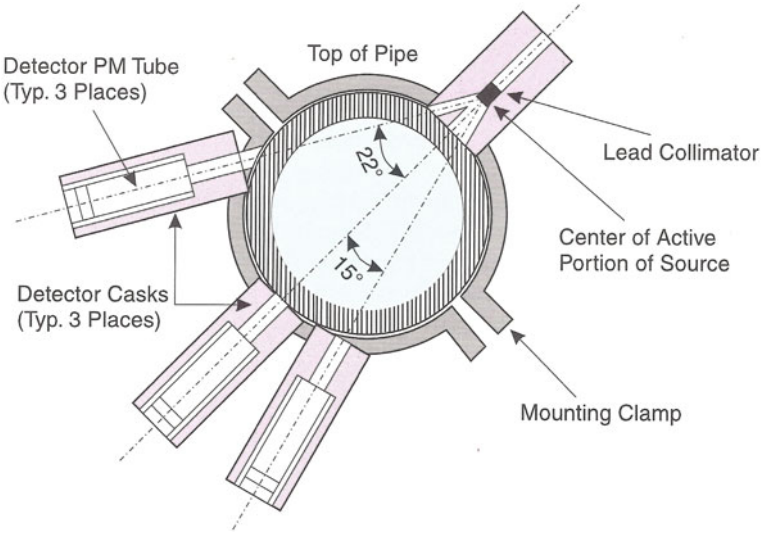

Fig. 1.11 An early realization of a three-beam gamma densitometer measuring three chordal-average void fractions that can be combined to obtain the cross-sectional-average value (Lassahn 1977; redrawn figure courtesy of EPRI)

$$R_k(t) = \frac{1}{A}\int_A P_k(\mathbf{r}, t)\, dA$$

where we have ignored the theoretical difficulties present in the integration of a discontinuous function. The instantaneous cross-sectional void fraction can be integrated in time to provide a time-averaged value over a time integral [T]

$$\bar{R}_G = \frac{1}{T}\int_{[T]} R_G(t)dt = \frac{1}{T}\int_{[T]}\frac{1}{A}\int_A P_G(\mathbf{r}, t)\, dA\, dt.$$

Similarly, we can space average the local statistical void fraction

$$\langle \bar{\varepsilon}_G \rangle = \frac{1}{A}\int_A \bar{\varepsilon}_G(\mathbf{r})dA = \frac{1}{A}\int_A \frac{1}{T}\int_{[T]} P_G(\mathbf{r}, t)\, dt\, dA.$$

We realize that thanks to the *commutativity* of the space (<·>) and time ($\bar{\cdot}$) averaging operators the two expressions above are identical and we have, indeed for either phase

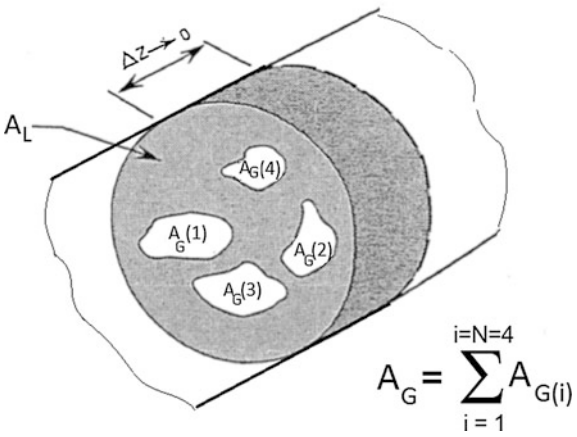

Fig. 1.12 The cross-sectional void fraction is obtained by summing all the areas occupied by gas in the cross section

$$\langle \bar{\varepsilon}_k \rangle = \bar{R}_k. \tag{1.7.4}$$

The cross-sectional void fraction can be obtained by integrating chordal-average measurements over the cross section as shown in Fig. 1.11, or by using the "one-shot" technique, or by a neutron scattering technique. Integration of chordal-average measurements can be done either by traversing a collimated beam across the channel (this obviously can be used only for steady-state measurements) or by using a multi-beam arrangement, as illustrated in Fig. 1.13 that shows multi-beam *gamma densitometers* that produce an estimate of the cross-sectional-average void fraction by weighting appropriately the chordal void fractions measured by many beams.

The "one-shot" method uses a broad radiation beam (as wide as the channel) with special collimators to adjust for the different path length and wall absorption.

In the remainder of this volume, we will practically always use the cross sectional and time-average void fraction $<\varepsilon_G>$ or $<\varepsilon>$ (where we dropped the overbar to alleviate the notation).[1]

[1]Mathematically, the use of a cross-sectional-average void fraction may lead to some difficulties. Therefore, it should really be understood as a volume-average void fraction defined over a length δz, as $\delta z \rightarrow 0$.

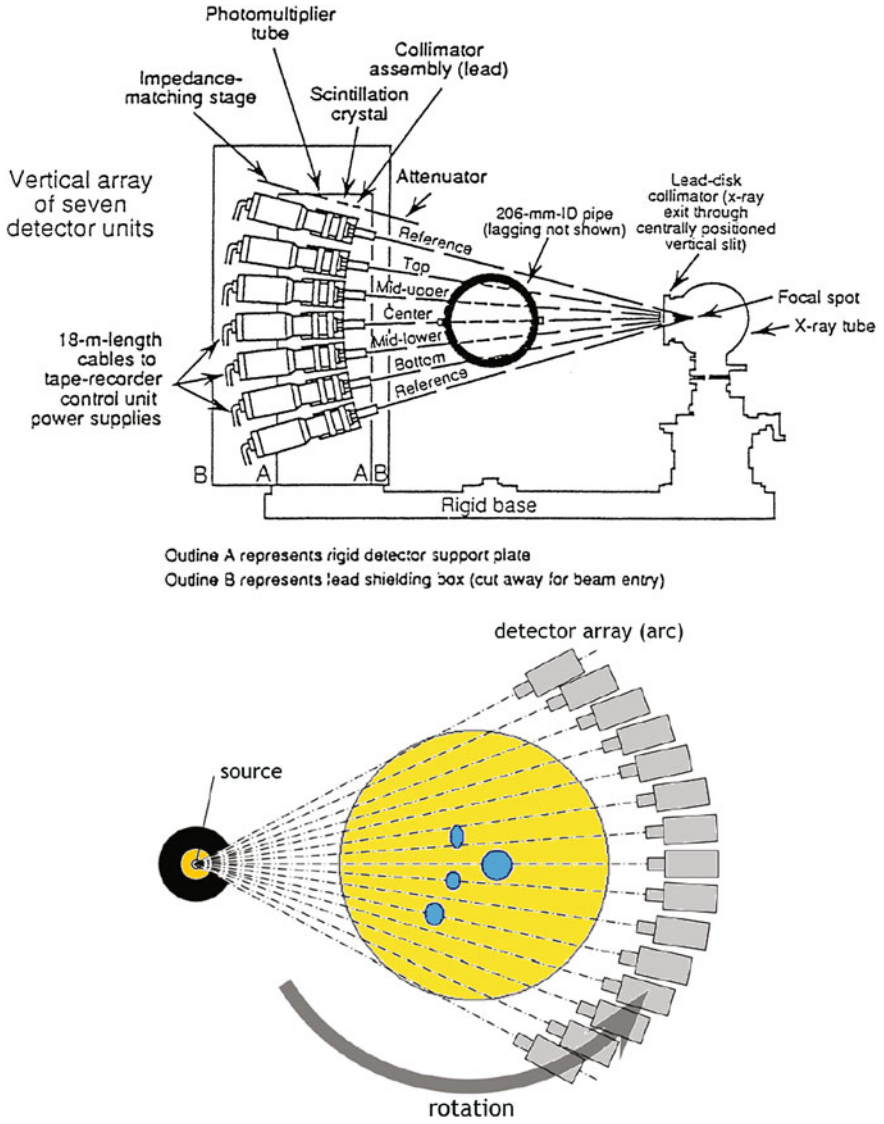

Fig. 1.13 Multi-beam x-ray systems for determination of multiple chordal-mean void fraction and hence cross-sectional-average void fractions. *Top* One of the first instruments (Smith 1975). *Bottom* Source and an array of rotating detectors can produce tomographic images (courtesy HM Prasser)

1.7.4 The Volume-Average Void Fraction

The channel (volume) average void fraction is defined as:

$$\varepsilon_{G3} = \frac{V_L}{V_L + V_G},$$

where V_G is the volume occupied by the gas and V_L is the volume occupied by the liquid in a certain volume $V_G + V_L$ of the channel. The average void fraction over a full length of the channel can be obtained by integrating many local or cross-sectional averages or by the *quick-closing-valve technique*. In this method two valves which can be simultaneously and quickly operated are placed at the two ends of the test section. At the appropriate time, the two valves are actuated and the volume of liquid in the test section is captured. The liquid is left to settle and its volume measured.

1.7.5 Averages of Products

In integrating over the flow cross section or in time to obtain average quantities, we often encounter averages of products of variables. Difficulties will arise when such products, e.g. products of void fraction, velocity and enthalpy have to be cross-sectionally averaged.

Time averages

The time average of the product of a phase-related quantity f_k (such as the phase velocity) by the *local presence function* P_k can also be written as an integral in $[T_k]$, as P_k is zero outside this interval:

$$\frac{1}{T}\int\limits_{[T]} f_k(\mathbf{r},t)P_k(\mathbf{r},t)dt = \frac{1}{T}\int\limits_{[T_k]} f_k(\mathbf{r},t)\,dt$$

that can be written as $\overline{f_k P_k} = \frac{T_k}{T}\overline{f_k}^k$.

We can verify that when $f_k = 1$, this equation produces the identity $\frac{T_k}{T} = \frac{T_k}{T}$.

We have already shown that thanks to the *commutativity* of the space and time averaging operators, Eq. (1.7.4), we have

$$\langle \bar{\varepsilon}_k \rangle = \bar{R}_k$$

Space averages

Let us consider now space averages of products of the void fraction and another phase variable f_k, e.g. velocity—such terms will appear when the momentum conservation equation is averaged in space:

$$\frac{1}{A}\int\limits_{A} \bar{\varepsilon}_k \bar{f}_k dA.$$

We will derive first a fundamental relation (Delhaye 1981) that will be useful in dealing with such space averages of products. It is going to be a fairly long derivation; we will first show that

$$\overline{\varepsilon_k}\,\overline{f_k}^{k} = \overline{P_k f_k}. \tag{1.7.5}$$

The left-hand side, using Eq. (1.7.5), can be written as $\overline{\varepsilon_k}\overline{f_k}^{k} = \frac{T_k}{T}\overline{f_k}^{k}$. The right-hand side can be expanded using the definition of time averaging, Eq. (1.6.3), and considering the fact that a time average of $P_k f_k$ over [T] is the same as a time averaging of f_k over [T_k] as

$$\overline{P_k f_k} \equiv \frac{1}{T}\int\limits_{[T]} P_k f_k dt = \frac{1}{T}\int\limits_{[T_k]} f_k dt = \frac{1}{T} T_k \overline{f_k}^{k}.$$

We have found identical expressions for both sides of Eq. (1.7.5) proving its validity.

We integrate now Eq. (1.7.5) over the cross-sectional area, i.e. we apply the operator <·> and expand the product using the definition of the time and space averaging operators:

$$\left\langle \bar{\varepsilon}_k \overline{f_k}^{k} \right\rangle = \left\langle \overline{P_k f_k} \right\rangle \equiv \frac{1}{A}\int\limits_{A} dA \left(\frac{1}{T}\int\limits_{[T]} P_k f_k dt \right).$$

Inverting the order of space/time integration, this expression becomes

$$\frac{1}{T}\int\limits_{[T]} \left(\frac{1}{A}\int\limits_{A} P_k f_k dA \right) dt = \frac{1}{T}\int\limits_{[T]} \left(\frac{1}{A}\int\limits_{[A_k]} f_k dA \right) dt = \frac{1}{T}\int\limits_{[T]} \left(\frac{1}{A} A_k \langle \varepsilon_k \rangle_k \right) dt \equiv \overline{R_k \langle f_k \rangle_k}.$$

We have found the *fundamental relationship*:

$$\left\langle \bar{\varepsilon}_k \overline{f_k}^{k} \right\rangle = \overline{R_k \langle f_k \rangle_k} \tag{1.7.6}$$

meaning that the time average of the instantaneous cross-sectional void fraction R_k times the space average of a phase property is equal to the space average of the local void fraction times the true time average of the phase property. In particular, if $f_k = 1$,

$$\langle \bar{\varepsilon}_k \rangle = \overline{R_k}$$

denoting that the space and time-averaged void fraction can be obtained either by space averaging local time-average values or by time averaging instantaneous space averages, as we have already seen above, Eq. (1.7.4).

We will be dealing usually with time-averaged quantities. If we neglect the difference between the time average of a product and the product of the time averages, i.e. if we write

$$\overline{R_k \langle f_k \rangle} = \overline{R_k} \cdot \overrightarrow{\langle f_k \rangle}$$

Equation (1.7.6) becomes

$$\left\langle \bar{\varepsilon}_k \overline{f_k}^k \right\rangle = \overline{R_k \langle f_k \rangle} = \overline{R_k} \cdot \overrightarrow{\langle f_k \rangle} = \langle \bar{\varepsilon}_k \rangle \overrightarrow{\langle f_k \rangle_k}$$

where we used the relation $\langle \bar{\varepsilon}_k \rangle = \bar{R}_k$, that is

$$\left\langle \bar{\varepsilon}_k \overline{f_k}^k \right\rangle = \langle \bar{\varepsilon}_k \rangle \overrightarrow{\langle f_k \rangle_k}. \tag{1.7.7}$$

From now on we will omit time-averaging bars and consider that we are dealing with properly time-averaged properties only. The notation $\langle \varepsilon_k \rangle$, k = L,G denotes the time and cross-sectionally averaged liquid and gas fractions. Equation (1.7.7) is then simplified as

$$\langle \varepsilon_k f_k \rangle = \langle f_k \rangle_k \langle \varepsilon_k \rangle. \tag{1.7.8}$$

This relationship will allow us to "open" the angle brackets of products of the void fraction with another variable, for example, the cross-sectional-average phase velocity:

$$< \varepsilon_k u_k > \; = \; < u_k >_k < \varepsilon_k > . \tag{1.7.9}$$

A similar relationship does *not* exist, however, for products of variables not containing the void fraction, e.g. *uh*. In this case, the angle brackets *cannot* be opened, $\langle fg \rangle \neq \langle f \rangle \langle g \rangle$. This fact will be again revisited during the derivation of the conservation equations.

Later, during the discussion of the drift-flux model in Chap. 5, we will have to make a distinction between local quantities and cross-sectional averages. For this reason we will maintain the practice of using angle brackets (<·>) to denote cross-sectional-average quantities, in spite of the fact that it burdens considerably the notations.

1.8 Phase Flow Rates and Flow Quality

The *flow quality* is defined as the ratio of the *gas mass-flowrate* $\dot{M}_G$ to the *total mass flowrate* (in kg/s):

$$x \equiv \frac{\dot{M}_G}{\dot{M}}, \qquad \dot{M} = \dot{M}_L + \dot{M}_G. \tag{1.8.1}$$

This *mass flow rate-based* definition is different from the common thermodynamic definition of quality, usually also denoted by the symbol *x,* which is the ratio of steam *mass* to total mass. To be fully consistent and clear we should have used the symbol $\dot{x}$ instead of simply x for the flow quality. As we will practically never use the mass-based definition, we are not going to do this to simplify the notation.

The flow rates of the phase k were denoted as $\dot{M}_k$ (kg/s). The corresponding volumetric flow rates are $\dot{Q}_k = \dot{M}_k/\rho_k$ (m^3/s) where ρ_k is the cross-sectional-average density of phase k. The phase *mass fluxes* are the phase flow rates per unit flow area:

$$\dot{m} = \frac{\dot{M}}{A}, \quad \dot{m}_k = \frac{\dot{M}_k}{A}.$$

Similarly, we can define the *cross-sectional-average* volumetric fluxes; departing, however, from the rule of using the same lower-case symbol for the fluxes, we will follow the usual practice and denote these by <*j*> (rather than $\dot{q}$):

$$\langle j_k \rangle = \frac{\dot{Q}_k}{A} = \frac{\dot{m} x_k}{\rho_k}, \quad \langle j_L \rangle = \frac{\dot{Q}_L}{A} = \frac{\dot{m}(1-x)}{\rho_L}, \quad \langle j_G \rangle = \frac{\dot{Q}_G}{A} = \frac{\dot{m} x}{\rho_G}. \tag{1.8.2}$$

Their sum is the *total volumetric flux* <*j*>:

$$\langle j \rangle = \langle j_L \rangle + \langle j_G \rangle = \dot{m}\left(\frac{x}{\rho_G} + \frac{1-x}{\rho_L}\right). \tag{1.8.3}$$

The volumetric fluxes are cross-sectional-average quantities. They have units of velocity, (m^3/s per m^2 or m/s). For this reason, the channel-average volumetric fluxes are also called *superficial phase velocities* U_{sG} and U_{sL}.:

$$\langle j_k \rangle = \frac{\dot{Q}_k}{A} \equiv U_{sk}. \tag{1.8.4}$$

The German term *Leerrohrgeschwindigkeit*, meaning "velocity in the empty pipe" explains well the situation: the superficial phase velocities are the ones that the phases would have had *if* they were flowing *alone* in the pipe.

We used $<j_k>$ to denote the *cross-sectional-average* value. The distinction between j_k, a *local* value and its cross-sectional average $<j_k>$ will become necessary later.[2]

1.8.1 Determination of the Flow Quality

In flows with no phase change—typically non-miscible, two-component flows such as air–water—we usually have ways of knowing the flow rates of the two phases, and the quality can be obtained from its basic definition, Eq. (1.8.1). For example, if the two phases are injected and mixed in the channel, they can be metered before injection. In this case the quality does not change along the channel.

When there is phase change in the channel, e.g. if the channel is heated and boiling takes place, then the quality increases along the channel. The inverse is true for condensation, the quality decreases along the channel in this case. In two-component flows, the quality can change also, if for example, the gas is getting dissolved in the liquid or the liquid evaporates into the gas.

More generally, in the case of multiple-component, same-phase flows, such as oil–water we may speak of *flowing mass fraction*. For example:

$$x_{oil} = \frac{\dot{M}_{oil}}{\dot{M}_{oil} + \dot{M}_{water}}, \quad x_{water} = \frac{\dot{M}_{water}}{\dot{M}_{oil} + \dot{M}_{water}}.$$

Petroleum engineers call x_{water} the "water cut" (the ratio of water produced to the volume of total liquids from an oil well).

For *single-component flows with phase change*, the determination of the quality is more complex. First, we need to calculate the enthalpy of the flowing mixture. At *steady state*, the enthalpy distribution along the channel $h(z)$ can be determined using the enthalpy balance for the channel that will be discussed in Chap. 2 as:

$$h(z) = h_{in} + \frac{1}{\dot{M}} \int_0^z q'(z) dz \tag{1.8.5}$$

where h_{in} is the enthalpy at the inlet, $\dot{M}$ the mass flow rate and q' the total "linear" energy input into the fluid per unit channel length. The total linear heat input term q' (W/m) may contain in addition to the heat flux from the wall q'' (W/m^2) other sources of "volumetric" heating of the fluid such as absorption of radiation or heat from chemical reactions that we denote by q''' (W/m^3). The *total linear heat input* from all sources is given as:

[2] In Chap. 5, we will introduce the *local* volumetric fluxes.

$$q' = q'' P_h + q''' A$$

where P_h is the heated perimeter of the channel and A its cross-sectional area. It is easy to understand the meaning of this equation, if its terms are multiplied by an elementary channel length dz: $P_h \cdot dz$ is the heat transfer area for the heat flux q'' and Adz is volume where the volumetric heating q''' takes place.

Thermodynamically, the enthalpy of a two-phase, single-component flowing mixture, e.g. steam-water flow in a steam generator, is given as a mass flow rate weighted quantity as we will see later:

$$h = x h_G + (1 - x) h_L \tag{1.8.6}$$

where, in simplified notation without the angle brackets, h_L and h_G are the (cross-sectional average) enthalpies of the two phases, $< h_k >_k$. In general, the (*actual*) local quality of the mixture will be given from Eq. (1.8.6) as

$$x = \frac{h - h_L}{h_G - h_L}. \tag{1.8.7}$$

Since often there is no thermal equilibrium between the phases (this will be further discussed elsewhere), one cannot calculate easily the phase enthalpies and then the quality merely by knowing the local enthalpy from Eq. (1.8.5) and getting the quality from Eq. (1.8.6); we need to know the values of the average local phase enthalpies h_L and h_G and these may have evolved along the channel in complex ways. Consequently, it is difficult to calculate or even measure with high precision the phase enthalpies and the quality of the liquid–vapour mixture flowing in a channel where phase change takes place.

A very simple "asymptotic" or limiting case is when both phases are saturated, i.e. if they have both the thermodynamically given *saturation* enthalpy h_{sat} corresponding to the local pressure in the channel *p(z)*

$$h_k(z) = h_{sat,k}(p(z)), \quad \mathrm{k} = \mathrm{L}, \mathrm{G}.$$

The $h_{sat,k}$ are the enthalpies we get from the so-called *Steam Tables* (e.g. Grigull et al. 2012) or more generally from fluid-property tables (Lemmon et al. 2010) for fluids other than water.

Notwithstanding the state of the fluid regarding thermal equilibrium, a *fictitious* quality, the so-called *thermal-equilibrium quality* can be calculated by *assuming* that both phases are saturated, i.e. that their temperatures are equal to the saturation temperature corresponding to their local pressure. The thermal-equilibrium quality is:

$$x_{eq} = \frac{h(z) - h_{L,sat}}{h_{LG,sat}}, \qquad h_{LG,sat} \equiv h_{G,sat} - h_{L,sat}$$

where $h_{LG,sat}$ is the latent heat of vaporization.

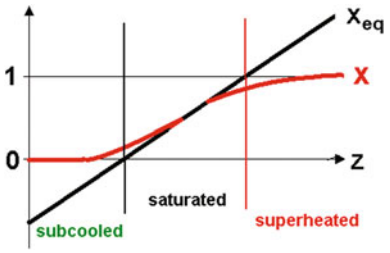

Fig. 1.14 Variation of the actual quality x and of the equilibrium quality x_{eq} along the channel. The equilibrium quality varies linearly in case of a uniform heat input along the channel

The thermal-equilibrium quality is the asymptotic, limiting value that a flowing mixture may reach in a well-mixed flow. In many situations, e.g. in the long tubes of steam generators, it may be a good approximation to the actual quality.

The notion of the thermal-equilibrium quality is a very useful one as it characterizes the properties of the flowing mixture, even when the latter is not in equilibrium. It is widely used as a characteristic of the flow, because it is easily available and it determines the equivalent state of the fluid that would have existed in the presence of thermal equilibrium. Often the authors neglect even to mention that they are referring to the thermal-equilibrium quality in their formulations; they simply speak of "quality". Note that, as defined above, x_{eq} can be negative or greater than one. A negative value of x_{eq} denotes that the mixture would have been subcooled liquid, while $x_{eq} > 1$ means that it would have been superheated vapour, Fig. 1.14.

1.9 Velocities, the Triangular Relationship and Other Useful Relations

There are several velocities which one can define, and we must be clear about what the definitions mean. In general, the two phases will not have the same velocity and there will be a relative velocity between them, as discussed below.

The *true instantaneous, local* velocities of the phases u_G and u_L are the velocities by which the phases actually travel at a given instant and at a given point. Their *phase cross-sectional averages* can be obtained as:

$$\langle u_k \rangle_k = \frac{\dot{M}_k}{\rho_k A_k} = \frac{\dot{Q}_k}{A_k} = \frac{A}{A_k} \langle j_k \rangle \tag{1.9.1}$$

where $\dot{M}_k$ is the mass flow rate of phase k, ρ_k its density and $\dot{Q}_k = \dot{M}_k / \rho_k$ the volumetric flow rate.

The cross-sectional-average velocities calculated *over the entire flow area* (as if the phase were flowing alone in the entire flow area) already defined by Eq. (1.8.2) are also called *superficial velocities* (subscript s)

$$U_{sk} = \frac{\dot{M}_k}{\rho_k A} = \frac{\dot{Q}_k}{A} \equiv \langle j_k \rangle \tag{1.9.2}$$

These are also the *volumetric fluxes* that we defined earlier; this second name represents better the physical situation and is easily understood by looking at the last equality in Eq. (1.9.2). The sum of the volumetric fluxes is the *total volumetric flux <j>*:

$$\langle j \rangle = \langle j_L \rangle + \langle j_G \rangle \text{or} U_s = U_{sL} + U_{sG}$$

The total volumetric flux can also be called the *velocity of the centre of volume;* we will discuss this further in the following section.

Using Eqs. (1.9.1) and (1.9.2), one obtains the relationship between the true cross-sectional-average velocity and the superficial velocity of each phase:

$$\langle u_G \rangle_G = \frac{U_{sG}}{\langle \varepsilon_G \rangle} = \frac{\langle j_G \rangle}{\langle \varepsilon_G \rangle}, \qquad \langle u_L \rangle_L = \frac{U_{sL}}{\langle \varepsilon_L \rangle} = \frac{\langle j_L \rangle}{\langle \varepsilon_L \rangle} \tag{1.9.3}$$

The *velocity ratio S* is the ratio of the cross-sectional average of the true velocities of the phases, i.e.

$$S \equiv \frac{\langle u_G \rangle_G}{\langle u_L \rangle_L}.$$

This useful parameter is often misleadingly called the *slip ratio*. Clearly, however, it is not a "slip", i.e. a velocity difference. Using Eq. (1.9.2),

$$S = \frac{\dot{Q}_G}{A_G} \Big/ \frac{\dot{Q}_L}{A_L} = \frac{\dot{Q}_G}{\dot{Q}_L} \frac{A_L}{A_G} = \frac{\dot{Q}_G}{\dot{Q}_L} \frac{\langle \varepsilon_L \rangle}{\langle \varepsilon_G \rangle} = \frac{\dot{Q}_G}{\dot{Q}_L} \frac{\langle 1 - \varepsilon_G \rangle}{\langle \varepsilon_G \rangle} = \frac{\langle j_G \rangle \langle \varepsilon_L \rangle}{\langle j_L \rangle \langle \varepsilon_G \rangle} \tag{1.9.4}$$

Solving for the void and liquid fractions,

$$\langle \varepsilon_G \rangle = \frac{\langle j_G \rangle}{S \langle j_L \rangle + \langle j_G \rangle}, \qquad \langle \varepsilon_L \rangle \equiv \langle 1 - \varepsilon_G \rangle = \frac{S \langle j_L \rangle}{S \langle j_L \rangle + \langle j_G \rangle} \tag{1.9.5}$$

To express the velocity ratio in terms of the quality, we recall that

$$\dot{M}_G = x\dot{M} = \rho_G \dot{Q}_G \quad \text{and} \quad \dot{M}_L = (1 - x)\dot{M} = \rho_L \dot{Q}_L$$

and substituting into Eq. (1.9.4) we readily obtain the *triangular relationship:*

$$S \equiv \frac{\langle u_G \rangle_G}{\langle u_L \rangle_L} = \frac{\rho_L}{\rho_G} \frac{x}{1 - x} \frac{\langle 1 - \varepsilon_G \rangle}{\langle \varepsilon_G \rangle} \tag{1.9.6}$$

As the phase densities are normally known, this relationship links the three variables, S, x and $<\varepsilon_G>$. Usually, we know or we can calculate the quality x. However, we need some additional information to get the void fraction such as S or a correlation for the void fraction in terms of x. We will spend later the entire Chap. 5 on methods to estimate the void fraction.

Solving Eq. (1.9.6) for the void and liquid fractions in terms of quality and velocity ratio:

$$\langle \varepsilon_G \rangle = \frac{\rho_G x}{S\rho_G(1-x)+\rho_L x}, \qquad \langle 1-\varepsilon_G \rangle = \frac{S\rho_G(1-x)}{S\rho_G(1-x)+\rho_L x} \tag{1.9.7}$$

Another two useful relationships between the quality and the volumetric fluxes can be obtained starting from the definition of the quality x and of 1-x and expanding these

$$x \equiv \frac{\dot{M}_G}{\dot{M}} = \frac{A\langle \varepsilon_G \rangle \rho_G \langle u_G \rangle_G}{\dot{M}} = \frac{A\langle j_G \rangle \rho_G}{\dot{M}}.$$
$$1-x \equiv \frac{\dot{M}_L}{\dot{M}} = \frac{A\langle \varepsilon_L \rangle \langle \varepsilon_L \rangle \rho_L \langle u_L \rangle_L}{\dot{M}} = \frac{A\langle j_L \rangle \rho_L}{\dot{M}}$$

Dividing these expressions, member by member, we find the useful relationships,

$$\frac{1-x}{x} = \frac{\langle \varepsilon_L \rangle \rho_L \langle u_L \rangle_L}{\langle \varepsilon_G \rangle \rho_G \langle u_G \rangle_G} = \frac{\langle j_L \rangle \rho_L}{\langle j_G \rangle \rho_G} \qquad \text{or} \qquad \frac{\langle j_L \rangle}{\langle j_G \rangle} = \frac{\rho_G}{\rho_L}\frac{1-x}{x} \tag{1.9.8}$$

that can be solved for x:

$$x = \frac{\langle j_L \rangle \rho_G}{\langle j_L \rangle \rho_L + \langle j_G \rangle \rho_G}. \tag{1.9.9}$$

1.9.1 Velocities of the Centre of Volume and Mass

Figure 1.15a shows a two-phase flow past a plane having an area A and moving with the velocity $<j>$. Let us assume that the flow is stratified as shown in the figure. Assuming that the gas flows faster, a volume of gas equal to $<\varepsilon>(<u_G>_G - <j>)A$ will cross the plane in the positive z direction, while a volume of liquid equal to $<1-\varepsilon>(<j_L> - <j>)A$ will cross it in the opposite direction (we use $\varepsilon = \varepsilon_G$). Summing up the two:

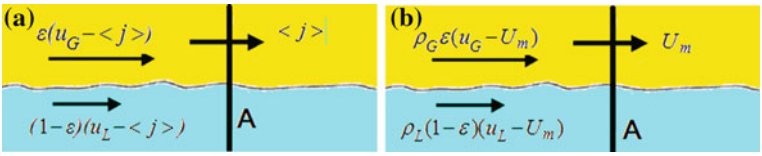

Fig. 1.15 Flows of volume and mass crossing plane A: **a** moving with velocity $\langle j \rangle$, **b** with the velocity U_m

$$\langle \varepsilon \rangle \left(\langle u_G \rangle_G - \langle j \rangle \right) A + \langle 1 - \varepsilon \rangle (\langle j_L \rangle - \langle j \rangle) A$$
$$A(\langle j_G \rangle + \langle j_L \rangle) - \langle j \rangle (\langle \varepsilon \rangle - \langle 1 - \varepsilon \rangle) = A(\langle j \rangle - \langle j \rangle) = 0$$

proving that no net volume will cross this plane (Yadigaroglu and Lahey 1976). In a somewhat more sophisticated way we can show the same thing for the general case, starting from the local quantities shown in Fig. 1.15a; we obviously obtain the same result:

$$\int_A [\varepsilon(u_G - \langle j \rangle) + \langle 1 - \varepsilon \rangle (u_L - \langle j \rangle)] \, dA$$
$$= \langle \varepsilon u_G \rangle - \langle \varepsilon \langle j \rangle \rangle + \langle (1 - \varepsilon) u_L \rangle - \langle (1 - \varepsilon) \langle j \rangle \rangle$$
$$= \langle \varepsilon u_G \rangle + \langle (1 - \varepsilon) u_L \rangle - \langle \varepsilon \rangle \langle j \rangle - \langle 1 - \varepsilon \rangle \langle j \rangle$$
$$= \langle \varepsilon \rangle \langle u_G \rangle_G + \langle 1 - \varepsilon \rangle \langle u_L \rangle_L - \langle j \rangle = \langle j_G \rangle + \langle j_L \rangle - \langle j \rangle = 0.$$

A second useful velocity is the *velocity of the centre of mass* defined as:

$$U_m \equiv \frac{\dot{m}}{\langle \rho \rangle} = \frac{\rho_L \langle u_L \rangle_L \langle \varepsilon_L \rangle + \rho_G \langle u_G \rangle_G \langle \varepsilon_G \rangle}{\rho_L \langle \varepsilon_L \rangle + \rho_G \langle \varepsilon_G \rangle}.$$

This one is the velocity of a plane traversed by zero net mass flux as:

$$\int_A [\rho_G \varepsilon(u_G - U_m) + \rho_L (1 - \varepsilon)(u_L - U_m)] \, dA$$
$$= \langle \rho_G \varepsilon u_G \rangle - \langle \rho_G \varepsilon U_m \rangle + \langle \rho_L (1 - \varepsilon) u_L \rangle - \langle \rho_L (1 - \varepsilon) U_m \rangle$$
$$= \rho_G \langle \varepsilon \rangle \langle u_G \rangle_G + \rho_L \langle 1 - \varepsilon \rangle \langle u_L \rangle_L - \rho_G \langle \varepsilon \rangle U_m - \rho_L \langle 1 - \varepsilon \rangle U_m$$
$$= \dot{m} - \langle \rho \rangle U_m = 0$$

by the definition of U_m.

1.9.2 Homogeneous Flow

Flows with equal phase velocities, i.e. if the velocity ratio $S = 1$, are called *homogeneous* flows. Our usage of the term does not imply any other "homogeneity" in the flow (e.g. well mixed). For *homogeneous flow*, setting $S = 1$ in Eq. (1.9.7) we obtain the *homogeneous* void fraction, often denoted by β:

$$\langle \varepsilon_G \rangle_{\text{hom}} \equiv \beta = \frac{\rho_L x}{\rho_G (1-x) + \rho_L x} \tag{1.9.10}$$

and in terms of volumetric fluxes, Eqs. (1.9.5) yield

$$\beta = \frac{\langle j_G \rangle}{\langle j_L \rangle + \langle j_G \rangle}, \qquad 1 - \beta = \frac{\langle j_L \rangle}{\langle j_L \rangle + \langle j_G \rangle} \tag{1.9.11}$$

Comparing Eqs. (1.9.7) and (1.9.10), one can immediately see that, as in most cases $S > 1, \langle \varepsilon_G \rangle < \beta$. Indeed, as the gas flows faster, it needs less cross-sectional flow area.

Another useful relationship is obtained for homogeneous flow from Eq. (1.9.3):

$$\langle u_G \rangle_G = \frac{\langle j_G \rangle}{\langle \varepsilon_G \rangle} = \langle u_L \rangle_L = \frac{\langle j_L \rangle}{\langle \varepsilon_L \rangle} \quad \text{or} \quad \frac{\langle j_G \rangle}{\langle \varepsilon_G \rangle} = \frac{\langle j_L \rangle}{\langle \varepsilon_L \rangle} \tag{1.9.12}$$

In the case of homogeneous flow, all mixture and phase velocities become equal:

$$\langle u_G \rangle_G = \langle u_L \rangle_L = \langle j \rangle = U_m = \frac{\dot{M}}{\langle \rho \rangle A}.$$

The equilibrium quality was considered a limiting or asymptotic situation for equal phase temperatures and used as an *index* characterizing the flow. Similarly, the homogeneous void fraction can also be considered as the limiting case of equal phase velocities and used as a useful two-phase flow index.

1.10 A Few Useful Non-dimensional Numbers

A few non-dimensionless numbers or groups of variables that are very often used will be introduced in this section, in anticipation of their actual use in the following chapters.

The density ratio

One of the most commonly used non-dimensional parameter is the density ratio ρ_L/ρ_G that appears naturally on many occasions. It provides also a useful way of considering the effect of system pressure as, e.g. in boiling flows the ratio of saturated densities is uniquely linked to the pressure.

The Martinelli X

Martinelli and co-workers suggested during the mid 40s (Martinelli et al. 1944, Lockhart and Martinelli 1949) a *separated flow* model for the frictional pressure drop, i.e. a model for flow with two distinct phase velocities (that will be discussed in Chap. 6). In the formulation of their model, they arrived at the parameter

$$X^2 = \frac{(dp/dz)_{frLP}}{(dp/dz)_{frGP}} \tag{1.10.1}$$

where $(dp/dz)_{frLP}$ is the frictional pressure gradient of the liquid as if it were flowing *alone* in the pipe at the liquid flow rate, i.e. the frictional pressure gradient based on the superficial velocity of the liquid. The subscripts LP are used to denote this "flowing alone" condition. $(dp/dz)_{frGP}$ is the corresponding gradient for the gas.

Note that the computation of the two frictional pressure gradients should be based on a Reynolds number and a friction factor consistent with the $(dp/dz)_{frkP}$ assumptions, i.e. using the volumetric flux as the velocity, computing first

$$\begin{aligned} \mathrm{Re}_{LP} &= \frac{\rho_L \langle j_L \rangle D}{\mu_L} = \frac{\langle j_L \rangle D}{\nu_L} = \frac{\dot{m}\,(1-x) D}{\mu_L} \\ \mathrm{Re}_{GP} &= \frac{\rho_G \langle j_G \rangle D}{\mu_G} = \frac{\langle j_G \rangle D}{\nu_G} = \frac{\dot{m}\,x\,D}{\mu_G} \end{aligned} \tag{1.10.2}$$

and then the corresponding (Fanning) friction factors f_{kP}, according to whether the flow is laminar or turbulent, using the appropriate correlations, for example:

for laminar flow, $f_{kP} = \frac{16}{\mathrm{Re}_{kP}}, \quad k = L, G$

and for turbulent flow, $f_{kP} = \frac{C}{\mathrm{Re}_{kP}^{m}}$

where C and m are empirical constants. The pressure gradients are then given as

$$-\left[\frac{dp}{dz}\right]_{frkP} = \frac{4 f_{kP}}{D} \frac{\dot{m}^2 (x_k)^2}{2\rho_k} = \frac{4 f_{kP}}{D} \frac{\rho_k \langle j_k \rangle^2}{2}.$$

The Martinelli parameter can be computed in terms of known quantities. For the case of turbulent flow in both phases (X with subscript tt), and with the exponent of the friction factor correlation $m = 0.2$, it takes the simple form

$$X_{tt} = \left[\frac{1-x}{x}\right]^{0.9} \left[\frac{\rho_G}{\rho_L}\right]^{0.5} \left[\frac{\mu_L}{\mu_G}\right]^{0.1} \tag{1.10.3}$$

This parameter involves the ratios of the main quantities determining the pressure gradient to the appropriate powers and is a quite useful reference parameter introduced in various correlations for void fraction, and pressure drop or even

boiling heat transfer. X^2 is also a measure of the degree to which the two-phase mixture is closer to liquid, i.e. $X^2 \gg 1$, or to gas, i.e. $X^2 << 1$.

It is useful to express X_{tt} in terms of volumetric fluxes; we use Eq. (1.9.8) to obtain

$$X_{tt} = \left[\frac{\langle j_L \rangle}{\langle j_G \rangle}\right]^{0.9} \left[\frac{\rho_L}{\rho_G}\right]^{0.4} \left[\frac{\mu_L}{\mu_G}\right]^{0.1} \tag{1.10.4}$$

The variation of X_{tt} with x (for constant properties), together with the ratio of $<j_G>/<j_L>$, Eq. (1.9.8) vs x, are plotted in Fig. 1.16 to give the reader a feeling for these dependencies.

Figure 1.17 is a plot of the Martinelli parameter X_{tt} and of the ratio of volumetric fluxes $<j_L>/<j_G>$ versus quality of saturated steam/water flows. The purpose of the plot is to show that both vary widely with the quality. Even within the "more reasonable" quality range (0.05–0.95), the variations are of two to three orders of magnitude, mainly due to the wide variation of the density with pressure, as shown in Fig. 1.17 for saturated water/steam and air/water systems.

The Laplace wavelength

As we will see in Chap. 4 on interfacial instabilities, a non-dimensional length characterizing the balance between surface tension and gravity forces is the so-called Laplace length of wavelength:

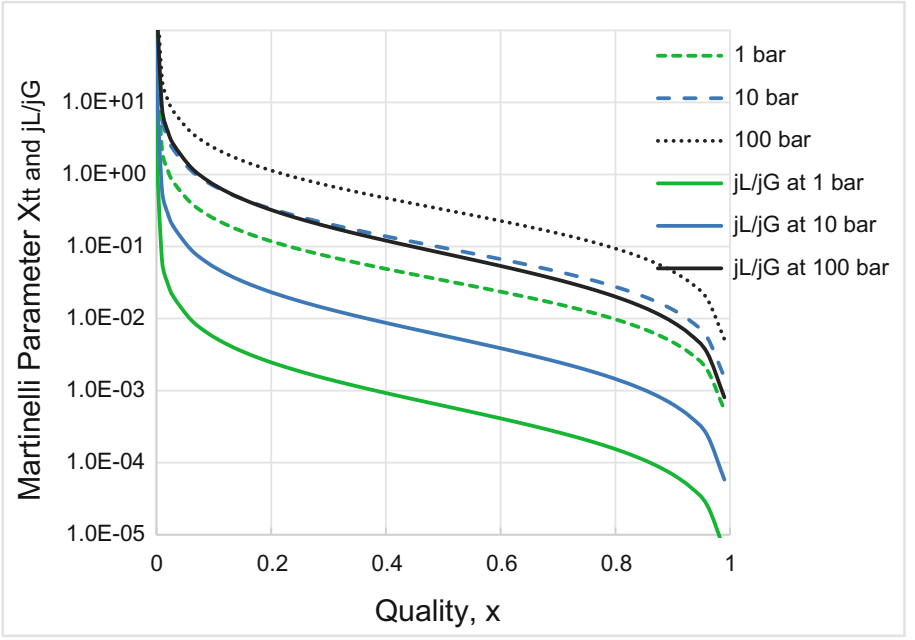

Fig. 1.16 Variation of the Martinelli parameter X_{tt} and of the ratio of volumetric fluxes j_L/j_G with quality; saturated steam/water flow at three different pressures

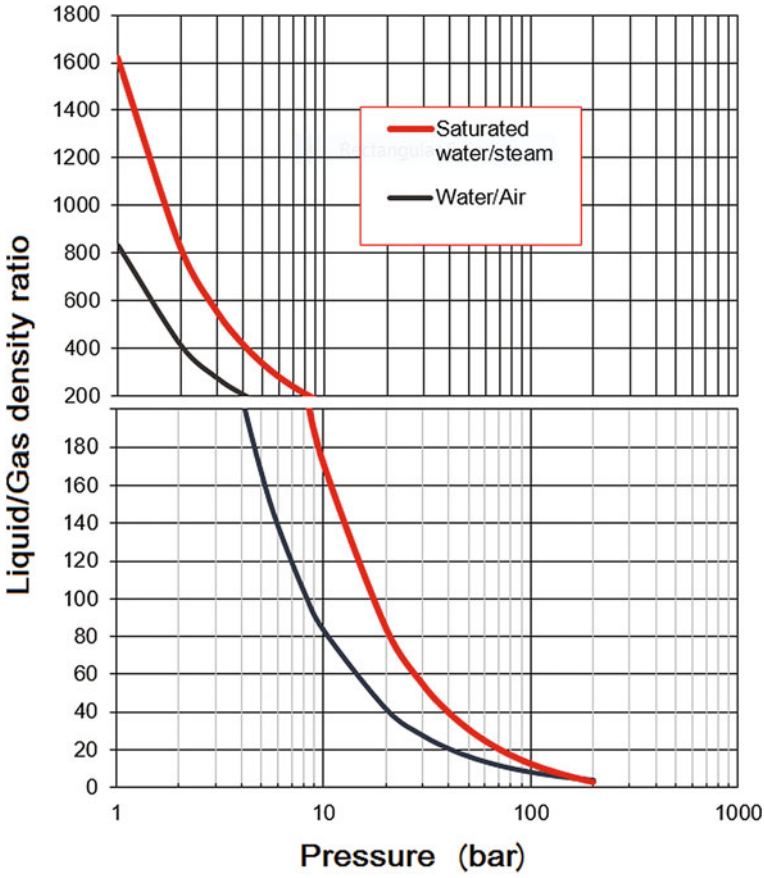

Fig. 1.17 Variation of the liquid/gas density ratio for water/air and saturated water/steam

$$L \equiv \sqrt{\frac{\sigma}{g(\rho_L - \rho_G)}}$$

Non-dimensional volumetric fluxes

Wallis (1969) introduced the non-dimensional volumetric fluxes that find many uses as

$$j_k^* \equiv \frac{\langle j_k \rangle}{\sqrt{\frac{gD(\rho_L - \rho_G)}{\rho_k}}}, \quad \mathrm{k} = \mathrm{L}, \mathrm{G}$$

where D is a characteristic system dimension, usually the diameter. There are cases, however, where a characteristic system dimension is not available, and the

phenomena may depend on some intrinsic length scale such as the Laplace length. For such cases we would rather use the Kutateladze numbers[3]:

$$K_k \equiv \frac{\langle j_k \rangle}{\sqrt{4\frac{\sigma g(\rho_L - \rho_G)}{\rho_k^2}}}, \quad k = L, G$$

where the Wallis diameter D was replaced by the Laplace length L.

1.11 System of Units

The internationally accepted SI system of units will be used, unless otherwise necessary. This is a self-consistent set of units, which makes it easy to check equations and eliminate ambiguities such as kg-mass or kg-force.

The basic units are: length: m (meter), mass: kg (kilogram), time: s (second), temperature: °C or K (by convention, degree Kelvin is written as K, not °K).

Other units are derived from these, such as force: N (Newton = kg m s^{-2}); pressure: Pa (Pascal = N m^{-2}). Unfortunately, Pa is a very small unit and MPa (= 10^6 Pa) or bar (= 10^5 Pa) are frequently used instead; energy: J (Joule = Nm = kg m^2 s^{-2}); power: W (Watt = J s^{-1}); thermal conductivity (W m^{-1} $°C^{-1}$ = J s^{-1} m^{-1} $°C^{-1}$), etc.

A large number of older texts and papers on multiphase flows were written using the British system of units. Appendix II gives the most often needed but more difficult to find conversion factors for the heat-transfer and fluid-mechanics areas.

Appendix III lists the general nomenclature used in this volume. Additional nomenclature is defined locally, as needed.

1.12 Sources of Information

There are several textbooks that have been written on the subject of two- or multiphase flows and heat transfer with phase change and several journals that publish regularly on these topics.

Two of the first books on two-phase flow are the classical Tong (1965) and the excellent book by Wallis (1969). A second edition by Tong and Tang (1997) has been published more recently. The monograph byWallis (1969) has not "aged" and remains a very valuable source of information.

The early first edition by Collier and its third edition by Collier and Thome (1994) provide the basic information on boiling phenomena. The more recent book by Carey (1992) contains a wealth of information on phase change phenomena.

[3]There are other Kutateladze numbers in addition to the ones given here.

Ishii and Hibiki (2011) provide detailed discussions and derivations of the fundamental conservation equations and various models used for two-phase flows. Noticeable in the German speaking area are the books by Mayinger (1982) and Stephan (1988). Handbooks on multiphase systems have been published by Hetsroni (1982), Kandlikar et al. (1999), and Crowe (2005).

More specialized textbooks are those of Hewitt (2013) on annular flows, Levy (1999), Kleinstreuer (2003), Ghiaassiaan (2008) on "miniature systems", Govier and Aziz (1972) on "complex mixtures in pipes" (petroleum engineering flows). Lahey and Moody (1977, 1993) and Tong and Weisman (1979) published books on Boiling and Pressurized Water Reactors, respectively, that contain a lot of two-phase flow related material. Kolev (2012a,b,c, 2015a,b) has published five volumes containing a lot of detailed information on modelling and computing two-phase flows. Computational methods for multiphase flows are presented in the books by Prosperetti and Tryggvason (Prosperetti and Tryggvason 2007) and by Tryggvason et al. (2011).

A monograph specialized on flow regimes is that of Cheng et al. (2008); Yarin et al. (2009) wrote on two-phase flows and boiling in microchannels. Finally, there are notable handbooks or specialized monographs sponsored by companies, such as those of Wolverine Tube, Inc. (2014–2010) and the two monographs by Chexal et al. (1997, 1999). The latter contain most recent models and methods for computing pressure drop and void fraction in two-phase flows as well as the computer tools for their implementation.

The interested reader will find some of the early seminal work in the proceedings of workshops that were organized and attracted prominent researchers. The proceedings of such a meeting that took place in Istanbul were published by Kakac and Mayinger (1977). The book by Delhaye et al. (1980) contains a series of chapters on several topics of industrial interest. One could also mention here three Workshops organized by the US Department of Energy (DOE) (jointly with the US Electric Power Institute, EPRI, the third time) on "Two-Phase Flow Fundamentals" at the National Bureau of Standards, Gaithersburg, Maryland (1985), at the Rensselaer Polytechnic Institute, Troy, New York (1987), and for the last time at Imperial College in London (DOE/EPRI 1992). The objective of the first workshop was to identify, formulate and prioritize research problems in the field of multiphase flow and heat transfer. A selection of "numerical benchmark sets" and "physical benchmark exercises" was also chosen. These were then performed by various international participants who compared their findings at the second workshop. Presentations on the two-phase flow models and on interfacial relationships, and the selected Data Sets and Numerical Benchmark Tests are included in Volume 3 of *Multiphase Science and Technology* (Hewitt et al. 1987). There is also a report on the first meeting by Kestin and Podowski (1985). The results of the second workshop were published in Vols. 5, 6, and 8 of *Multiphase Science and Technology*.

Most of the articles on boiling heat transfer and two-phase flow can be found in the following journals:

International Journal of Multiphase Flow, IJMPF
International Journal of Heat and Mass Transfer, IJHMT
Journal of Heat Transfer, Transactions ASME, JHT
American Inst. of Chemical Engineers Journal, AIChE Journal
Chemical Engineering Progress, Symposium Series
Multiphase Science and Technology (reviews), etc.

In addition, applications to nuclear systems are found mostly in:

Nuclear Science and Engineering
Nuclear Technology
Nuclear Engineering and Design
Annals of Nuclear Energy, etc

Petroleum-industry related papers can be found in:

Petroleum Science and Technology
Journal of Petroleum Technology
Oil and Gas Journal, etc

References

Banerjee S, Hussein E, Meneley DA (1978) Simulation of a neutron scattering method for measuring void fraction in two-phase flow. Nucl Eng Des 53:393–405
Brown NP, Heywood NI (1991) Slurry handling design of solid-liquid systems. Elsevier Applied Science, London and New York
Carey VP (1992) Liquid-vapor phase-change phenomena. Hemisphere Publ, Corp, Washington
Cheng L, Ribatski G, Thome JR (2008) Two-phase flow patterns and flow-pattern maps: fundamentals and applications. Appl Mech Rev 61(5). doi:050802
Chexal B et al (1997) Void fraction technology for design and analysis. EPRI—Siemens. http://www.epri.com/abstracts/Pages/ProductAbstract.aspx?ProductId=TR-106326
Chexal B et al (1999) Pressure drop technology for design and analysis. EPRI—Siemens. http://www.epri.com/abstracts/Pages/ProductAbstract.aspx?ProductId=TR-113189
Collier JG, Thome JR (1994) Convective boiling and condensation, 3rd edn. Oxford University Press
Crowe CT (2005) Multiphase flow handbook. Taylor & Francis
Danel F, Delhaye JM (1971) Optical probe for measuring the local voidage in two-phase flow systems. Mes Regul Automat 36(8–9):99–101
Delhaye JM (1981) Local instantaneous equations, local time-averaged equations, and composite-averaged equations. In: Delhaye JM, Giot M, Riethmueller ML (ed) Thermohydraulics of two-phase systems for industrial design and nuclear engineering. Hemisphere, Washington
Delhaye JM, Giot M, Riethmuller ML (eds) (1980) Thermodynamics of two-phase systems for industrial design and nuclear engineering. Hemisphere Publishing Corp, Washington DC
DOE/EPRI (1992) Proceedings of the third international workshop on two-phase flow fundamentals, 15–19 June 1992, London, US DOE and EPRI
Fan L-S, Zhu C (1998) Principles of gas-solid flows. Cambridge University Press, New York
Ghiaasiaan SM (2008) Two phase flow boiling and condensation in conventional and miniature Systems. Cambridge University Press
Govier GW, Aziz K (1972) The flow of complex mixtures in pipes. Van Nostrand Reinhold, New York

Grigull U, Straub J, Schiebener P (2012) Steam Tables in SI-Units/Wasserdampftafeln: concise steam tables in SI-Units (Student's Tables) Properties of ordinary water substance up to 1000° C and 1000 bar. Springer Science & Business Media, Third enlarged edition

Hetsroni G (1982) Handbook of multiphase systems. Hemisphere. McGraw-Hill

Hewitt G (2013) Annular two-phase flow. Elsevier

Hewitt GF, Delhaye JM, Zuber N (1987, 1990, 1992, 1994) Multiphase science and technology, vols 3, 5, and 6, Hemisphere, Washington

Ishii M, Hibiki T (2011) Thermo-fluid dynamics of two-phase flow, 2nd edn. Springer Science & Business Media, New York

Kakac S, Mayinger F (1977) Two-phase flows and heat transfer, Proceedings NATO advanced study institute on two-phase flows and heat transfer, Istanbul, Turkey, 16 Aug 1976, vols 1–III. Hemisphere Publishing Corp, Washington, DC

Kandlikar SG, Shoji M, Dhir VK (1999) Handbook of phase change: boiling and condensation. Taylor & Francis

Kestin J. Podowski MZ (1985) Report on international workshop on two-phase flow fundamentals, held at the National Bureau of Standards, Gaithersburg, Maryland, 22–27 Sept 1985

Kleinstreuer C (2003) Two-phase flow—Theory and application. Taylor & Francis

Kolev NI (2012a) Multiphase Flow dynamics 2—Mechanical interactions. Springer, Berlin Heidelberg

Kolev NI (2012b) Multiphase flow dynamics 3—Thermal interactions. Springer, Berlin, Heidelberg Kolev NI (2009)

Kolev NI (2012c) Multiphase flow dynamics 4—Turbulence. Diesel fuel properties. Springer, Berlin Heidelberg, Gas Adsorption and Release

Kolev NI (2015a) Multiphase flow dynamics 1 – Fundamentals, 5th edn. Springer, Berlin, Heidelberg

Kolev NI (2015b) Multiphase flow dynamics 5—Nuclear Thermal Hydraulics, 3rd edn. Springer-Verlag, Berlin Heidelberg

Lahey RT, Moody FJ (1977, 1993) The thermal-hydraulics of a boiling water nuclear reactor. Amer Nuclear Society

Lassahn GD (1977) LOFT 3 Beam Densitometer Data Interpretation. US NRC report NUREG-1111

Ledinegg M (1938) Instability of flow during natural and forced circulation. Die Wärme 61 (8):891–898 (English translation as report AEC-tr-1861 (1954))

Lemmon EW, Huber ML, McLinden MO (2010) NIST Reference fluid thermodynamic and transport properties—REFPROP Version 9.0 User's guide thermophysical properties Division National Institute of Standards and Technology Boulder, Colorado 80305

Levy S (1999) Two-phase flow in complex systems. John Wiley & Sons Inc

Lockhart RW, Martinelli RC (1949) Proposed correlation of data for isothermal two-phase, two-component flow in pipes. Chem Eng Prog 45:39–48

Martinelli RC, Boelter LK, Taylor TH, Thomsen EG, Morrin EH (1944) Isothermal pressure drop for two-phase two-component flow in a horizontal pipe. Trans ASME 66(2):139–151

Mayinger (1982) Strömung und Wärmeübergang in Gas-Flüssigkeitsgemischen, Springer-Verlag, Wien

Nukiyama S (1934) The maximum and minimum value of the heat transmitted from metal to boiling water under atmospheric pressure. J Japan Soc of Mech Engrs 37: 367–374. See also translation in Int J Heat Mass Transfer (1966) 9:1419-1433

Prosperetti A, Tryggvason G (2007) Computational methods for multiphase flow. Cambridge University Press

Rousseau JC, Riegel B (1978) SUPER CANON experiments. Transient two-phase flow. In: Proceedings of the second CSNI specialists meeting, Paris, 12–14 June 1978

Shapiro AH (1953) The dynamics and thermodynamics of compressible fluid flow, Vol 1, Chap 4. Ronald Press, New York

Smith AV (1975) Fast response multi-beam X-ray absorption technique for identifying phase distributions during steam-water blowdowns. J Br Nucl Energy Soc 14(3):227–235

Stephan K (1988) Wärmeübergang beim Kondensieren und beim Sieden. Springer-Verlag, Berlin
Tong LS (1965) Boiling heat transfer and two-phase flow. Wiley, New York
Tong LS, Tang YS (1997) Boiling heat transfer and two-phase flow. CRC Press
Tong LS, Weisman J (1979) Thermal analysis of pressurized water reactors
Tryggvason G, Scardovelli R, Zaleski S (2011) Direct Numerical Simulations of gas-liquid multiphase flows, Cambridge University Press
Wallis GB (1969) One dimensional two phase flow. McGraw-Hill
Wolverine Tube, Inc. (2004–2010) Heat transfer data book. http://www.wlv.com/heat-transfer-databook/
Yarin LP, Mosyak A, Hetsroni G (2009) Fluid flow, heat transfer and boiling in micro-channels. Springer Verlag

Chapter 2
Modelling Strategies and Two-Phase Flow Models

Geoffrey F. Hewitt and George Yadigaroglu

2.1 Two-Phase Flows and Their Analysis

We will recall first the general methods of solution of thermal-hydraulic problems and then show how these are complicated by the presence of multiphase flows before entering in the following sections into the descriptions of the various approaches.

2.1.1 General Methods of Solution

The design and transient behaviour problems are treated in a similar manner. Starting from the general conservation laws:

- conservation of mass
- conservation of momentum
- conservation of energy,

we express these by *partial differential equations*. We choose the minimum required number of space variables and consider, if necessary, time dependence. Very often we deal with *one-dimensional systems* and with cross-sectionally averaged variables. We then "close" or complete the set of equations by including the necessary *constitutive laws and relations,* namely,

G.F. Hewitt (✉)
Department of Chemical Engineering and Chemical Technology,
Imperial College, London, UK
e-mail: g.hewitt@imperial.ac.uk

G. Yadigaroglu
ETH Zurich, Zurich, Switzerland
e-mail: yadi@ethz.ch

G. Yadigaroglu and G.F. Hewitt (eds.), *Introduction to Multiphase Flow*,
Zurich Lectures on Multiphase Flow, DOI 10.1007/978-3-319-58718-9_2

- *equations of state* that govern the physical properties of the materials involved
- *general laws of nature* or *rate equations*, e.g. the Fourier law of conduction, Newton's law of viscosity, etc. These describe in an idealized or simplified manner natural behaviour. For multiphase flows, new needs appear in this category, or the corresponding laws become much more complex (e.g. how is heat conducted in a two-phase mixture)
- *semi-empirical* relations for parameters such as friction factors, heat transfer coefficients, turbulence parameters, etc. These often appear in the conservation equations because of the idealizations or reductions in space variables made, e.g. instead of resolving all details of the flow in three dimensions and getting the heat transfer law at the wall, we work in one dimension and use a heat transfer coefficient for the heat transfer between the wall and the average temperature of the fluid. Again, here the situation becomes much more complex for multiphase flows, e.g. in the determination of frictional pressure drop or of the heat transfer law in boiling. In particular, in two-phase flows, we should make sure that the empirical relations used remain valid in the domain of application as most available data cover rather narrow domains.

We then define the boundary conditions of the problem. These are prescribed according to our physical understanding of the problem and are often approximations of reality.

Finally, we solve the resulting set of equations subject to the boundary conditions. Exact analytical solutions are rare; approximate analytical solutions are sometimes possible; numerical methods embedded in computer codes are most often used.

As said in Chap. 1, we are dealing here mainly with one-dimensional systems and corresponding formulations. Multidimensional formulations of multiphase flow problems will be only briefly discussed below and treated in other volumes with methods based on Computational Fluid Dynamics (CFD).

2.1.2 *Special Features of Two-Phase Flows*

The most important feature of gas–liquid flows, when compared to single-phase flows, is the existence of deformable interfaces. This, coupled with the naturally occurring turbulence in gas–liquid flows, makes them highly complex. Some simplification is possible by classifying the types of interfacial distributions (their topology) under various headings, known as *flow regimes* or *flow patterns*. The two-phase flow regimes for gas–liquid flow in vertical tubes are illustrated in Fig. 2.1 and range from bubble flow to wispy annular flow. Vertical flows are, on average, axi-symmetric but with horizontal flows, gravity induces the liquid to move preferentially towards the bottom of the channel as shown in Fig. 2.2. Flow patterns and their prediction will be discussed in another chapter.

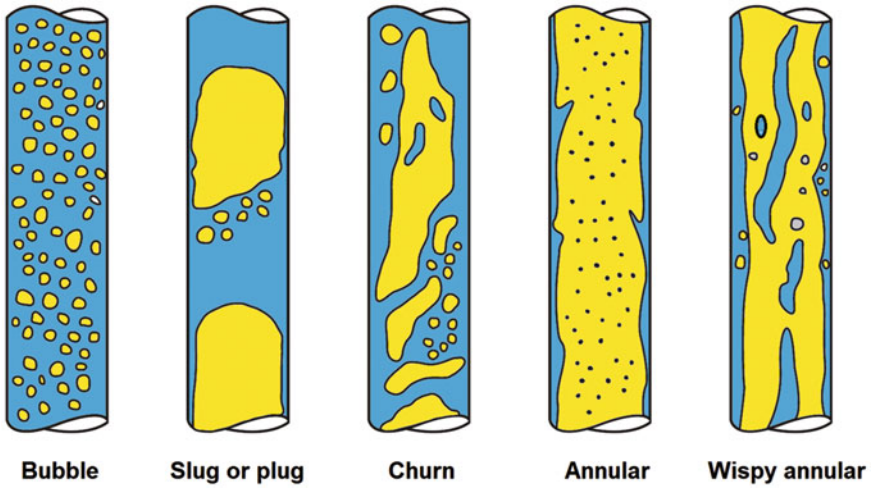

Fig. 2.1 Main flow regimes in upwards gas–liquid flow in vertical tubes

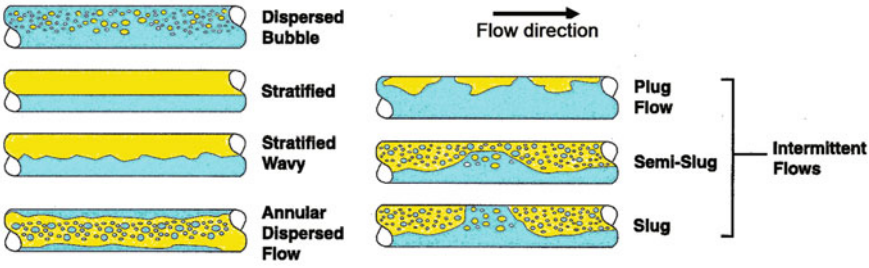

Fig. 2.2 Main flow regimes in gas–liquid flow in horizontal tubes

An exact formulation of the two-phase flow problem would have required the description of the evolution in time of the fields (pressure, velocity, temperature, etc.) for each phase, together with a prediction of the geometry of the interfaces. Such an approach is impractical, except in some relatively very simple situations, for example in horizontal stratified flow, where the geometrical configuration of the two phases is a priori known or can be computed by interface tracking methods (discussed later in Sect. 2.7). In most situations, however, the flow field and the topographical distribution of the phases are chaotic and must be described using statistical, average properties. There are two general approaches, the *two-fluid approach* and the *mixture formulation*; we will discuss them in Sect. 2.5.

2.1.3 Two-Phase Flow Equipment

Two-phase gas–liquid flow is important in a wide variety of equipment types which include the following.

Vapour Generation Systems
In these systems, vapour is generated by the addition of heat and joins the liquid in flowing through the system. Vapour generation equipment includes power station boilers, waste heat boilers, coiled tube boilers and package boilers. Vapour generation is also a vital component of many process plants, with equipment ranging from fired heaters to various kinds of reboilers (kettle, horizontal thermosiphon and vertical thermosiphon). The generic problems in all this equipment are the prediction of void fraction and pressure drop (and hence pumping power or, in the case of natural circulation systems, circulation rate), critical heat flux, heat transfer, system stability and fouling of the heat transfer surfaces.

Nuclear Power Plants (NPP)
Vapour generation is also, of course, vital in nuclear power generation and can occur directly within the reactor itself (as in the Boiling Water Reactor, BWR) or in the steam generators which are heated by hot fluid from the reactor (as in the Pressurized Water Reactor, PWR). Two-phase flow and heat transfer with phase change are important for the normal operation of NPPs but become very complex in case of transient and accidental situations. A very large number of situations and phenomena can be encountered; these will be discussed in another volume in this series.

Vapour Condensers
Most condensers are of the *indirect contact* type and there is a preponderance of the shell-and-tube type of condenser, with both condensation on the tube side and the shell side. However, air-cooled condensers are important as are matrix (brazed aluminium) condensers for cryogenic systems, for instance. Condensation can also be carried out in the *direct contact* mode with various types of equipment being used (pool type condensers, spray condensers, baffle column condensers, etc.). Again, the principal requirements for design are prediction of void fraction and pressure drop and heat transfer coefficients. In many systems, the fluids are multi-component in nature and condensation involves simultaneous heat and mass transfer. Where the condensation is done in counter-current flow, flooding can be an important limitation on operation.

Mass Transfer Equipment
Many mass transfer operations (absorption, stripping, humidification, dehumidification, distillation, etc.) involve gas–liquid two-phase flows. Equipment used includes bubble columns, wetted wall columns, plate columns (having bubble caps or sieve plates, etc.), packed columns and spray chambers. Again, the key problems in design are the prediction of mass transfer coefficients and pressure

drop. However, questions of stability, bypass and phase separation are of considerable importance in this type of equipment.

In carrying out designs, information is required on the *fluid physical properties* and on the expected *flow rates* of the respective phases. The prediction requirements for design are of three categories:

(1) *Steady-state design parameters.* These include pressure drop, heat and mass transfer laws and coefficients and mean gas phase content (void fraction).
(2) *Limiting conditions.* These include critical heat flux (i.e. the heat flux at which the heat transfer coefficient deteriorates, possibly leading to damage of the channel surface), critical mass flux (the condition at which the flow rate becomes independent of downstream pressure), mechanical vibration, erosion and corrosion and instability.
(3) *Plant transients.* These cover a whole range of situations including plant start-up and shutdown, emergency events (such as the loss of site power in a nuclear power station), Loss Of Coolant Accidents (LOCAs) and atmospheric release and dispersion of multiphase mixtures.

To meet the above design requirements, a number of approaches to prediction can be taken. These include

(1) The empirical approach
(2) Phenomenological modelling
(3) Multi-fluid modelling
(4) Computational fluid dynamics modelling (CFD).

These various approaches will be discussed in the following sections; each approach has limitations and there is no general "best" modelling scheme for multiphase systems. In Sect. 2.8, some conclusions are drawn about the subject of modelling methodologies.

2.2 The Empirical Approach

The empirical approach proceeds as follows:

(1) *Data collection*. A large number of data points are collected, for example, for the pressure gradient (*dp/dz*), for a range of mass flux, quality, physical properties and tube orientation and diameter.
(2) *Correlation.* Empirical (or semi-empirical) relationships are developed between the *dependent* variables (pressure gradient *(dp/dz)* or pressure drop Δp, for instance) and the *independent* variables (mass flow, quality, geometry and fluid physical properties).
(3) *Application.* The correlations developed are then applied in hand and computer calculations to predict the design variables. Since the correlations are largely empirical, they are insecure outside the range of data which they cover even at

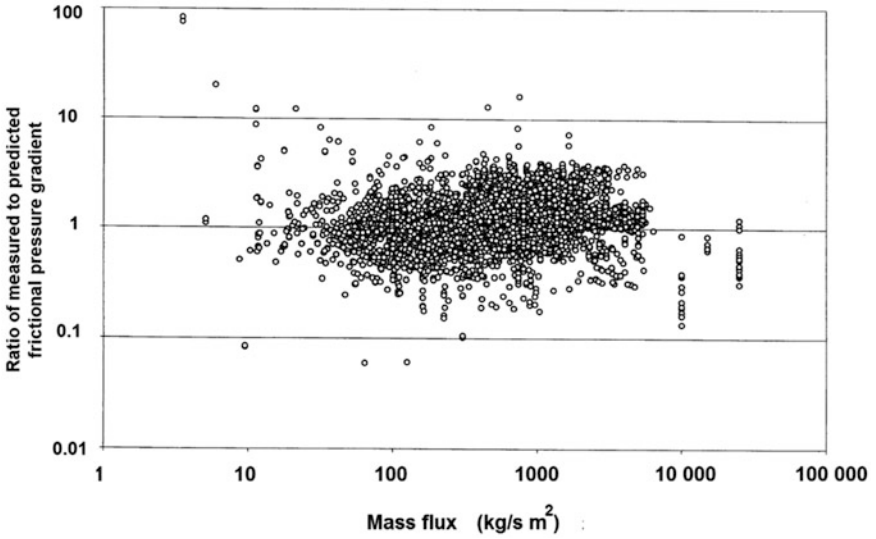

Fig. 2.3 Comparison of experimental data with the "best" correlation selected for each group of data (ESDU 2002)

steady state. For lack of a better alternative, empirical correlations are often, however, applied also to transient conditions, where they may not be successful (an example is given in Sect. 2.4.4).

An illustration of the errors associated with empirical models is amply provided by an exercise carried out by the former Engineering Sciences Data Unit in the UK (ESDU 2002) on pressure gradient in horizontal two-phase gas–liquid flow. A data bank of 6453 experimental data points forpressure gradient was assembled. This database covered a wide range of physical properties (though with a natural preponderance of low-pressure, air–water data). The database was compared with ten published pressure gradient correlations. The comparisons were grouped into bands of mass flux and quality and the best correlation identified for each respective band. Comparison of the data with these "best" correlations is shown in Figs. 2.3 and 2.4.

Figure 2.3 plots the ratio of measured to predicted frictional pressure gradient as a function of mass flux and it will be seen that in a few cases errors of more than a factor of ten may occur, though the preponderance of the data is (as would be expected) in better agreement than that. Figure 2.4 shows the distribution of errors which essentially gives the same message. The ESDU publication gives methods of assessing the uncertainties in the use of these empirical correlations and, within the range covered by the data base, gives the expected confidence level in a range around the central prediction. The designer is therefore able to make an assessment of the uncertainty (which may be large) and to consider how it affects the system design.

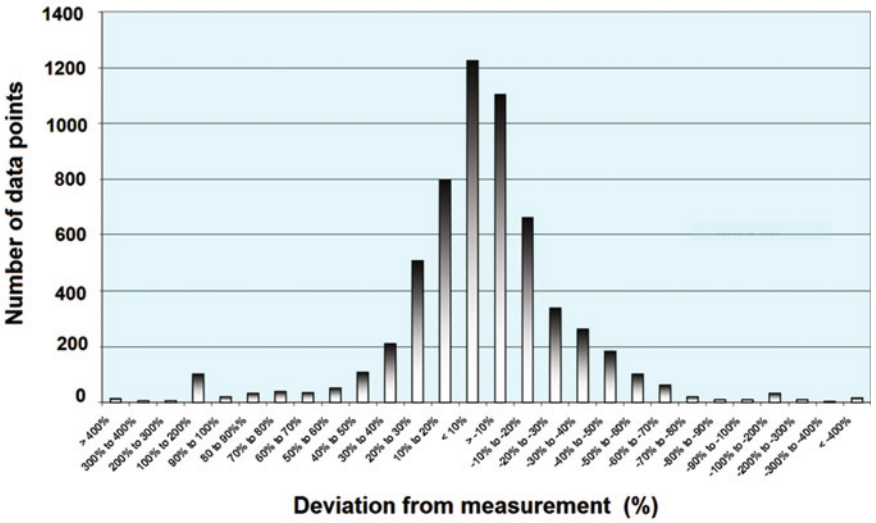

Fig. 2.4 Distribution of errors in comparisons of predicted and measured values of pressure drop in vertical pipes (ESDU 2002)

The relative failure of empirical correlations for pressure drop, void fraction, etc. has led to the search for improved models and these will be reviewed below. However, it should be stressed that the "improved" models do not necessarily give better results than do the empirical correlations.

The inaccuracies in empirical correlations arise because of a number of factors[1]:

(1) The experimental data may itself be in error. Measurements in gas–liquid systems are quite difficult but, with adequate attention to detail, one would have expected maximum inaccuracies in measurement of the order of 10–20%.
(2) The correlation form may be unsuitable. Even with the existence of many adjustable constants, if the form is not adequate, then a good data fit will not be possible.
(3) The data may be basically uncorrelatable. Factors here include the following:
    (a) Not all the relevant parameters may be known, particularly local physical properties.
    (b) There may be unrecognised effects. For example, surface tension can have a large effect on pressure gradient and is hardly ever taken full account of in correlations.
    (c) The flow may not have reached hydrodynamic equilibrium. In single-phase flows, pressure gradient becomes relatively constant after typically ten tube diameters. In gas–liquid two-phase flow, reaching constant values of

[1]The following discussion is mainly directed to the accuracy of the pressure gradient; similar considerations apply, however, in all other areas.

pressure gradient may take many hundreds of diameters. Experimental data are rarely obtained under these conditions and, in any case, changes in pressure may occur which give rise to expansion of the gas phase and changes in the gas velocity and hence pressure gradient. In this context, it has been found that approximately constant values of pressure gradient are obtained at *fixed outlet pressure* after several hundred diameters. Thus, even with adiabatic flows, the pressure gradient data may contain significant errors due to lack of equilibrium. Moreover, with diabatic (evaporating or condensing) flows, the potential equilibrium value is in itself changing along the channel and equilibrium conditions rarely pertain in such cases.

(d) A starting assumption in many calculations is that the phases are in thermodynamic equilibrium. However, this is patently not so in systems with heat transfer where bubbles may exist in the presence of bulk liquid subcooling and droplets may exist in the presence of bulk vapour superheat.

It is in the context of the non-equilibrium situations that the real benefits of improved modelling are likely to accrue.

2.2.1 The Empirical Approach Versus Phenomenological Modelling

As we have shown above, it is clear that the various two-phase flow and boiling heat transfer variables of interest, such as the pressure gradient, the void fraction, the heat transfer coefficient, etc., will depend on the particular flow regime. Thus, in principle, one should model each flow regime separately. This is indeed often done; flow-regime-dependent modelling becomes a necessity if high prediction accuracy is needed; for example, in calculating phenomena taking place in pipelines. When flow-regime-specific models are used, one can "mechanistically" take into consideration the particularities of each regime. However, one drawback of the flow-regime-oriented approach is that one must first predict the prevailing flow regime before undertaking any calculation; this is not always easy. Moreover, the calculation procedure is also considerably lengthened and complicated if many flow regimes can take place.

The alternative approach often used is to largely ignore the flow regimes and derive methods (most often empirical correlations) covering all flow regimes continuously. When the variables used as inputs in the correlations are the same as the ones used in determining the flow regime, such methods can be successful. For example, if mass flux and flow quality are the two variables determining the flow regime (they are not the only ones…), then a correlation of the frictional pressure gradient in term of these two variables has the potential of inherently taking into account the prevailing flow regime.

2.3 Phenomenological Modelling

If one looks at Figs. 2.1 and 2.2, it seems obvious that a flow in the bubble flow regime will behave quite differently to one which is in the annular flow regime. In spite of this, empirical correlations often do not take particular account of regimes, and this must be one of the main reasons for their relative failure. In the *phenomenological* approach, the calculations are made for specific flow regimes; this presents a new problem of course, which is the identification of which flow pattern applies for the set of conditions of interest, as already mentioned. Empirical correlations (in the form of flow regime maps, etc. discussed in Chap. 4) exist for flow regime transitions, but these, too, often lack generality and phenomenological modelling is also used in the context of the flow pattern transitions themselves. Thus, the steps for a given flow regime modelling are as follows:

(1) Observations and detailed measurements are made not only of global parameters such as pressure drop and void fraction, but also of local parameters such as film thickness and entrainment in annular flow, bubble size and bubble distribution in bubbly flow, slug length and slug frequency in slug flow, etc.
(2) On the basis of the measurements and observations made, physical models of theoretical or semi-theoretical type are formulated to describe the phenomena; these are sometimes called *mechanistic models.*
(3) The local models are then integrated to achieve a system description, which may notably take account of hydrodynamic and thermodynamic non-equilibrium by modelling the evolution of the flow along the channel.

2.3.1 Example: Case of Annular Flow

By way of example, consider the case of annular flow as illustrated in Fig. 2.5.

In order to predict the important system variables (pressure gradient, local phase contents, heat transfer coefficients and critical heat flux) it is necessary to predict the local film and droplet flow rates (e.g. the film flow rate becomes zero at the critical heat flux or dryout condition). The essential components of the phenomenological model for annular flow are as follows:

(1) Establishment of the local film flow rate ($\dot{M}_{LF}$, kg/s). This is done by applying the equation:

$$\frac{d\dot{M}_{LF}}{dz} = P(D - E - q''/h_{LG}) \tag{2.3.1}$$

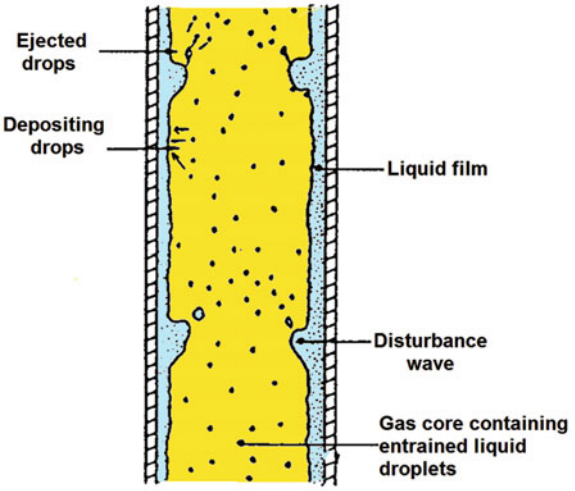

Fig. 2.5 Schematic illustration of annular flow

where P(m) is the channel periphery, D is the rate of deposition of droplets, E is the rate of entrainment of droplets per unit peripheral area (kg/m^{2}s), q'' is the wall heat flux and h_{LG} is the latent heat of vaporization. This equation is integrated along the channel starting from a given initial or boundary condition to give the film flow rate downstream, at any point. A typical boundary condition would be the fraction entrained at the onset of annular flow; for evaporating flows, the initial condition for film flow rate corresponds to the onset of annular flow. There is a difficulty in providing an accurate value of the initial condition for film flow rate (or entrainment) but, for long enough channels, the initial condition may not be too significant as there will be sufficient time to reach equilibrium between entrainment and deposition.

(2) If the film flowrate is known, then local values of film thickness and wall shear stress (frictional pressure gradient) can be obtained by combining two relationships as follows:

   (a) The *triangular relationship* which links film thickness δ, interfacial shear stress τ_i, and film flowrate. The interfacial shear stress τ_i is related to pressure gradient dp/dz and the triangular relationship can be expressed in the form

$$\dot{M}_{LF} = \dot{M}_{LF}(\delta, \tau_i) = \dot{M}_{LF}(\delta, dp/dz). \tag{2.3.2}$$

The relationship implicit in Eq. (2.3.2) can be obtained by determining the velocity profile and integrating this profile through the film.

(b) The interfacial shear stress τ_i is affected by interfacial waves and, of course, by the gas core velocity. It is conveniently expressed in terms of an interfacial friction factor f_i which has been found to be approximately a function only of δ/D where D is the tube diameter. This relationship implies that the effective roughness of the interface depends only on the film thickness for a given tube diameter and this implies geometrical similarity between the waves on the interface for a given film thickness, which is confirmed by experimental measurements.

Annular flow modelling has been widely applied and is particularly useful in predicting the onset of dryout. Typical dryout predictions using this kind of model are illustrated in Fig. 2.6. Dryout occurs when the flow rate of the liquid film on the wall goes to zero.

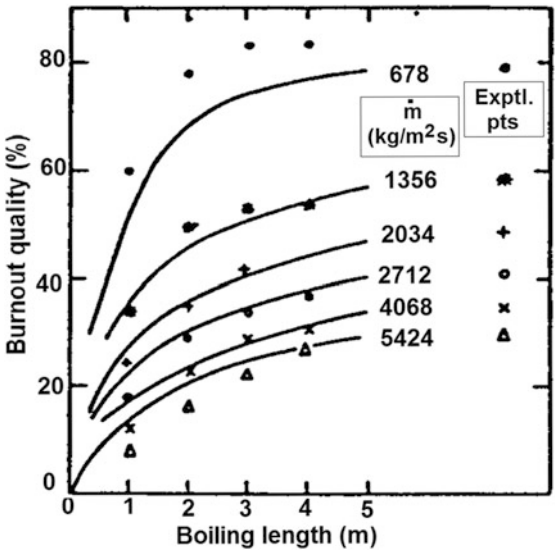

Fig. 2.6 Prediction of dryout for uniformly heated tubes (continuous lines) and comparison with experimental data (points)—water flow at 70 bar, subcooled inlet condition (Whalley et al. 1974, 1978). Reprinted from Whalley et al. 1974 with permission from Begell House, Inc

2.4 Multi-fluid Models and One-Dimensional Conservation Equations

As mentioned above, the formulation of the two-phase-flow problem that would have required the description of the evolution in time of the fields (pressure, velocity, temperature, etc.) for each phase, together with a prediction of the geometry of the interfaces, is generally impractical. The often chaotic flow fields must be treated in terms of statistical, average properties. There are two general approaches, the *two-fluid, or more generally the multi-fluid approach* and the *mixture formulation*.[2] A simple presentation of the two-fluid approach will be given in this section. The basis of the method is to write conservation equations for each phase and to include in these equations terms which represent the interaction between the phases.

The two-fluid (or more generally, the multi-fluid) formulation is an *interpenetrating media* approach to the problem: each phase is present at every point, but with a given fractional presence time or frequency or probability, which happens to be the local void fraction. In reality, the phases interact with one another at the *interfaces* separating them. If the gas, for example, has a higher velocity than the liquid, it will create a shear force (a drag force) acting on the liquid at the interface. An equal drag force of opposite sign will act on the gas. This mutual interaction at the interface can be described as an *interfacial momentum exchange*. When the phases exchange energy and mass, there are also *interfacial* energy and *mass exchanges*.

In the interpenetrating media approach, the interfacial transfers are modelled as interfacial terms acting on each phase to explicitly take them into consideration. We write two sets of phase conservation equations (one mass, momentum and energy conservation equation for each phase) in terms of phase-average properties. The dynamics of the interactions between the two phases are described by *closure laws* governing the interfacial mass, momentum and energy exchanges.

When two fluids are used, this approach results in the so-called "six-equation models". If additional fluids or fields are used, one gets additional equations. For example, if one considers two liquid fields—droplets and film on the wall—and the gas, one gets nine equations. No particular assumptions are made regarding, for example, thermal equilibrium or the velocity ratio; these are obtained naturally from the solution of the set of conservation equations; the phases interact *dynamically* according to the interfacial exchange laws specified.

Starting from the two-fluid formulation, if the phase conservation equations are added together, the interfacial exchange terms cancel out and we end up with three

[2]We recall here what was discussed in Chap. 1 regarding the term *mixture* that is most of the time used to denote the two (or more) phases flowing together and does not necessarily imply that these are intimately *mixed*.

mixture conservation equations that will be discussed next. In this case, instead of specifying closure laws for the interfacial exchanges, we must specify, for example, how the void fraction or the temperatures of the two phases vary as a function of the quality obtained from the energy equation. We may specify, for instance, a certain value of the velocity ratio, or a velocity ratio that is function of the local quality, etc. Another example would be to "force" one of the phases or both to remain saturated, i.e. to specify phase temperatures that are functions of the local pressure only. Dynamic, thermal interaction of the phases does not take place, however, in this case; the relative behaviour of the phases and the development of the mixture have been prescribed externally and a priori.

The choice between the two alternative approaches depends on the nature of the problem to be solved. The full six-equation model might be needed, for example, for calculating the evolution of the mixture during a fast transient during which strong departures from equilibrium are expected to occur. Slower transients during which there is more time to reach equilibrium may be adequately described by a mixture model.

In the simplest possible mixture model, the *homogeneous equilibrium model (HEM)* equal phase velocities *and* thermal equilibrium between the phases is assumed.[3]

Local, instantaneous conservation equations can be derived rigorously and then averaged over the entire cross-sectional area of a duct surrounded by a wall, to arrive at instantaneous, space-averaged equations. These can then be time (or ensemble) averaged to arrive at *space and time-averaged equations* (e.g. Delhaye 1981; Ishii and Mishima 1984, Lahey and Drew 1988; Nigmatulin 1979). These derivations will be discussed in more detail in another volume. Here, we will proceed with a more intuitive and simplified derivation of the space *and* time-averaged equations. This derivation, in spite of being rather primitive, yields equations that have the form and contain practically all the terms obtained from the much more sophisticated derivations mentioned above; they will be useful for the needs of his volume.

2.4.1 Simple Derivation of Two-Fluid Conservation Equations

The equations are derived below in a simplified manner (see, e.g. Zuber 1967; Yadigaroglu and Lahey 1976) with reference to a simple flow configuration (in this case annular or stratified flow) where the two phases flow separately, as shown in

[3]The term "separated flow" is often used loosely to denote two-phase flows where the two phases have different average velocities. This distinguishes such flows from the *homogeneous* ones, where the phases have the same average velocity; such flows may strictly speaking not be homogeneous at all.

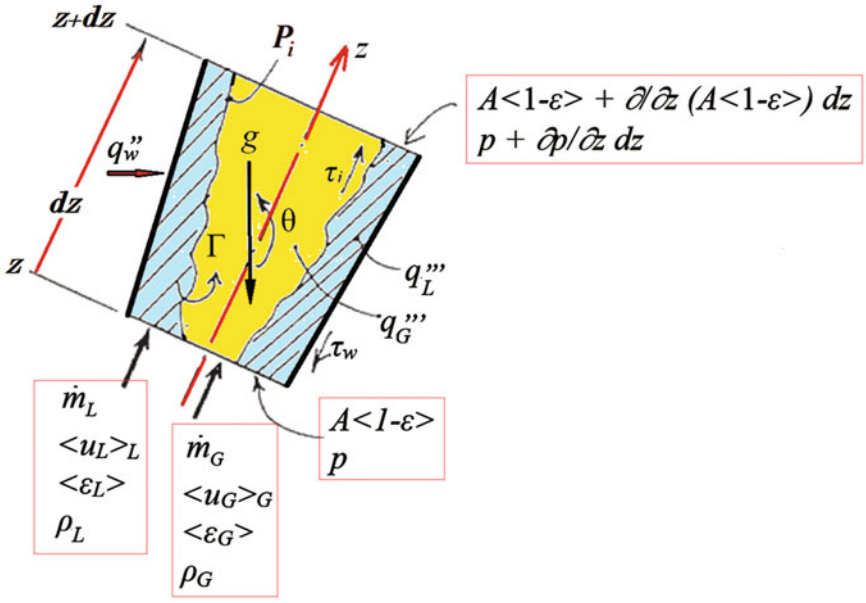

Fig. 2.7 Control volume used for writing the two-fluid conservation equations and the variables involved in the derivations

Fig. 2.7 that shows the control volume used for the derivation. The simple flow configuration allows deriving the conservation equations for the liquid and the gas phases separately. As noted, above, in most situations, the distribution of the phases is much more complex and a rigorous derivation must follow mathematically much more complex procedures. As a result of the simplicity of the derivation, certain additional terms that appear when the rigorous path is followed (e.g. the *virtual mass*[4] term) will not appear.

The pressure is assumed to be uniform in a cross-sectional plane; in reality the average pressure in the liquid phase may be different from the pressure in the gas phase (an obvious example is horizontal, stratified flow) and the pressure at the interface may have a value between the two. The pressure may also fluctuate locally in time and spatially within a phase. It is such fluctuations that give rise to phenomena such as the virtual mass effect for bubbles which are not considered here. The equations are written for one-dimensional flow in a duct having, however, variable area A. All the variables are considered to be time-averaged values (as discussed in Chap. 1). The reader is referred to the derivation of the conservation equations for single-phase flow as a basis, given, for example, in the excellent textbook by Bird et al. (1960).

[4]A bubble accelerating in a liquid entrains the fluid surrounding it and appears to have much larger inertia than that of the mass of gas it contains; the *virtual mass* effect.

Mass Continuity

With reference to Fig. 2.7, a notable difference from the single-phase flow formulations is the presence now of the interfacial mass transfer term. Mass continuity for phase k becomes

$$\frac{\partial}{\partial t}[\langle \rho_k \varepsilon_k \rangle] + \frac{1}{A}\frac{\partial}{\partial z}[\langle \rho_k \varepsilon_k u_k \rangle A] = \Gamma_k \quad \mathrm{k = L, G}, \tag{2.4.1}$$

where Γ_k is the volumetric mass transfer rate *into* phase k (it has units of kg/m^{3}s). In case of boiling flow, for example, Γ_G is the rate of vapour generation per unit volume. The first term of the equation above represents the rate of change of mass within the control volume, while the second term is the net convective mass flux into the control volume, as the reader can confirm by examining the various terms in Fig. 2.7. Since there is no mass stored at the interface,

$$\Gamma_L + \Gamma_G = 0,$$

which is the so-called *jump condition* for mass conservation at the interface. We can define

$$\Gamma \equiv \Gamma_G = -\Gamma_L. \tag{2.4.2}$$

Momentum Conservation

The assumption was made here that the pressure is uniform across the flow area and equal in both phases. This assumption is sometimes justified by the observation that radial pressure differences are usually small and in most cases non-measurable; it is not *always* true, however, as already mentioned. Momentum conservation for phase k is written as

$$\begin{aligned} &\frac{\partial}{\partial t}[\langle \rho_k \varepsilon_k u_k \rangle] + \frac{1}{A}\frac{\partial}{\partial z}\left[\langle \rho_k \varepsilon_k u_k^2 \rangle A\right] \\ &= -\langle \varepsilon_k \rangle \frac{\partial p}{\partial z} + g\langle \rho_k \varepsilon_k \rangle \cos\theta - \frac{P_{wk}\tau_{wk}}{A} - \frac{P_i \tau_i}{A} + u_i \Gamma_k. \end{aligned} \tag{2.4.3}$$

The first term on the left is again the rate of change of momentum within the control volume, while the second one is the net momentum flux term. The terms on the right are the forces acting on phase k: the first term is the net pressure force acting on phase k—it includes contributions due to variable duct area and to variable phase area fraction along the duct. The second term is the gravity force, where θ is the angle between the positive z direction and the acceleration of gravity, Fig. 2.7.

The shear stresses acting on the phase at the wall and at the interface are denoted by τ_{wk} and τ_{ik}, respectively. The part of wall perimeter wetted by phase k is P_{wk}, while P_i is the interfacial perimeter. The last term represents the momentum addition into phase k by mass exchange at the interface; as mass crosses the

interface and enters the other phase, it carries with it its original momentum. The mass entering phase k has a velocity u_i characteristic of the interface.

Considering the momentum exchanges taking place at the interface (i.e. the jump condition for momentum exchange), we must have

$$\tau_{iL} + \tau_{iG} = 0,$$

and we can define

$$\tau_i \equiv \tau_{iG} = -\tau_{iL}. \tag{2.4.4}$$

Total Enthalpy Conservation

Defining the total enthalpy of phase k, i.e. the sum of the intrinsic enthalpy h_k, and of the kinetic and potential energies by

$$h_k^0 = h_k + \frac{u_k^2}{2} - gz\cos\theta,$$

we can write

$$\begin{aligned} &\frac{\partial}{\partial t}\left[\langle \rho_k \varepsilon_k h_k^0 \rangle\right] + \frac{1}{A}\frac{\partial}{\partial z}\left[\langle \rho_k \varepsilon_k h_k^0 u_k \rangle A\right] \\ &= q_k'''\langle \varepsilon_k \rangle + \frac{q_{ik}'' P_i}{A} + \frac{q_{wk}'' P_{hk}}{A} + \Gamma_k h_{ik}^0 + \langle \varepsilon_k \rangle \frac{\partial p}{\partial t} - \zeta_k \frac{P_i}{A}\tau_i u_i, \end{aligned} \tag{2.4.5}$$

with τ_i given by Eq. (2.4.4).

The first term on the right is the internal heat generation in phase k due to a volumetric source q_k'''. The second and third terms are the sensible heat inputs from the interfacial perimeter P_i and from the heated portion of the perimeter wetted by phase k, P_{hk}. The fourth term accounts for energy addition to phase k due to interfacial mass transfer; h_{ik}^0 is the specific total enthalpy characteristic of this exchange. The fifth term, $<\varepsilon_k > \partial p/\partial t$, accounting for the reversible work due to expansion or contraction of the phases should has been written as

$$-\frac{p}{A}\frac{\partial}{\partial t}(\langle \varepsilon_k \rangle A).$$

Using, however, the identity $\partial(ab)/\partial t = a \cdot \partial b/\partial t + b \cdot \partial a/\partial t$, we obtain

$$-\frac{p}{A}\frac{\partial}{\partial t}(\langle \varepsilon_k \rangle A) = -\frac{1}{A}\frac{\partial}{\partial t}(p\langle \varepsilon_k \rangle A) + \frac{1}{A}(A\langle \varepsilon_k \rangle)\frac{\partial p}{\partial t}. \tag{2.4.6}$$

The second term on the right side is the one appearing in Eq. (2.4.5). Moreover, the first $\partial/\partial t$ term on the left side of Eq. (2.4.5) should have contained the internal energy e_k, not the enthalpy h_k. However, it has been combined with the $\partial p/\partial t$ term on the right side as follows. Expanding

$$\frac{\partial}{\partial t}\left[\left\langle \rho_k e_k^0 \varepsilon_k \right\rangle\right] = \frac{\partial}{\partial t}\left[\left\langle \rho_k \varepsilon_k \left(e_k^0 + \frac{p}{\rho_k} - \frac{p}{\rho_k} \right) \right\rangle\right] = \frac{\partial}{\partial t}\left[\left\langle \rho_k \varepsilon_k h_k^0 \right\rangle\right] - \frac{\partial}{\partial t}\left[\left\langle \rho_k \varepsilon_k \frac{p}{\rho_k} \right\rangle\right]$$

and moving the second term to the right side of Eq. (2.4.5) where we combine it with the first term on the right side of Eq. (2.4.6), we have

$$-\frac{1}{A}\frac{\partial}{\partial t}\left[p\langle \varepsilon_k \rangle A\right] + \frac{\partial}{\partial t}\left[\langle \varepsilon_k \rangle p\right] = -\frac{A}{A}\frac{\partial}{\partial t}\left(p\langle \varepsilon_k \rangle\right) - \left(\langle \varepsilon_k \rangle p\right)\frac{\partial A}{\partial t} + \frac{\partial}{\partial t}\left[\langle \varepsilon_k \rangle p\right] = 0,$$

provided that the flow area is time independent.

The very last term of Eq. (2.4.5) is related to the interfacial energy dissipation. Although such a term does not appear when the *mixture* is considered, the term shows up in the *phase* energy equations, signifying that the dissipation energy created at the interface is distributed in a certain way, specified by ζ_k, between the two phases. We must have

$$\zeta_L + \zeta_G = 0 \quad \text{or} \quad \zeta \equiv \zeta_G = -\zeta_L.$$

The jump condition for energy conservation will be given and discussed below.

2.4.2 Practical Set of Two-Fluid Equations

Inspection of the conservation equations derived above reveals the presence of cross-sectional averages of products such as $<\rho_k \varepsilon_k>$, $<\rho_k \varepsilon_k u_k>$ and $<\rho_k \varepsilon_k h_k u_k>$. Within the framework of the one-dimensional theory presented here, we would like to deal with cross-sectionally averaged variables only, e.g. $<u_k>_k$. It is evident that the averages of products of several variables cannot be evaluated and replaced by the product of their averages unless the cross-sectional *distributions* of these variables (e.g. the phase velocities u_k and enthalpies h_k) are known. Such information is not, however, included in the one-dimensional treatment; it was essentially "lost" during the averaging process; at most it can be provided externally, from knowledge about these distributions obtained by other means.

The angle brackets for the double products containing the void fraction can be "opened" (i.e. the average of the product replaced by the product of averages) using the relationship derived in Chap. 1, Eq. (1.7.8),

$$\langle \varepsilon_k f_k \rangle = \langle \varepsilon_k \rangle \langle f_k \rangle_k,$$

and defining and using an appropriate cross-sectional-average value of the density. This cannot be done, however, for the products of three or four variables.

Regarding the triple products, if the density of a phase is sufficiently constant over the cross section, it can be taken again out of the angle brackets. The constant-density assumption may be an excellent approximation for the liquid, but it may not be always adequate for the gas, for example, in the presence of strong radial temperature gradients. Ignoring the density variations, the remaining double products with the void fraction ($<\varepsilon_k u_k>$ and $<\varepsilon_k h_k>$) can then be "opened."

Finally, there is a fundamental difficulty with the products of four variables, e.g. $<\rho_k \varepsilon_k u_k^2>$. If the velocity and enthalpy profiles can be evaluated or guessed independently, then one can use *correlation coefficients* C to "open the angle brackets", for example, to write

$$\langle \rho_k h_k u_k \rangle = C \langle \rho_k \rangle_k \langle h_k \rangle_k \langle u_k \rangle_k.$$

If the values of such correlation coefficients are close to unity (as in the case of single-phase turbulent flow where the velocity profile is quite flat), this poses no great problems. We will assume that all correlation coefficients are equal to one in the following treatment.

Terms resulting from the variation of the pressure over the cross section are not included, as already mentioned (the virtual mass terms, for example). The terms dealing with viscous dissipation at the interfaces are also usually ignored. With these simplifications, and using the definitions of Γ, τ_i, etc. given above, the two-fluid conservation equations take the following practical form:

Mass Continuity

$$\frac{\partial}{\partial t}[\rho_L \langle 1-\varepsilon \rangle] + \frac{1}{A}\frac{\partial}{\partial z}\left[\rho_L \langle 1-\varepsilon \rangle \langle u_L \rangle_L A\right] = -\Gamma \tag{2.4.7}$$

$$\frac{\partial}{\partial t}[\rho_G \langle \varepsilon \rangle] + \frac{1}{A}\frac{\partial}{\partial z}\left[\rho_G \langle \varepsilon \rangle \langle u_G \rangle_G A\right] = \Gamma. \tag{2.4.8}$$

Momentum Conservation

$$\begin{aligned} &\frac{\partial}{\partial t}\left[\rho_L \langle 1-\varepsilon \rangle \langle u_L \rangle_L\right] + \frac{1}{A}\frac{\partial}{\partial z}\left[\rho_L \langle 1-\varepsilon \rangle \langle u_L \rangle_L^2 A\right] \\ &= -\langle 1-\varepsilon \rangle \frac{\partial p}{\partial z} + g\rho_L \langle 1-\varepsilon \rangle \cos\theta - \frac{P_{wL}\tau_{wL}}{A} + \frac{P_i \tau_i}{A} - u_i \Gamma \end{aligned} \tag{2.4.9}$$

$$\begin{aligned} &\frac{\partial}{\partial t}\left[\rho_G \langle \varepsilon \rangle \langle u_G \rangle_G\right] + \frac{1}{A}\frac{\partial}{\partial z}\left[\rho_G \langle \varepsilon \rangle \langle u_G \rangle_G^2 A\right] \\ &= -\langle \varepsilon \rangle \frac{\partial p}{\partial z} + g\rho_G \langle \varepsilon \rangle \cos\theta - \frac{P_{wG}\tau_{wG}}{A} - \frac{P_i \tau_i}{A} + u_i \Gamma. \end{aligned} \tag{2.4.10}$$

Total Enthalpy Conservation

$$\begin{aligned}&\frac{\partial}{\partial t}\left[\rho_L\langle 1-\varepsilon\rangle\left\langle h_L^0\right\rangle_L\right]+\frac{1}{A}\frac{\partial}{\partial z}\left[\rho_L\langle 1-\varepsilon\rangle\left\langle h_L^0\right\rangle_L\langle u_L\rangle_L A\right]\\&=q_L'''\langle 1-\varepsilon\rangle+\frac{q_{iL}''P_i}{A}+\frac{q_{wL}''P_{hL}}{A}-\Gamma h_{iL}^0+\langle 1-\varepsilon\rangle\frac{\partial p}{\partial t}\end{aligned}\tag{2.4.11}$$

$$\begin{aligned}&\frac{\partial}{\partial t}\left[\rho_G\langle\varepsilon\rangle\left\langle h_G^0\right\rangle_G\right]+\frac{1}{A}\frac{\partial}{\partial z}\left[\rho_G\langle\varepsilon\rangle\left\langle h_G^0\right\rangle_G\langle u_G\rangle_G A\right]\\&=q_G'''\langle\varepsilon\rangle+\frac{q_{iG}''P_i}{A}+\frac{q_{wG}''P_{hG}}{A}-\Gamma h_{iG}^0+\langle\varepsilon\rangle\frac{\partial p}{\partial t}.\end{aligned}\tag{2.4.12}$$

The symbols have the following meaning:

Γ	volumetric mass generation rate (positive for vaporization) [kg/m^{3}s]
q'''	internal heat generation rate in phase k
P_i	"interfacial perimeter"
P_{wk}	wall perimeter wetted by phase k
P_{hk}	heated wall perimeter in contact with phase k
q_{ik}''	interfacial heat flux from the interface into phase k
q_{wk}''	heat flux from the wall into phase k
ε	the void fraction (ε_G)
τ_i	interfacial shear stress acting on the gas (see Eq. (2.4.4))
τ_{wk}	shear between wall and phase k
u_i	interface velocity
θ	angle between positive z direction and acceleration of gravity

Note that the phase conservation equations listed above have the general form:

$$\frac{\partial}{\partial t}\left[\rho_k\langle\varepsilon_k\rangle\Psi_k\right]+\frac{1}{A}\frac{\partial}{\partial z}\left[\rho_k\langle\varepsilon_k\rangle\langle u_k\rangle_k\Psi_k A\right]=\text{efflux term}\ +\ \text{body source term},$$

where Ψ_k is 1, $\langle u_k\rangle_k$ and $\langle h_k\rangle_k$ for mass, momentum and enthalpy continuity, respectively. In Chap. 4 we will have the opportunity to make use of this set of equations for the simple case of horizontal stratified flow.

2.4.3 Closure Laws Required

The set of one-dimensional two-fluid conservation equations given above requires knowledge of the following eight terms governing the exchanges at the interface between the phases and at the wall:

- the volumetric mass exchange rate between the phases, Γ
- the wall shear force applied to each phase, $P_{wL}\tau_{wL}$ and $P_{wG}\tau_{wG}$

- the interfacial shear force, $P_i\tau_i$
- the heat supplied from the wall to each phase, $q''_{wL}P_{hL}$ and $q''_{wG}P_{hG}$
- the interfacial energy transfer rates, $q''_{iL}P_i$ and $q''_{iG}P_i$.

However, one needs only seven exchange laws, since the interfacial heat fluxes and the mass exchange rate Γ are linked through the following energy *jump condition* at the interface:

$$\Gamma(h_{iG} - h_{iL}) + \frac{P_i}{A}(q''_{iG} + q''_{iL}) = 0, \tag{2.4.13}$$

where h_{ik} are the enthalpies of the phases at the interface, usually assumed to be at saturation. Contributions from minor terms, such as the kinetic energies and surface tension, were ignored in this jump condition. If one assumes that the interface is saturated, Eq. (2.4.13) yields a simple relationship between mass transfer at the interface, the latent heat of vaporization h_{LG} and the heat fluxes into the phases:

$$\Gamma h_{LG} + \frac{P_i}{A}(q''_{iG} + q''_{iL}) = 0.$$

Figure 2.8a illustrates this interfacial jump condition. If one considers a control volume enclosing the interface and having an infinitesimal thickness (and therefore no mass or energy storage), Eq. (2.4.13) constitutes an energy balance for this volume. Figure 2.8b shows an application of the jump condition. In the *presence of superheated steam and subcooled liquid (a possible condition in post-dryout heat*

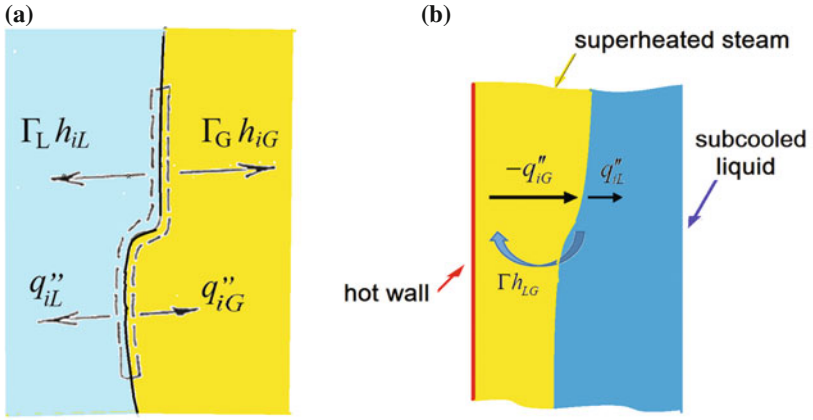

Fig. 2.8 **a** Control volume used to illustrate interfacial energy exchanges and the jump condition. **b** Application to heat transfer at the interface between superheated steam and subcooled liquid

transfer[5]), there will be heat transfer from the steam to the interface. A fraction q''_{iL} of the heat flux q''_{iG} from the interface penetrates into the liquid and is used to heat it up. The remaining fraction produces saturated steam at the interface.

2.4.4 Implementation Difficulties: Application to Horizontal Stratified Flow

The use of multi-fluid modelling implies certain basic assumptions about the averaging of the conservation equations. Although more advanced than a purely empirical approach, the approach still relies on lumped-parameter representation of the quantities. An example is the assignment of a given average velocity to each phase, which is often clearly unrealistic. An example of this would be annular flow where a large fraction of the liquid phase may be entrained as droplets and travelling at a much higher velocity than the liquid film. One could, of course, represent such a situation using a nine-equation model (three equations each for the liquid film, gas core and entrained droplets) but even this may not be sufficient to represent the subtleties of the flow. Lahey and Drew (2001) proposed a *four-field model* that could accurately predict the distribution of the fields of continuous vapour and liquid as well as dispersed vapour and liquid.

The major difficulty with one-dimensional multi-fluid models is that of obtaining sufficiently general relationships for the wall and interface shear terms; these can rarely be directly measured and correlated. An example is discussed here to point at difficulties. The closure laws will be discussed extensively in another volume.

Shaha (1999) made a wide range of measurements on stratified gas–liquid flow which were sufficient to determine τ_{wL}, τ_{wG} and τ_i independently. Expressing the shear stresses in terms of friction factors, Shaha was able to show that, though the values of τ_{wG} were reasonably predicted by existing models, there were large variations between the data and the models for both wall-to-liquid shear stress and interfacial shear stress or friction factors, as illustrated in Figs. 2.9 and 2.10, respectively. It should be noted that the models themselves show large variations in prediction.

For liquid-to-wall shear stress in laminar flows, it is commonly assumed that the friction factor is given by

$$f_L = \frac{16}{\mathrm{Re}_L}, \tag{2.4.14}$$

[5]Post-dryout heat transfer refers to the heat transfer regimes that are present after the critical heat flux condition or dryout is reached.

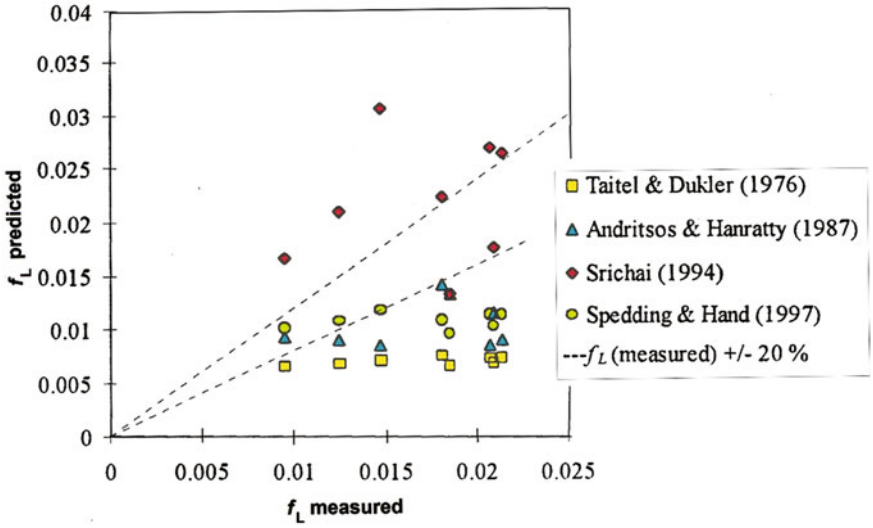

Fig. 2.9 Comparison of measured liquid-wall friction factor with various correlations (Shaha 1999)

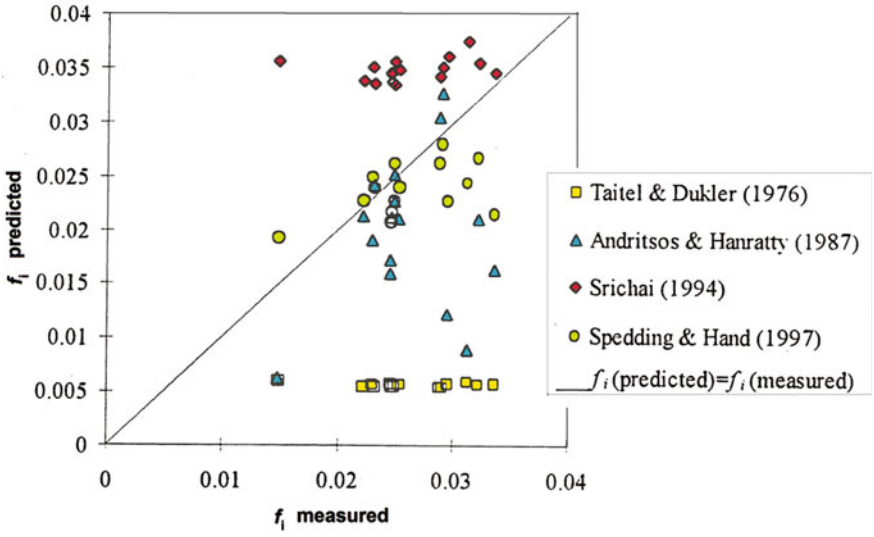

Fig. 2.10 Comparison of experimental interfacial friction factors with various correlations (Shaha 1999)

where the Reynolds number, Re_L is given by

$$\mathrm{Re}_L = \frac{u_L D_H \rho_L}{\mu_L},$$

and D_H is the hydraulic diameter (which may be defined either with or without inclusion of the interfacial periphery). Calculations on laminar liquid flows with a turbulent gas above them are described by Ng (2002); it was possible to deduce the actual value of the constant in Eq. (2.4.14) from these calculations for a range of conditions. The values obtained can be as low as 4 and approach the classical 16 at the two ends of the liquid fraction spectrum (0 to 1) when the interface is not included in D_h and are definitively lower (roughly between 2 and 8) when it is included. As expected, the constant approaches the standard value of 16 for a liquid-phase fraction of unity.

The one-dimensional two-fluid models are commonly also used to calculate transients. This adds further uncertainties to those already shown in Figs. 2.9 and 2.10. Shaha (1999) explored the interfacial structure in stratified flow using multiple twin-wire conductance probes. Figures 2.11a–c typify the results obtained for a transient increase in gas flow rate. Figure 2.11a shows the interfacial configuration before the transient. Figure 2.11b shows the interfacial structure during a transient in which the gas superficial velocity was increased from 5.0 to 6.46 m/s. Eventually, the interface settled down to the configuration shown in Fig. 2.11c at the new value of gas superficial velocity. It is clear from these figures that the interfacial structure during the transient is very different from what would be expected by interpolation between the starting and final values. During the transient, the interfaces are far rougher which implies a much higher value of interfacial shear stress and, indeed, this is borne out by the measurements which suggest that the transient will not be well predicted using steady-state correlations. Such difficulties were already announced in Sect. 2.2.

2.4.5 *The Drift Flux Model*

The presence of two momentum equations in the two-fluid formulation dictates the explicit specification of the momentum exchange terms between the phases. There are, however, difficulties in determining the interfacial closure laws, that most of the time cannot be directly measured, as the example of the preceding section has shown, as well as difficulties in the numerical solution of the equations.

The drift flux model, or DF model for short, (Zuber and Findlay 1967) provides an interesting alternative: the two momentum equations are replaced by a mixture equation where the relative motion between phases is taken into account by a kinematic constitutive relation. The DF model will be discussed in detail in Chap. 5 as it is primarily a way of determining the void fraction. Formulations of the two-phase problems based on the DF concept will be discussed in the volume

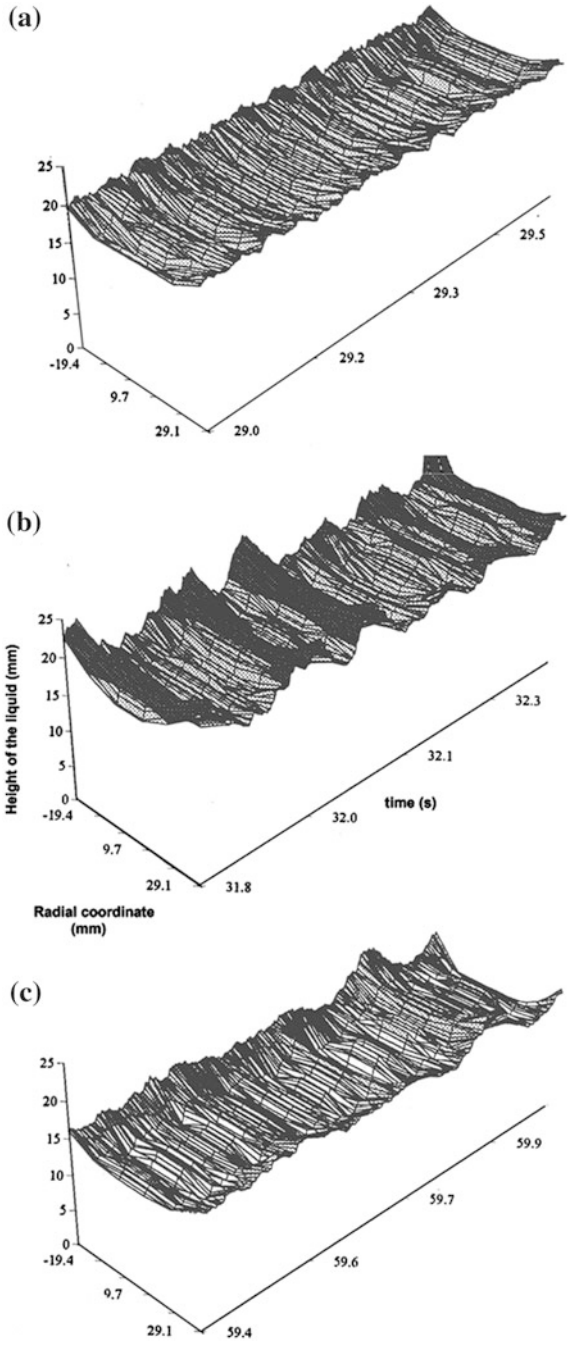

Fig. 2.11 Variation of the interfacial structure in an air–water stratified flow during a transient variation of the gas superficial velocity. **a** steady state with U_{sG} = 5.0 m/s and U_{sL} = 0.039 m/s; **b** the superficial velocity U_{sG} is now increased to 6.46 m/s; **c** a new steady state is reached with U_{sG} = 6.46 m/s and U_{sL} = 0.039 m/s (Shaha 1999)

dealing with the conservation equations. We can note, however, here that the DF model provides an excellent alternative to the two-fluid model when the phases are closely coupled and "mixed".

2.5 Separated Flow and Mixture Models

As mentioned above, the phase conservation equations may be summed up to yield *mixture conservation equations*. In doing so, we lose *explicit* consideration of the interactions between the phases; as we will see below, the interfacial exchange terms are no longer visible. The interfacial exchanges between the phases can be considered *implicitly* only, e.g. by the empirical correlations describing the mixture.

The forms obtained when the mass, momentum and energy equations, Eqs. (2.4.7) to (2.4.12) are summed up are given below.

Mass Conservation

$$A\frac{\partial}{\partial t}\langle\rho\rangle + \frac{\partial}{\partial z}(\dot{m}A) = 0, \tag{2.5.1}$$

where the *mixture density* <ρ> and the mixture mass flux $\dot{m}$ are given by

$$\langle\rho\rangle \equiv \rho_L\langle 1-\varepsilon\rangle + \rho_G\langle\varepsilon\rangle \tag{2.5.2}$$

$$\dot{m} = \rho_L\langle u_L\rangle_L\langle 1-\varepsilon\rangle + \rho_G\langle u_G\rangle_G\langle\varepsilon\rangle. \tag{2.5.3}$$

Momentum Conservation

$$\frac{\partial}{\partial t}\dot{m} + \frac{1}{A}\frac{\partial}{\partial z}A\left(\rho_L\langle 1-\varepsilon\rangle\langle u_L\rangle_L^2 + \rho_G\langle\varepsilon\rangle\langle u_G\rangle_G^2\right) = -\frac{\partial p}{\partial z} + g\langle\rho\rangle\cos\theta - \frac{P_w\tau_w}{A}. \tag{2.5.4}$$

Starting from the left, the terms in the momentum equation are identified as the inertial or temporal acceleration, the spatial acceleration, the total pressure gradient, the gravitational pressure gradient and the frictional pressure gradient. One notes that the terms containing the interfacial shear have disappeared now since we are dealing with the mixture. This mixture momentum equation will be used in Chap. 6 as the basis for calculating two-phase pressure drop.

Total Enthalpy Conservation

$$\frac{\partial}{\partial t}\left(\rho_L\langle h_L^0\rangle_L\langle 1-\varepsilon\rangle+\rho_G\langle h_G^0\rangle_G\langle\varepsilon\rangle\right)$$
$$+\frac{1}{A}\frac{\partial}{\partial z}A\left(\rho_L\langle 1-\varepsilon\rangle\langle h_L^0\rangle_L\langle u_L\rangle_L+\rho_G\langle\varepsilon\rangle\langle h_G^0\rangle_G\langle u_G\rangle_G\right)=q'''+\frac{P_h q_w''}{A}+\frac{\partial p}{\partial t}. \tag{2.5.5}$$

Again we notice that the interfacial exchanges do not appear any longer in this equation and the heat flux from the wall heats the mixture rather than the phases separately.

In the momentum Eq. (2.5.4), only the momentum flux term (second term) is "different" from the corresponding terms in the single-phase momentum equation. This term can also be written, however, in a "single-phase fluid" form by defining (Meyer 1960) the *momentum density* ρ' (or specific volume v'),

$$\frac{1}{\rho'}\equiv\frac{(1-x)^2}{\rho_L\langle 1-\varepsilon\rangle}+\frac{x^2}{\rho_G\langle\varepsilon\rangle}\equiv v'. \tag{2.5.6}$$

The mixture *momentum conservation equation* then takes the form

$$\frac{\partial}{\partial t}\dot{m}+\frac{1}{A}\frac{\partial}{\partial z}\left[\frac{A\dot{m}^2}{\rho'}\right]=-\frac{\partial p}{\partial z}+g\langle\rho\rangle\cos\theta-\frac{P_w\tau_w}{A}. \tag{2.5.7}$$

Regarding the energy equation, we will generally neglect the contribution to the total enthalpy due to kinetic and potential energy, i.e. we will assume that $h_k^0\approx h_k$. Indeed in most problems of thermal hydraulics the changes in kinetic energy and potential energy are very small compared to the changes in enthalpy; this is not true, e.g. in turbomachinery where the kinetic energy of the gas varies very significantly to produce work.

The proper definition of mixture enthalpies can be obtained from the energy equation. Two definitions will be needed since the enthalpy is *volume* or *mass* weighted in the time derivative term (stemming from the rate of change of the *contents* of the infinitesimal control volume), while it is *mass flux* weighted in the enthalpy *flux* (the $\partial/\partial z$) term. Since

$$\rho_L\langle 1-\varepsilon\rangle\langle u_L\rangle_L\equiv(1-x)\,\dot{m}\quad\text{and}\quad\rho_G\langle\varepsilon\rangle\langle u_G\rangle_G\equiv x\,\dot{m},$$

it follows that we must have two mixture enthalpies defined: a new, *mass* weighted $\bar{h}$ and the conventional, *mass-flow-rate* weighted h:

$$\bar{h} \equiv \frac{\rho_L \langle 1-\varepsilon \rangle \langle h_L \rangle_L + \rho_G \langle \varepsilon \rangle \langle h_G \rangle_G}{\langle \rho \rangle} \tag{2.5.8}$$

$$h \equiv (1-x)\langle h_L \rangle_L + x \langle h_G \rangle_G. \tag{2.5.9}$$

With these definitions, the total enthalpy equation takes the *visually* simple form resembling the single-phase enthalpy equation:

$$\frac{\partial}{\partial t}\left[\langle \rho \rangle \overline{h}\right] + \frac{1}{A}\frac{\partial}{\partial z}[A\dot{m}h] = q''' + \frac{P_h q''_w}{A} + \frac{\partial p}{\partial t}. \tag{2.5.10}$$

The equation above shows that, at steady state (i.e. without the $\partial/\partial t$ term), the enthalpy h of the mixture at a given point in the channel can be obtained from a simple heat balance. Indeed, by integrating the steady-state form of Eq. (2.5.10) (with the volumetric heating q''' term "included" in q''_w):

$$h(z) - h_{in} = \frac{P_h}{\dot{M}} \int_0^z q''_w dz = \frac{1}{\dot{M}} \int_0^z q'_w dz, \tag{2.5.11}$$

where $q'_w = P_h q''_w + A q'''$ is the total, equivalent, linear heat generation rate.

If one assumes that the two phases are in *thermal equilibrium*, i.e. that their enthalpies are equal to the saturation enthalpies corresponding to the local pressure,

$$h_L = h_{L,sat}(p) \quad \text{and} \quad h_G = h_{G,sat}(p),$$

then one can calculate from Eq. (2.5.9) the local *equilibrium* quality x_{eq}:

$$x_{eq} = \frac{h - h_{L,sat}}{h_{LG}}, \tag{2.5.12}$$

where h_{LG} is the heat of vaporization, $h_{LG} = h_{G,sat} - h_{L,sat}$.

2.6 The Homogeneous Model

If one assumes that the two-phase velocities are equal, $<u_L>_L = <u_G>_G$, then all the equations are very much simplified and one obtains the homogeneous model. Note that no assumption about any other "homogeneity" of the flow is required, the condition $S = 1$, is sufficient to derive the homogeneous model conservation equations that look very much like the single-phase conservation equations. The various definitions of the density or specific volume and of the enthalpy of the

mixture that were needed to write the mixture conservation equations for the separated flow model all merge into their unique homogeneous model form

$$\langle \rho \rangle = \frac{1}{\langle v \rangle} = \frac{1}{v_L + x v_{LG}} \quad \text{or} \quad \frac{1}{\langle \rho \rangle} = \frac{1-x}{\rho_L} + \frac{x}{\rho_G}$$
$$\bar{h} = h = (1-x)\langle h_L \rangle_L + x \langle h_G \rangle_G$$

and the homogeneous model conservation equations become

$$A \frac{\partial}{\partial t} \langle \rho \rangle + \frac{\partial}{\partial z} (\dot{m} A) = 0 \tag{2.5.13}$$

$$\frac{\partial}{\partial t} \dot{m} + \frac{1}{A} \frac{\partial}{\partial z} A \left[\frac{A \dot{m}^2}{\langle \rho \rangle} \right] = - \frac{\partial p}{\partial z} + g \langle \rho \rangle \cos \theta - \frac{\tau_w P_w}{A} \tag{2.5.14}$$

$$\frac{\partial}{\partial t} [\langle \rho \rangle \langle h \rangle] + \frac{1}{A} \frac{\partial}{\partial z} A [\langle \rho \rangle \langle h \rangle] = q''' + \frac{P_h q''_w}{A} + \frac{\partial p}{\partial t}. \tag{2.5.15}$$

For homogeneous flow, the unique mixture velocity is then simply

$$\langle u \rangle = \frac{\dot{m}}{\langle \rho \rangle} = \langle j \rangle. \tag{2.5.16}$$

Another advantage of the homogeneous model, beyond its inherent simplicity, is that when an expression for the quality and consequently for $<\rho>$ is available, and the fluid properties can be considered constant along the channel, the conservation equations can often be analytically integrated (for example, to compute the pressure drop along a channel).

Example: Computation of the Local Equilibrium Quality and of the Homogeneous Void Fraction

The purpose of this small exercise is to familiarize the reader with the use of the equations derived above, show the ease with which the homogeneous model can produce analytical results and provide a flair for the orders of magnitude. We consider a uniformly heated tube with a length L = 10 m and a diameter of 20 mm, receiving a mass flow rate of 1 kg/s of water (for the 20 mm diameter tube this corresponds to a mass flux of 3183 kg/m^{2}s and a velocity of 4.3 m/s) with an inlet subcooling of 30 °C (i.e. 30 °C below the saturation temperature corresponding to the system pressure) and operating at a system pressure of 70 bar (assumed constant along the tube as it should vary little with respect to its absolute value). The total power input to the tube is uniform and amounts to 1 MW, yielding a linear heat input rate q' = 100 kW/m. We will calculate now the variation (along the length of the tube z) of the equilibrium quality x_{eq}, and, under the assumption of homogeneous flow, the specific volume v, the density $\rho = <\rho>$ of the mixture and the void fraction $<\varepsilon>_{hom} = \beta$.

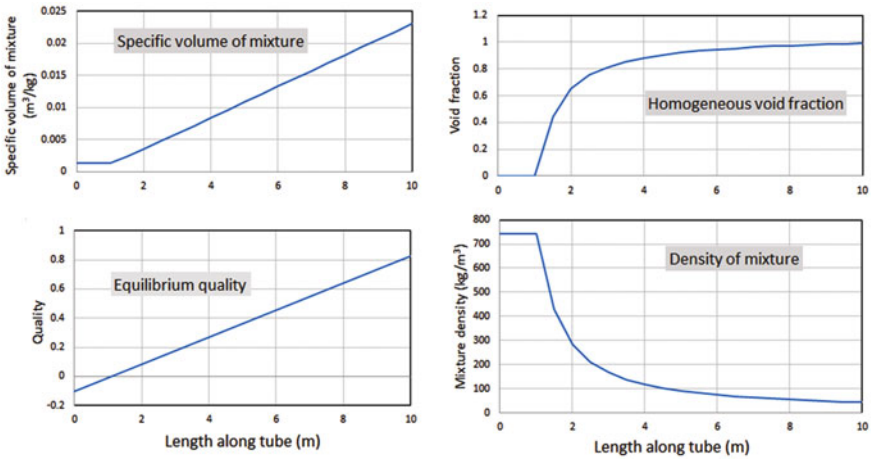

Fig. 2.12 Variation along the length of a heated tube of the equilibrium quality, of the specific volume and density of the mixture and of the void fraction

Equations (2.5.12) and (2.5.11) allow us to compute the local equilibrium quality x_{eq}

$$x_{eq} = \frac{h(z) - h_{L,sat}}{h_{LG}} = \frac{1}{h_{LG}}\left[\frac{1}{\dot{M}}\int_0^z q' dz + h_{in}\right] - \frac{h_{L,sat}}{h_{LG}} = \frac{q'z}{\dot{M}h_{LG}} - \frac{\Delta h_{in}}{h_{LG}},$$

where $\Delta h_{in} \equiv h_{L,sat} - h_{in}$ is the inlet subcooling in terms of enthalpy. The first term on the right side is a dimensionless enthalpy addition and the second the dimensionless inlet subcooling; in both cases the non-dimensionalization is provided by dividing by the latent heat, a fundamental phase change and fluid parameter. Knowing the quality, we can compute the specific volume of the mixture

$$v = v_L + x v_{LG} \text{ with } v_{LG} \equiv v_G - v_L.$$

Clearly, $\rho = 1/v$. The homogeneous void fraction is given by Eq. (1.9.10) of Chap. 1 as

$$\beta = \frac{x v_G}{v_L + x v_{LG}}.$$

Figure 2.12 shows the results for the case considered. One notes the linear increases of the quality and of the specific volume (following the linear increase of the quality), the fast drop of the density of the mixture and the corresponding rise of the void fraction that, even at this relatively high pressure, reaches values near unity for qualities above about 0.5.

2.7 Computational Multiphase Flow Dynamics

We will introduce in this section summarily these relatively new developments that rely on computational methods to analyse and simulate multi- and two-phase flows. As the purpose, at this point, is to make the reader only aware of their existence, we will limit ourselves to an introduction as these will be covered in other volumes. We will also briefly mention only the extension to 3D of the 1D methods presented above, in particular the two-fluid approach.

Computational Fluid Dynamics (CFD) has been widely applied industrially to single-phase flow problems, but the extension of related methods to multiphase flows is new and at its infancy; the difficulties are much greater. We proposed to label this relatively new discipline Computational *Multi*-Fluid Dynamics or C*M*FD for short (Yadigaroglu 2003). The CMFD techniques are "CFD like" in the sense that they are based on the well-established bases of Fluid Mechanics, are three-dimensional, consider the turbulence and use computational techniques. In complexity and difficulty, however, they are clearly one step beyond the classical CFD of single-phase flows. As it happened for single-phase flows, detailed numerical CMFD experimentation is again providing an alternative to laboratory investigations in multiphase flow situations.

The computational developments need inputs from new experiments to provide the detailed data necessary to verify the much more detailed computations. Advanced instrumentation needed for future work is discussed in another volume.

2.7.1 Treatment of Separated Phases as Single-Phase Flow

We start the discussion with an example where the two phases are treated separately by a single-phase CFD code. Indeed, in general, if the position of the interface is known, and if the distribution of shear stress and pressure can be specified along the interface, then solutions can be obtained which may throw valuable light on the flow behaviour. Results of one such an early calculation (Jayanti and Hewitt 1997) are illustrated in Fig. 2.13, which shows predicted velocity vectors within a disturbance wave in annular flow, based on the use of empirical correlations for the interfacial shear stress. The profile of the interface was *assumed* (and was kept fixed throughout the calculations). The wall was moved at the wave velocity in a direction opposite to the flow so as to keep the shape of the interface fixed, thus permitting a steady-state calculation of the flow field. The geometry and flow conditions specified were typical of those encountered in gas–liquid annular flow. The results showed that the flow in the substrate layer was laminar while that in the disturbance wave region was turbulent, leading to a local enhancement of the transport coefficients.

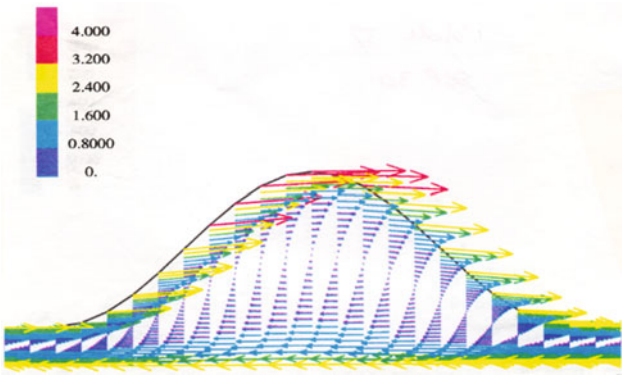

Fig. 2.13 Predicted velocity vectors in a disturbance wave in annular flow (Jayanti and Hewitt 1997). Note that the view of the wave is considerably foreshortened in the axial direction to allow a better view of the velocity vectors. The velocities are coloured in m/s

2.7.2 One-Fluid Formulation with Interface Tracking Versus Two-Fluid Formulations

The One-Dimensional, Two-Fluid Model

At this point, it is worth recalling the basic premise of the two-fluid model. The separate phase conservation equations are derived from an averaging procedure that allows both phases to co-exist at any point, according to a certain phase indicator function, or essentially a probability, that is the local instantaneous void fraction, Fig. 2.14. The approach is also referred to as the "interpenetrating media" formulation, a term that reminds us of the basic assumption made. With the two-fluid model, each phase, governed by its own conservation equations, moves and develops independently. The interfacial exchange terms provide the interactions between the phases.

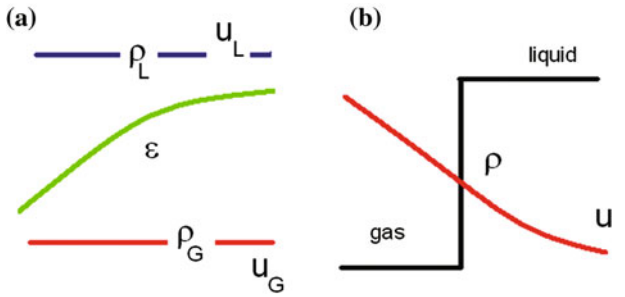

Fig. 2.14 Two-fluid (*left*) versus one-fluid (*right*) formulation; in this case the velocity field is unique but, e.g. the density changes abruptly at the interface

Although the presence of the interfaces *has* been considered during the local averaging process (and led to the definition of the local interfacial area concentration for the inter-phase exchanges), the characteristics of the interfaces (their exact shape and position) are "lost" in the interpenetrating media, formulation. The exact topology of the phases cannot be obtained and consequently the flow regimes cannot really be determined, except by correlation with the average flow conditions. The two-fluid, 1D model cannot tell if, say at a 30% void fraction, the flow is stratified or bubbly. This is fine with many problems, but there are situations where the two phases are sharply separated (at a large scale, such as that of the duct) and an understanding of the situation requires knowledge of the positions of the interfaces. This could be, for example, the case of injection of subcooled water in a pipe with stratified two-phase flow; clearly one needs to know the characteristics of the steam-water interface to estimate the rate of condensation taking place there.

Multidimensional Implementation of the Two-Fluid Model and Alternatives

Some of the limitations mentioned above can be removed by applying the two-fluid model to three-dimensional situations. Indeed, it is possible to write multidimensional equations analogous to the one-dimensional equations described above (e.g. Lahey and Drew 1988; Ishii and Hibiki 2011). Solutions of these equations allow flow fields and phase fraction distributions to be determined. Of course, in three dimensions, the closure challenge is even greater.

For example, the injection of a large bubble from a vent into water and its condensation is a situation where the shape and extent of the liquid–gas interface are important. Although the two-fluid model could, in some way, deal with this vent discharge and similar problems, in practice this is not totally satisfactory. Indeed, one could start the vent flow problem with the volume occupied by gas characterized as a region of void fraction unity, and the liquid volume as a region of void fraction zero. Numerical diffusion will very quickly mix the two phases, however, and the interface will lose its sharpness and disappear. *Interface sharpening methods* (Štrubelj et al. 2009; Gauss et al. 2016) can be used to overcome this problem, but there are better solutions, namely the *Interface Tracking (IT)* methods discussed below.

There are also cases where prediction of the location of the phases, leading essentially to the definition of the flow pattern, is needed. Other situations that are good candidates for application of IT methods are those for which the stability of the interface plays an important role: the stability and break-up of jets is a good example.

One-Fluid Formulation with Interface Tracking (IT)

All the IT methods are associated with a "one-fluid" description of the two-phase flow system: while in the interpenetrating media formulation the conservation equations were appropriately averaged (for example, over volume) *for each phase separately,* in the *one-fluid, IT* formulation, the same conservation equations are used for the entire computational domain, but the fluid properties such as density and viscosity vary sharply across the interface as we move from one phase into the other, Fig. 2.14. Thus, the two-phase system is treated as a continuous fluid whose

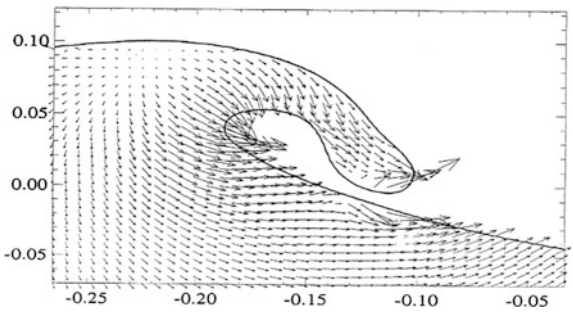

Fig. 2.15 Example of the application of the VOF method: prediction of a breaking wave (Chen et al. 1999). Reproduced from Chen et al. 1999 with the permission of AIP publishing

properties vary from those of the liquid to those of the gas over a narrow range of values of a phase-indicating scalar or "colour function" (that is typically given limiting values of 0 and 1 for the two phases). An equation is written for the transport of the scalar with the fluid. Kataoka (1986) discusses the bridge between the two (one- or two-fluid) approaches.

The position of the interface is tracked using a variety of procedures; our purpose is only to mention these here (and refer to some of the related seminal work) as they will be treated in other volumes. Rider and Kothe (1998) and Lakehal et al. (2002) review these methods that can be classified as either Lagrangian or Eulerian according to the way the motion of the interface is tracked.

The most frequently employed Eulerian IT methods are the *Volume-of-Fluid (VOF)* method that is based on the earlier multi-fluid simulations using the so-called *Marker-And-Cell (MAC)* approach (see the classical work of Hirt and Nichols (1981) and a recent implementation by Scardovelli and Zaleski (1999)) and its *Level Set (LS)* variant (Osher and Sethian 1988; Sussman et al. 1994). Figure 2.15 illustrates an early, two-dimensional, VOF computation of a breaking wave.

In *Lagrangian or embedded interface methods* (Unverdi and Tryggvason 1992; Tryggvason et al. 2001), particles are typically used to track the motion of the interfaces. The grid that they form can adapt to account for any changes in the interfacial shape. Again, an early application of this method is shown in Fig. 2.16 where the structure of an array of bubbles (originally equally spaced) has been calculated.

The so-called "second gradient method" offers alternative capabilities (Jamet et al. 2001). The relative merits of VOF and LS, as well as other possibilities, are discussed by Rider and Kothe (1998) and Scardovelli and Zaleski (1999).

2.7.3 Multiplicity of Scales

System behaviour and the various physical phenomena taking place in the system can sometimes be best addressed at a multiplicity of time and space scales. Let us refer to these as the micro-, the meso- and the macro-scale. For example, an entire

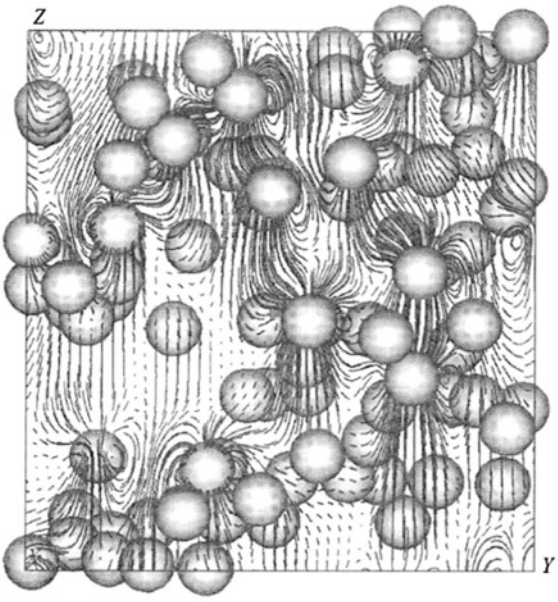

Fig. 2.16 Application of the front tracking method to the prediction of the motion of a three-dimensional array of bubbles (Bunner and Tryggvason 2002)

large-scale system such as a nuclear plant or a steam generator can be modelled at the macro-scale; a system component may need to be examined at the meso-scale. Local flow in a critical part of a component may need to be addressed at the micro-scale, Fig. 2.17. At each level of the scale hierarchy, the physics of the flow are best amenable to numerical prediction by scale-specific strategies.

Cross-scale interactions (feedback and forward transfer of information) between the micro-, meso- and macro-scales) require merging of the solutions delivered by the scale-specific approaches at each level of the scale hierarchy. As shown in Fig. 2.17, considering the top-down path, the computations at each level provide the boundary conditions needed at the lower levels. On the inverse path, starting from the bottom-up, the computations at each level will deliver the closure laws needed at the higher level. For example, local, detailed CFD computations may deliver the heat transfer coefficient needed to describe the behaviour of a component, and component behaviour will provide the information needed at the system level.

Instances where a full understanding of a situation or phenomenon requires solution of such a "cascade" of problems at various scales with a corresponding panoply and hierarchy of tools were discussed by Yadigaroglu (2005), Yadigaroglu and Lakehal (2003) and Chauliac et al. (2011). For example, for nuclear systems, the behaviour of the entire system is typically obtained using a system code based on the two-fluid approach and operating at macro-scales comparable to the dimensions of the system and its components. Local phenomena, or the behaviour of parts of the system, may be addressed at the meso-scale level, with tools considering smaller scales and more detailed description of phenomena. Finally, one

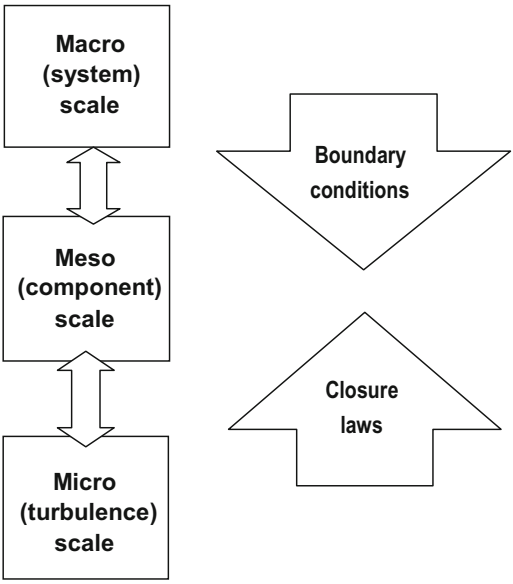

Fig. 2.17 Multiplicity of scales and transfers of information

may obtain, for example, wall and interfacial momentum, heat and mass transfer laws by performing studies at micro-scales, for example, via *Direct Numerical Simulation* (DNS)[6]; such level of spatial resolution is indeed needed to resolve the gradients determining transfers at the interfaces.

A recent example of advanced VOF simulation *and* of multi-scale computing is given in Fig. 2.18. The study by Ling et al. (2015) proposes a model for atomization simulations, where the large-scale interfaces are resolved by the VOF method and the resulting small droplets by a Lagrangian point-particle model.

Molecular Dynamics

Pushing the computations and the scales to the infinitesimal level, *Molecular Dynamics*, studying the physical behaviour and movements of atoms and molecules, is the ultimate tool in CFD and CMFD (e.g. Alder and Wainwright 1957; Long et al. 1996). We will only mention here the possibility of investigating phenomena such as the vaporization of an ultra-thin liquid layer on a hot metallic surface by molecular dynamics simulations (e.g. Yi et al. 2002). In this case, the forces acting between all combinations of pairs of wall and fluid molecules are

[6]Contrary to other authors, we do not use the term DNS to characterize all "fully resolved" computations, but apply it only to computations where all the scales of *turbulence* are resolved. In this sense, an exact analytical solution for laminar flow is not a DNS (Yadigaroglu 2005).

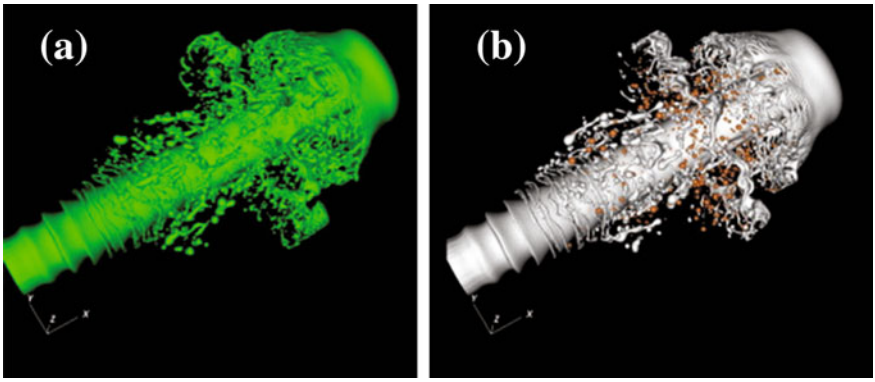

Fig. 2.18 Example of VOF computations coupled with a particle tracking method to track the small droplets. The figure shows a snapshot of the liquid–gas interface of an atomizing pulsed jet. **a** using fully resolved droplets. **b** using the coupled-model method where the orange droplets are from the tracked ones (Ling et al. 2015)

modelled and the evolution of the system is simulated numerically; the results of Yi et al. (2002) show resemblance to our knowledge of such vaporization events.

2.7.4 DNS of Turbulent Multiphase Flows

Contrary to terminology used by other authors, by Direct Numerical Simulation (DNS), we mean *capturing the entire turbulence spectrum of length and time scales without resorting to modelling* (Yadigaroglu 2003). In two-phase flow, so far, DNS has been primarily applied to study the physics of small particle dispersion using Eulerian–Lagrangian point tracking, or, occasionally, using the Eulerian, two-fluid formulation; as an example, we can cite the bubble-laden mixing layer work by Druzhinin and Elghobashi (2001).

Interface tracking methods, although not limited *in theory* to consideration of turbulence in the fluids by an associated DNS, are *in practice* not adequate for the purpose. Even inLarge Eddy Simulation (LES) where the large scales of turbulence are resolved, while the small ones are modelled, the scales still needed for resolving the large scales of turbulence may be much smaller than those of the interfaces. Thus, even rather simple *turbulent* bubbly flows are still often far from DNS. Conducting true DNS studies in multiphase flows has proven, however, possible for certain relatively very simple flow situations, for example, for counter-current gas liquid flows separated by a sheared interface; the latter can be deformable within limits, i.e. without the presence of breaking waves (Fulgosi et al. 2003; Lakehal et al. 2003). As this approach tackles all the physics of the problem without recourse to modelling, this method can be regarded as a true DNS *of turbulence in*

multiphase flow. Such sophisticated techniques are understandably limited to a narrow range of applications, where they can serve as "numerical experiments" for exploring small-scale, turbulence-induced transport phenomena at the interface.

2.8 Conclusions

One may make the following general observations about the state of prediction methods in multiphase flow systems:

- The prediction of multiphase systems represents a formidable challenge and great accuracy cannot be expected.
- The widely used empirical models do not predict data outside their range of derivation.
- *Phenomenological* (or *mechanistic*) modelling offers insight into the processes occurring but needs sub-models (e.g. for droplet entrainment and deposition) which may not yet have a secure base.
- Multi-fluid (two-fluid) models provide an elegant framework but are less flexible than phenomenological models. The identification of general closure relationships has proved a difficult goal.
- CFD and CMFD modelling are already a useful research tools, giving insights into flow phenomena. They are far from being readily applicable to all industrial problems.
- Single-phase CFD techniques are mature; their application to large systems is only limited by available computing power. The commercial CFD codes are readily usable in many areas, but specific models need often to be added to consider particular phenomena.
- CMFD techniques can already tackle certain flow regimes. Interface tracking methods such as VOF and level sets are capable of dealing with flows where the interfaces are relatively simple, e.g. stratified flows or wavy annular flows. There are much greater difficulties in dealing with flow regimes presenting complex interfaces, such as churn flows.
- Cascades of computations at different scales are needed to address certain problems.
- DNS and more specifically the future DNS of two-phase flows is likely to be successfully used to investigate microscopic phenomena that are not amenable to experimental observation in the manner of numerical experiments.

Multiphase flow is a diverse and complex subject with many subtleties and a whole variety of solution approaches. We hope that by presenting a whole variety of viewpoints, the richness of the subject will become apparent.

References

Alder BJ, Wainwright TE (1957) Phase transition of a hard sphere system. J Chem Phys 27(5):1208

Andritsos N, Hanratty TJ (1987) Influence of interfacial waves in stratified gas-liquid flows. AIChE J 33(3):444–454

Bird RB, Stewart WE, Lightfoot EN (1960) Transport phenomena. Wiley, New York

Bunner B, Tryggvason G (2002) Dynamics of homogeneous bubbly flows. Part 1. J Fluid Mech 446:17–52

Chauliac C, Aragonés JM, Bestion D, Cacuci DG, Crouzet N, Weiss FP, Zimmermann MA (2011) NURESIM–A European simulation platform for nuclear reactor safety: multi-scale and multi-physics calculations, sensitivity and uncertainty analysis. Nucl Eng Des 241(9): 3416–3426

Chen G, Kharif C, Zaleski S, Li J (1999) Two-dimensional Navier-Stokes simulation of breaking waves. Phys Fluids 11(1):121–133. doi:10.1063/1.869907

Delhaye JM (1981) Local instantaneous equations, local time-averaged equations, and composite-averaged equations. In: Delhaye JM, Giot M, Riethmueller ML (eds) Thermohydraulics of two-phase systems for industrial design and nuclear engineering. Hemisphere, Washington

Druzhinin OA, Elghobashi S (2001) Direct numerical simulation of a three-dimensional spatially developing bubble-laden mixing layer with two-way coupling. J Fluid Mech 429:23–61

ESDU (2002) Frictional pressure gradient in adiabatic flows of gas-liquid mixtures in horizontal pipes: prediction using empirical correlations and data base. Engineering Sciences Data Unit, Data Item 01014 (ISBN 1 86246 171 6). ESDU International Ltd, London

Fulgosi M, Lakehal D, Banerjee S, De Angelis V (2003) Direct numerical simulation of turbulence in a sheared air-water flow with a deformable interface. J Fluid Mech 482:319–3457

Gauss F, Lucas D, Krepper E (2016) Grid studies for the simulation of resolved structures in an Eulerian two-fluid framework. Nucl Eng Des 305:371–377

Hirt CW, Nichols BD (1981) Volume of Fluid method (VOF) for the dynamics of free boundaries. J Comput Phys 39:201–225

Ishii M, Hibiki T (2011) Thermo-fluid dynamics of two-phase flow, 2nd edn. Springer, New York

Ishii M, Mishima K (1984) Two-fluid model and hydrodynamic constitutive relations. Nucl Eng Des 82:107–126

Jamet D, Lebaigue O, Coutris N, Delhaye JM (2001) The second gradient method for the direct numerical simulation of liquid-vapor flows with phase change. J Comput Phys 169:624–651

Jayanti S, Hewitt GF (1997) Hydrodynamics and heat transfer in wavy annular gas-liquid flow: a computational fluid dynamics study. Int J Heat Mass Transf 40:2445–2660

Kataoka T (1986) Local instant formulation of two-phase flow. Int J Multiphase Flow 12:745

Lahey Jr RT, Drew DA (1988) The three-dimensional time and volume averaged conservation equations of two-phase flow. In: Advances in nuclear science and technology. Springer, US, pp 1–69

Lahey RT Jr, Drew DA (2001) The analysis of two-phase flow and heat transfer using a multidimensional, four field, two-fluid Model. Nucl Eng Des 204(1):29–44

Lakehal D, Meier M, Fulgosi M (2002) Interface tracking towards the direct simulation of heat and mass transfer in multiphase flows. Int J Heat Fluid Flow 23(3):242–257

Lakehal D, Fulgosi M, Yadigaroglu G, Banerjee S (2003) Direct numerical simulation of heat transfer at different Prandtl numbers in counter-current gas-liquid flows. ASME J Heat Transf 125(6):1129–1140

Ling Y, Zaleski S, Scardovelli R (2015) Multiscale simulation of atomization with small droplets represented by a Lagrangian point-particle model. Int J Multiphase Flow 76:122–143

Long LN, Micci MM, Wong BC (1996) Molecular dynamics simulations of droplet evaporation. Comp Phys Commun 96(2):167–172

Meyer JE (1960) Conservation laws in one-dimensional hydrodynamics. Bettis Technical Review, p 61 https://www.osti.gov/scitech/servlets/purl/4127649#page=68
Ng TS (2002) Interfacial structure in stratified pipe flow. Ph.D. thesis, University of London, June 2002
Nigmatulin RI (1979) Spatial averaging in the mechanics of heterogeneous and dispersed systems. Int J Multiph Flow 5(5):353–385
Osher S, Sethian JA (1988) Fronts propagating with curvature-dependent speed: algorithms based on Hamilton-Jacobi formulations. J Comput Phys 79:12–49
Rider WJ, Kothe DB (1998) Reconstructing volume tracking. J Comput Phys 141:112–152
Scardovelli R, Zaleski S (1999) Direct numerical simulation of free-surface and interfacial flow. Annu Rev Fluid Mech 31(1):567–603
Shaha J (1999) Phase interactions in transient stratified flow. Ph.D. thesis, University of London, August 1999
Spedding PL, Hand NP (1997) Prediction in stratified gas-liquid co-current flow in horizontal pipelines. Int J Heat Mass Transf 40(8):1923–1935
Štrubelj L, Tiselj I, Mavko B (2009) Simulations of free surface flows with implementation of surface tension and interface sharpening in the two-fluid model. Int J Heat Fluid Flow 30(4):741–750
Srichai S (1994) High pressure separated two-phase flow. Doctoral dissertation, Imperial College, London
Sussman M, Smereka P, Osher S (1994) A level set approach for computing solutions to incompressible two-phase flow. J Comput Phys 114:146–159
Taitel Y, Dukler AE (1976) A model for predicting flow regime transitions in horizontal and near horizontal gas-liquid flow. AIChE J 22(1):47–55
Tryggvason G, Bunner B, Esmaeeli A, Juric D, Al-Rawahi N, Tauber W, Han J, Nas S, Jan YJ (2001) A front tracking method for the computations of multiphase flow. J Comput Phys 169:708–759
Unverdi SO, Tryggvason G (1992) A front tracking method for viscous incompressible flows. J Comput Phys 100:25–37
Whalley PB, Hutchinson P, Hewitt, GF (1974). The calculation of critical heat flux in forced convective boiling. Heat transfer. In: Proceedings of the 1974 International Heat Transfer Conference, vol 4, pp 290–294
Whalley PB, Hutchinson P, James PW (1978). The calculation of critical heat flux in complex situations using an annular flow model. In: Proceedings of 6th International Heat Transfer Conference, Toronto, vol 5, pp 65–70
Yadigaroglu G (2003) Letter to the Editor, CMFD (a brand name) and other acronyms. Int J Multiphase Flow 29:719–720
Yadigaroglu G (2005) Computational fluid dynamics for nuclear applications: from CFD to multi-scale CMFD. Nucl Eng Des 235(2):153–164
Yadigaroglu G, Lakehal D (2003) New challenges in computational thermal hydraulics, invited plenary lecture. In: The 10th international topical meeting on nuclear reactor thermal hydraulics (NURETH-10), Seoul, Korea, 5–9 October 2003
Yadigaroglu G, Lahey RTL Jr (1976) On the various forms of the conservation equations in two-phase flow. Int J Multiphase Flow 2:477–494
Yi P, Poulikakos D, Walther J, Yadigaroglu G (2002) Molecular dynamics simulation of vaporization of an ultra-thin liquid argon layer on a surface. Int J Heat Mass Transf 45: 2087–2100
Zuber N (1967) Conservation laws for two-phase flow with a change of phase. Int J Heat Mass Transf 10:1637–1642
Zuber N, Findlay (1965) Average volumetric concentration in two-phase flow systems. J Heat Transf 87:453–468

Chapter 3
Interfacial Instabilities

George Yadigaroglu

3.1 Introduction: The Stability of Two Fluid Layers

In the chapter we will discuss *instabilities of the gas-liquid interface*. The behaviour of interfaces is clearly an important consideration in two-phase flows as it determines many flow parameters such as the sizes of inclusions (bubbles in liquid, droplets in gas), flow regimes, interfacial exchanges, etc. After a brief introduction of the basic interfacial stability or rather *instability* concepts, we will apply them to various cases such as the stability of films in boiling, stability of the dispersed phase (droplets or bubbles) in two-phase flow, etc.

In this chapter we will consider instabilities at the "microscopic" scale of the *interface*. In another volume in these series we will deal with the "macroscopic" stability of two-phase *systems*, such as boiling channels, loops, etc.

The basis of all the work in this area is consideration of the stability of the interface between two parallel layers of fluids having different properties and velocities. We will consider for simplicity the general one-dimensional situation which is depicted in Fig. 3.1. The figure shows a one-dimensional perturbation of the surface along the x-direction only (there is no variation in the y-direction, the object considered is something like a very wide wave on the sea surface or a wave created in a long, narrow flume).

The two fluids are distinguished by the subscripts 1 and 2. They are flowing in a channel with velocities U_1 and U_2 and occupy heights h_1 and h_2. The problem of the stability of the interface under these conditions can be found in several classical treatises on hydrodynamics such as the books of Lamb (1945), Milne-Thompson (1955), and Chandrasekhar (1968).

The literature on this subject is very rich, both in mathematical formulations of physical variations of the problem as well as in applications to particular physical

G. Yadigaroglu (✉)
ETH Zurich, Zurich, Switzerland
e-mail: yadi@ethz.ch

G. Yadigaroglu and G.F. Hewitt (eds.), *Introduction to Multiphase Flow*,
Zurich Lectures on Multiphase Flow, DOI 10.1007/978-3-319-58718-9_3

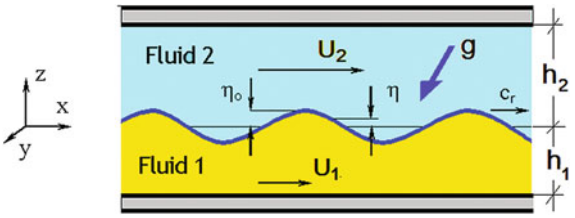

Fig. 3.1 Stability of the interface between two layers of fluids

situations. The effects of viscosity will not be considered below, although they have been taken into consideration in certain analyses (e.g. Barnea and Taitel 1993).

In all linearized analyses of the problem, one considers a small-amplitude perturbation (wave) of the interface and examines its growth under the influence of the various forces acting on it. For the general, inviscid flow case consider here, the analysis is conducted by considering potential flow of two incompressible fluids.

If one considers a non-flow situation (or if $U_1 = U_2$) in the two horizontal layers, the forces acting on the two fluids and at their interface are gravity and surface tension. In this case we speak of the *Rayleigh-Taylor instability*. The same instability may appear, however, if two fluids of different densities are under the influence of an acceleration field (other than gravity), for example, if one fluid is propelled on the other.

The second simple case is that of the parallel flow of two fluids with different velocities in the absence of gravity or other fields. In this case we speak of the *Kelvin-Helmholtz instability*.

The surface tension and the pressure difference across the interface Δp_i are related to its deformation by the classical force balance relationship, Fig. 3.2,

$$\Delta p_i = \sigma\left[\frac{1}{R_1} + \frac{1}{R_2}\right] \tag{3.1.1}$$

where R_1 and R_2 are the principal radii of curvature of the interface. For a sphere, $R_1 = R_2 = R$, and Eq. (3.1.1) becomes $\Delta p_i = 2\sigma/R$, as shown in Fig. 3.2.

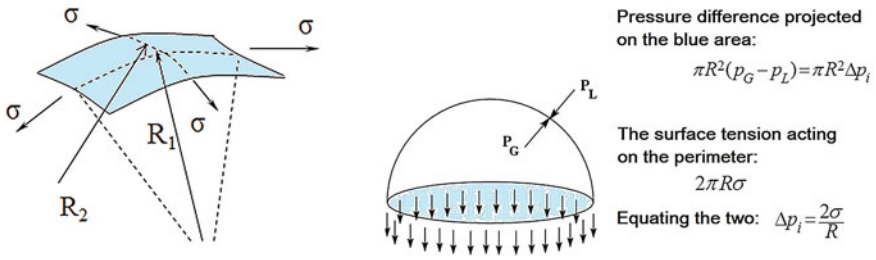

Fig. 3.2 An interfacial element and the principal radii of curvature. *Left* the figure helps intuitively understand the interfacial balance of forces in the general case, Eq. (3.1.1). *Right* for the case of a hemisphere, the exact derivation is given in the figure

The principal radii of curvature can be related to deformation of the interface $\eta(x)$. In the case of Fig. 3.1, the principal radii are R_1 in the plane of the figure and $R_2 \to \infty$ perpendicular to it. The principal radius in the case of the figure is approximated as usual by

$$\frac{1}{R_1} \approx \frac{\partial^2 \eta}{\partial x^2}$$

and Eq. (3.1.1) becomes

$$\Delta p_i = \sigma \left[\frac{\partial^2 \eta}{\partial x^2} \right] \tag{3.1.2}$$

The continuity and momentum equations for the two fluids are used and, for the one-dimensional case considered for simplicity here, solutions are sought for a periodic interfacial perturbation

$$\eta(x,t) = \eta_0 \exp(ik(x - ct)) \tag{3.1.3}$$

where η_0 is the amplitude of the initial perturbation, k the *wave number*, $k = 2\pi/\lambda$, where λ is the *wavelength* of the perturbation, and c the complex wave *celerity,*

$$c = c_r + ic_i$$

Thus η takes the form

$$\eta(x,t) = \eta_0 \, e^{ik(x - c_i t)} e^{kc_i t} \tag{3.1.4}$$

We see now the reason for introducing a complex wave celerity: Eq. (3.1.4) has a first exponential term that produces a sinusoidal variation, while the second one is a real *growth or decay factor*, depending on the sign of kc_i. Regarding the stability of the perturbed interface, if kc_i is positive the perturbations will grow, while any perturbation will be damped for kc_i negative.

Assuming that the perturbed flow is potential (using the Bernoulli equation for the two fluid layers), that the amplitude of the perturbation is small, and introducing the pressure difference across the interface given by Eqs. (3.1.1) and (3.1.2) that couples the pressure fields in the two fluid layers, the *growth factor* kc_i can be obtained (e.g. Yih 1980) as

$$kc_i = \left[\frac{\rho_1 \rho_2 \coth(kh_1)(U_1 - U_2)^2 k^2}{[\rho_1 \coth(kh_1) + \rho_2 \coth(kh_2)]^2} - \frac{\sigma k^3 - g(\rho_1 - \rho_2)k}{\rho_1 \coth(kh_1) + \rho_2 \coth(kh_2)} \right]^{\frac{1}{2}} \tag{3.1.5}$$

where σ is the interfacial tension (or the surface tension if we are dealing with a liquid in contact with a gas). When the fluid layers are thick, h_1 and $h_2 \to \infty$ and $\coth(kh_1)$ and $\coth(kh_2) \to 1$ and Eq. (3.1.5) takes the simpler form,

$$kc_i = \left[\frac{\rho_1\rho_2(U_1 - U_2)^2k^2}{[\rho_1 + \rho_2]^2} - \frac{\sigma k^3 - g(\rho_1 - \rho_2)k}{\rho_1 + \rho_2}\right]^{\frac{1}{2}} \tag{3.1.6}$$

The term inside the square brackets must be positive for a solution to exist, i.e.

$$\begin{aligned} &\frac{\rho_1\rho_2(U_1 - U_2)^2k^2}{[\rho_1 + \rho_2]^2} - \frac{\sigma k^3 - g(\rho_1 - \rho_2)k}{\rho_1 + \rho_2} > 0 \\ \text{or} \quad &\frac{\rho_1\rho_2(U_1 - U_2)^2k}{\rho_1 + \rho_2} - \sigma k^2 + g(\rho_1 - \rho_2) > 0 \end{aligned} \tag{3.1.7}$$

If this condition is satisfied, the system may be unstable. Marginal stability will be reached when $kc_i = 0$. Solving then Eq. (3.1.6) for k one obtains the wave number corresponding to this stability limit. This will be done for the two particular cases considered below.

3.2 Rayleigh-Taylor (RT) Instability

We are considering now two horizontally stratified layers without relative movement of the fluids, i.e. $U_1 - U_2 = 0$. Equation (3.1.6) in this case becomes

$$(kc_i)^2 = -\frac{\sigma k^3 - g(\rho_1 - \rho_2)k}{\rho_1 + \rho_2} \tag{3.2.1}$$

and the instability condition (from Eq. (3.1.7) is

$$-\sigma k^2 + g(\rho_1 - \rho_2) > 0 \tag{3.2.2}$$

The *marginal stability* criterion is obtained by setting kc_i equal to zero in Eq. (3.2.1); in this case the wavelength for marginal stability is given by:

$$\lambda_{ms} \equiv \frac{2\pi}{k_{ms}} = 2\pi\sqrt{\frac{\sigma}{g(\rho_1 - \rho_2)}} \tag{3.2.3}$$

This marginal stability wavelength for a liquid and a gas, without the 2π, is called the *Laplace length scale:*

$$L = \sqrt{\frac{\sigma}{g(\rho_L - \rho_G)}} \tag{3.2.4}$$

The fastest growing wave or *most dangerous wavelength,* λ_m, can be obtained by finding the maximum of $(kc_i)^2$ given by Eq. (3.2.1); $\partial(kc_i)^2/\partial k = 0$ yields:

$$\lambda_m \equiv \frac{2\pi}{k_m} = 2\pi\sqrt{\frac{3\sigma}{g(\rho_1 - \rho_2)}} = \sqrt{3}\,\lambda_{ms} \tag{3.2.5}$$

We conclude that the arrangement is stable for disturbances having a wavelength shorter than λ_{ms}; in this case the stabilizing effect of the surface tension overcomes the destabilizing effect of gravity. Physically speaking, gravity tends to accentuate any existing perturbation, while the surface tension "stretches" the surface and tries to restore it back to its original flat shape, Fig. 3.3.

For $\lambda > \lambda_{ms}$, the arrangement is unstable and the disturbance grows most rapidly with a wavelength λ_m. Figure 3.4 illustrates the two situations: the liquid cannot remain in a large tube characterized by its dimension L, while it forms a stable meniscus in a capillary one.

Figure 3.5 shows an interesting physical phenomenon that must have its roots in a RT-like instability. Intense volcanic activity pushed highly fluid molten basalt

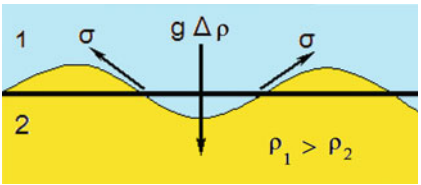

Fig. 3.3 Balance of forces in Rayleigh-Taylor instability

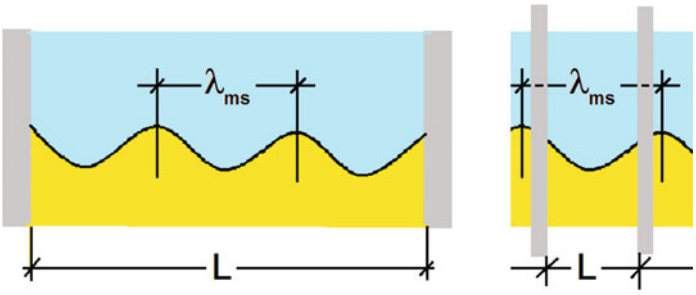

Fig. 3.4 Illustration of stable (*right*) and unstable (*left*) situations with respect to the RT instability

Fig. 3.5 Giant's causeway, Northern Ireland

upwards to form an extensive lava plateau. As the lava cooled, contraction fractured the material, like drying mud, creating the patters or hexagons whose dimensions must correspond to the Laplace length. Assuming a surface tension value of 0.3 N/m for the magma and a liquid density of 3000 kg/m^3, Eq. (3.2.4) yields a value of 0.06 m for the most unstable wavelength, smaller but of the same order of magnitude to what we see in the photograph.

3.2.1 Case when σ = 0

We consider the case of two fluid layers subjected to an acceleration perpendicular to their interface (Taylor 1950) by setting $\sigma = 0$ in Eq. (3.2.1), which yields:

$$(kc_i)^2 = g\frac{(\rho_1 - \rho_2)k}{\rho_1 + \rho_2}$$

and the instability condition becomes $g(\rho_1 - \rho_2) > 0$.The net acceleration g is positive in the direction of the z-axis, Fig. 3.1. We find, as expected, that under gravity only, the situation with the heavier fluid on top ($\rho_2 > \rho_1$) is unstable under all circumstances. The presence of normal gravity is not necessary, such a situation arises if, for example, a sheet of liquid is accelerated by air pressure (Taylor 1950). Instabilities develop and the sheet breaks down. Figure 3.6 shows the sudden expansion of superheated liquid that was initially contained in a glass flask. One clearly observes the creation of "fingers" resulting from the growth of RT instabilities as the fluid expands violently.

The instability of interfaces accelerated by a shock-like perturbation has been studied theoretically by Richtmyer (1960) and experimentally by Meshkov (1992).

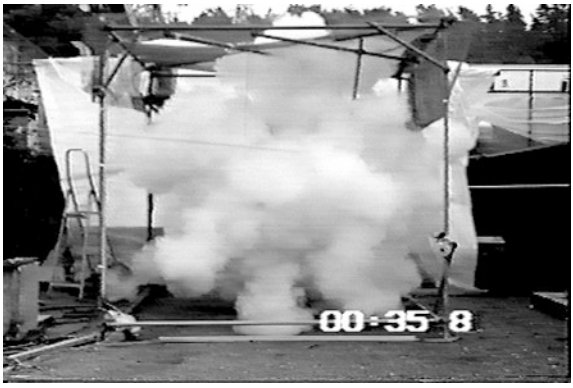

Fig. 3.6 Frame from a high-speed movie showing the violent expansion of fluid that was suddenly depressurized by breaking the flask containing it (Reinke 1996)

The long-time evolution of these Richtmyer-Meshkov instabilities, i.e. the growth of initial surface corrugations, can be well described as an impulsive RT instability.

3.2.2 Generalization

The linear treatment outlined above can be generalized to include other physical effects such as the viscosity (e.g. Drazin and Reid 1981), compressibility, non-uniform accelerations, heat and mass transfer at the interface, shocks, density gradients, sphericity of the interface, etc. The literature is very rich and corresponding references are too numerous to be listed here, but some can be found in the review papers by Sharp (1984) and Kull (1991) who also includes a historical overview of the development of the theory. Sharp also considers the non-linear growth of the disturbances that takes place after their amplitude reaches a few tenths of the wavelength.

Rayleigh-Taylor instabilities appear in many phase-change situations, such a boiling, melting, condensation, and evaporation (see, e.g., Taghavi-Tafreshi and Dhir 1980; Kutateladze and Sorokin 1969).

A typical application of the concept is the determination of the unstable wavelength in film boiling from a horizontal surface (Dhir and Lienhard 1973). Figure 3.7 shows film boiling from a horizontal cylindrical heater. Gerstmann and Griffith (1967) report that the pattern of waves on the condensate appearing below a cold plate is also described as a Taylor instability.

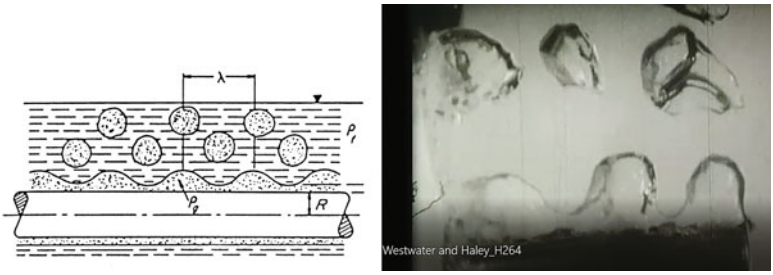

Fig. 3.7 *Left* illustration of film boiling from a horizontal cylindrical heater (Dhir and Lienhard 1973). *Right* frame from a high-speed movie by Haley and Westwater (1965) for film boiling around a cylindrical fin

3.3 Kelvin-Helmholtz Instability

In this case, we consider the parallel flow of two layers of fluid with different velocities U_1 and U_2. Gravity does not have to play a role; an initial perturbation (say a small wave pointing upwards) restricts the passage available for the upper fluid, the velocity of the upper fluid is locally increased, and the pressure above the interface is reduced due to the Bernoulli effect. The decrease in pressure tends to further destabilize the interface. It is the surface tension again that has a stabilizing effect, Fig. 3.8, since it tries to keep the interface flat. From Eq. (3.1.7), the flow is unstable, if

$$-\frac{g}{k}\frac{\rho_1-\rho_2}{\rho_1+\rho_2}+\frac{\sigma k}{\rho_1+\rho_2}<\rho_1\rho_2\left[\frac{U_1-U_2}{\rho_1+\rho_2}\right]^2 \tag{3.3.1}$$

In the absence of gravity, by setting $g = 0$, we obtain

$$\sigma k<\rho_1\rho_2\frac{(U_1-U_2)^2}{\rho_1+\rho_2} \tag{3.3.2}$$

This equation can be used to derive stability criteria for a number of two-phase flow situations: fragmentation of liquid jets flowing parallel to a gas stream, fragmentation of droplets, etc. Indeed, replacing the subscript 1 by L (liquid) and 2 by G (gas) and noting that $\rho_L \gg \rho_G$, Eq. (3.3.2) takes the form

$$\sigma k<\rho_G(U_G-U_L)^2$$

which suggests the use of a *Weber number*,

$$\mathrm{We}\equiv\frac{\rho_G(U_G-U_L)^2L}{\sigma} \tag{3.3.4}$$

where L is a characteristic dimension of the liquid volume (droplet or jet diameter, for example). Indeed, constant-Weber-number criteria have been extensively used to define the stability limits of droplets, jets, etc.

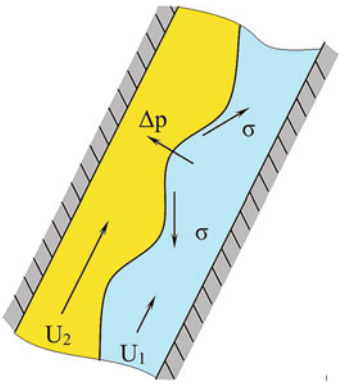

Fig. 3.8 Balance of forces in Kelvin-Helmholz instability

3.3.1 Applications

The basic considerations outlined above have been applied to many physical situations, as already noted (see e.g. Taghavi-Tafreshi and Dhir 1980). Kolev (1993) reviews fragmentation and coalescence in two-phase flows. Two interfacial stability cases related to pool boiling are briefly outlined below, followed by a discussion on the application of Weber-number criteria.

3.3.2 Departure from Nucleate Boiling (DNB) in Pool Boiling

At high heat fluxes, "jets" of vapour leave the heated surface; the liquid has to reach the wall by flowing in the areas left between the vapour columns, Fig. 3.9. This situation (parallel flow of two non-miscible fluids) leads eventually to a Kelvin-Helmholtz instability and breakdown of the vapour-liquid interfaces; this happens when the relative velocity of the vapour with respect to the liquid attains a certain critical value. Thus in the usual models of DNB in pool boiling, the controlling parameter is the volumetric flux of the vapour away from the surface:

$$\frac{q''_{crit}}{\rho_G h_{LG}} \tag{3.3.5}$$

This volumetric flux or superficial vapour velocity is compared to the critical relative velocity for the Helmholtz instability which is obtained from a Weber number, where λ, the most unstable wavelength given by Eq. (3.2.5), or the Laplace length scale, is used as the characteristic length. Combining these expressions, one obtains DNB (or CHF) correlations of the form

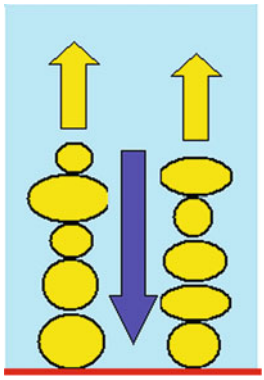

Fig. 3.9 Columns of vapour rising while liquid flows downwards to cool the surface near the DNB point

$$\frac{q''_{crit}}{h_{LG}\rho_G} = \text{const}\left[\frac{g\sigma(\rho_L - \rho_G)}{\rho_G^2}\right]^{1/4} \cdot \text{f}\left(\frac{\rho_L}{\rho_G}\right) \tag{3.3.6}$$

where the last factor f, function of the density ratio, correlates the remaining effect of pressure.

Son and Dhir (1997) computed the shape of the interface in film boiling on a flat plate and examined differences between the predictions of the linear theory discussed here and their CFD predictions.

3.3.3 *Minimum Film Boiling (MFB) Point*

MFB denotes the point in film boiling at which vapour is no longer generated at a sufficient rate to keep the liquid from wetting the wall: below a certain wall temperature, the vapour generation rate is not sufficiently large to supply the vapour demanded for the growth of the bubbles spaced on the interface according to its the Taylor instability wavelength. It is interesting to note that, as a result of the dependence on the parametric groups controlling the Taylor instability, the heat flux at the MFB point is correlated by expressions quite similar to those used for CHF, q''_{crit}. For example, Zuber and Tribus (1958) arrive at the following expression:

$$\frac{q''_{min}}{\rho_G h_{LG}} = \text{const}\left[\frac{g\sigma(\rho_L - \rho_G)}{(\rho_L + \rho_G)^2}\right]^{1/4} \tag{3.3.7}$$

where the value of the constant varies between 0.1 and 0.2 according to various authors. For a cylindrical heater of radius R, Lienhard and Wong (1964) give

$$\frac{q''_{min}}{\rho_G h_{LG}} = \frac{\pi^2}{60}\sqrt{43}\frac{1}{R}\left[2g\frac{\rho_L - \rho_G}{\rho_L + \rho_G} + \frac{\sigma}{(\rho_L + \rho_G)R^2}\right]^{1/2}\left[\frac{g(\rho_L - \rho_G)}{\sigma} + \frac{1}{2R^2}\right]^{-3/4}$$

3.3.4 Weber-Number Stability Criteria for Drops, Jets, etc.

Weber-number stability criteria are widely used in practice to predict the stability of the liquid-gas interface. Some applications are mentioned below. The classical reference book by Clift et al. (1978) provides useful information about the stability of bubbles and droplets. Stone (1994) describes the dynamics of drop deformation and breakup in viscous flows at low Reynolds numbers. Common situations include the cases given below.

Freelyfalling liquid drops in gaseous media (Hinze 1955): We $\sim$ 22 (in this case U_L is the terminal velocity of the droplet).

Drops in a high-velocity gas stream: We $\sim$ 12 to 17.

Kataoka et al. (1983) also present a correlation for dispersed flow in a pipe:

$$\mathrm{We} = 0.031\ \mathrm{Re}_{cd}^{2/3}\left(\frac{\rho_L}{\rho_G}\right)^{-1/3}\left(\frac{\mu_G}{\mu_L}\right)^{2/3} \tag{3.3.8}$$

where μ is the dynamic viscosity, and $\mathrm{Re_{cd}}$ is the continuous (gas) phase Reynolds number based on the hydraulic diameter of the flow channel.

The breakup of *liquid jets* has been reviewed by Sirignano (1993), by Chigier and Reitz (1996) and by Lin (1996). Lin and Reitz (1998) focus on the physical mechanisms that cause jet breakup. Jet breakup was also studied in the context of inverted-annular film boiling[1] by De Jarlais et al. (1986).

3.3.5 Stability and Breakup of Fluid Particles

Kitscha and Kocamustafaogullari (1989) presented *unified breakup criteria for fluid particles,* which were probably the first that are based on consideration of the simultaneous, combined development of Rayleigh–Taylor and Kelvin-Helmholtz instabilities. Their analysis starts from Eq. (3.1.5) above, but considers particles having the characteristic shapes of droplets and bubbles, namely spherical caps and half-spheres. The curvature of the surface is assumed not to affect the stability criterion (derived for a flat interface), but Eq. (3.1.5) is modified to account for the flow field (tangential velocity) around such particles, Fig. 3.10. Potential flow theory is used to compute the flow field. The effects of viscosity are neglected in the theoretical analysis but later brought into play as correction factors to the resulting correlations.

Since the flow field and the "thickness" h_d of the liquid layer vary around the particle (Fig. 3.8), the speed of propagation of interfacial perturbations and the growth factor will depend on the location of the disturbance. To answer the

[1]This is a situation occurring in post-dryout heat transfer in a tube: the vapour forms a film on the dry wall while the liquid flows in the middle of the channel .

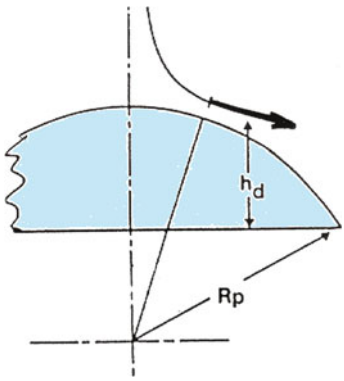

Fig. 3.10 Flow around a rising cap bubble considered by Kitscha and Kocamustafaogullari (1989)

question of whether the waves that are created can lead to breakup of the particle or not, it is necessary to know the time required for these waves to grow to a certain amplitude and compare it to the time they need to travel to the edge of the particle. Breakup will occur if the growth rate of interfacial waves is faster than the rate at which the waves propagate around the interface to the sides of the particles.

To complete the analysis and arrive at breakup criteria, one also needs additional information such as the geometry of the particles, their terminal velocity, etc. There is also an upper limit on the wavelength imposed by the fact that too large a disturbance represents a gross deformation of the particle, rather than a perturbation of its surface. The authors found that the most unstable wavelengths were larger than the particle sizes; instead of the most unstable wave, the wave which minimizes the ratio of the propagation time to growth time was used. This leads to a theoretical expression for the breakup criterion containing, however, the "critical" ratio of the propagation to growth times, C_g. Defining the non-dimensional quantities,

$$\mathrm{We} \equiv \frac{\rho_c d_e u_c^2}{\sigma}, \quad d_e^* \equiv \left[\frac{g|\Delta\rho|d_e^2}{\sigma}\right], \quad \rho^* \equiv \frac{\rho_d \coth(k_{min}h_d)}{\rho_c}, \quad k_{min}h_d$$
$$= \frac{2\pi}{\theta_w}\sin\left(\frac{3\theta_w}{4}\right)\sin\left(\frac{\theta_w}{4}\right)$$

(the last one being a geometric factor), a general breakup criterion having the functional form

$$\mathrm{F}(\mathrm{We},\ \rho_e^*,\ \mathrm{N}\mu_c\ ,\theta_w\ ,C_e) = 0$$

is derived. C_e is the ratio between the mean curvature of the particle d_p and its volume-equivalent diameter d_e, and

$$\mathrm{N}\mu_c \equiv \left[\frac{\mu_c^2}{\rho_c\left(\frac{\sigma^3}{g\,\Delta\rho}\right)^{1/2}}\right]^{1/2}$$

is a viscosity number correction for the continuous phase. The subscripts c and d denote the continuous and dispersed phases, respectively. A correlation for C_g is also given. The authors propose also several more practical correlations specialized for various particular situations.

For example, for *freely falling drops:* $d_e^* \approx 3.52$. One notes that when the slight effects of ρ^* and $\mathrm{N}\mu_c$ are neglected, one obtains the classical form We = 14 (instead of the value of 22 mentioned earlier).

For *drops in a high-velocity field* the breakup criterion is $(d_e^*)^2 + 0.26 \cdot \mathrm{We}_m d_e^* - 4 = 0$ where We_m is a modified Weber number, $\mathrm{We}_m \equiv \mathrm{We}/d_e^*$

For *bubbles rising in stagnant liquids*, $d_e^* = 27.07 \cdot (1 + \mathrm{N}\mu_c)^{0.83}$

A fairly complex expression is also given for drops falling or rising in stagnant liquids. Good correlation with available experimental data is shown.

Nigmatulin (1991) identifies six possible modes of droplet breakup depending on the value of the Weber number, each resulting in different daughter droplet spectra, Fig. 3.11. Wierzba (1990) also discusses the effect of Weber number on breakup and the scatter in the critical Weber numbers found in the literature.

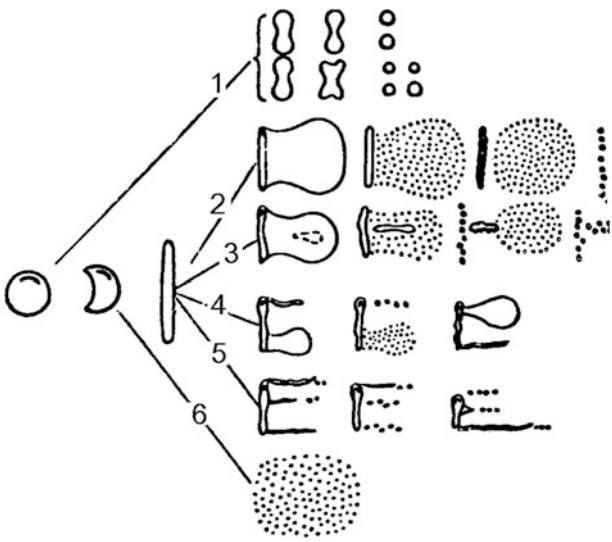

Fig. 3.11 Possible mechanisms of drop deformation and fragmentation with increasing Weber number (Nigmatulin 1991). Mode 1: droplet oscillates and breaks up; Modes 2–5: bag mode; Mode 6: complete fragmentation. Modes 2–5 produce droplet size distributions having two or more peaks according to the origin of the fragments (surface of rim of the bag)

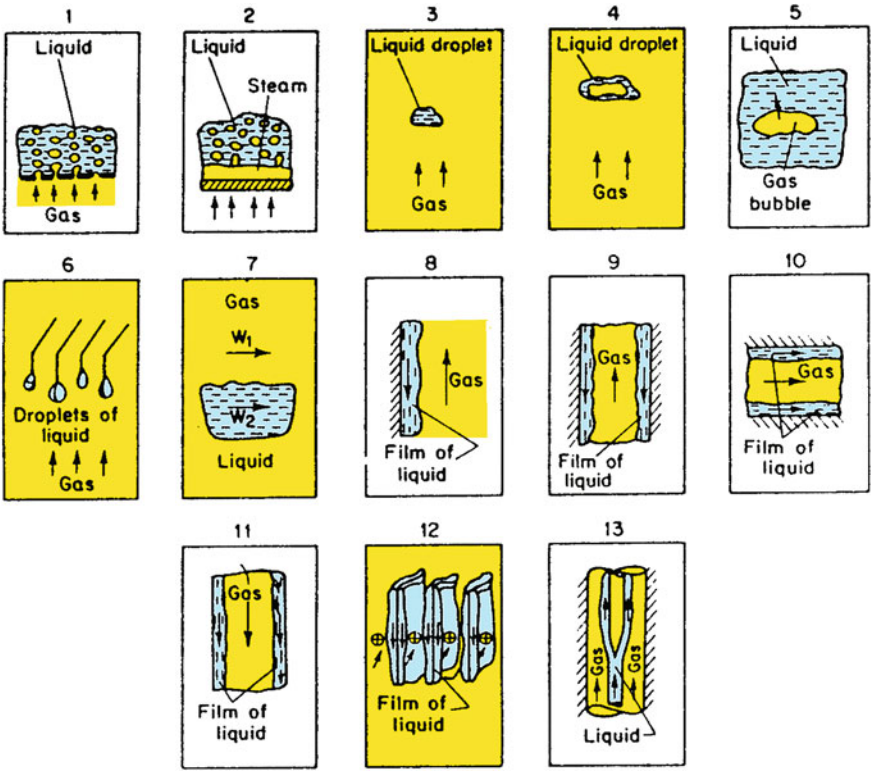

Fig. 3.12 Various processes where interfacial instabilities play an important role (Kutateladze and Sorokin 1969)

Interfacial instabilities are important for many two-phase flow and phase change phenomena. Certain of these are illustrated in Fig. 3.12 taken from Kutateladze and Sorokin (1969). The authors sketch also a general theory that governs interfacial instability problems in terms of non-dimensional numbers and provide numerous relationships covering the situations illustrated in the figure.

References

Barnea D, Taitel Y (1993) Kelvin-Helmholz stability criteria for stratified flow: viscous versus non-viscous (inviscid) approaches. Int J Multiphase Flow 19:639–649

Chandrasekhar S (1968) Hydrodynamic and hydromagnetic stability. Oxford Univ Press, Oxford Chapters X and XI

Chigier N, Reitz RD (1996) Regimes of jet breakup and breakup mechanisms (physical aspects). In: Kuo KK (ed) Recent advances in spray combustion: spray atomization and drop burning phenomena. AIAA, Reston, VA, pp 109–135

Clift R, Grace JR, Weber ME (1978) Bubbles, drops and particles. Academic Press, New York

De Jarlais G, Ishii M, Linehan J (1986) Hydrodynamic stability of inverted annular flow in an adiabatic simulation. J Heat Transf Trans ASME 108:84–92

Dhir VK, Lienhard JH (1973) Taylor stability of viscous fluids with application to film boiling. Int J Heat Mass Transf 16:2097–2109

Drazin PG, Reid WH (1981) Hydrodynamic stability. Cambridge University Press, Cambridge

Gerstmann J, Griffith P (1967) Laminar film condensation on the underside of horizontal and inclined surfaces. Int J Heat Mass Transf 10:567–580

Hinze JO (1955) Fundamentals of the hydrodynamic mechanism of splitting dispersion processes. AIChE J 1:289–295

Kataoka I, Ishii M, Mishima K (1983) Generation and size distribution of droplets in annular two-phase flow. J Fluids Eng 105:230–238

Kitscha J, Kocamustafaogullari G (1989) Breakup criteria for fluid particles. Int J Multiphase Flow 15:573–588

Kolev NI (1993) Fragmentation and coalescence dynamics in multiphase flows. Exp Therm Fluid Sci 6:211–251

Kull HJ (1991) Theory of the Rayleigh-Taylor instability. Phys Rep 206(5):197–325

Kutateladze S, Sorokin L (1969) The hydrodynamic stability of vapour-liquid systems. In: Kutateladze, S (ed) Problems of heat transfer and hydraulics of two-phase media, Pergamon, pp 385–395

Lamb H (1945) Hydrodynamics, 6th edn. Dover Publications, New York, pp 370–378, 471–475

Lienhard JH, Wong PTY (1964) The dominant unstable wavelength and minimum heat flux during film boiling on a horizontal cylinder. J Heat Transf Trans ASME 86(2):220–226

Lin SP (1996) Regimes of jet breakup and breakup mechanisms (mathematical aspects). In: Kuo KK (ed) Recent advances in spray combustion: spray atomization and drop burning phenomena. AIAA, Reston, VA, pp 137–160

Lin SP, Reitz RD (1998) Drop and spray formation from a liquid jet. Ann Rev Fluid Mech 30:85–105

Milne-Thompson LM (1955) Theoretical hydrodynamics, 3rd edn. Macmillan, New York, pp 374–431

Nigmatulin RI (1991) Dynamics of multiphase media. Hemisphere Publishing Corp, New York

Meshkov EE (1992) Instability of shock-accelerated interface between two media. Adv Compressible Turbulent Mixing 8810234:473

Reinke P (1996) Surface boiling of superheated liquid. Doctoral Dissertation No. 11598, Swiss Federal Institute of Technology, Zurich, Switzerland

Richtmyer RD (1960) Taylor instability in shock acceleration of compressible fluids. Commun Pure Appl Math 13(2):297–319

Sharp DH (1984) An overview of Rayleigh-Taylor instability. Physica D Nonlinear Phenom 12(1):3–18

Sirignano WA (1993) Fluid dynamics of sprays. J Fluid Eng 115:345–378

Son G, Dhir VK (1997) Numerical simulation of saturated film boiling on a horizontal surface. J Heat Transf 119(3):525–533

Stone HA (1994) Dynamics of drop deformation and breakup in viscous fluids. Ann Rev Fluid Mech 26:65–102

Taghavi-Tafreshi K, Dhir VK (1980) Taylor instability in boiling, melting and condensation or evaporation. Int J Heat Mass Transf 23:1433–1445

Taylor Sir G (1950) The instability of liquid surfaces when accelerated in a direction perpendicular to their planes. Proc R Soc A-201: 192–196

Haley KW, Westwater JW (1965) Heat transfer from a fin to a boiling liquid. Chem Eng Sci 20(7):711–712
Wierzba A (1990) Deformation and breakup of liquid drops in a gas stream at nearly critical weber numbers. Exp Fluids 9(1–2):59–64
Yih CH (1980) Stratified flows, 2nd edn. Academic Press, New York
Zuber N, Tribus M (1958) Further remarks on the stability of boiling heat transfer. AECU 3631

Chapter 4
Flow Regimes

George Yadigaroglu, Gad Hetsroni and Geoffrey F. Hewitt

4.1 Introduction

One of the major difficulties in modelling multiphase, or more specifically two-phase flows that are our concern here, is to determine the geometry of the flow, i.e. the topology or distribution of the phases, and the geometry of the interfaces, which are not necessarily known a priori, but are rather a part of the solution of the problem. This particular problem is not, however, solvable in general. It is only in a very restricted number of cases that the shape of the interfaces is roughly predictable: dispersed flow of spherical particles (bubbles or droplets) and smooth stratified or annular flow are such examples. Methods to predict the shape of interfaces by CFD or CMFD techniques are still at their infancy and are discussed in another volume.

In *single-phase* flow in a conduit, we know the geometry (the shape of the conduit) and we are left to determine the velocity distribution, pressure drop, etc—either experimentally or theoretically. In contrast, when there are two or more fluids flowing simultaneously in a conduit, one cannot tell a priori how the phases are going to distribute themselves, e.g. are the bubbles going to be distributed uni-

Gad Hetsroni—Deceased Author.

G. Yadigaroglu (✉)
ETH-Zurich, Zurich, Switzerland
e-mail: yadi@ethz.ch

G. Hetsroni
Technion - Israel Institute of Technology, Haifa, Israel

G.F. Hewitt
Department of Chemical Engineering and Chemical Technology, Imperial College, London, UK
e-mail: g.hewitt@imperial.ac.uk

G. Yadigaroglu and G.F. Hewitt (eds.), *Introduction to Multiphase Flow*,
Zurich Lectures on Multiphase Flow, DOI 10.1007/978-3-319-58718-9_4

formly throughout the liquid, are they going to cluster in certain areas, or are they going to coalesce and form slugs?

The geometrical and topological configurations of the interfaces determine what is referred to as the *flow regime* or *flow pattern*. These are a small number of idealizations of the real situation, useful for modelling. Their definition and the discrimination between flow regimes are, however, often quite subjective. The main two-phase flow regimes for horizontal and vertical upwards flows are illustrated in Figs. 4.1 and 4.2 containing both sketches as well as photographs.

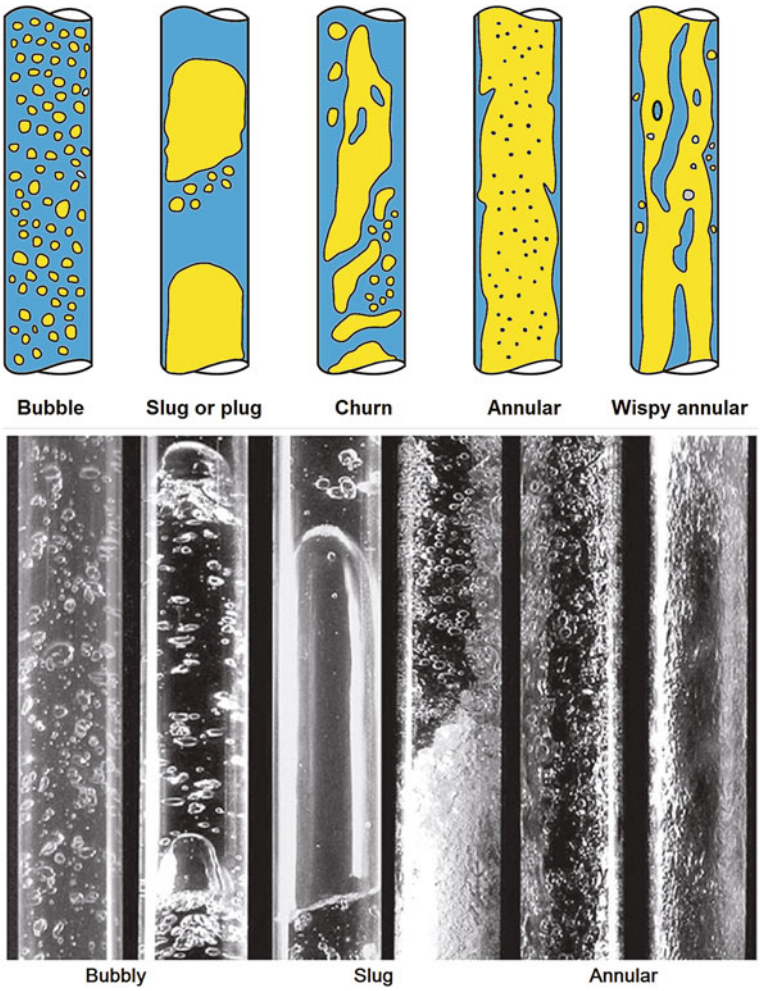

Fig. 4.1 *Top* Sketches of main flow patterns in vertical upwards flow. *Bottom* selected photographs of flow regimes (Rosa et al. 2012) © IOP Publishing; reproduced with permission; all rights reserved. The authors are indebted to Eugenio Spano Rosa, University of Campinas—Brazil, School of Mechanical Engineering for providing the original photographs

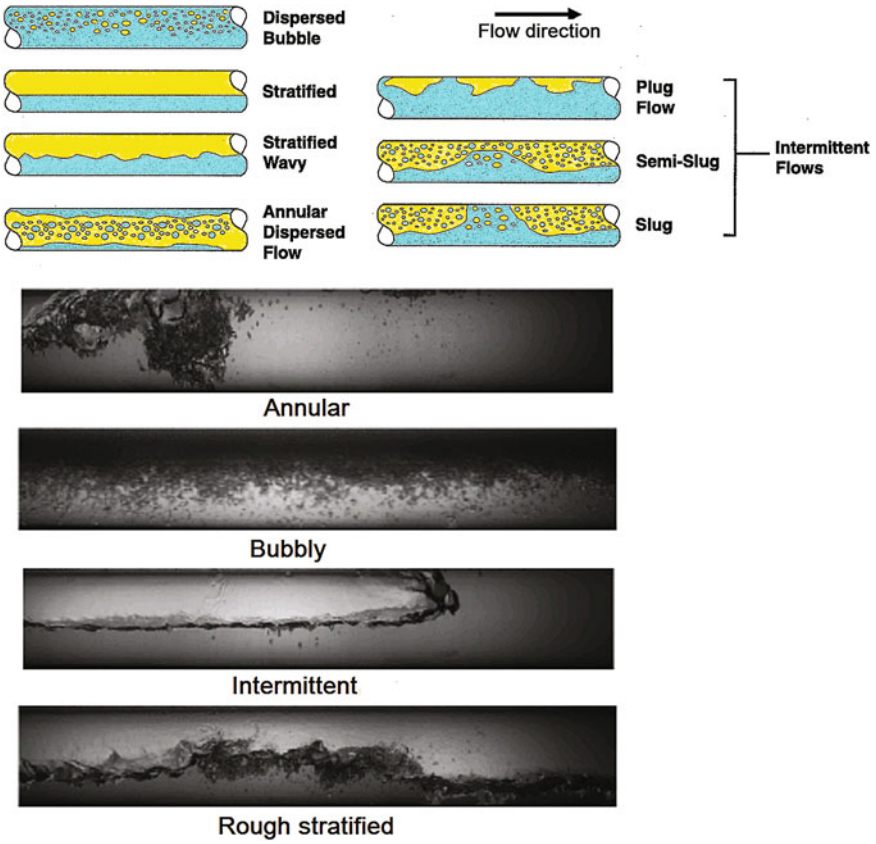

Fig. 4.2 *Top* Sketches of main flow patterns in horizontal flow. *Bottom* selected photographs (Barbosa et al. 2010)

4.1.1 Flow Regime Observations and Maps

Flow regime determinations are based either on direct "visual" observations, including photography, X-ray pictures, or cross-sectional void fraction plots (based on instruments such as optical or electrical contact probes, or multi-beam, gamma densitometers, wire-mesh sensors, etc.), or on indirect determinations via the analysis of signals such as the static pressure or the attenuation of an X-ray beam. Visual observations are difficult to interpret and can be biased by the subjectivity of the observer. Thus it may appear that an automatic determination using the signature of a (fluctuating) signal (e.g. Jones (1973); Mi et al. (1998) or Barbosa et al. (2010), who used advanced instrumentation and neural networks) and a set of criteria may be more objective, but this may amount to moving the subjectivity to the determination of the criteria. This is one of the reasons that the flow regime maps have or should be shown to have "broad" transition boundaries. Indeed, in

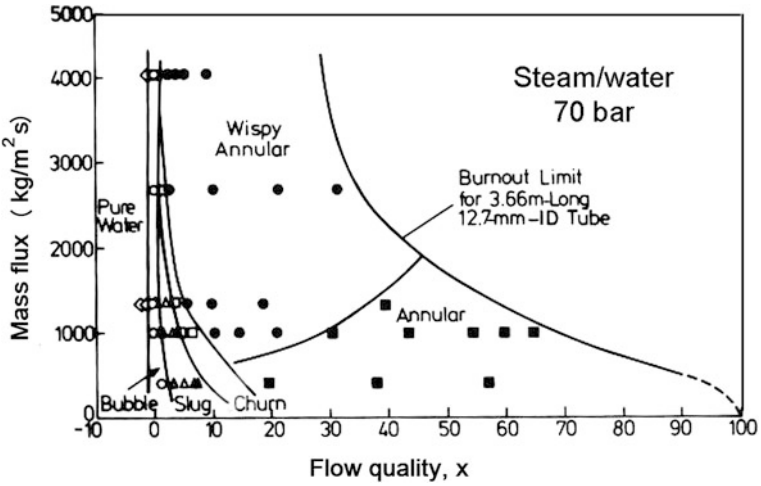

Fig. 4.3 The Bennet et al. (1965) map for steam flow at high pressure (70 bar). One problem of the presentation with the quality as the abscissa is that the data points get all crowded in the very low quality region (as at small quality the void fraction that determines the flow regime changes dramatically with quality)

many flow regime mappings, sub-regimes or additional flow patterns for intermediate situations have also been used.

Experimental observations can be used to generate a *flow regime map*, i.e. a mapping of the areas occupied by each flow regime in a plane having as coordinates variables characterizing the flow, for example quality and mass flux. Such a flow regime map is given in Fig. 4.3. A flow regime map produced using experimental observations can then be used to predict the flow regime in new but necessarily similar situations.

4.1.2 Flow Regime Transitions

Flow regime transitions take place when certain flow conditions are met and the flow pattern changes. Alternatively a flow regime map can be produced by assembling a set of *flow-regime transition criteria* for the transitions between the different flow regimes. Having such a set one can then produce the corresponding flow regime map, or use the criteria alone to determine analytically the flow regime for a given flow condition. This transition criteria-based approach should produce much more reliable results than the look-up in an empirical map as the criteria could be based on first principles and could be universally applicable. We will see lots of such examples in this chapter.

4.1.3 Need to Know the Flow Regime

Naturally, the cross-sectional distribution of the gas phase in the pipe determines other design parameters such as heat transfer, pressure drop, etc. and without knowing this distribution, i.e. the flow regime, one cannot accurately calculate the other variables of engineering significance, such as pressure drop, as we have discussed in Chap. 2. So, we should in principle start by considering flow regimes.

As more and more data has become available for two-phase fluid flows, some of the inadequacies of the more traditional, empirical prediction methods for, say, pressure drop, have become more apparent. The older style, but still widely used, regime-independent methods (such as the homogeneous model and prediction methods based on empirical correlations that we will review in Chap. 6) give predictions which may be in extreme cases up to an order of magnitude in error. Attempts to better correlate the data for parameters such as pressure gradient and void fraction have led to a whole series of more recent and better correlations which may, however, still give typical standard deviations, when compared with the data, of up to 20–30%. Thus, the best available empirical correlations may be in many cases unsatisfactory when compared with the existing data over broad ranges of flow conditions. In many practical situations (for instance the flow of multiphase mixtures in oil/gas sub-sea pipelines), one has conditions which are well outside the range of existing data, and the empirical correlations cannot be extrapolated with any certainty to these new ranges of conditions. This has led to the search for prediction methods which are more securely based on the actual physics of the flow taking place and consequently to an even greater interest in the classification of these processes into general categories of flow patterns.

As we have seen in Chap. 2, the application of multi-fluid models, and in particular the six-equation model, to two-phase flows requires closure relationships for the calculation of parameters such as interfacial heat transfer, interfacial friction, wall friction and wall heat transfer. It is clear that these closure relationships would be affected strongly by the flow regime; for instance, the interfacial friction will be expected to be very different in bubble flow and, say, stratified flow. Thus, the identification of flow regimes and the associated selection of appropriate closure relationships form an essential part of the multi-fluid modelling approach.

We shall begin by describing the various regimes. Then, flow pattern maps will be presented and the ways in which these may be generalized, will be discussed. Following this, there will be a discussion of the analytical description of some individual flow pattern transitions and, finally, the generation of sets of criteria that can be used to build flow pattern maps will be described. This touches closely to the whole area of flow regime-based phenomenological or mechanistic modelling of multiphase flows that is, however, the subject of another volume.

An excellent historical presentation and discussion of the flow regime transition criteria and flow regime maps can be found in a keynote lecture presented by Taitel (1990). Not much new work has been presented since except for the particular case of mini and microchannels; we will not deal in this chapter with this ongoing work.

More recently, Cheng et al. (2008) produced a review including discussion of the empirical as well as of the analytical transition criteria and maps that includes several useful commented tables of experimental works as well as analytical efforts and covers also topics that are not treated in depth here such as flow regimes under diabatic conditions (boiling and condensation), microchannels, etc. One should remember that flow regimes depend on many parameters such as pressure, choice of fluids, complexity of the geometry, inclination of the tube, etc. and therefore, the discussion here cannot be totally general. In fact, one would expect to find many engineering applications where the flow regimes are unknown.

This chapter is very extensive and long as it goes well beyond the description of the flow regimes and introduces the mechanistic methods used to define the transitions between regimes and their assembly into analytical flow regime maps. Once the flow regimes have been established here, their phenomenological, mechanistic description (rather than an empirical one) is discussed in another volume.

4.2 Flow Patterns—Physical Descriptions

Flow patterns in simple geometries such as round tubes will depend on the orientation of the duct (vertical, inclined, horizontal; upwards, downwards) and its dimensions, and on whether the two-phases flow co- or counter-currently. All the fluid parameters (density, viscosity, surface tension) and the operating conditions (pressure, mass fluxes of the phases) will of course also play a major role. There are several key publications on flow pattern observation and predictions, including Spedding and Nguyen (1980), Taitel et al. (1980), Barnea et al. (1980), Mishima and Ishii (1983), etc. Most of the work deals with adiabatic flows without phase change.

4.2.1 Flow Patterns in Vertical Co-current Flow

The more common flow patterns which are encountered in an upwards, co-current flow of, say, air/water in a vertical tube were shown in Fig. 4.1 and are summarily described now. Other couples of fluids may, or may not, exhibit similar flow patterns depending on their properties.

4.2.1.1 Bubble or Bubbly Flow

The gas is dispersed as *discrete bubbles* in *continuous liquid*. The bubbles may have different shapes and sizes but they are smaller than the pipe diameter. The bubble flow regime can be encountered under two different sets of conditions: *Bubbly* flow (B) at low liquid flow rates and *Dispersed Bubble* (DB) flow at high

liquid flow rates. At low liquid flow rates the bubbles may simply keep wandering within the liquid as its turbulence is not sufficient to disturb or destroy them. On the contrary, in highly turbulent DB flow small bubbles are created by the breakup of larger volumes of gas. This distinction is, however, not always made and authors may use the terms *bubbly* or *bubble* flow indiscriminately. In strictly adhering to the definition based on "discrete bubbles in continuous liquid," foams can also be considered bubbly flows.

4.2.1.2 Slug Flow

When the quality—or the void fraction—increase, the bubbles coalesce and form larger bubbles of a size similar to that of the pipe diameter. These are called *Taylor bubbles* or *plugs* (or by some authors, *gas slugs*); they have a characteristic spherical cap nose and are somewhat abruptly terminated. The elongated gas bubbles are separated by liquid *slugs*, which may have smaller bubbles in them (the *aerated slug* area). The Taylor bubbles (Davis and Taylor 1950) are separated from the wall by a film of liquid, which may locally flow downward, even though the net flow of the liquid is upward. The length of the slug-flow *cells* (plug and liquid slug) as well as that of the individual Taylor bubbles and liquid slugs may vary considerably.

4.2.1.3 Churn Flow

When the velocity of the flow is increased, the slugs break-down into a seemingly unstable regime. Liquid may be flowing up and down in an oscillatory fashion. This is a flow regime in between the slug flow where the liquid and the gas are separated mainly *axially* and the annular flow where the separation becomes mainly *radial* as most of the liquid is finally displaced to the tube wall. In small-diameter tubes the chum-flow regime may not develop, and the transition slug-annular may be a smooth one.

Slug and churn flows produce highly fluctuating signals (e.g. pressure at the wall) and are called *intermittent*.

4.2.1.4 Annular Flow

The bulk of the liquid flows now on the wall as a *film* and the gas as the continuous phase at the centre of the duct. Normally there is some *liquid entrained* in the continuous *gas core* in the form of droplets, and there may be some gas in the liquid film in the form of bubbles. If the gas velocity is sufficiently high, large-amplitude waves may be created at the liquid–gas interface, which break up producing entrainment. The breakup of the waves is the continuous source of droplets for the gas core (*entrainment*). The droplets may deposit, however, from the gaseous core on

the liquid film (*deposition* or *redeposition*). There is really no simple explanation for the fact that the liquid wets the wall and forms annular flow.

4.2.1.5 Wispy Annular Flow

When the liquid flow rate is higher, there is a considerable amount of liquid in the gas core. These liquid droplets then coalesce to form large lumps or *wisps of liquid* (Bennett et al. 1965; Hawkes et al. 2000). This regime has not been much investigated and is difficult to detect by ordinary visual methods, except using X-rays. It occurs at high mass velocities, when the dimensionless superficial velocities (or volumetric fluxes)

$$U^*_{sG} > 1 \quad \text{and} \quad U^*_{sL} > 2.5 \text{ to } 3.0,$$

where the U^*_{sk}, $k = L, G$, are non-dimensional superficial velocities, defined in Sect. 1.10 of Chap. 1:

$$U^*_{sk} \equiv \frac{U_{sk}\rho_k^{1/2}}{[gD(\rho_L - \rho_G]^{1/2}} = j^*_k$$

This gave us an early opportunity to rely on two very commonly used non-dimensional variables in defining a transition criterion based on these. Transition criteria will be discussed extensively below.

4.2.2 Flow Patterns in Horizontal Co-current Flow

The more common flow patterns which are encountered in co-current flow of, say, air/water in a horizontal tube are shown in Fig. 4.2. Other fluids may, or may not, exhibit similar flow patterns.

The flow patterns in horizontal flow differ, naturally, from the vertical-flow ones, because of the effects of gravity, which tend to stratify the flow. In bubble and plug flow (as shown in Fig. 4.2), the gas bubbles tend to flow toward the top of the tube. In stratified flow, the gas phase interacts with the liquid, causing surface waves (stratified-wavy flow) which can grow to large sizes (semi-slug flow); the waves sometimes reaching the top of the tube leading to the formation of slug flow. Annular-dispersed flow can exist in horizontal tubes and is characterized usually by a large difference in film thickness between the lower and upper parts of the tube. It is convenient to classify elongated bubble, plug, semi-slug and slug flows as a general class of *intermittent flows*. The effects of gravity will become less important as the volumetric fluxes increase and axial momentum effects tend to dominate.

4.2.2.1 Bubble Flow

Bubbles are dispersed in the continuous liquid, though their concentrations tend to be higher in the upper part of the tube. At higher velocity, as the relative importance of gravity is lesser, the bubbles tend to be more dispersed in the tube, i.e. their concentration is more uniform.

4.2.2.2 Stratified Flow

The two phases are separated, with liquid at the bottom of the tube under normal gravity conditions. This flow pattern occurs at low liquid and gas velocities and can be either stratified-smooth and stratified-wavy. The stratified-smooth occurs at low gas velocities. As the gas velocity is increased, waves are formed on the liquid–gas interface, travelling in the direction of the flow. The amplitude of the waves depends on the relative velocity between the phases and the properties of the fluids, such as their densities and surface tension.

4.2.2.3 Annular Flow

Higher gas flow rates will cause the liquid to form a film on the tube wall, somewhat similar to that observed in vertical flow, with the important exception that the film at the bottom of the tube may be much thicker than the film at the top (the thickness variation depends on the velocity of the gas, i.e. on the relative importance of gravity). The film may or may not be continuous around the periphery of the tube. The film may be wavy, as in vertical flow, and droplets are usually dispersed in the gas core.

The question of having a continuous film around the periphery of the tube may be of crucial importance to tube integrity in case the tube is exposed to some heat flux around the periphery.

4.2.2.4 Plug Flow

The pattern is an intermittent flow that occurs at low flow rates and moderate liquid rates. In this regime, liquid plugs, free of entrained gas bubbles, are separated by zones of elongated gas bubbles. Plug flow is also termed *elongated bubble flow*.

4.2.2.5 Slug Flow

When the gas velocity is increased at plug flow (or elongated bubble flow), the liquid slugs become aerated and contain small bubbles. The flow is more chaotic, compared with plug flow, and the interface between the liquid slugs and the gas elongated bubbles is not sharp.

4.2.3 Flow Patterns in Other Situations

There are scant experimental observations of flow patterns in *inclined tubes*; these seem to be similar to the flow patterns in vertical and horizontal tubes but are very sensitive to pipe inclination. We will deal with inclined tubes in Sect. 4.5.2 where a map covering all inclinations is discussed. The inclined-tube patterns obviously must "converge" towards the horizontal or vertical situations when these inclinations are reached. Hewitt (1982) discusses this topic. A notable difference is the suppression of the churn regime that exists only in vertical flows.

Other situations include *vertical downward flow* (Crawford et al. 1985) and flow inside and around *tube bundles*. Some information can be found in the book by Collier and Thome (1994) about flow regimes in special geometries (such as rectangular channels, helical inserts, expansions, contractions, bends and coils, and annuli. Hewitt (1982) presents information on flow patterns in bundle geometries—inside and around rod bundles. Rouhani and Sohal (1983) also provide general information of flow regimes and consider also the case of co-current flow. Counter-current flows with the liquid flowing downwards will lead to flooding; this limits their presence. The effect of pipe diameter is discussed by Kaji and Azzopardi (2010). Ohnuki and Akimoto (2000) and Oddie et al. (2003) provide data on transitions in unusually large pipes.

Figure 4.4 shows an example of the cross-flow patterns around rows of heat exchanger tubes; clearly the regimes in such situations will depend on the complex geometry of the equipment, in addition to the flow parameters. Here, the regimes are analogous to those found in tubes but there are both local and overall separation phenomena; for instance, it is possible to have an overall stratification (Fig. 4.3d) coupled with a spray flow (with films being formed on the tube in the spray region).

All the work discussed so far concerned adiabatic conditions. The work on flow patterns at adiabatic condition*s* may be extended to *diabatic conditions* for lack of better information; indeed Fig. 4.5 (Collier and Thome 1994) shows flow regimes similar to the ones expected in adiabatic vertical two-phase flow. Frankum et al. (1997) also provide flow patterns for *evaporating flow*.

Consider a heated tube with subcooled flow at the inlet. As Fig. 4.5 shows, somewhere downstream of the inlet boiling takes place (the point is referred to as the point of Onset of Nucleate Boiling or ONB) and the first voids appear. Another important point in the channel is the point where the *Critical Heat Flux* (*CHF*) *condition* or *Burnout* occurs. There is *post-burnout heat transfer* beyond this point, but if the heat flux is sufficiently high the heat transfer will be insufficient and the channel wall will overheat and fail. Figure 4.5 shows also the *point of suppression of nucleate boiling*; indeed, as the quality increases and the annular-flow film on the wall becomes thin, it may be unable to support a superheat sufficient for nucleation and nucleation will be suppressed. Beyond this point boiling will take place only by evaporation of the liquid at the annular-flow liquid/vapour interface; this boiling regime is called *forced-convection vapourization.*

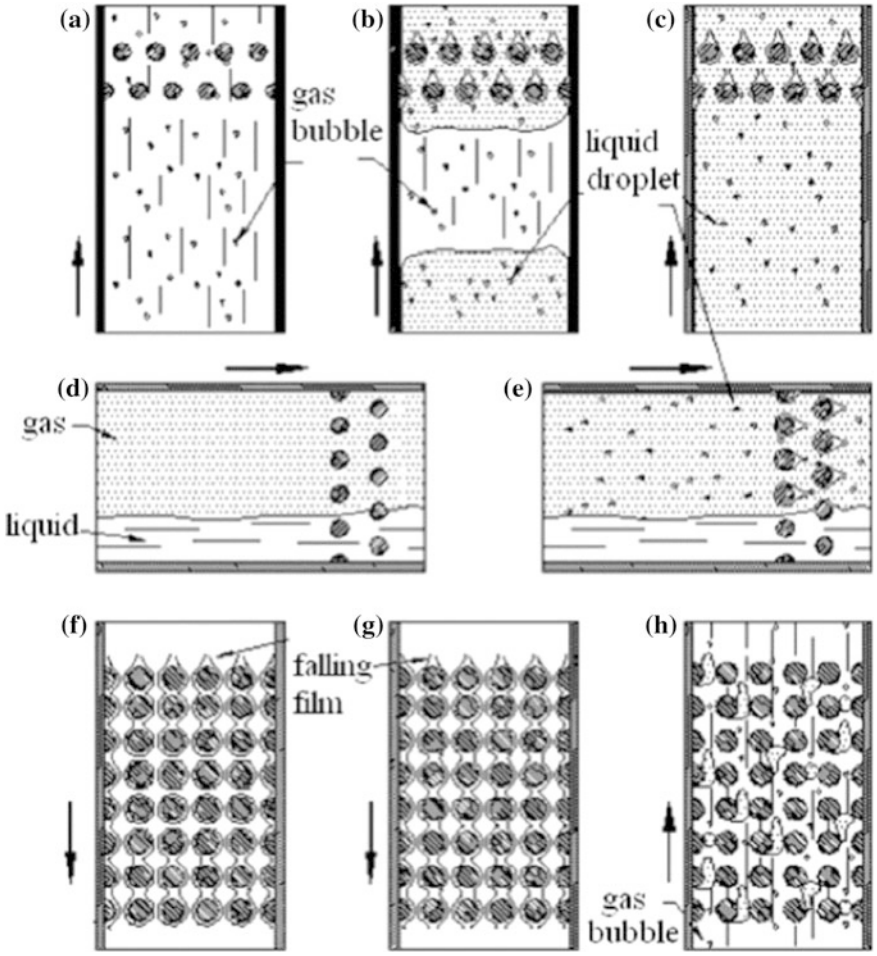

Fig. 4.4 Flow patterns in cross flow over rows of heat exchanger tubes (Ribatski and Thome 2007; Grant and Chisholm 1979; Xu et al. 1988. Part of the figure with ASME permission

The boiling mechanisms and regimes will be considered in another volume, but we would like to show here the succession of situations that will be present in the channel as the heat input is increased in steps, Fig. 4.6: the various points just mentioned will move down the channel as shown in the figure. As the equilibrium quality at a location z is given (Sect. 1.8.1 of Chap. 1) by

$$x_{eq}(z) = \frac{h(z) - h_{L,sat}}{h_{LG,sat}} = \frac{1}{h_{LG,sat}}\left[h_{in} + \frac{\dot{Q}(0 \to z)}{\dot{M}}\right] - \frac{h_{L,sat}}{h_{LG,sat}}$$
$$= \frac{h_{in} - h_{L,sat}}{h_{LG,sat}} + \frac{\dot{Q}(0 \to z)}{\dot{M}},$$

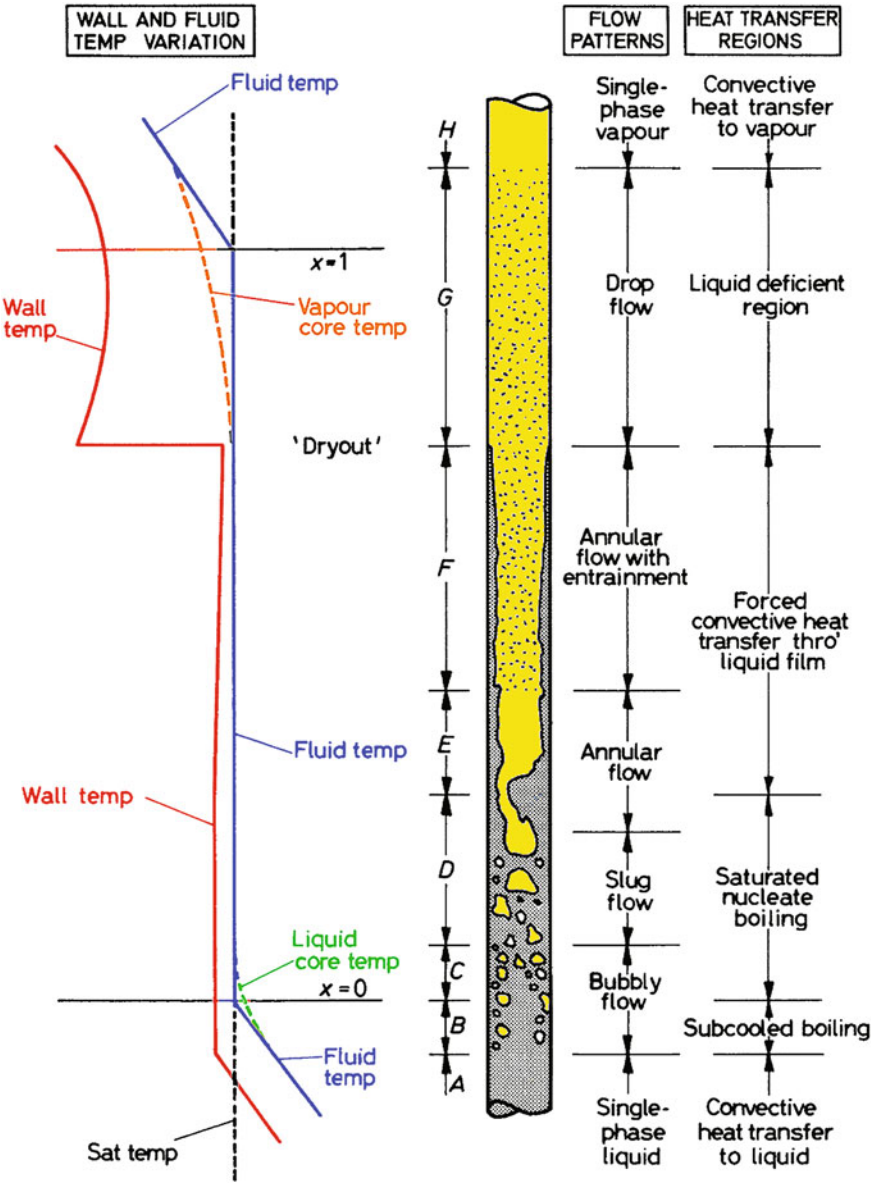

Fig. 4.5 The succession of boiling regimes and the corresponding flow regimes in a heated, boiling tube; adapted from Collier (1972) (or Collier and Thome 1994). © and courtesy of Prof. J. Thome

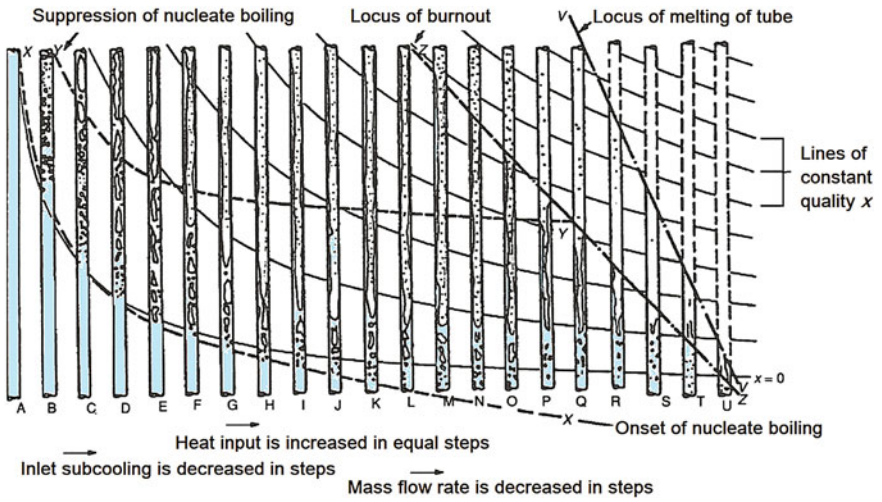

Fig. 4.6 As the heat input is increased, or mass flux is decreased, or inlet subcooling is decreased, the succession of regimes in the channel moves. Only one variable was varied at a time

where $\dot{Q}(0 \rightarrow z)$ is the heat input from the entrance to point z, we note that one can produce the succession of regimes shown in Fig. 4.6 either by increasing the heat input or by reducing the mass flow rate $\dot{M}$ or by decreasing (in absolute value) the inlet subcooling $h_{in} - h_{L,sat}$. The fundamental effects produced by the variation of these three operating parameters, (heat input, mass flow rate and inlet subcooling), are important to visualize and keep in mind so that the performance and the dynamic behaviour of a boiling channel are well understood.

Thome and collaborators (Cheng et al. 2008; Kattan et al. 1998; El Hajal et al. 2003) studied the flow regimes taking place under diabatic conditions in a horizontal tube and their two-way impact on two-phase heat transfer and pressure drop. Figure 4.7 from Thome's work shows the flow patterns in a horizontal tube where either evaporation or condensation taking place. The figures show the non-axisymmetric conditions produced by gravity. Cheng et al. (2008) note that from a heat transfer viewpoint there is a possibility of intermittent drying and rewetting of the upper surfaces of the tube in slug and wavy flows resulting in progressive dryout of the upper circumference of the tube wall in annular flow.

Mini- and microchannels

The currently available methods for predicting the flow regimes and their transitions were established mainly from observations of gas–liquid flows in pipe diameters ranging from a few centimetres to about 13 cm (0.5- to 5-inch pipes) and should not be expected to properly apply to mini and microchannels. Indeed, for small diameters there is an increased role of the surface tension and the corresponding

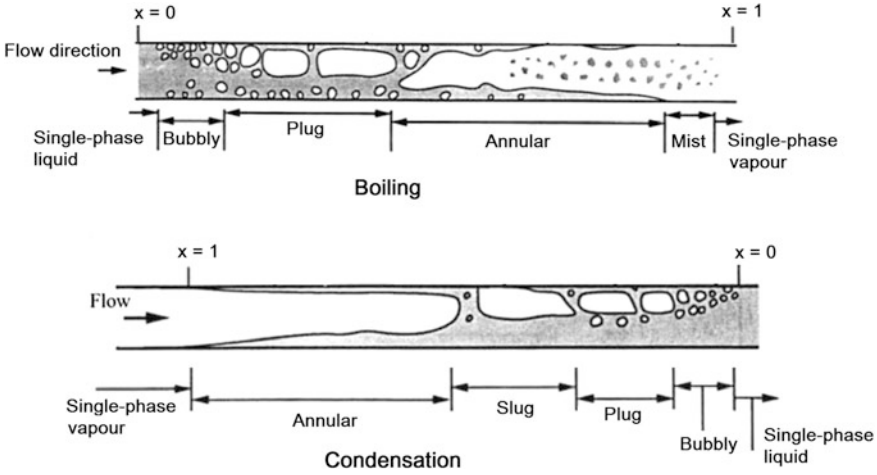

Fig. 4.7 The flow patterns in a horizontal tube where the fluid evaporates (*top*) or condenses (*bottom*) (adapted from Collier and Thome (1994) and Palen et al. (1979))

wetting effects (Ullman and Brauner, 2007). Kandlikar (2002) attempted a classification of channel size according to its hydraulic diameter D_h as

- conventional channels: $D_h > 3$ mm
- minichannels: $D_h = 0.2$–3 mm
- microchannels: $D_h = 10$–200 μm

The physical distinction (Triplett et al. 1999) is better made if one compares the hydraulic diameter to the Laplace constant L determining the wavelength related to Taylor instabilities (Sect. 1.10 in Chap. 1).

$$L = \sqrt{\frac{\sigma}{g(\rho_L - \rho_G)}}$$

The Laplace constant characterizes the effects of surface tension vs gravity. Here g is the acceleration of gravity, ρ_L and ρ_G the liquid and gas vapour densities, respectively, and σ the surface tension. Small channels, $D_h < L$, will clearly be affected by capillary effects that will also influence the flow regime. The reader interested in microchannels should consult the works of Kawahara et al. (2002), Serizawa et al. (2002), Triplett et al. (1999) and Ullmann and Brauner (2007).

4.3 Empirical Flow Regime Maps

Flow pattern, or flow regime maps are normally drawn as follows: the experimental equipment is set to get a certain liquid superficial velocity U_{sL} and gas superficial velocity U_{sG}. The flow pattern is then determined and a mark is made on, say, a U_{sL} vs U_{sG} map as shown in the examples of Figs. 4.3 and 4.8; other mappings according to combinations of dimensional or non-dimensional variables are of course possible. The state of the system (e.g. the valves) is then changed, the flow pattern is again observed and a new mark is made corresponding to the new flow pattern. When the whole velocity ranges are covered this way, boundaries are drawn delimiting the marks indicating the presence of a certain regime. Obviously the map obtained this way will be applicable in principle only to the experimental system used. The challenge is to find map coordinates that will make the map more universally applicable, to other setups, fluids, etc.

The reader should also be aware of the fact that observations and their predictions under steady-state conditions (the vast majority of the published work) may vary significantly under *transient conditions* such as flow reversals, rapid flow changes, etc. However, in view of the fact that *all* the empirical correlations are obtained at steady state and then often used for transient conditions, this is not a limitation only for the flow regime maps. Taitel et al. (1978) provide an example of differences between steady-state and transient situations.

Flow pattern data for a given pair of fluids are often represented in terms of flow parameters such as mass flux $\dot{m}$ and quality x or phase superficial velocities, U_{sG}

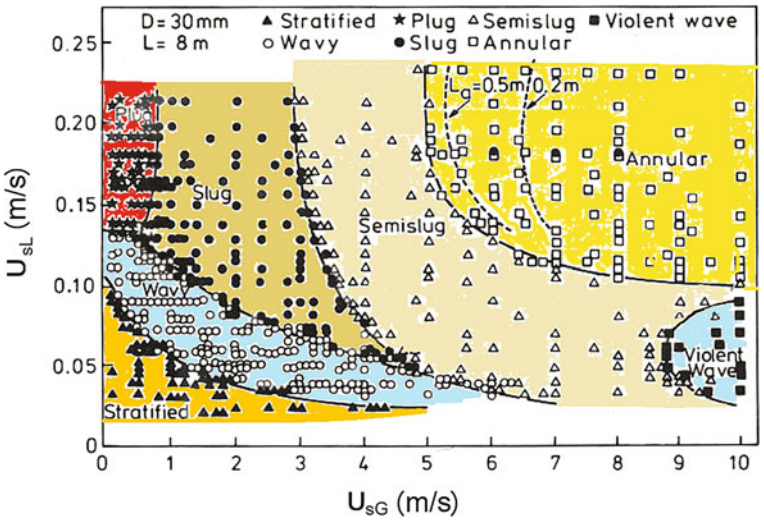

Fig. 4.8 The classical Sakaguchi et al. (1979) map for horizontal, air-water flow in a 300 mm diameter tube. L_a is the length required for the establishment of fully developed annular flow; indeed, certain flow patterns need a certain length to develop

and U_{sL} for the gas and the liquid phase, respectively. Two typical, classical maps of this form are shown in Figs. 4.3 and 4.8 for upflow, high pressure steam-water and horizontal, low-pressure air-water, respectively. Although the presentation of the data in this form is useful in describing a particular set of experiments, such maps cannot be extrapolated to other fluid conditions. This has led to the search for more generalized flow pattern maps, as discussed next.

There were many attempts to generalize the flow pattern maps, but this is obviously very difficult to achieve since there can be up to a dozen relevant physical variables: the superficial velocities, the densities, viscosities, surface tension, pipe geometry (length, diameter, roughness, inclination) and acceleration due to gravity. With these, one can have eight or nine dimensionless groups (the number of variables minus the number of basic units according to the Pi theorem). Some of the variables may be of lesser importance, but the number of dimensionless groups is still quite large. Some maps are now discussed and simplified modellings are then presented, which attempt to generalize the maps and to predict the transitions from one regime to another. Yet, it should be emphasized that the flow regime maps are not general and should be extrapolated cautiously, since, for example, there is experimental evidence of substantial effects of pipe diameter, pressure, etc. that may not be included in their construction.

4.3.1 The Baker Map for Horizontal Flow

For historic reasons, but also because his work has still some relevance, we will present the map produced by Baker (1954) who published the earliest flow-pattern map for *horizontal flow*, presented in Fig. 4.9. In an attempt to produce a map having a certain generality, Baker used

$$\frac{\dot{m}_G}{\lambda} \quad \text{vs} \quad \frac{\dot{m}_L}{\dot{m}_G}\lambda\psi$$

as coordinates, where

$$\lambda \equiv \left[\frac{\rho_G}{\rho_{air}} \cdot \frac{\rho_L}{\rho_{water}}\right]^{0.5} \quad \text{and} \quad \psi \equiv \frac{\sigma_{water}}{\sigma}\left[\frac{\mu_L}{\mu_{water}} \cdot \left(\frac{\rho_{water}}{\rho_L}\right)^2\right]^{2/3}$$

One notes that in the Baker map the horizontal coordinate is dimensionless while the vertical one has dimensions of mass flux (the units should be British, namely, $lb_m/hr\ ft^2$). This suggests that this map cannot be very general. Note that λ and ψ are dimensionless parameters that should take into account the variation in the properties of the fluids with respect to air and water: λ and ψ are equal to unity for the "standard" case of water–air, under standard atmospheric pressure and at room temperature. In this case, the map reduces to a plot of $\dot{m}_G$ vs $\dot{m}_L/\dot{m}_G$. Rouhani and

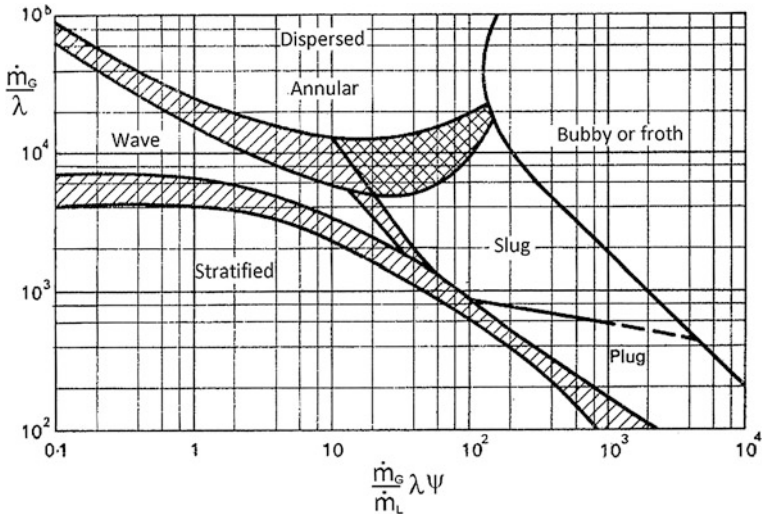

Fig. 4.9 The old Baker (1954) map for horizontal flow as modified by Scott (1963) who broadened its borders to reflect the inherent uncertainty

Sohal (1983) have shown that indeed Baker's map does not adequately predict horizontal flow regimes in numerous situations.

4.3.2 *The Hewitt and Roberts Generalized Map*

Hewitt and Roberts (1969) presented a more generalized map for vertical tubes in terms of the momentum fluxes of the phases $\rho_k U_{sk}^2$ or $\rho_k j_k^2$, Fig. 4.10. This

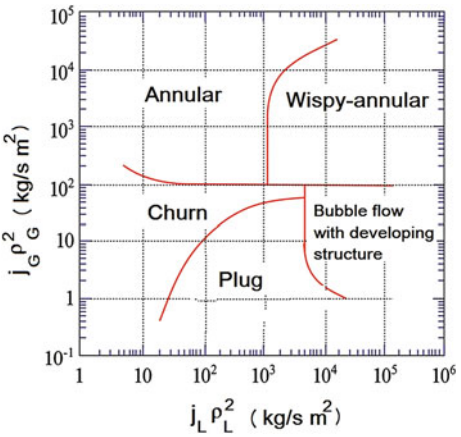

Fig. 4.10 The generalized map of Hewitt and Roberts (1969) where the coordinates are the phase momentum fluxes, $\rho_k U_{sk}^2 = \rho_k j_k^2$ calculated with the superficial phase velocities or volumetric fluxes

representation is still recommended as fitting a fairly wide range of data for both low and high pressures and with several fluid pairs.[1]

4.4 Analytical Treatment of Flow Pattern Transitions—Flow Pattern Maps

As an alternative to the use of empirical flow regime maps, one can specify the boundaries between the various flow regimes by examining phenomenologically the particular mechanisms involved in the transition. In this case a flow pattern map can be constructed using a collection of transition criteria. One of the advantages of this analytical, mechanistic approach is that each transition may be best described using the most appropriate variables and can take into account in a natural way effects such as the inclination of the channel, flow direction, fluid properties, etc.

Although there have been many attempts to model the transitions from one flow pattern to another, most of the relevant literature is limited to one or a few transitions at a time. A few research groups collected, however, the flow regime transition mechanisms and corresponding criteria and came up with *comprehensive* and *unified* analytical sets of transition criteria covering all regimes and transitions in terms of non-dimensional numbers. Such sets can then be used to construct flow regime maps for specific applications.

In particular Dukler, Taitel, Barnea (DTB) and their co-workers who collaborated very closely and extensively, started from maps mainly for the horizontal flows of interest to the oil-and-gas industry and extended over the years their approach that finally culminated in a unified map covering all orientations. Another group consisting of Ishii and his collaborators published extensively criteria mainly for the vertical flows of interest to the nuclear and power industries. Both groups of workers produced comprehensive sets of criteria that can be used to assemble a flow regime map. The DTB work is highlighted in Sect. 4.5 and the work of Ishii and co-workers in Sect. 4.6.

In addition to these works, the interested reader could also consult other flow-pattern transition models, such as those proposed by Weisman et al. (1979) for horizontal pipes, Weisman and Kang (1981) for vertical or upward inclined pipes, Taitel and Barnea (1983) for vertical counter-current flows, Ito et al. (2004) who propose "a simplified model," and Crawford and Weisman (1984) for diabatic conditions.

Before discussing in the following sections the approaches of the two groups mentioned above, we will review first a few key mechanism for selected, particular transitions that lead to appropriate transition criteria, as good examples of mechanistic modelling. We are not going to be exhaustive, as the following two sections

[1]To simplify the notation, the angle brackets are eliminated in this chapter. Consequently, we write j_k *for* $< j_k >$ and u_k for $< u_k >$ *and* ε for $< \varepsilon >$.

on comprehensive analytical maps will cover the remaining cases. Flow transitions will also be discussed in another volume on phenomenological modelling. As examples of the numerous studies that have focused on *specific* flow regime transitions, we cite the Hurlburt and Hanratty (2002) and Johnston (1985) works on the transitions from stratified flows, the paper by Matuszkiewicz et al. (1987) for the transition from bubble to slug flow.

4.4.1 The Bubbly-to-Slug Flow Transition

In bubble flow, there is a natural process of bubble growth due to bubble collisions and coalescence. The frequency of bubble collisions increases rapidly with increasing gas volumetric fraction (void fraction) in the channel. It is this coalescence of the bubbles that creates the gas slugs. Since the coalescence depends on the bubble population and on the transit time of the mixture, given enough time in the channel (or a sufficiently long entrance length) most bubbly flows will revert to slug flow. Typically this transition occurs for values of the void fraction between 0.1 and 0.3.

When the void fraction is increased, bubbles tend to coalesce more. One can assume that the coalescence is proportional to the distance between the bubbles, but it increases sharply as the distance between the bubbles is less than half their radius. With a dense packing of the bubbles, this corresponds to $\varepsilon = 0.25$, which is the transition boundary from bubble flow at low liquid velocities.

In the presence of foaming agents, the flow may, however, remain bubbly for void fractions up to nearly one; foam is an extreme case of bubbly flow. Whalley et al. (1972) found that the transition void fraction could rise to around 0.6 with very small amounts of hexanol or butanol present in the water. This points to the importance of usually poorly controlled variables such as the surface tension in determining the flow regime.

If the flow is highly turbulent, then the bubbles may be breaking up and bubble flow may persist due to an equilibrium between bubble breakup and coalescence. Taitel and Dukler (1980) describe an approximate theory for turbulent breakup of bubbles.

In small tubes, spherically capped bubbles that have sizes larger than those of the smaller distributed bubbles, have slower rise velocities; the smaller bubbles overtake these and can coalesce with them forming progressively larger bubbles that end up as gas slugs.

Mishima and Ishii (1984) suggested a simple bubbly-to-slug flow transition criterion, namely

$$\varepsilon = 0.3$$

This criterion in terms of void fraction may not fit, however, into the framework of computing codes not using the void fraction as primary variable or for producing

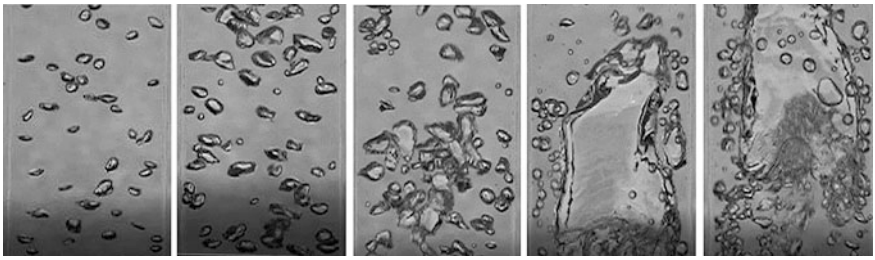

Fig. 4.11 Five shots showing the transition from bubbly to slug flow if one moves upwards in the channel (extracted from a movie made by Milenkovic et al. 2006)

flow pattern maps in terms of superficial velocities. For this reason, Mishima and Ishii (1984) convert the void fraction based criterion into the superficial velocities framework; clearly a void fraction correlation or the equivalent information is needed for this and the Drift Flux Model (DF) of Zuber and Findlay (1965) that we will cover in Chap. 5 on void fraction was used. The result is

$$j_L = \left(\frac{3.33}{C_0} - 1\right) j_G - \frac{0.76}{C_0}\left(\frac{\sigma g \Delta\rho}{\rho_L^2}\right)^{1/4},$$

where C_0 is the DF *distribution* parameter and $\Delta\rho \equiv \rho_L - \rho_G$.

Figure 4.11 shows five shots from a film documenting a transition from bubbly to slug flow (air-water). The shots were taken as the camera moves up the rectangular (1 × 5 cm) channel. One notices first the growth of the bubbles due to agglomeration and then the formation of larger structures very much resembling slugs and plugs; the liquid remains, however, highly aerated, i.e. contains lots of small bubbles.

4.4.2 *The Slug-to-Churn Transition in Vertical Upwards Flow*

Several mechanisms have been proposed for the slug-to-churn transition. These can be essentially grouped into two categories: models that consider the destruction of the liquid slug between two Taylor bubbles, and models based on flooding of the liquid film surrounding the Taylor bubble, Fig. 4.12. Flooding refers to the condition occurring when a counter-current smooth falling-liquid–rising-gas flow becomes disrupted and chaotic as the gas velocity is increased. For the transition in question, flooding occurs as the velocity of the rising-gas slug is increased and disrupts the falling liquid film surrounding it; the long gas slug breaks up, resulting in churn flow. More specifically various published models make the following assumptions for the transition:

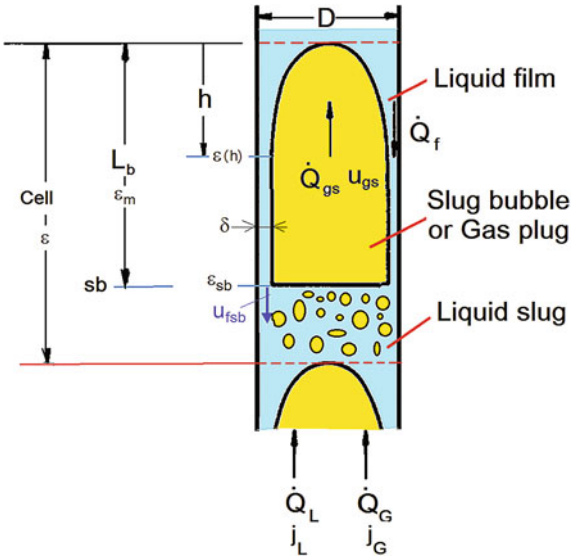

Fig. 4.12 Schematic representation of slug flow and definition of variables

- the liquid slug separating two consecutive Taylor bubbles becomes so short that the wake behind the Taylor bubble destroys it (Dukler and Taitel 1977; Mishima and lshii 1984)
- Taitel et al. (1980) treat churn flow as an entrance phenomenon, part of the process of formation of stable slug flow further downstream; they develop a method for calculating the entry length required to develop stable slug flow
- the mean void fraction of the entire slug cell exceeds that of the Taylor-bubble area (Mishima and lshii, 1984)
- the void fraction within the liquid slug reaches the maximum bubble, cubic, volumetric packing of 0.52 (Brauner and Barnea 1986; Barnea 1987)
- flooding of the liquid film surrounding the Taylor bubble (Nicklin and Davidson 1962; Wallis 1969; Porteous 1969; McQuillan and Whalley 1985; Govan et al. 1991; Jayanti and Hewitt 1992)

McQuillan and Whalley (1985) and Jayanti and Hewitt (1992) review these mechanisms and the relative merits of the corresponding models.

We will give here some details about the McQuillan and Whalley (1985) model, Fig. 4.12, based on the flooding assumption that builds up on the earlier works listed above, as a good example of mechanistic modelling involving well-established methods. The authors solve first a set of relationships to find the thickness of the falling film and the volumetric flow rates of the falling liquid film and of the gas slug (that they call *gas plug*),$\dot{Q}_f$, $\dot{Q}_{gs}$, respectively.

The thickness of the falling-film δ, assumed to be laminar, can be calculated according to the classical Nusselt (1916) solution

$$\delta = \delta_{lam} = \left(\frac{3\dot{Q}_f \mu_L}{\pi g D \rho_L}\right)^{1/3} \tag{4.4.1}$$

The rise velocity of the gas plug u_{gs} is given by an expression developed by Nicklin (1962)

$$u_{gs} = 1.2\ (j_L + j_G) + 0.35\ \left[\frac{gD(\rho_L - \rho_G)}{\rho_L}\right]^{1/2} \tag{4.4.2}$$

essentially stating that the plug moves at the total volumetric flux velocity plus the velocity of the rising Taylor bubble (the second term). The factor 1.2 accounts for the velocity profile in turbulent flow. The volumetric fluxes of the liquid and the gas are j_L and j_G, respectively. The gas volumetric flow rate in the slug can be calculated as the product of the slug velocity times its flow area $\pi D^2/4 - 2\pi D\delta = A(1 - 4\delta/D)$ as

$$\dot{Q}_{gs} = \left(1 - \frac{4\delta}{D}\right) A u_{gs} \tag{4.4.3}$$

Continuity of volume in the entire slug-flow cell is expressed as

$$\dot{Q}_{gs} = -\ \dot{Q}_f + (\dot{Q}_G + \dot{Q}_L) \tag{4.4.4}$$

with the volumetric flow of the film being positive in the downflow direction. The set of four Eqs. (4.4.1) to (4.4.4) can be solved to find the unknowns, δ, $\dot{Q}_{gs}$, $\dot{Q}_f$ and u_{gs} in terms of j_L and j_G.

As mentioned, the McQuillan and Whalley (1985) model is based on the assumption of flooding between the liquid film and the Taylor bubble. Several authors have developed flooding correlations having the form

$$\sqrt{j_G^*} + m\sqrt{j_L^*} = C \quad \text{with} \quad j_k^* \equiv \frac{j_k}{\sqrt{\frac{gD(\rho_L - \rho_G)}{\rho_k}}}, \quad k = LG$$

where the j_k^* are the non-dimensional volumetric fluxes introduced in Chap. 1, Sect. 1.10. McQuillan and Whalley (1985) develop their transition criteria in terms of such non-dimensional volumetric fluxes; however, they define these using the volumetric fluxes of the gas slug and of the liquid film, $j_{gs} \equiv \dot{Q}_{gs}/A$ and $j_f \equiv \dot{Q}_f/A$, respectively, rather than the usual j_L and j_G:

$$j_f^* \equiv \frac{j_f}{\sqrt{\frac{gD(\rho_L - \rho_G)}{\rho_L}}} \quad \text{and} \quad j_{gs}^* \equiv \frac{j_{gs}}{\sqrt{\frac{gD(\rho_L - \rho_G)}{\rho_G}}},$$

Their correlation is

$$\sqrt{j_f^*} + \sqrt{j_{gs}^*} = 1 \tag{4.4.5}$$

Jayanti and Hewitt (1992) proposed an improved, more sophisticated model based on the McQuillan and Whalley (1985) approach accounting, however, for the effect of the Taylor-bubble length on flooding and of the turbulence in the falling film.

Chen and Brill (1997) proposed a new model developed on the basis of the wake effect behind the Taylor bubble, an idea already present in earlier models (e.g. Duklert and Taitel, 1977; Mishima and Ishii 1984). The transition from slug to churn is attributed to the destruction of the highly aerated liquid slug by the strong effect of the wake behind the preceding Taylor bubble.

Alternatively, Mishima and Ishii (1984) consider the slug-to-churn transition to occur when the average void fraction over the "cell" including the gas slug (Taylor bubble) and the liquid plug that follows it exceeds the value over the slug-bubble section. A criterion developed on this basis is presented in Sect. 4.6 below.

4.4.3 Transitions in Horizontal Flow

These will be discussed summarily here as a more comprehensive discussion will be given while discussing the analytical horizontal flow maps. Figure 4.13 gives a

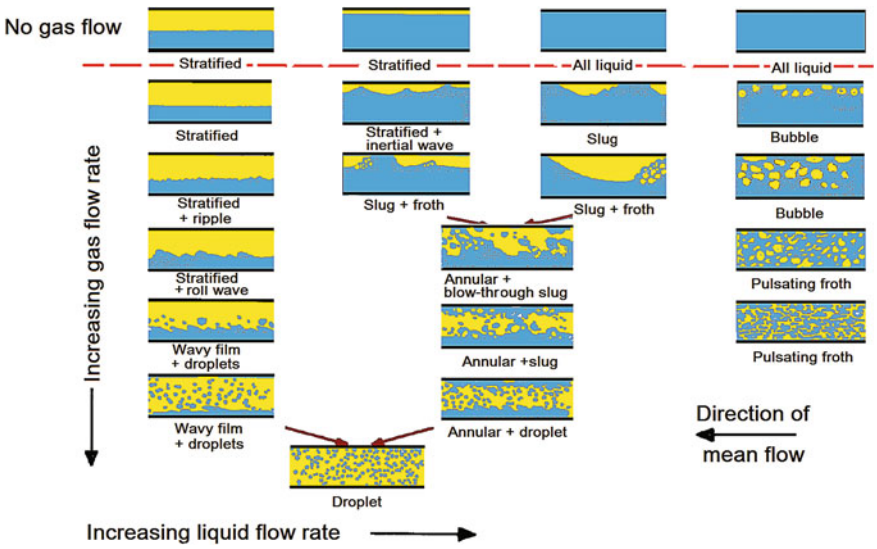

Fig. 4.13 A very comprehensive diagram showing the possible flow transitions in horizontal flow (adapted from Spedding and Nguyen 1980)

very comprehensive view of the various possible transitions in horizontal flow. We will not enter into such detail and will cover only the main transitions sketched in Fig. 4.2.

4.4.3.1 Transition from Horizontal-Stratified to Intermittent or Annular Flow

The transition can be explained in terms of a solitary wave of finite amplitude growing as the Bernoulli forces (i.e. the under-pressure created by the acceleration of the gas flow above the wave) overcome the stabilizing effect of gravity—an interfacial instability (Taitel and Dukler 1976; Hurlburt and Hanratty 2002). If the wave grows sufficiently and the level of the stratified flow in the pipe is sufficiently high, it bridges the pipe, blocks the flow of gas, and slug-flow results. If there is not enough liquid in the channel to form a complete bridge and block the flow of the gas, annular flow results. This model is an essential part of the maps presented in the next section.

4.4.3.2 Appearance of Waviness in Stratified Horizontal Flow

The velocity of the gas must be sufficient to cause waves, but lower than the critical value needed for rapid wave growth that would trigger a transition to intermittent or annular flow. Jeffreys (1925, 1926) suggested the following criterion for wave generation:

$$(u_G - c)^2 c > \frac{4 v_L g (\rho_L - \rho_G)}{s \rho_G},$$

where c is the velocity of propagation of the waves and s a "sheltering" coefficient; the kinematic viscosity of the liquid is v_L. Taitel and Dukler (1976) starting from this relationship, used $c = u_L$ and developed the transition criterion for the appearance of waves presented in the analytical maps section below.

4.4.3.3 Transition from Intermittent Horizontal to Dispersed Bubbly Flow

This transition will take place when the turbulent fluctuations in the liquid will be high enough to overcome the stabilizing effect of the buoyancy forces keeping the gas at the top of the channel.

4.5 Flow Regime Maps Based on Transition Criteria: The Dukler-Taitel-Barnea Work

We will discuss in this section the unified approach that resulted from the extensive collaborations between Dukler, Taitel, Barnea and their co-workers, generically referred to here as the DTB work. Highlights of this work will be presented as examples of well accepted approaches showing what can be accomplished in this fashion.

The major accomplishments of the DTB work can be found in the publications related to their maps: the early Taitel and Dukler (1976) map for horizontal or near-horizontal flow; the Taitel et al. (1980) map for vertical flow; the Barnea et al. (1982a,b) map for downward or downward inclined flow; and finally the unified map presented by Barnea (1986,1987) for *inclined* flows continuously ranging from horizontal to vertical. Barnea et al. (1983) includes a model and experimental results for flow pattern transitions for small-diameter pipes where surface tension effects are not negligible. Taitel (1990) gives an excellent summary of all the developments. To make the chapter manageable, we will not be able to give here all the details necessary for practical use of the maps, however, we will treat at some length the development of transition criteria as these are excellent exercises in mechanistic modelling of two-phase flows.

During the 90s Taitel and Barnea published papers on the transition from separated flow (stratified and annular) based on linear and nonlinear interfacial and structural stability analyses with applications to flow pattern transitions. These were summarized in a recently published volume by Taitel and Barnea (2016).

4.5.1 Transitions from Horizontal or Near-Horizontal Flows—the Taitel and Dukler Map

The Taitel and Dukler (1976) analysis begins by finding the condition determining whether the flow is stratified or not. When gas and liquid are in a horizontal, or near-horizontal pipe (under normal gravity conditions), the heavier liquid flows on the bottom of the pipe, whereas the gas takes its place above it, as expected, Fig. 4.14. Stratified flow prevails unless the interface becomes unstable and wavy. It is assumed that the instability is of a Kelvin–Helmholz type (Chap. 4) in the presence of a gravity field, i.e. a balance between surface tension, gravity and Bernoulli forces due to differences of velocity of two parallel steams.

4.5.1.1 The Equilibrium Liquid Height

We will start the analysis by finding the equilibrium liquid height in the pipe, i.e. the liquid level in terms of the volumetric fluxes. The integral momentum balance

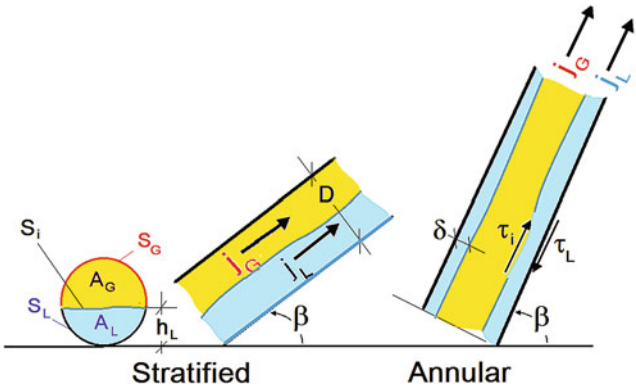

Fig. 4.14 Definition of the dimensions of the pipe considered and of the main variables; two different flow regimes depicted

equations that will be used for the liquid and the gas provide a good opportunity to use the two-fluid momentum conservation equations derived in Chap. 2.

$$\frac{\partial}{\partial t}\left[\rho_L\langle 1-\varepsilon\rangle\langle u_L\rangle_L\right] + \frac{1}{A}\frac{\partial}{\partial z}\left[\rho_L\langle 1-\varepsilon\rangle\langle u_L\rangle_L^2 A\right] = -\langle 1-\varepsilon\rangle\frac{\partial p}{\partial z} + g\rho_L\langle 1-\varepsilon\rangle\cos\theta - \frac{P_{wL}\tau_{wL}}{A} + \frac{P_i\tau_i}{A} - u_i\Gamma \tag{2.4.9}$$

$$\frac{\partial}{\partial t}\left[\rho_G\langle\varepsilon_G\rangle\langle u_G\rangle_G\right] + \frac{1}{A}\frac{\partial}{\partial z}\left[\rho_G\langle\varepsilon\rangle\langle u_G\rangle_G^2 A\right] = -\langle\varepsilon\rangle\frac{\partial p}{\partial z} + g\rho_G\langle\varepsilon\rangle\cos\theta - \frac{P_{wG}\tau_{wG}}{A} - \frac{P_i\tau_i}{A} + u_i\Gamma \tag{2.4.10}$$

At steady state and for fully developed flow, the time and space derivative terms vanish; we also assume no interfacial mass exchange and we are left with

$$0 = -\langle 1-\varepsilon\rangle\frac{\partial p}{\partial z} + g\rho_L\langle 1-\varepsilon\rangle\cos\theta - \frac{P_{wL}\tau_{wL}}{A} + \frac{P_i\tau_i}{A}$$

$$0 = -\langle\varepsilon\rangle\frac{\partial p}{\partial z} + g\rho_G\langle\varepsilon\rangle\cos\theta - \frac{P_{wG}\tau_{wG}}{A} - \frac{P_i\tau_i}{A}$$

Noting that $<\varepsilon> = A_G/A$ and $<1-\varepsilon> = A_L/A$, we obtain

$$\begin{aligned} A_L\left.\frac{dp}{dz}\right|_L - \tau_{wL}S_L + \tau_i S_i - \rho_L A_L g\sin\beta = 0 \\ A_G\left.\frac{dp}{dz}\right|_G - \tau_{wG}S_G - \tau_i S_i - \rho_G A_G g\sin\beta = 0, \end{aligned} \tag{4.5.1}$$

where $\beta = \theta - \pi/2$ is the angle of inclination now to the horizontal (θ was the angle between gravity and the z coordinate) and is taken as positive for upward flow. We also kept here the nomenclature of Taitel and Dukler, namely $S_i \equiv P_i, S_L \equiv P_{wL}$ and $S_L \equiv P_{wL}$. All these geometric parameters depend uniquely on the height of the liquid in the channel (i.e. the liquid fraction) and the pipe diameter.

Eliminating the pressure gradient (by assuming that the gradients in the two phases are equal), yields a single equation

$$-\frac{\tau_{wL}S_L}{A_L} + \frac{\tau_{wG}S_G}{A_G} + \tau_i S_i\left(\frac{1}{A_L} - \frac{1}{A_G}\right) - (\rho_L - \rho_G)g\,\sin\beta = 0 \qquad (4.5.2)$$

The shear stresses at liquid-wall, τ_{wL}, gas-wall, τ_{wG}, and gas–liquid interface, τ_i, control the height of the liquid in the pipe and consequently the dependent geometrical parameters S_L, S_G and S_i. The stresses can be approximated using the relevant usual friction factors, f_{wL}, f_{wG} and f_i

$$\tau_{wL} = f_L\frac{\rho_L u_L^2}{2}, \qquad \tau_{wG} = f_G\frac{\rho_G u_G^2}{2}, \qquad \tau_i = f_i\frac{\rho_G(u_L - u_G)|u_L - u_G|}{2},$$

where the use of the absolute value of the difference of velocities allows to take into account the flow direction. The friction factors for smooth pipes f_L and f_G and the interfacial friction factor f_i are given as

$$f_L = C_L\mathrm{Re}_L^{-n} = C_L\left[\frac{4A_L u_L}{S_L v_L}\right]^{-n}, \quad f_G = C_G\mathrm{Re}_G^{-m} = C_G\left[\frac{4A_G u_G}{S_G v_G}\right]^{-m} \quad \text{and} \quad f_i \approx f_G,$$

where $C_L = C_G = 0.046$, $n = m = 0.2$ for turbulent flow and $C_L = C_G = 16$ and $n = m = 1$ for laminar flow. Note that by taking $f_i = f_G$, it is tacitly assumed that the interface is smooth and that the liquid velocity is negligible compared with the gas velocity. This assumption is quite good even when the interface is wavy.

Parenthetically, let us mention here that more recently, Gomez et al. (2000) found that it is better to calculate f_G from a standard friction-factor chart, but f_L from a correlation developed by Ouyang and Aziz (1996) that considers both the liquid and gas flow rates

$$\text{For} \quad \mathrm{Re}_G \le 2300, \quad f_G = \frac{16}{\mathrm{Re}_G}$$

$$\text{For} \quad \mathrm{Re}_G > 2300, \quad f_G = 0.001375\left[1 + \left(2\cdot 10^4\frac{\varepsilon_r}{D} + \frac{10^6}{\mathrm{Re}_G}\right)^{1/3}\right]$$

$$f_L = \frac{1.6291}{\mathrm{Re}_L^{0.5161}}\left(\frac{j_G}{j_L}\right)^{0.0926}$$

The interfacial friction factor f_i for stratified-smooth flow is again taken as the friction factor f_G. However, for stratified-wavy flow, a friction factor by Baker et al. (1988) is used.

Dimensionless quantities, denoted by a tilde over the symbol, are now defined by dividing the actual lengths by the pipe diameter D, the areas by D^2, and the actual average phase velocities by the volumetric fluxes of the phases. The various lengths and areas are defined in Fig. 4.14.

We have given above the balance of pressure drops in the two phases that determines the liquid level, Eq. (4.5.2). Taitel and Dukler show that this equation can be solved for the non-dimensional height of the liquid $\tilde{h}_L \equiv h_L/D$ that depends only on two parameters X and Y that appear and the pipe geometry

$$\tilde{h}_L \equiv \frac{h_L}{D} = f(\mathrm{X}, Y)$$

The first parameter X is the Lockhart–Martinelli parameter, defined in Chap. 1, Sect. 1.10 as the ratio between the pressure gradients which would have occurred if the fluids were flowing alone in the pipe at their flow rate

$$\mathrm{X} \equiv \left[\frac{dp/dz|_{LP}}{dp/dz|_{GP}}\right]^{1/2},$$

where the frictional pressure gradients and the Reynolds numbers are also calculated assuming that each phase is flowing alone in the channel, subscript kP (i.e. using the volumetric fluxes j_k or superficial velocities of each phase)

The second parameter Y is an inclination parameter, namely the ratio of the gravitational pressure gradient component along the pipe axis to the frictional pressure gradient in the gas phase

$$\mathrm{Y} \equiv \frac{(\rho_L - \rho_G) g \ \sin\beta}{\left|(dp/dz)_{GP}\right|}, \tag{4.5.3}$$

where β is the angle between the pipe axis and the horizontal. The results of this computation are plotted in Fig. 4.15 for turbulent flows, when X = $\mathrm{X_{tt}}$ becomes an expression involving the ratio of volumetric fluxes and fluid properties only, Chap. 1, Eq. (1.10.3):

$$X_{tt} = \left[\frac{j_L}{j_G}\right]^{0.9} \left[\frac{\rho_L}{\rho_G}\right]^{0.4} \left[\frac{\mu_L}{\mu_G}\right]^{0.1}$$

Therefore, the abscissa of Fig. 4.15 can be interpreted practically as j_L/j_G (see Fig. 1.16 in Chap. 1). The results for laminar flow were shown by Taitel and Dukler to be very similar. Note that negative Y values denote downflow; for fixed liquid and gas flowrates, i.e. at constant X, the thickness of the liquid layer is decreasing

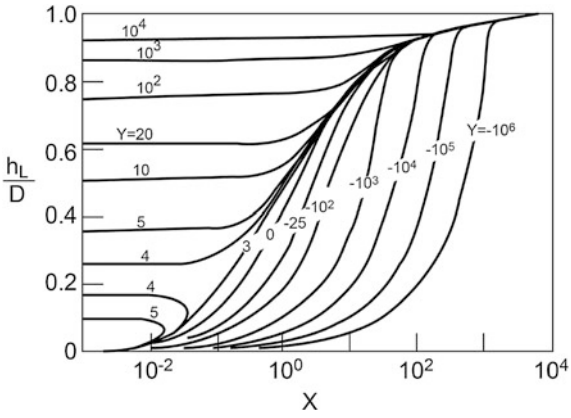

Fig. 4.15 The equilibrium level of the liquid h_L in the pipe of diameter D for various pipe inclinations β (that are embedded in Y) (Barnea 1987)

and the liquid is accelerating for decreasing inclination Y. Positive Y indicates upflow and now the film thickness increases as Y increases. Notice that there are two lines for Y = 4 and 5, which probably means that there could be multiple possible solutions.

Stability of the interface

We will next investigate whether any waves present on the interface become unstable due to the Kelvin–Helmholz instability. The Kelvin–Helmholz theory discussed in Chap. 3 provides a stability criterion for infinitesimal-amplitude waves. A simplified version of the Kelvin–Helmholz instability theory that takes into account the finite wave amplitude and the circular geometry is considered as follows. Assume a stationary solitary wave on the stratified flow interface, Fig. 4.16, and neglect the effect of surface tension. We can identify two competing forces that act on the wave crest. Gravity is the force that tends to flatten the wave and thereby stabilize the stratified configuration. The Bernoulli force, which results from the increased gas velocity above the wave and the decrease of the pressure in the narrow air gap, tends to increase the wave amplitude. Considering a small volume of fluid on the wave (darker, hatched area in Fig. 4.16), the condition for stability is reached when gravity dominates, namely when

$$(h_G - h'_G)(\rho_L - \rho_G)g\cos\beta \;\; > \frac{1}{2}\rho_G(u'^2_G - u^2_G)$$

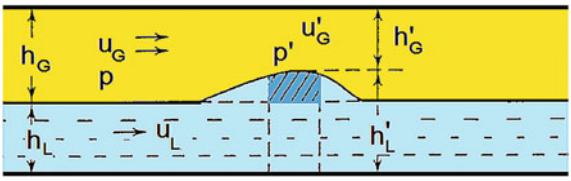

Fig. 4.16 Instability of a solitary wave in stratified flow

The criterion for stability then becomes

$$u_G < C\left[\frac{(\rho_L - \rho_G) g \cos\beta A_G}{\rho_G \frac{dA_L}{dh_L}}\right]^{1/2}, \tag{4.5.4}$$

where

$$C^2 \equiv 2\frac{(A'_G/A_G)^2}{1 + A'_G/A_G}$$

For infinitesimally small disturbances, $A'_G \approx A_G$ and $C \approx 1$ as suggested by the Kelvin–Helmholz theory. For large disturbances, the value of C depends on the liquid level. When the liquid level is very low, $C = 1$, since any disturbance is small compared to the gas cross section which is almost equal to the pipe cross section. On the other hand, when the liquid level is very high, close to the top, then any disturbance will result in closure of the gas passage; thus we take $C = 0$. For any other liquid level, Taitel and Dukler (1976) suggest a linear relation between these two extreme cases

$$C = 1 - \frac{h_L}{D}$$

Equation (4.5.4) can be written in a dimensionless form as

$$\mathrm{F}^2\left[\frac{1}{C^2}\frac{(u_G/j_G)^2 D\,(dA_L/dh_L)}{A_G}\right] < 1 \quad \text{or} \quad \mathrm{F}^2\left[\frac{1}{C^2}\frac{\tilde{u}_G^2\,(d\tilde{A}_L/d\tilde{h}_L)}{\tilde{A}_G}\right] < 1 \tag{4.5.5}$$

The term in the square parentheses is a dimensionless quantity that depends only on h_l/D, and F is a non-dimensional Froude number modified by the density ratio

$$\mathrm{F} \equiv \sqrt{\frac{\rho_G}{\rho_L - \rho_G}}\frac{j_G}{\sqrt{Dg\cos\beta}}$$

expressing the fact that waves of finite size will grow and tend to block the pipe when the balance between the Bernoulli force—tending to make the wave grow—is greater than the gravity force tending to flatten the wave. All the terms in the square brackets of Eq. (4.5.5) are functions of h_l/D, which is a function of X, Y only (as plotted in Fig. 4.15). We can plot now using Eq. (4.5.5) the transition from stratified flow to other regimes as line A with F vs X as coordinates in the Taitel and Dukler (1976) map given below, Fig. 4.17.

We are not going to enter into the details here of the derivation of the other transition criteria needed to construct the Taitel and Dukler map as similar ones will be covered in the following section regarding the Barnea map for inclined pipes. We will rather summarize the Taitel and Dukler transition criteria.

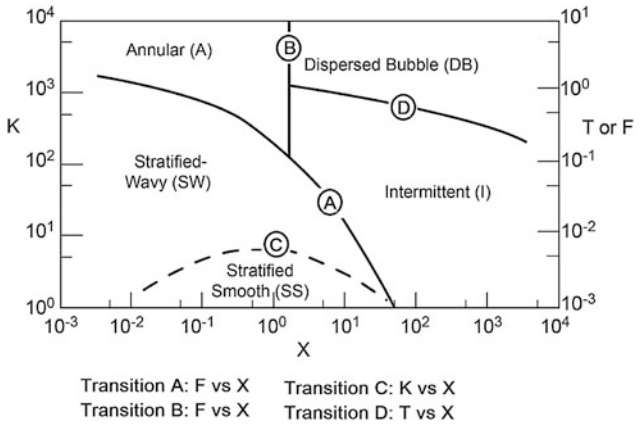

Fig. 4.17 The Taitel and Dukler (1976) flow regime map showing the transition boundaries between the flow regimes for horizontal or near-horizontal flows

The Taitel and Dukler (1976) map for near-horizontal flows

The following set of five non-dimensional numbers is used; three of these X, Y and F have already been defined and used above

$$\mathrm{X} \equiv \left[\frac{dp/dz|_{LP}}{dp/dz|_{GP}}\right]^{1/2} \tag{4.5.6}$$

$$\mathrm{Y} \equiv \frac{(\rho_L - \rho_G)g\ \sin\beta}{\left|(dp/dz)_{GP}\right|} \tag{4.5.7}$$

$$\mathrm{F} \equiv \sqrt{\frac{\rho_G}{\rho_L - \rho_G}}\frac{j_G}{\sqrt{Dg\ \cos\beta}} \tag{4.5.8}$$

In addition, we define the ratio of the frictional pressure gradient in the liquid phase to the component of the gravitational pressure gradient in the direction normal to the pipe axis

$$\mathrm{T} \equiv \frac{\left|(dp/dz)_{LP}\right|}{(\rho_L - \rho_G)g\ \cos\beta} \tag{4.5.9}$$

and the product of F times the Reynolds number for the liquid phase

$$\mathrm{K} \equiv \mathrm{F}\sqrt{\mathrm{Re}_L} = \mathrm{F}\sqrt{\frac{\rho_L D\, j_L}{\mu_L}} \tag{4.5.10}$$

Figure 4.17 Shows the Taitel and Dukler (1967) flow regime map for (Y = 0); maps for other small inclinations can be constructed. Note that the ordinate of the map can be either T, F or K, as shown under the figure.

Curve A plotted using F versus X represents the transition from stratified (S) to intermittent (I) or annular—dispersed-liquid (AD) flows that satisfies the criterion given by Eq. (4.5.5) above.

Curve B is the transition between intermittent (I) or dispersed bubble (DB) and annular-dispersed-liquid (AD) flows. This occurs at a constant value of X. It is based on the argument that the growing waves will have a sufficient liquid supply to form a slug only when the height of the liquid is sufficient, i.e. when $h_L/D \geq 0.5$. Lower liquid heights will produce an annular configuration.

Curve C is the transition line between stratified-smooth (SS) and stratified-wavy (SW) flow. It is the locus of the planes plotted in the K-X plane that satisfy

$$K = \frac{2}{\sqrt{\tilde{u}_L} \cdot \tilde{u}_G \sqrt{s}} \tag{4.5.11}$$

This criterion is based on the model by Jeffreys (1925, 1926) describing the condition for transfer of energy to the liquid to create waves: the wave velocity is estimated from the mean velocity of the liquid film and a sheltering coefficient determined from the analysis of Benjamin (1968).

Curve D, the transition between intermittent (I) and dispersed bubble (DB) flow, represents the situation when the turbulent fluctuations in the liquid balance the buoyancy that makes the gas rise according to

$$T^2 = \frac{8\tilde{A}_G}{\tilde{S}_i \tilde{u}_L^2 (\tilde{u}_L \tilde{D}_L)^{-n}} \tag{4.5.12}$$

The transition depends on the value of Y that can be calculated or obtained from Fig. 4.15.

To account for the effect of pipe roughness, the authors suggest that the (dp/dz) values be calculated using the appropriate roughness parameters.

The criteria listed above can be used to construct a flow regime map in the (j_L, j_G) plane. Such a map is shown in Fig. 4.18. The agreement with the "classical" experimental data of Mandhane et al. (1974) is quite good. It is, of course, not necessary to use a flow regime map at all. Given any one set of flow conditions (rate, pressure, line size and inclination), the flow pattern that exists for that condition can be determined rather simply by using hand calculations from the equations given above.

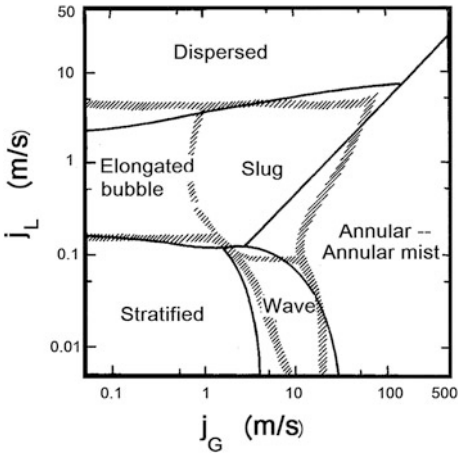

Fig. 4.18 Comparison of the Taitel and Dukler flow boundary predictions with the experimental map of Mandhane et al. (1974). Water/air, 25 °C, 1 atm, 2.5 cm diameter, horizontal. Lines: continuous line: theory: Mandhane

4.5.2 The DTB Map and Unified Model for the Whole Range of Inclinations

Building up on the previous work for horizontal flows discussed above, various criteria developed by the group were assembled in two publications (Barnea 1986, 1987) to continuously cover all inclinations in a unified model. Indeed previously existing work considered horizontal flows, near-horizontal flows and vertical flows separately, while flows in inclined tubes were rarely treated. These theories do not offer a smooth transition between vertical and horizontal flow, with all the angles included in between. In the unified model, previously formulated transition mechanisms were re-evaluated and modified and some new ones were presented to yield a complete theory for transition boundaries applicable to all angles of inclination. Although the validity of this approach may be still subject to extensive experimental testing (Taitel 1990), especially for large-diameter pipes or high pressures, it does handle the dependence of the flow pattern on the inclination angle rather well, as shown in Fig. 4.19 presenting experimental data for the flow regimes that take place as a function of the inclination of the pipe and the corresponding Barnea transition lines for horizontal, upward and downward flows. The differences made by one degree of inclination (first column of results) are striking.

The DTB unified map (Barnea 1987) is considering the following flow regimes:

- Dispersed-Bubble flow (DB) taking place at high liquid flow rates
- Annular flow (A)
- Stratified flows (ST) that can be either Smooth (SS) or Wavy (SW)
- Intermittent flows (I) that can be either Slug (SL), Elongated Bubbles (EB) or Churn (CH)
- Bubbly flows (B) at low liquid flow rates

and the following regime transitions (or bifurcations, or conditions for existence):

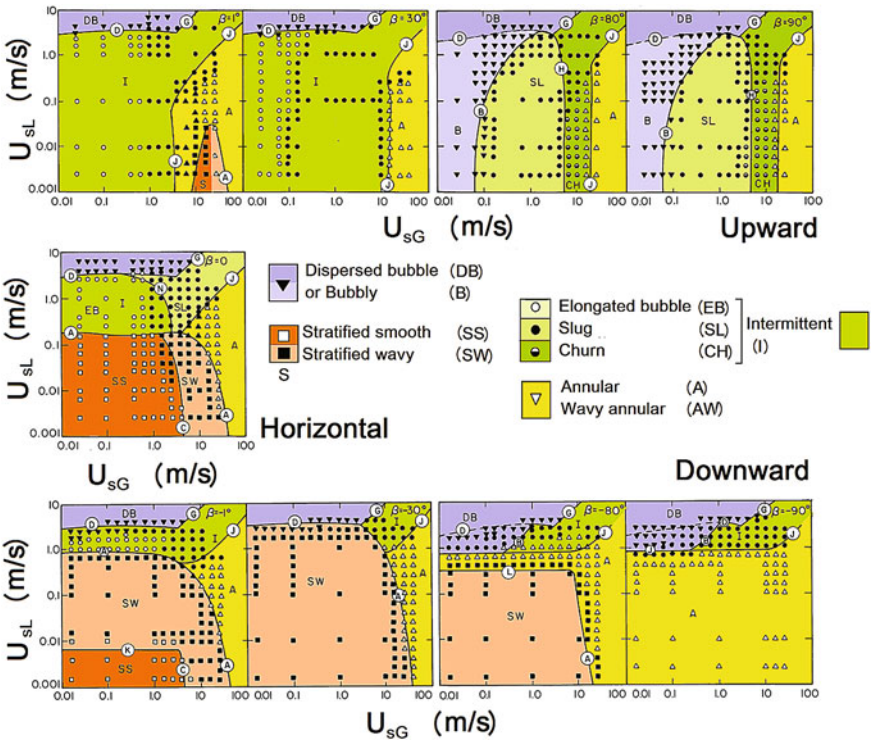

Fig. 4.19 Flow regimes in inclined pipes (Barnea, 1987). The example is drawn for air/water at atmospheric pressure and at 25 °C in a 5.1 cm diameter pipe. The symbols designate the experimental data, while the lines are the DTB map predictions. (The author is grateful to Y. Taitel and D. Barnea for providing the original figures; they are not responsible for the colour rendition of their map)

- Transition to Dispersed Bubble due to high turbulent fluctuations in the liquid (line D)
- Transition from Dispersed Bubble due to high void fraction (condition for existence of dispersed bubbles, line G)
- Stratified flow condition (line A)
- Stratified—Annular transition (line L)
- Annular—Intermittent transition (line J)
- Stratified-Smooth—Stratified-Wavy transition due to downward flow (line M)
- Stratified-Smooth—Stratified-Wavy transition due to high gas velocity ("wind," line C)
- Slug—Elongated-Bubble transition (line N)
- Slug—Churn transition (line H)
- Bubble flow—Intermittent-flow transition (line B).

The flow regime map is based on the volumetric fluxes j_k (or superficial velocities U_{sk}) of the phases, pipe diameter D, inclination to the horizontal β, and fluid properties. With many regimes and ten transition criteria, the logic for detecting the flow regime (as well as the logic of the presentation of the transition criteria) becomes quite complex; Barnea (1987) provides a logical flow chart to accomplish this. We follow essentially the logic of this chart while stressing the physics of the phenomena.

A few preliminary words can be said here about the importance of inclination with respect to gravity under certain flow conditions. If the flows are dominated by shear forces, the effects of gravity should be small and the transition criteria should be applicable to all flow directions and inclinations; an example is the transition from highly turbulent, dispersed-bubble flow to annular flow. On the contrary, when gravity dominates, the transition criteria will depend strongly on flow inclination and direction; the examples are stratified flows.

The transition A from stratified flow is modelled as shown above for the Taitel and Dukler map. The other transitions are briefly discussed below.

4.5.2.1 Transitions D and G from Dispersed-Bubble (DB) Flow

Taitel (1990) notes that there are two distinct cases of bubble flows. At very high liquid flow rates dispersed-bubble (DB) flow usually appears when the bubbles are created and dispersed by high liquid turbulence. At low flow rates, small discrete bubbles can also appear, however, and this flow regime can be designated as *Bubbly flow* denoted as B. Dispersed-bubble flows can exist at any pipe inclination, while the bubbly flow pattern is observed only in vertical or near-vertical flows and for relatively large-diameter tubes. Indeed, in small-diameter pipes the rise velocity of small bubbles exceeds the rise velocity of the Taylor bubbles and these coalesce with the Taylor bubbles creating slug flow as discussed in Sect. 4.4.1.

The *persistence* of bubble flow can result from different reasons at low or high liquid flow rates. At low liquid flow rate, the bubbles may stay separated simply for lack of coalescence forces. At high liquid flow rates, the turbulence of the liquid causes large bubbles to break up into smaller ones; this turbulent dispersion of bubbles does not allow them to agglomerate into other forms.

4.5.2.2 Case of High Flow Rates (Transitions D and G)

The maximum diameter d of stable bubbles is given by (Barnea et al. 1982b) as

$$d_C = (0.725 + 4.15 \cdot \varepsilon^{1/2}) \left(\frac{\sigma}{\rho_L}\right)^{3/5} \kappa^{-2/5} \qquad \text{with} \qquad \kappa \equiv \frac{2f_j}{D} j^2, \qquad (4.5.13)$$

where κ is the rate of turbulent kinetic energy dissipation per unit mass, and f_j is the friction factor based on the mixture velocity $j = j_L + j_G$. This equation applies to

bubbles sufficiently small to retain approximately their spherical shape. Larger bubbles tend to deform and coalesce. Barnea et al. (1982b) use the following expression for the critical size of such bubbles:

$$d_{CD} = 2\left[\frac{0.4\sigma}{(\rho_L - \rho_G)g}\right]^{1/2} \tag{4.5.14}$$

A first condition to be used as a transition criterion becomes then $d_C < d_{CD}$. However, this criterion alone is not sufficient for the persistence of bubble flow. In horizontal and inclined pipes, buoyancy makes bubbles rise and concentrate at the upper part of the pipe (*creaming*) and agglomerate to large *elongated bubbles*. The critical bubble size below which creaming is prevented is obtained comparing the buoyance forces F_B to the turbulent forces F_T which tend to disperse the bubbles in the pipe (Levich 1962). The forces in the radial direction are

$$F_B = (\rho_L - \rho_G)g\,\cos\beta\frac{\pi d^3}{6}$$

$$F_T = \frac{1}{2}\rho_L v'^2\frac{\pi d^2}{4},$$

where v' is the radial velocity fluctuations whose rms is estimated to be approximately equal to the friction velocity $u^* = \sqrt{\tau_w/\rho}$:

$$\sqrt{\overline{(v'^2)}} = u^* = j\sqrt{\frac{f}{2}}$$

Migration of the dispersed bubbles upwards will occur when $F_B > F_T$, i.e. when the bubble diameter d_{CB} obtained by equating F_B and F_T, is smaller than the bubble diameter d

$$d > d_{CB} = \frac{3}{8}\frac{\rho_L}{\rho_L - \rho_G}\frac{f j^2}{g\,\cos\beta} \tag{4.5.15}$$

In order to maintain the dispersed-bubble flow, neither distortion of the bubbles nor creaming should take place. In addition, one should consider the effect of maximum possible packing of bubbles that takes place at $\varepsilon < 0.52$. To fit into the map, this criterion should be expressed in terms of the volumetric fluxes. Assuming homogeneous flow, (using Eq. 1.9.12 of Chap. 1) we obtain the equivalent criterion in terms of phase volumetric fluxes

$$\frac{j_L}{j_G} = \frac{\varepsilon_L}{\varepsilon_G} = \frac{0.52}{0.48} \approx 1.1 \tag{4.5.16}$$

The set of transition criteria then becomes

$$d_C < d_{CD} \quad \text{and} \quad d_C < d_{CB} \quad \text{and} \quad \varepsilon < 0.52 \quad \text{or} \quad \frac{j_L}{j_G} < 1.1 \tag{4.5.17}$$

The first two conditions produce the transition boundary D in the DTB map (Fig. 4.19), while the second one the line G.

Existence of Bubbly flow (transition B)
Taitel (1990) lists the four conditions necessary for the existence of bubbly blow (B). The pipe diameter should be large or the inclination angle should be larger than a certain value *and* the void fraction should be lower than 0.25 *and* the flow should not be annular. Alternatively, we can say (Barnea 1987) that the bubbly flow will not become Intermittent (transition B). This transition bubbly to intermittent flow is discussed now; the interested reader should refer to Barnea (1987) or Taitel (1990) for the transitions *inside* the intermittent-flow area.

4.5.2.3 Transition B to Intermittent Flow

The condition ε < 0.25 can be translated again using Eq. (1.9.12) of Chap. 1 as

$$\frac{j_L}{j_G} = \frac{\varepsilon_L}{\varepsilon_G} < \frac{0.25}{0.75} = 0.33 \quad or \quad j_L < 0.33\, j_G \tag{4.5.18}$$

If the component of the free-rise velocity of small bubbles u_0 along the direction of the flow $u_0 \sin\beta$ is roughly equated to $j_G - j_L$, using again the homogeneous-flow relationship (Eq. 1.9.12 of Chap. 1), $j_L/j_G = (1-\varepsilon)/\varepsilon$, we obtain

$$j_L = j_G \frac{1-\varepsilon}{\varepsilon} - (1-\varepsilon)\, u_0 \sin\beta$$

The free-rise velocity of the bubbles is given by Harmathy (1960) as

$$u_0 = 1.53 \left[\frac{g(\rho_L - \rho_G)\sigma}{\rho_L^2}\right]^{1/4}$$

Combining the last two expressions,

$$j_L = \frac{1-\varepsilon}{\varepsilon} j_G - (1-\varepsilon) \left[\frac{g(\rho_L - \rho_G)\sigma}{\rho_L^2}\right]^{1/4} \sin\beta \tag{4.5.19}$$

One can then compute ε from Eq. (4.5.19) and make sure it is smaller than 0.25, or alternatively set ε = *0.25* in Eq. (4.5.19) and get

$$j_L < 3j_G - 1.15\left[\frac{g(\rho_L - \rho_G)\sigma}{\rho_L^2}\right]^{1/4} \tag{4.5.20}$$

as the condition for existence of bubbly flow for the transition from slug to bubbly flow. This is line B in the Barnea map.

4.5.2.4 Transition J from Annular to Intermittent Flow

The transition from annular to intermittent flow is assumed to occur (Barnea 1986) as a result of either: (a) a gas velocity decrease that reduces the interfacial shear allowing the liquid to flow downward creating intermittent flow (flow reversal); or (b) a void fraction decrease making the thicker annulus of liquid to collapse and block the flow of gas (high liquid holdup case). These two cases are discussed in detail by Barnea (1986) and by Taitel (1980) and lead to transition J.

Transition L: stratified to annular in steep downflow

So far annular flow was assumed to exist due to the violent action of the gas stream in dispersing the liquid all around the pipe periphery. The exception to this type of flow is the special case of flow down a steep incline at low gas velocities. Usually under these conditions one would expect stratified flow to take place. However, at steep downward inclinations the liquid level is small, the liquid velocity is very high and the liquid tends to spread around the pipe periphery resulting in annular flow. This type of annular flow takes place within the region of the stratified/non-stratified transition. It is designated as transition L in Fig. 4.19; for more details see Barnea (1987).

In summary: The first step is to check whether we have dispersed bubble flow (transitions D or G). If the flow is not DB, we should check next whether it is stratified (transition A). If the flow is neither of the above, we check for annular flow (transition J). Finally, if the flow is also not annular, it will be intermittent.

Figure 4.20 shows some of the transitions (A, C, M, L) in a non-dimensional map where F, K, W and Z are plotted versus the non-dimensional liquid height h_L/D. Two of the non-dimensional parameters, F and K given again below, were

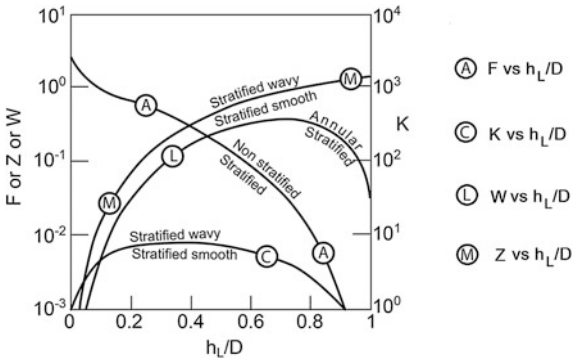

Fig. 4.20 Generalized transition boundaries according to the DTB work (Barnea 1987)

already used for the Taitel and Dukler map (Sect. 4.5.1, Eqs. (4.5.8) and (4.5.10), respectively) and also govern the A and C transitions. The new parameters W and Z control the transitions M and L, respectively and are given as

$$\mathrm{F} \equiv \sqrt{\frac{\rho_G}{\rho_L - \rho_G}} \frac{j_G}{\sqrt{Dg\ \cos\beta}}, \quad \mathrm{K} \equiv \mathrm{F}\sqrt{\mathrm{Re}_L} = \mathrm{F}\sqrt{\frac{\rho_L D\, j_L}{\mu_L}}, \quad \mathrm{W} \equiv \frac{j_L}{\sqrt{gD}},$$
$$\mathrm{Z} \equiv \frac{[dp/dz]_{LP}}{\rho_L g\ \cos\ \beta}$$

Z is similar to the Taitel and Dukler T, except that now the nominator has a directional sign. The TDB map has the non-dimensional liquid height (equivalent to the liquid fraction) as abscissa, while the Taitel and Dukler map has X that is proportional to j_L/j_G.

4.6 Flow Regime Maps and Transition Criteria for Vertical Upwards Flow—Ishii and Co-workers

The work by Dukler, Taitel, Barnea (DTB) and their collaborators discussed in Sect. 4.5 produced a unified map and criteria for all inclinations. Many researchers have been interested in vertical flows but we will concentrate here on the work of Ishii, Mishima, Hibiki and co-workers whose reference applications were mostly for two-phase flows in nuclear water reactors and their point of view is somewhat different. Indeed Mishima and Ishii (1984) note that the transition criteria in terms of the superficial velocities developed by the DTB group may not be consistent with the framework of the two-fluid formulation of the conservation equations (used in the modern codes developed for reactor safety analysis and other transient applications, including pipelines). In this case the void fraction and other parameters such as the interfacial area as inputs to the models are better suited to their structure. They also expect the flow regimes to be controlled mainly by the void fraction and the interfacial area rather than the superficial velocities. While it is true that the void fraction and the superficial velocities are uniquely related under steady-state conditions, the steady-state relationship may not apply under rapid transients. Thus criteria in terms of the void fraction should be preferable as these variables are more amenable to describe the transient situations. The transition criteria proposed by Mishima and Ishii (1984) are briefly discussed below.

Bubbly-to-slug flow transition
The very simple Mishima and Ishii (1984) criterion

$$\varepsilon \approx 0.3$$

is the one or very close to the one based on bubble-packing geometrical considerations, already discussed in Sect. 4.4.1. This transition criterion expressed in

terms of the volumetric fluxes (as discussed in Sect. 4.4.1) is plotted as line A in Fig. 4.20.[2]

Slug-to-churn flow transition

Figure 4.12 shows the control area used by Ishii and Mishima who postulate that the transition occurs when the mean void fraction over the entire control volume ε exceeds that of the average value over the Taylor-bubble section ε_{sb}, which essentially says that the void fraction in the aerated area exceeds the void fraction in the Taylor-bubble region—the aerated area "becomes Taylor bubble also." The authors also give as an explanation that, just before the transition, the Taylor bubbles almost touch each other, the liquid slugs become unstable due to the strong wake effect of the downstream bubble, leading to regime transition. Without entering into the long derivation presented, we summarize here the procedure used to obtain the transition criterion.

The local void fraction—or the film thickness—along the Taylor bubble is first established using a Taylor-bubble or gas slug (subscript gs) velocity based on the drift flux (DF) model

$$u_{gs} = C_0 j + 0.35\sqrt{\frac{gD\Delta\rho}{\rho_L}}, \tag{4.6.1}$$

where the second term is the Taylor-bubble velocity in stagnant flow and the first adds the volumetric flux of the mixture corrected for the radial profile by the DF distribution parameter C_0.

The Bernouilli equation for the pressure in the liquid film, continuity, and equality of pressures in the liquid film and the bubble are then used to obtain the axial void fraction distribution in the Taylor-bubble region

$$\varepsilon(h) = \frac{\sqrt{\frac{2gh\,\Delta\rho}{\rho_L}}}{\sqrt{\frac{2gh\,\Delta\rho}{\rho_L}} + + (C_0 - 1)j + 0.35\sqrt{\frac{gD\,\Delta\rho}{\rho_L}}} \tag{4.6.2}$$

The average value of this axial void fraction ε_m is obtained by integration; a complex expression results, but it is numerically approximated by

$$\varepsilon_m \approx 1 - 0.813 \cdot X_I^{3/4} \tag{4.6.3}$$

with

$$X_I \equiv \sqrt{\frac{\rho_L}{2g\,\Delta\rho\,L_b}} \cdot \left[(C_0 - 1)j + 0.35\sqrt{\frac{gD\Delta\rho}{\rho_L}}\right]. \tag{4.6.4}$$

[2]The labelling of the transition lines is different in this section from that used in the DTB map.

The expression for the Taylor-bubble length L_b that is contained in X_I is obtained by assuming that the void fraction at the bottom of the Taylor bubble is equal to ε_{sb}, This void fraction is obtained from a force balance (gravity vs shear) in the liquid film around the Taylor bubble that yields the following expressions relating the terminal (i.e. under equilibrium between gravity and shear) film velocity u_{fsb}, and the corresponding void fraction ε_{sb} (the subscript *sb* stands for the tail-end of the slug bubble). This force balance finally yields $u_{fsb,}$ and ε_{sb}

$$u_{fsb} = \frac{\varepsilon_{sb} u_{gs} - j}{1 - \varepsilon_{sb}} \tag{4.6.5}$$

$$\varepsilon_{sb} = \frac{3ab(1 - \varepsilon_{sb})^{1.67}}{C_0 j + 0.35b} \tag{4.6.6}$$

with

$$a \equiv \left(\frac{g\ \Delta\rho\ D^3}{\rho_L u_L^2} \right)^{1/18} \approx 3, \quad b \equiv \sqrt{\frac{g\ \Delta\rho\ D}{\rho_L}}, \quad \Delta\rho \equiv (\rho_L - \rho_G) \tag{4.6.7}$$

The approximation for a is valid for weakly viscous fluids such as water only.

The expression for $\varepsilon(h)$ of Eq. (4.6.2) for $h = L_b$ is equated to ε_{sb} from Eq. (4.6.6), $\varepsilon(L_b) = \varepsilon_{sb}$, leading to an expression for L_b

$$\sqrt{\frac{2g\ \Delta\rho\ L_b}{\rho_L}} = j + 075\, ab \tag{4.6.8}$$

that can be used to extract L_b and insert in Eq. (4.6.4), leading to

$$X_I = \frac{1}{j + 0.75ab} \left[(C_0 - 1)j + 0.35 \sqrt{\frac{gD\Delta\rho}{\rho_L}} \right]$$

The criterion for slug-churn transition is $\varepsilon \geq \varepsilon_m$ or

$$\varepsilon \geq 1 - 0.813\, X_I^{3/4} \quad \text{or} \quad \varepsilon \geq 1 - 0.813 \left[\frac{(C_0 - 1)j + 0.35\, b}{j + 0.75\, ab} \right]^{3/4} \tag{4.6.9}$$

where the coefficients a and b are given by Eqs. (4.6.7). This transition line is plotted in Fig. 4.21 as line B.

Churn-to-annular flow transition

Two transition mechanisms are postulated, namely flow reversal of the liquid films along large bubbles and destruction of large waves or liquid slugs; transition criteria are developed for each. For flow direction reversal in the liquid film flowing along the wall, the starting point is $j_L = 0$. Using DF correlations, this leads to the criterion

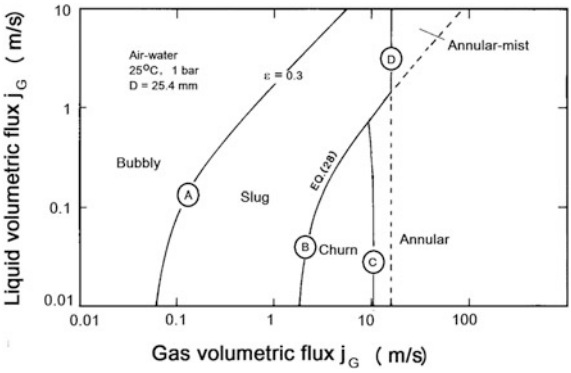

Fig. 4.21 Flow regime map developed using the Mishima and Ishii criteria

$$j_G \geq \sqrt{\frac{g\,\Delta\rho\,D}{\rho_G}}\cdot(\varepsilon - 0.11) \tag{4.6.10}$$

where the void fraction must also satisfy the slug-flow criterion, Eq. (4.6.9). Equation (4.6.10) is plotted as line C in Fig. 4.20.

For destruction of the liquid slug by liquid droplet entrainment, droplet entrainment is considered via a force balance on the liquid wave crest opposing the shearing force of the vapour drag and the surface tension that tends to keep the surface flat; this yields

$$\frac{\mu_L j_G}{\sigma}\sqrt{\frac{\rho_G}{\rho_L}} = \mathrm{N}_{\mu L}^{0.8}$$

with

$$\mathrm{N}_{\mu L} \equiv \mu_L \left[\rho_L \sigma \sqrt{\frac{\sigma}{g\,\Delta\rho}}\right]^{1/2}$$

valid for low-viscous fluids at relatively high liquid Reynolds number. The criterion is expressed as

$$j_G \geq \left(\frac{\sigma g \Delta\rho}{\rho_G^2}\right)^{1/4} \mathrm{N}_{\mu L}^{-0.2} \tag{4.6.11}$$

and is applicable to large-diameter tubes, i.e. when

$$D > \frac{\sqrt{\frac{\sigma}{g\,\Delta\rho}}\cdot \mathrm{N}_{\mu L}^{-0.4}}{\left[\frac{1-0.11\cdot C_0}{C_0}\right]^2}$$

Figure 4.20 shows this limiting condition as line D.

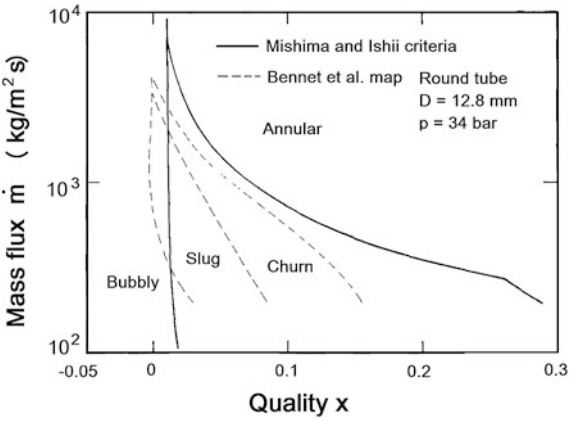

Fig. 4.22 Flow regime map obtained using the Mishima and Ishii criteria and comparison with the empirical map of Bennet et al. (1965) for 34 bar, steam-water flow entering under subcooled-inlet conditions

Mishima and Ishii maps

Figure 4.21 shows the application of the criteria developed by Ishii and Mishima and the resulting map for air-water flow at atmospheric conditions. This map could be compared with the TDB map, Fig. 4.19, in Sect. 4.5.2.

Figure 4.22 shows a flow regime map obtained using the relationships of Mishima and Ishii and compares it to the empirical flow regime map obtained by Bennet et al. (1965), Fig. 4.3, for steam-water flow at high pressure.

Hibiki and Mishima (1996) extended the Mishima-Ishii model to vertical upward flows in narrow rectangular channels.

References

Baker O (1954) Simultaneous flow of oil and gas. Oil Gas J 2:185–195

Baker A, Nielsen K, Gabb A (1988) Pressure loss, liquid holdup calculations developed. Oil Gas J 14(March):55

Barbosa PR, Crivelaro KC, Seleghim P Jr (2010) On the application of self-organizing neural networks in gas-liquid and gas-solid flow regime identification. J Braz Soc Mech Sci Eng 32 (1):15–20

Barnea D (1986) Transition from annular mow and from dispersed-bubble flow—unified models for the whole range of pipe inclination. Int J Multiphase Flow 5:733–744

Barnea D (1987) A unified model for prediction of flow pattern transitions in the whole range of pipe inclination. Int J Multiphase Flow 13:1–12

Barnea D, Shoham O, Taitel Y, Dukler AE (1980) Flow pattern transition for gas-liquid flow in horizontal and inclined pipes. Comparison of experimental data with theory. Int J Multiphase Flow 6(3):217–225

Barnea D, Shoham O, Taitel Y (1982a) Flow pattern transition for vertical downward two phase flow. Chem Eng Sci 37:741–746

Barnea D, Shoham O, Taitel Y (1982b) Flow pattern transition for downward inclined two phase flow; horizontal to vertical. Chem Eng Sci 37(5):735–740

Barnea D, Luninsky Y, Taitel Y (1983) Flow pattern in horizontal and vertical two phase flow in small diameter pipes. Can J Chem Eng 61:617–620

Benjamin TB (1968) Gravity currents and related phenomena. J Fluid Mech 2:209–248
Bennett AW, Hewitt GF, Kearsey HA, Keeys RKF (1965) Flow visualization studies of boiling at high pressure. Proc Inst Mech Eng Conf Proc 180(3):260–283
Brauner N, Barnea D (1986) Slug/churn transition in upward gas-liquid flow. Chem Eng Sci 41 (1):159–163
Chen XT, Brill JP (1997) Slug to churn transition in upward vertical two-phase flow. Chem Eng Sci 52(23):4269–4272
Cheng L, Ribatski G, Thome JR (2008) New prediction methods for CO_2 evaporation inside tubes, Part 2-An updated general flow boiling heat transfer model based on flow patterns. Int J Heat Mass Transf 51:125–135
Collier JG, Thome JR (1994) Convective boiling and condensation, 3rd edn. Oxford University Press
Crawford T, Weisman J (1984) Two-phase (vapor-liquid) flow pattern transitions in ducts of non-circular cross-section and under diabatic conditions. Int J. Multiphase Flow 10:385–391
Crawford TJ, Weinberger CB, Weisman J (1985) Two-phase flow patterns and void fractions in downward flow. Part I: Steady-state flow patterns. Int J Multiphase Flow 11(6):761–782
Davis RM, GI Taylor (1950) The mechanism of large bubbles rising through liquids in tubes. Proc R Soc Lond, Ser A 200:375
El Hajal J, Thome JR, Cavallini A (2003) Condensation in horizontal tubes, Part 1: Two-phase flow pattern map. Int J Heat Mass Transf 46:3349–3363
Frankum DP, Wadekar VV, Azzopardi BJ (1997) Two-phase flow patterns for evaporating flow. Exp Thermal Fluid Sci 15(3):183–192
Gomez LE, Shoham O, Schmidt Z, Chokshi RN, Northug T (2000) Unified mechanistic model for steady-state two-phase flow: horizontal to vertical upward flow. SPE J 5(03):339–350
Govan AH, Hewitt GF, Richter HJ, Scott A (1991) Flooding and churn flow in vertical pipes. Int J Multiphase Flow 17(1):27–44
Grant IDR, Chisholm D (1979) Two-phase flow on the shell-side of a segmentally baffled shell-and-tube heat exchanger. J Heat Transf 101(1):38–42
Harmathy TZ (1960) Velocity of large drops and bubbles in media of infinite or restricted extent. AIChE J 6:281–288
Hawkes NJ, Lawrence CJ, Hewitt GF (2000) Studies of wispy-annular flow using transient pressure gradient and optical measurements. Int J Multiphase Flow 26(10):1565–1582
Hewitt GF (1982) Liquid-gas systems. In: Hetsroni G (ed) Handbook of multiphase systems. Hemisphere, Washington, DC
Hewitt GF, Roberts DN (1969) Studies of two-phase flow patterns by simultaneous X-ray and flash photography. Atomic Energy Research Establishment report AERE-M2159
Hurlburt ET, Hanratty TJ (2002) Prediction of the transition from stratified to slug and plug flow for long pipes. Int J Multiphase Flow 28:707–729
Ito K, Inoue M, Ozawa M, Shoji M (2004) A simplified model of gas-liquid two-phase flow pattern transition. Heat Transf Asian Res 33(7):445–461
Jayanti S, Hewitt GF (1992) Prediction of the slug-to-churn flow transition in vertical two-phase flow. Int J Multiphase Flow 18(6):847–860
Jeffreys H (1925) On the formation of water waves by wind. Proc R Soc Lond Ser A (Containing Papers of a Mathematical and Physical Character) 107(742):189–206
Jeffreys H (1926) On the formation of water waves by wind (second paper). Proc R Soc Lond Ser A (Containing Papers of a Mathematical and Physical Character) 110(754):241–247
Johnston AJ (1985) Transition from stratified to slug regime in countercurrent flow. Int J Multiphase Flow 11:31–41
Jones OC (1973) Statistical considerations in heterogeneous two-phase flowing systems. Doctoral dissertation, Rensselaer Polytechnic Institute, USA
Kaji R, Azzopardi BJ (2010) The effect of pipe diameter on the structure of gas/liquid flow in vertical pipes. Int J Multiphase Flow 36(4):303–313
Kandlikar SG (2002) Fundamental issues related to flow boiling in minichannels and microchannels. Exp Them Fluid Sci 26:389–407

Kattan N, Thome JR, Favrat D (1998) Flow boiling in horizontal tubes, Part I: development of a diabatic two-phase flow pattern map. ASME J Heat Transf 120:140–147
Kawahara A, Chung PY, Kawaji M (2002) Investigation of two-phase flow pattern, void fraction and pressure drop in a microchannel. Int J Multiphase Flow 28(9):1411–1435
Levich VG (1962) Physicochemical hydrodynamics. Prentice Hall
Matuszkiewicz A, Flamand JC, Boure JA (1987) The bubble-slug flow pattern transition and instabilities of void fraction waves. Int J Multiphase Flow 13:199–217
McQuillan KW, Whalley PB (1985) Flow patterns in vertical two-phase flow. Int J Multiphase Flow 11(2):161–175
Mi Y, Ishii M, Tsoukalas LH (1998) Vertical two-phase flow identification using advanced instrumentation and neural networks. Nucl Eng Design 184(2):409–420
Milenkovic R, Fehlman M, Sigg B, Yadigaroglu G (2006) Frames from a movie made at PSI, Switzerland
Mishima K, Hibiki T (1996) Some characteristics of air-water two-phase flow in small diameter vertical tubes. Int J Multiphase Flow 22(4):703–712
Mishima K, Ishii M (1983) Flow regime transition criteria consistent with two-fluid model for vertical two-phase flow. [PWR]. Argonne National Lab, IL (USA)
Mishima K, Ishii M (1984) Flow regime transition criteria for upward two-phase flow in vertical tubes. Int J Heat Mass Transf 27(5):123–731
Nicklin DJ (1962) Two-phase bubble flow. Chem Eng Sci 17(9):693–702
Nicklin DJ, Davidson JF (1962) The onset of instability in two-phase slug flow. In: Proceedings of the symposium on two-phase fluid flow. Institution of Mechanical Engineers, London, Paper No. 4
Nusselt W (1916) The surface condensation of water vapour. VDI Z 60:541–546
Oddie G, Shi H, Durlofsky LJ, Aziz K, Pfeffer B, Holmes JA (2003) Experimental study of two and three phase flows in large diameter inclined pipes. Int J Multiphase Flow 29(4):527–558
Ohnuki A, Akimoto H (2000) Experimental study on transition of flow pattern and phase distribution in upward air–water two-phase flow along a large vertical pipe. Int J Multiphase Flow 26(3):367–386
Ouyang LB, Aziz K (1996) Development of new wall friction factor and interfacial friction factor correlations for gas/liquid stratified flow in wells and pipes. Paper SPE 35679 presented at the 1996 SPE western regional meeting, Anchorage, 22–24 May 1996
Palen JW, Breber G, Taborek K (1979) Prediction of flow regimes in horizontal tube-side-condensation. Heat Transf Eng 1(2):47–57
Porteous A (1969) Prediction of upper limit of slug flow regime. British Chemical Engineering 14 (9):117–119
Ribatski G, Thome JR (2007) Two-phase flow and heat transfer across horizontal bundles. A review. Heat Transf Eng 28(6):508–524
Rosa ES, Flora BF, Souza MASF (2012) Design and performance prediction of an impedance void meter applied to the petroleum industry. Meas Sci Technol 23:055304–055328. doi:10.1088/0957-0233/23/5/055304
Rouhani SZ, Sohal MS (1983) Two-phase flow patterns: A review of research results. Prog Nucl Energy 11(3):219–259
Sakaguchi T, Akagawa K, Hamaguchi H, Imito M, Ishida S (1979) Flow regime maps for developing steady air water two-phase flow in horizontal tubes. Mem Fac Eng Kobe Univ 25:192–202
Scott DS (1963) Properties of concurrent gas-liquid flow. In: Advances in chemical engineering, vol 4. Academic Press, New York
Serizawa A, Feng Z, Kawara Z (2002) Two-phase flow in microchannels. Exp Thermal Fluid Sci 26(6):703–714
Spedding PL, Nguyen VT (1980) Regime maps for air water two phase flow. Chem Eng Sci 35 (4):779–793
Taitel Y (1990) Flow pattern transition in two phase flow. In: 9th international heat transfer conference, vol 1, Jerusalem, Israel, 19–24 Aug 1990, pp 237–254 (Keynote lecture)

Taitel Y, Barnea D (1983) Counter current gas-liquid vertical flow, model for flow pattern and pressure drop. Int J Multiphase Flow 9:637–647
Taitel Y, Barnea D (2016) Modeling of gas liquid flow in pipes. In: Thome J (ed) Encyclopedia of two-phase heat transfer and flow. I. Fundamentals and methods, vol 1. World Scientific Publishers, New Jersey
Taitel Y, Dukler AE (1976) A model for predicting flow regime transitions in horizontal and near horizontal gas-liquid flow. AIChE J 22(1):47–55
Taitel Y, Dukler AE (1977) Flow regime transitions for vertical upward gas-liquid flow: A preliminary approach through physical modeling. In: AIChE 70th annual meeting
Taitel Y, Lee N, Dukler AE (1978) Transient gas-liquid flow in horizontal pipes: Modeling the flow pattern transitions. AIChE J 24(5):920–934
Taitel Y, Barnea D, Dukler AE (1980) Modelling flow pattern transitions for steady upward gas-liquid flow in vertical tubes. AIChE J 26(3):345–354
Triplett KA, Ghiaasiaan SM, Abdel-Khalik SI, Sadowski DL (1999) Gas–liquid two-phase flow in microchannels, Part I: two-phase flow patterns. Int J Multiphase Flow 25(3):377–394
Ullmann A, Brauner N (2007) The prediction of flow pattern maps in minichannels. Multiphase Sci Technol 19(1)
Wallis GB (1969) One-dimensional two-phase flow. McGraw-Hill Companies
Weisman J, Kang SY (1981) Flow pattern transitions in vertical and upwardly inclined limes. Int J Multiphase Flow 7:271–291
Weisman J, Duncan D, Gibson J, Grawford T (1979) Effect of fluid properties and pipe diameter on two-phase flow patterns in horizontal lines. Int J Multiphase Flow 5:437–462
Whalley PB, Hedley BD, Davidson JF (1972) Gas hold-up in bubble columns with liquid flow. VDI Berichte (No. 182):57–61
Xu GP, Tso CP, Tou KW (1998) Hydrodynamics of two-phase flow in vertical up and down-flow across a horizontal tube bundle. Int J Multiphase Flow 24(8):1317–1342
Zuber N, Findlay J (1965) Average volumetric concentration in two-phase flow systems. J Heat Transf 87(4):453–468

Chapter 5
Void Fraction—Empirical Methods

George Yadigaroglu

5.1 Introduction—the Empirical Methods

The *cross-sectional and time*-average void fraction $\langle\varepsilon\rangle$ (defined in Chap. 1) is the quantity of interest in practical, industrial applications of two-phase flow. For example, it determines the amount of liquid present in the core of a boiling water reactor (and therefore its neutronic state) or the "holdup" of liquid in a pipeline,[1] i.e. the volume fraction of liquid in the flowing mixture. The pressure gradient or pressure drop computation involves the void fraction, in particular when it is dominated by the gravitational term. Thus, we must have methods for predicting it.

In the present chapter dealing with the void fraction and in the following chapter on pressure drop we will discuss the empirical methods used to estimate these. Usually, these do not consider the flow regime, which, however, as we discussed in Chap. 1, is inherent or indirectly present to some extent in the empirical methods, as the variables that determine the void fraction and the pressure drop also largely determine the flow regime. In Chap. 2 we introduced phenomenological or mechanistic modelling considering the topology of the flow, i.e. the flow regime. The void fraction and the pressure drop can be determined for each flow regime separately by modelling mechanistically the situation corresponding to the particular regime. This may lead to better, more accurate predictions. Phenomenological methods are, however, more difficult to use and most often more difficult to insert in computer codes. They will be dealt with in another volume.

In this chapter and in Chap. 6 we will cover the most often used empirical methods for predicting the void fraction and the flow regime. These methods were developed

[1]The term *liquid holdup* is more usual in the petrochemical industries, denoting simply the liquid fraction.

G. Yadigaroglu (✉)
ETH Zurich, Zurich, Switzerland
e-mail: yadi@ethz.ch

G. Yadigaroglu and G.F. Hewitt (eds.), *Introduction to Multiphase Flow*,
Zurich Lectures on Multiphase Flow, DOI 10.1007/978-3-319-58718-9_5

for *mixture* models and are traditionally linked to homogeneous or separated flow models and formulations of the conservation equations of two-phase flow[2] that we introduced in Chap. 2. By extension, they are often used, however, also with two-fluid models where they may be substitutes for the closure laws needed in such models or they may be used to derive the closure laws needed. For example, the shear between the liquid and the wall may be obtained from an empirical, mixture pressure-gradient model or correlation. Indeed, in most situations, there is no direct way of measuring the shear between the wall and a phase.

In this chapter and Chap. 6 we deal mainly with relatively large-diameter ducts such as those used in the thermal and petrochemical industries. The extensive work related to measurements and empirical correlation of void fraction and pressure drop and the very numerous corresponding publications practically ceased in the 80s where the interest shifted to microchannels used for electronic equipment and chip cooling and similar applications or small channels used in refrigeration systems. These are treated elsewhere.

5.2 Void Fraction Measurement Techniques

Before considering the various empirical methods available for estimating the void fraction, we will give a brief survey on the experimental methods available for measuring it. In Chap. 1, we already mentioned the methods available for each type of void fraction, namely point (local optical or conductivity probes), chordal (radiation attenuation methods), cross-sectional-average (e.g. multi-beam radiation attenuation methods), and volume average measurements (e.g. quick closing valves). This discussion will not repeated here; additional possibilities will be presented. Only the well-established, classical techniques will be briefly discussed leaving the advanced methods to another volume. For exhaustive reviews of void fraction (and other two-phase flow parameter) measurement methods, the reader is referred to Hewitt (1978), Hewitt and Whalley (1980), Banerjee and Lahey (1981), Delhaye (1981), Delhaye and Cognet (1984), etc.

5.2.1 Photographic Techniques

Photographic techniques are relatively simple to use and can provide void or liquid fraction information if the dispersed phase is not densely distributed, so that the

[2]As discussed in Chap. 1, the term *mixture* is most of the time used to denote the two (or more) phases flowing together and does not necessarily imply that these are intimately *mixed*. The term *separated flow* is often used loosely to denote two-phase flows where the two phases have different average velocities in contrast to the *homogeneous flows*, where the phases have the same average velocity.

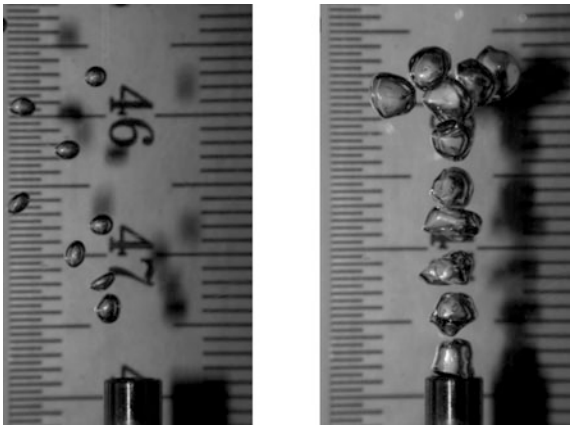

Fig. 5.1 Photographs of bubbles near the exit of a special injector designed to produce bubbles of given sizes (Milenkovic 2005)

field of view is not obstructed by the dispersed phase itself. Bubbly flows with very low void fractions lend themselves to such photographic measurement of the void fraction, provided that a transparent test section can be used. The same is true for highly dispersed liquid flows. An example of photographic recording of the void fraction is given in Fig. 4.11 of Chap. 4. Figure 5.1 shows another photographic recording of a few bubbles.

With conventional photographic techniques the depth of field is necessarily limited. Fairly short exposure times (as low as microseconds) may have to be used even for particles moving at modest speed, especially if they are small. Successive exposures on the same film can provide also information on particle speed and direction. The disadvantages regarding the depth of field are overcome when laser holographic techniques are used (e.g. Hawighorst 1984; Peterson et al. 1984). A pulsed ruby laser (20 ns) can be used to obtain a short-exposure, three-dimensional hologram, which is then reconstructed using a He–Ne continuous laser and examined photographically: the hologram is photographed by focusing the camera on narrow slices of the field. In this manner, truly three-dimensional instantaneous information is obtained and can be (painstakingly) analysed.

5.2.2 Optical or Electrical Techniques

Optical fibre sensors can be used to detect the instantaneous local presence of a phase, as already discussed in Chap. 1. The competing conductivity probes rely on the conductivity of the liquid to detect its local presence. Gases are normally not conducting, while certain liquids are or can be made conductive by addition of salts: a miniature resistive probe detects the presence of the conducting liquid between two electrodes. One of the electrodes is often a protruding needle isolated from a

coaxial sheath. The principle as well as the electronic realization are very simple. Electrochemical effects may, however, disturb the measurements.

Hot-wire anemometers, instruments very often used in gas flows, deliver a widely different signal when their sensing wires are immersed in liquid or gas phases as the heat transfer from the hot wire depends on the phase surrounding it. Thus they can be used as local void fraction detectors. They are usually, however, fragile. Hot surface anemometers are more rugged, but less suitable for such measurements.

One must note that the signal from all local, probes is more or less deformed due to the piercing of the liquid–gas interfaces by the probes.

5.2.3 *Techniques for Cross-Sectional Averages*

The multiple-beam radiation attenuation technique was mentioned in Chap. 1. Another possibility is the neutron scattering technique that uses a fast epithermal neutron beam and measures the scattered and transmitted neutrons, Fig. 5.2. The intensity of the scattered beam depends primarily on the amount of hydrogenous material in the cross section; thus, it is inversely proportional to the voids in the cross section.

Several methods for obtaining directly cross-sectional average values have been proposed (Banerjee and Lahey 1981). We will briefly discuss here only the electrical impedance method. The method is based on the fact that the impedance (resistance and capacitance) measured between two electrodes immersed in a two-phase mixture depends on the void fraction. To minimize the important sensitivity to liquid-phase resistivity changes, one uses a high-frequency excitation, so that the impedance is mainly capacitive. There is still, however, strong dependence of the dielectric constant of the liquid phase on temperature, and dependence of the dielectric constant of the two-phase mixture upon flow regime, i.e. the distribution of the two phases.

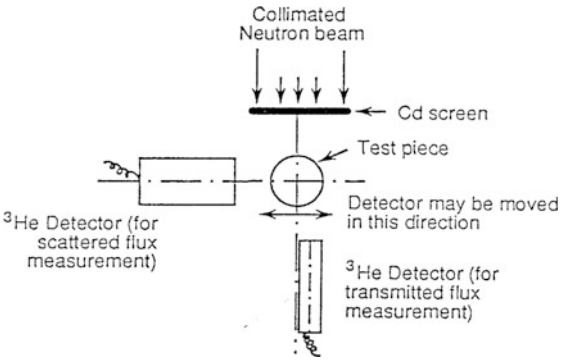

Fig. 5.2 Neutron scattering method for void fraction measurements (Rousseau and Riegel 1981; Banerjee et al. 1979)

According to the classical results of Maxwell, in uniform bubbly flow, the dielectric constant of the mixture, e, depends on the void fraction according to:

$$\frac{e - e_L}{e + 2e_L} = \langle \varepsilon_G \rangle \frac{e_L - e_G}{e_G + 2e_L},$$

where e_L and e_G are the dielectric constants of the two phases. In uniform droplet flow:

$$\left(\frac{e - e_G}{e + 2e_G}\right) = \langle \varepsilon_L \rangle \frac{e_L - e_G}{e_L + 2e_G}.$$

Thus the relationship between the measured mixture dielectric constant and average void fraction must, in general, be obtained from calibrations. Although quite complex impedance techniques attempting to eliminate some of the shortcomings mentioned have been developed, simpler techniques seem also to give satisfactory results, at least under certain conditions. An example is the impedance probe discussed by Andreussi et al. (1988) using two simple, ring electrodes flush mounted to the (non-conducting) tube wall, 1.5–2.5 diameters apart.

Cross-sectional averaging of local measurements

If the local void fraction has been measured in a sufficient number of points in the cross section, an average can be performed. In case of axisymmetric flow, measurement of a void fraction profile suffices. Figure 5.3 shows local void fraction profiles measured with an optical probe; it is also shown here to give the reader a

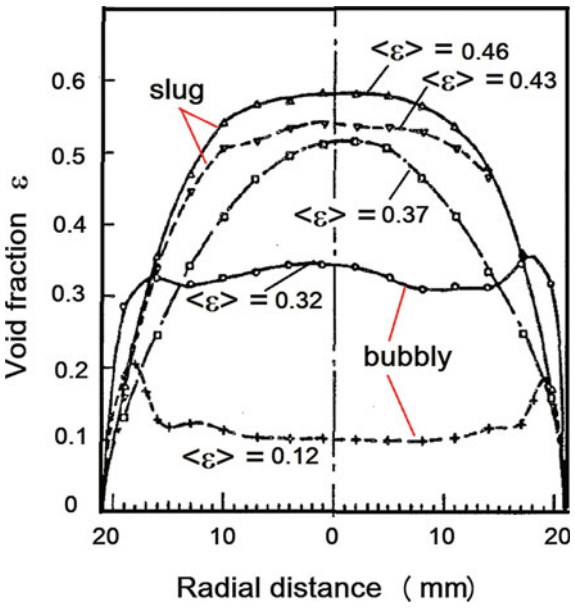

Fig. 5.3 Local void profiles measured for varying average void fraction (Gallaup and Delhaye 1976)

feeling regarding the distribution of the phases. The agreement between the cross-sectional averages calculated from these values and average measurements with a radiation absorption technique were good (Gallaup and Delhaye 1976).

5.2.4 Volume Average Void Fraction

Analytically, one usually deals with cross-sectional averages of the void fraction. (There are problems, however, when volume averages may be of interest, for example in level swell problems.) On the contrary, it is relatively easier to measure the volume average void fraction over a length of the test section. Such measurements are most interesting when the void fraction does not change rapidly over the length of the section. At the limit, as the length over which the void fraction is measured shrinks, one obtains an approximation of the cross-sectional average. Two such methods are widely used: the first one consists of measuring the pressure drop and extracting void fraction information from it. The frictional and acceleration pressure drops are calculated using a suitable model and extracted from the total measured pressure drop to arrive at the gravitational component; the void fraction can then be calculated, as we will see in Chap. 6. The method is usable only when the pressure drop is dominated by the gravitational term. Otherwise, the uncertainty in the frictional and acceleration corrections is too great. In fact one needs simultaneous independent measurements of the pressure drop *and* of the void fraction to arrive at correlations of both the frictional pressure drop and of the void fraction.

Quick Closing Valve Method

This second method consists of isolating very rapidly a segment of the test section by quick closing valves and measuring its liquid content. This method has been used for decades, and very rapidly closing valves are available (Agostini et al. 1969). Typical closing times for a 2-1/2 in valve can be 15 ms. The experiments with quick closing valves may have to be repeated many times to arrive at appropriately time- or ensemble-averaged values. This is particularly true in intermittent flows.

The method based on quick closing valves is used mostly to calibrate other techniques. It can be very accurate if care is taken to close the valves rapidly and simultaneously. At high void fractions, the accuracy of the method deteriorates due to the difficulty of measuring the small amounts of liquid left in the section between the valves. The method is mostly used at low pressure, since the valves may leak and produce significant errors at high pressure. The method is better suited for two component rather than single-component flows where condensation or vaporization of the trapped mass may alter the results.

5.3 Prediction Methods

We start by recalling here the *triangular relationship* between the velocity ratio S (also misleadingly called "slip ratio"), the cross-sectionally and time-averaged void fraction $<\varepsilon>$ and the quality x derived in Chap. 1, Eq. (1.9.6):

$$S \equiv \frac{\langle u_G \rangle_G}{\langle u_L \rangle_L} = \frac{\rho_L}{\rho_G} \frac{x}{1-x} \frac{\langle 1-\varepsilon_G \rangle}{\langle \varepsilon_G \rangle} \tag{5.3.1}$$

We recall that as the phase densities are normally known, this relationship links the three variables, S, x and $<\varepsilon>$. Usually, we know or we can calculate the quality x, but we need some additional information to get the void fraction, for example S, or a correlation for the void fraction in terms of x. We will deal now with the empirical or semi-empirical methods for estimating the void fraction, starting from the simplest one, the homogeneous model.

Experimental void fraction data have been used in the past to calculate and correlate the velocity ratio S in terms of the relevant parameters. This approach is not straightforward in general since the variation of S is not simple as we will see in Sect. 5.3.2. below. In general, the velocity ratio is a weak function of hydraulic diameter, pressure and total flow rate, but depends strongly on the void fraction.

5.3.1 The Homogeneous Void Fraction and Density

In the simplest possible model of two-phase flow, the homogeneous model, one assumes that the velocity ratio is equal to one. Then the void fraction can be calculated. The *homogeneous* void fraction is denoted by β and is obtained by solving Eq. (5.3.1) for $<\varepsilon>$ with $S = 1$:

$$\langle \varepsilon_G \rangle_{\text{hom}} \equiv \beta = \frac{x/\rho_G}{(1-x)/\rho_L + x/\rho_G} = \left(\frac{x v_G}{x\rho_G + (1-x)v_L} \right). \tag{5.3.2}$$

It can be easily shown that the homogeneous void fraction β is also equal to

$$\beta = \frac{\dot{Q}_G}{\dot{Q}_L + \dot{Q}_G} = \frac{\langle j_G \rangle}{\langle j_L \rangle + \langle j_G \rangle}. \tag{5.3.3}$$

If the quality x (or the mass fluxes of the two phases) are known, the volumetric fluxes and the homogeneous void fraction can be calculated from Eqs. (5.3.2) and (5.3.3) above.

The two-phase *mixture density* was given in Chap. 2, Eq. (2.5.2) as a volume-weighted quantity with a definition *not* restricted to homogenous flow,

$$\langle \rho \rangle \equiv \rho_L \langle 1 - \varepsilon_G \rangle + \rho_G \langle \varepsilon_G \rangle$$

Expressing the volumetric flow rates in terms of the flow quality x, i.e. using Eq. (5.3.2) to express the homogeneous void fraction in terms of the quality, one obtains the homogeneous density

$$\frac{1}{\langle \rho \rangle_{\text{hom}}} = \frac{x}{\rho_G} + \frac{1-x}{\rho_L} \tag{5.3.4}$$

that can be more conveniently written using the phase specific volumes (the inverse of the densities) as

$$\langle \rho \rangle_{\text{hom}} = \frac{1}{\langle v \rangle_{\text{hom}}} = \frac{1}{v_L + x v_{LG}} \quad \text{or} \quad \langle v \rangle_{\text{hom}} = v_L + x v_{LG},$$

where $v_{LG} \equiv v_G - v_L$.

Here, the quality x is the local value of the *true* quality, i.e. not necessarily the thermal equilibrium quality, provided of course that the true quality can be estimated. The *equilibrium* quality can generally be obtained from a heat balance, as we have seen in Chap. 1.

5.3.2 Empirical Correlations for Separated Flows

There is a large number of empirical correlations for the void fraction when the homogeneous flow assumption is not used. Lockhart and Martinelli (1949) proposed long time ago one of the most widely used ones. This correlation is mentioned here as an example. It relates the void fraction to the Lockhart–Martinelli parameter X_{tt} that we have introduced in Chap. 1,

$$X_{tt} = \left[\frac{1-x}{x}\right]^{0.9} \left[\frac{\rho_G}{\rho_L}\right]^{0.5} \left[\frac{\mu_L}{\mu_G}\right]^{0.1}$$

and is given originally in graphical form valid in principle for any pair of fluids. A useful numerical approximation to this correlation was proposed by McFarlane (1966):

$$\langle \varepsilon_G \rangle = 1 - \left[1 + \frac{21}{X_{tt}} + \frac{1}{X_{tt}^2}\right]^{-0.5}.$$

This numerical fit gives a very good match (within 2–4%) with the original Lockhart–Martinelli plot for $X_{tt} < 10$, but the errors can become as large as 10–20% for higher values of X_{tt}. For a given fluid at saturation, X_{tt} is only a function of

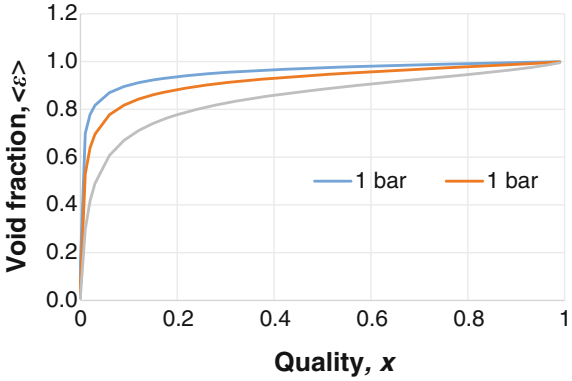

Fig. 5.4 Plot of the void fraction for saturated stream water at three different pressures according to the McFarlane (1966) formula

pressure and quality, and the void fraction can then be calculated or plotted directly as a function of these variables. Figure 5.4 shows a plot of the void fraction versus quality for saturated steam–water at different pressures obtained using this correlation.

The original empirical plot due to Martinelli and Nelson (1948) for saturated steam–water mixtures, where again the void fraction is simply given as a function of the quality x is given in Fig. 5.5. The figure is convenient for obtaining rapidly an estimate of the void fraction. One notes how rapidly the void fraction increases at low qualities and pressures. At the critical pressure of 3206 psia the relationship between quality and void fraction becomes linear.

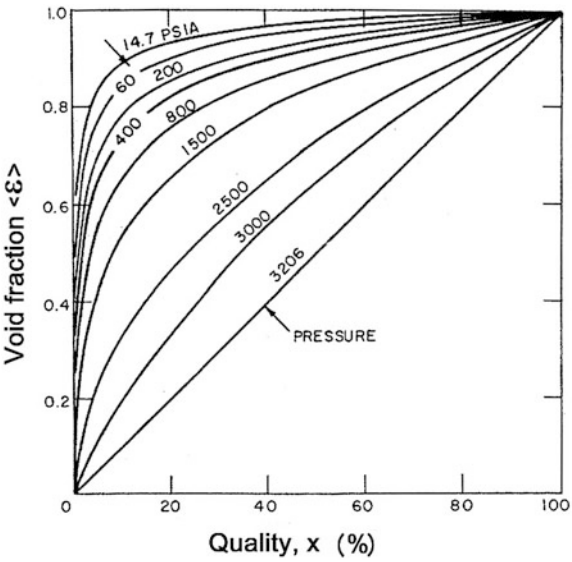

Fig. 5.5 The Martinelli-Nelson (1948) void fraction correlation for saturated steam–water mixtures; the pressure is given in British units (1 bar = 14.5 psia)

Several of the most commonly used void fraction correlations were compared against a very large data set (Hewitt 1985); the best results were obtained by a correlation proposed by the CISE laboratory in Italy (Premoli et al. 1971). The Premoli (or CISE) correlation, written in terms of the velocity ratio S and of the homogeneous void fraction β is given here:

$$S = 1 + E_1 \left[\frac{y}{1 + yE_2} - yE_2 \right]^{1/2}$$

with

$$y \equiv \frac{\beta}{1-\beta} = \frac{\langle j_G \rangle}{\langle j_L \rangle}$$

$$E_1 = 1.578 \cdot \mathrm{Re}^{-0.19} \left(\frac{\rho_L}{\rho_G} \right)^{0.22}, \quad E_2 = 0.0273 \cdot \mathrm{We} \cdot \mathrm{Re}^{-0.51} \left(\frac{\rho_L}{\rho_G} \right)^{0.08}.$$

The non-dimensional Reynolds and Weber groups are given as:

$$\mathrm{Re} \equiv \frac{\dot{m}_L D}{\mu_L}, \quad \mathrm{We} \equiv \frac{\dot{m}^2 D}{\sigma \rho_L}.$$

One notes that the correlating parameter is essentially the ratio of the volumetric fluxes y. In contrast to, say, the homogeneous model or the Martinelli-Nelson correlation mentioned above, the CISE correlation considers the mass flux and also includes a correction factor for the surface tension, something that most other correlations ignore.

More specialized correlations could give better results in particular cases; the interested reader may be find data and a more specialized and accurate correlation for very particular or unusual situations. The drift flux approach discussed next is the most widely used general method today.

5.4 The Drift-Flux Model

The "drift-flux formulation" or DF for short by Zuber and Findlay (1965) (see also Wallis 1969) is presently the best available mixture model framework for representation of two-phase flows. It should give sufficient accuracy for moderate transients in which the mixture evolves in a quasi-steady-state fashion, i.e. the transient relationships between the void fraction and the local, time-dependent parameters such as quality and mass flux can be approximated at each instant by the corresponding steady-state relationships. Two-fluid formulations with interfacial exchange terms may be needed for fast transients where the mixture does not have time to reach

equilibrium conditions.[3] The conservation equations based on the DF model will be presented in another volume. Here we focus on void fraction predictions using the DF framework.

5.4.1 Basic Derivation

We defined in Chap.1 the *cross-sectional average* volumetric fluxes (using here for simplicity the notation $\varepsilon = \varepsilon_G$):

$$\langle j_L \rangle = \langle u_L(1-\varepsilon) \rangle = \langle u_L \rangle_L \langle 1-\varepsilon \rangle = \frac{\dot{m}\,(1-x)}{\rho_L}$$

$$\langle j_G \rangle = \langle u_G \varepsilon \rangle \quad = \langle u_G \rangle_G \langle \varepsilon \rangle = \quad \frac{\dot{m}\,x}{\rho_G} \tag{5.4.1}$$

and their sum, the total volumetric flux

$$\langle j \rangle = \langle j_L \rangle + \langle j_G \rangle. \tag{5.4.2}$$

The derivation of the basic DF formulation that is given below uses the *local volumetric fluxes* of the phases,

$$j_L = u_L(1-\varepsilon) \text{ and } j_G = u_G \varepsilon \tag{5.4.3}$$

as well as their sum j,

$$j = j_L + j_G. \tag{5.4.4}$$

One understands easily the physical meaning of the *cross-sectional average* volumetric fluxes; they are the rates of volumetric flow per unit area. It is maybe more difficult to explain the physical meaning of the *local* volumetric fluxes; these can be thought, however, as being the limiting values of the volumetric fluxes as the cross-sectional area over which they are computed shrinks to zero.

We consider now the basis of the DF model, the *local drift velocity of the gas*, defined as

$$u_{Gj} = u_G - j. \tag{5.4.5}$$

This is the velocity with which the gas is locally drifting past the mixture velocity given by the local volumetric flux. We multiply this equation by the local void fraction ε and integrate across the channel:

[3]The interfacial closure relationships used in the two-fluid formulations will also be discussed in another volume.

$$\langle \varepsilon u_{Gj} \rangle = \langle \varepsilon u_G \rangle - \langle \varepsilon j \rangle. \tag{5.4.6}$$

Using Eq. (1.7.8) derived in Chap.1, we can "open" the angle brackets of the first term on the right that contains the void fraction and a *phase* property and we obtain:

$$\langle \varepsilon u_{Gj} \rangle = \langle \varepsilon \rangle \langle u_G \rangle_G - \langle \varepsilon j \rangle.$$

The opening of the angle brackets is not possible for the first and last terms, which are averages of products of ε with a variable that is *not* a phase property. Defining, however, the *distribution coefficient* C_o, which accounts for the non-uniformity of the volumetric flux velocity and of the void fraction profiles across the duct:

$$C_0 \equiv \frac{\langle \varepsilon j \rangle}{\langle \varepsilon \rangle \langle j \rangle} \tag{5.4.7}$$

and the *cross-sectional average drift velocity* of the gas, U_{Gj}, which brings into consideration the average effect of the local relative velocity (or drift) between the phases:

$$U_{Gj} \equiv \frac{\langle u_{Gj} \varepsilon \rangle}{\langle \varepsilon \rangle} = \langle u_{Gj} \rangle_G, \tag{5.4.8}$$

we can write

$$\langle \varepsilon \rangle U_{Gj} = \langle \varepsilon \rangle \langle u_G \rangle_G - C_0 \langle \varepsilon \rangle \langle j \rangle$$

or, eliminating the void fraction,

$$\langle u_G \rangle_G = C_0 \langle j \rangle + U_{Gj} \tag{5.4.9}$$

This last expression, the foundation of the DF model, clearly shows that the difference between $<u_G>_G$ and $<j>$ is due to the effects of the profiles (the C_o contribution), as well as to the averaged effect of the local drift (the U_{Gj} contribution).

A *mean* drift velocity between the gas and the mixture can be defined as:

$$\bar{U}_{Gj} \equiv \langle u_G \rangle_G - \langle j \rangle$$

and can be computed using Eq. (5.4.9):

$$\bar{U}_{Gj} = (C_0 \langle j \rangle + U_{Gj}) - \langle j \rangle = (C_0 - 1) \langle j \rangle + U_{Gj}. \tag{5.4.10}$$

We easily see that if $C_0 = 1$ and $U_{Gj} = 0$, there is no mean drift between the phases.

5.4.2 Physical Significance of the DF Model Parameters

A few more useful relationships will be derived now and the physical meaning of their terms discussed. The average velocity of the gas phase in terms of <j> and the DF parameters was given by Eq. (5.4.9). Starting from Eq. (5.4.9), recalling that $\langle j_G \rangle = \langle \varepsilon_G \rangle \langle u_G \rangle_G$, and performing some algebra, we can obtain the void fraction as follows

$$\langle \varepsilon_G \rangle = \frac{\frac{\langle j_G \rangle}{\langle j \rangle}}{C_0 + \frac{U_{Gj}}{\langle j \rangle}} = \frac{\langle j_G \rangle}{C_0 \langle j \rangle + U_{Gj}} = \frac{\beta}{C_0 + \frac{U_{Gj}}{\langle j \rangle}}. \tag{5.4.11}$$

The expression for the liquid volume fraction is more complex:

$$\langle \varepsilon_L \rangle = 1 - \langle \varepsilon_G \rangle = \frac{\langle j_L \rangle + (C_0 - 1)\langle j \rangle + U_{Gj}}{C_0 \langle j \rangle + U_{Gj}} = \frac{(1-\beta) + (C_0 - 1) + \frac{U_{Gj}}{\langle j \rangle}}{C_0 + \frac{u_{Gj}}{\langle j \rangle}}. \tag{5.4.12}$$

We see clearly that the two DF model parameters act as correction factors to the homogeneous void fraction β, as evident in Eq. (5.4.11). By its definition, C_0 brings into the model the effect of the combined void fraction and volumetric flux profiles, and U_{Gj} the average effect of the void drift, Fig. 5.6. It should be noted that U_{Gj} is not necessarily zero in horizontal flows as there may be still mechanisms promoting drift of the voids. Normally, the value of C_0 is greater than one, except when the voids peak near the wall where the velocity is low; this is the case, e.g. of subcooled boiling. C_0 depends generally on pressure, channel geometry and to some extent flow rate. The average drift velocity is rather independent of flow conditions and depends only on the flow regime and the size of the voids.

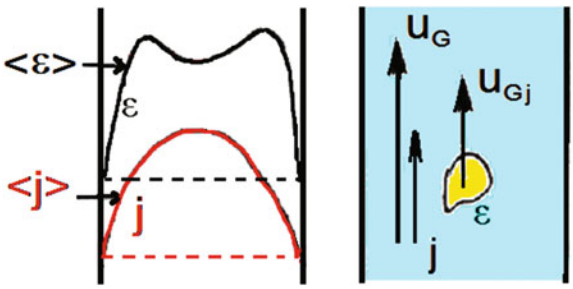

Fig. 5.6 Physical significance of the DF model parameters

Other useful expressions for the void and liquid fractions in terms of the quality, mass flux and the DF parameters can be obtained using Eqs. (5.4.11) and (1.8.2 and 1.8.3) of Chap. 1:

$$\langle \varepsilon_G \rangle = \frac{x}{C_0\left(x + \frac{\rho_G}{\rho_L}(1-x)\right) + \frac{\rho_G U_{Gj}}{\dot{m}}}$$

$$\langle \varepsilon_L \rangle = 1 - \langle \varepsilon_G \rangle.$$

An explicit expression for $<\varepsilon_L>$ can of course be developed with some algebra but it is complex and does not bring any particular insight. The corresponding phase velocities in terms of quality and mass flux are:

$$\langle u_G \rangle_G = \frac{\langle j_G \rangle}{\langle \varepsilon_G \rangle} = \frac{C_0\langle j \rangle + U_{Gj}}{\langle \varepsilon_G \rangle} = \frac{1}{\langle \varepsilon_G \rangle}\left[C_0\left(\frac{x}{\rho_G} + \frac{1-x}{\rho_L}\right)\dot{m} + U_{Gj}\right]$$

$$\langle u_L \rangle_L = \frac{\langle j_L \rangle}{\langle \varepsilon_L \rangle} = \frac{\dot{m}\,(1-x)\rho_L}{\langle \varepsilon_L \rangle},$$

where again the last term was left implicitly defined, as the expansion of the liquid velocity is complex and does not reveal anything very useful. Finally, the velocity ratio S can be expressed as:

$$S = C_0 + \frac{x(C_0 - 1)\rho_L}{\rho_G(1-x)} + \frac{\rho_L V_{Gj}}{\dot{m}\,(1-x)}.$$

5.4.3 Velocities in Terms of DF Parameters

It is useful to obtain the phase velocities in terms of the DF parameters and the volumetric fluxes. The gas velocity was can be obtained from the volumetric flux of the gas and the void fraction using Eq. (5.4.10) and rewritten as:

$$\langle u_G \rangle_G = \frac{\langle j_G \rangle}{\langle \varepsilon_G \rangle} = \frac{\langle j_G \rangle (C_0\langle j \rangle + U_{Gj})}{\langle j_G \rangle}.$$

Dividing top and bottom of the last fraction by $<j>$:

$$\langle u_G \rangle_G = \frac{\langle j_G \rangle \left(\frac{(C_0\langle j \rangle + U_{Gj})}{\langle j \rangle}\right)}{\frac{\langle j_G \rangle}{\langle j \rangle}} = \frac{\langle j_G \rangle}{\beta}\left(C_0 + \frac{U_{Gl}}{\langle j \rangle}\right). \tag{5.4.13}$$

The $<j_G>/\beta$ term can be recognized as the "homogeneous gas or mixture velocity" and the last term in the parentheses as the DF corrections to it. The liquid velocity is obtained now using Eq. (5.4.12) for the liquid volume fraction as:

$$\langle u_L\rangle_L = \frac{\langle j_L\rangle}{\langle \varepsilon_L\rangle} = \frac{\langle j_L\rangle}{\frac{(1-\beta)+(C_0-1)+\frac{U_{Gj}}{\langle j\rangle}}{C_0+\frac{u_{Gj}}{<j>}}} = \frac{\langle j_L\rangle(C_0+\frac{U_{Gj}}{\langle j\rangle})}{(1-\beta)+(C_0-1+\frac{U_{Gj}}{\langle j\rangle})} \tag{5.4.14}$$

Again, the presence of the $<j_L>/(1-\beta)$ "ratio" in the nominator and denominator of the last fraction can be recognized as the homogeneous velocity, while the other terms are the DF corrections.

Alternative expressions for the phase velocities in terms of the mass flux rather than the volumetric fluxes that can be obtained from $<j_G> = <\varepsilon_G><u_G>_G = <\varepsilon_G>(C_0<j> + U_{Gj})$ and $\dot{m} = \rho_L<j_L> + \rho_G<j_G>$ by eliminating $<j_L>$ and $<j_G>$, between the two, respectively:

$$\langle u_G\rangle_G = \frac{C_0\,\dot{m}/\rho_L + V_{Gj}}{1-\langle\varepsilon_G\rangle C_0(1-\rho_G/\rho_L)}$$

$$\langle u_L\rangle_L = \frac{(1-\langle\varepsilon_G\rangle C_0)\left(\dot{m}-\frac{\langle\varepsilon_G\rangle\rho_G V_{Gj}}{1-\langle\varepsilon_G\rangle C_0}\right)}{\rho_L\langle 1-\varepsilon_G\rangle[1-\langle\varepsilon_G\rangle C_0(1-\rho_G/\rho_L)]}.$$

These can also be expressed in terms of the mass and volumetric fluxes and the DF parameters (Yadigaroglu and Lahey 1976) as:

$$\langle u_L\rangle_L = \frac{\dot{m}}{\langle\rho\rangle} - \frac{\langle\varepsilon_G\rangle}{\langle\varepsilon_L\rangle}\frac{\rho_G}{\langle\rho\rangle}\left[(C_0-1)\langle j\rangle + U_{Gj}\right] = \frac{\dot{m}}{\langle\rho\rangle} - \frac{\langle\varepsilon_G\rangle}{\langle\varepsilon_L\rangle}\frac{\rho_G}{\langle\rho\rangle}\bar{U}_{Gj}$$

$$\langle u_G\rangle_G = \frac{\dot{m}}{\langle\rho\rangle} + \frac{\rho_L}{\langle\rho\rangle}\left[(C_0-1)\langle j\rangle + U_{Gj}\right] = \frac{\dot{m}}{\langle\rho\rangle} + \frac{\rho_L}{\langle\rho\rangle}\bar{U}_{Gj}.$$

where $\bar{U}_{Gj}$ was recognized above, Eq. (5.4.10), as the mean drift velocity between the gas and the mixture, $\bar{U}_{Gj} \equiv <u_G>_G - <j>$. Multiplying the first equation by the liquid fraction and the second by the void fraction and adding them, we obtain a relation linking the volume and mass fluxes and the mean drift velocity between the gas and the mixture:

$$\langle j\rangle = \frac{\dot{m}}{\langle\rho\rangle} + \frac{\Delta\rho\langle\varepsilon_G\rangle}{\langle\rho\rangle}\bar{U}_{Gj}.$$

In Sect. 1.9.1 of Chap.1, we had introduced the velocity of the centre of mass, U_m. It can be expressed now in terms of the DF parameters (Yadigaroglu and Lahey 1976)

$$U_m = \langle u_L \rangle_L + \frac{\langle \varepsilon_G \rangle}{\langle \varepsilon_L \rangle} \cdot \frac{\rho_G}{\langle \rho \rangle} \cdot \left[(C_0 - 1)\langle j \rangle + U_{Gj} \right] = \langle u_L \rangle_L + \frac{\langle \varepsilon_G \rangle}{\langle \varepsilon_L \rangle} \cdot \frac{\rho_G}{\langle \rho \rangle} \cdot \bar{U}_{Gj} = \langle u_G \rangle_G - \frac{\rho_L}{\langle \rho \rangle} \cdot \bar{U}_{Gj}, \tag{5.4.15}$$

the last two expressions containing the *mean drift velocity between the gas and the mixture,* Eq. (5.4.10): $\bar{U}_{Gj} \equiv <u_G>_G - <j> = (C_0 - 1)<j> + U_{Gj}$. For homogenous flow, $\bar{U}_{Gj} = 0$ and we obtain, as expected, $<u_G>_G = <u_L>_L = <j> = <j_G> = <j_L> = U_m$.

Finally, we can obtain the *relative velocity* between the phases (that could have been called the average *slip*) from Eqs. (5.4.15) as

$$U_r \equiv \langle u_G \rangle_G - \langle u_L \rangle_L = \left[\frac{\rho_L}{\langle \rho \rangle} + \frac{\langle \varepsilon_G \rangle}{\langle \varepsilon_L \rangle} \cdot \frac{\rho_G}{\langle \rho \rangle} \right] \cdot \bar{U}_{Gj} = \frac{1}{\langle 1 - \varepsilon_G \rangle} \cdot \bar{U}_{Gj}$$

or

$$U_r = \frac{1}{\langle 1 - \varepsilon_G \rangle} \cdot \bar{U}_{Gj}. \tag{5.4.16}$$

This last interesting result linking the relative velocity to the mean drift velocity is illustrated in Fig. 5.7 for the simple case of stratified flow. Considering the centre of volume plane moving with the velocity <*j*>, we can see that the volumes of gas

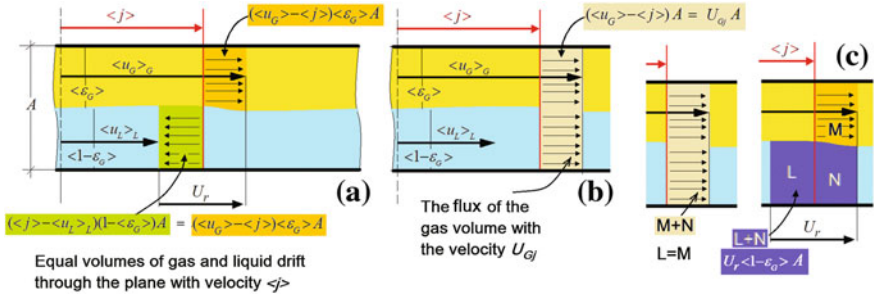

Fig. 5.7 A simple, graphical explanation of the relationship between the relative velocity and the mean drift velocity. **a** Illustration of the equal gas and liquid volumes crossing the plane moving with the velocity <*j*>. **b** Illustration of the gas flux associated with the average drift velocity of the gas U_{Gj}. **c** Geometrical proof of Eq. (5.4.16) according to the equality of the areas: $L + N = M + N$ as $L = M$ according to (**a**)

and liquid crossing it in opposite directions cancel out, as expected in Fig. 5.7a. Figure 5.7c demonstrates graphically the result obtained by Eq. (5.4.16).

We had several opportunities to notice that the DF model is not "symmetric" regarding the two phases and this leads to notable differences between the various phase-related quantities. The possibility of defining a DF model based on the drift velocity of the liquid with respect to j exists of course, but has not been used; it could be useful though in treating problems where the liquid is the dispersed phase, such as sprays.

5.4.4 Use of Experimental Data

When experimental data are plotted in a ($\langle u_G \rangle_G$, $\langle j \rangle$) plane, they often form a straight line and the DF model parameters are obtained as the slope and the intercept of the correlation line, as shown in Fig. 5.8. If the data do not fall on a straight line, this means that the drift flux parameters depend on certain flow variables, in particular the void fraction. The resulting C_0 and U_{Gj}correlations may then contain the void fraction and the method becomes implicit.

Figure 5.9 shows some old, actual data plotted in the ($\langle u_G \rangle_G$, $\langle j \rangle$) plane. The trend of the data shows a "knee" around $\langle j \rangle = 0.25$ m/s that is in fact revealing a change in the flow regime. Both the slope and the intercept (the DF model parameters) have different values, as shown in the figure for the two different regimes.

The drift-flux model is intrinsically best suited for bubbly and churn flows where there is indeed local drift between the phases. Its use becomes somewhat artificial in clearly separated flows, where there is really no local drift between the phases. Even in this case, however, it provides a good general framework for correlating void fraction data. Indeed, the drift flux model parameters C_o and U_{Gj} must *in principle* be provided on a case by case basis for each flow situation. Generally usable correlations for these parameters have also been developed, however, as we will see below.

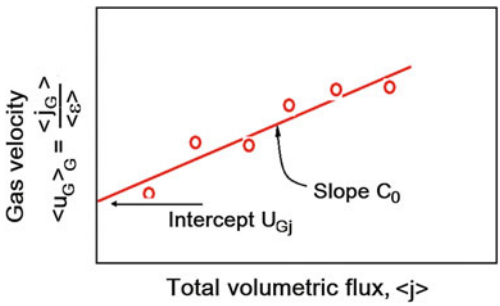

Fig. 5.8 Determination of the DF model parameters from experimental data plotted in the $\langle u_G \rangle_G$, $\langle j \rangle$ plane

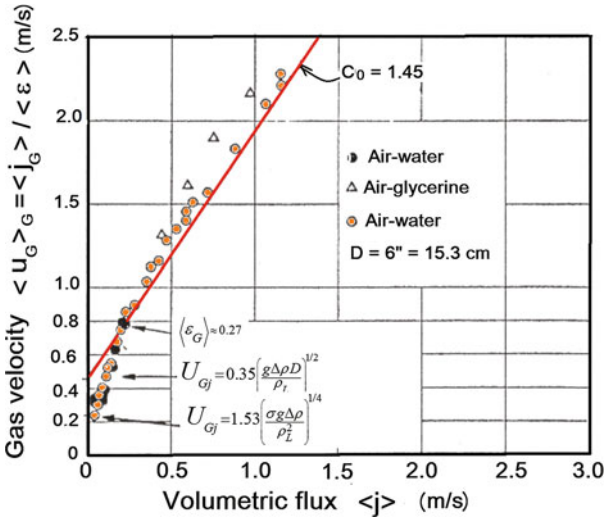

Fig. 5.9 Plot of experimental air–water data in the gas velocity—volumetric flux plane revealing a change in flow regime. Data of Bailey et al. (1956)

5.5 Determination of the Parameters of the DF Model

Certain recommendations for selection of the appropriate correlations for C_o and U_{Gj} are given in the original paper by Zuber and Findlay (1965), as well in more recent works (e.g. Hibiki and Ishii 2003a, 2005). Following the basic ideas of Zuber and Findlay, the DF parameters should be determined on a case-by-case basis for each situation or even data set. However, there is clearly an interest in making void fraction estimations and many authors have attempted to propose generally applicable correlations. The DF model parameters should behave at the limits of the range of void fraction and pressure values in a way compatible with the physical reality, yielding, e.g. the correct phase velocity values at the limits of zero or unity void fraction and the homogeneous flow solution as the pressure approaches the thermodynamic critical value.

Zuber and Findlay proposed the general framework but do not focus in their original paper much on the particular values of the DF parameters; they propose the general use of the following values for a churn-turbulent or bubbly flow regime:

$$C_0 = 1.2 \text{and} U_{Gj} = 1.53 \left[\frac{g\ \Delta\rho\ \sigma}{\rho_L^2} \right]^{1/4}, \quad \Delta\rho \equiv \rho_L - \rho_G, \tag{5.5.1}$$

where the U_{Gj} is the rise velocity of ellipsoid bubbles in an infinite medium (Harmathy 1960).

We will review now mainly the works of Ishii and co-workers and Chexal and co-workers that have been used rather extensively; the interested reader will find full lists of all available correlations in the comparative works mentioned below and in Sect. 5.6 Some of these may be more appropriate if the application is close to the origins of the data.

Average drift velocity U_{Gj}

According to the work of Hibiki and Ishii (2003a, 2005) also incorporated in the book by Ishii and Hibiki (2011), simplified expressions, already proposed earlier are confirmed for *gravity dominated flows,* namely:

For *bubbly* flow:

$U_{Gj} = \sqrt{2}\left(\frac{g_z \Delta\rho\ \sigma}{\rho_L^2}\right)^{1/4} \langle 1 - \varepsilon_G \rangle^{1.75}$ C_0 given as 1.2 or by Eq. (5.5.3) below,

where the first term of U_{Gj} is again, to a slight difference in the constant, Harmathy's single bubble rise velocity and g_z is the component of gravity along the flow path z (in case of an inclined pipe). The relation proposed for the distribution coefficient C_0 can be more complex and will be discussed below.

For *slug flow* Hibiki and Ishii (2003a, 2005) propose:

$$U_{Gj} = 0.35\left(\frac{g_z \Delta\rho\ D}{\rho_L}\right)^{1/2} \text{ and } C_0 = 1.2 - 0.2\sqrt{\frac{\rho_G}{\rho_L}},$$

where again the value of U_{Gj} is the one given for slugs of gas by Harmathy (1960). Finally, for *churn flow*:

$$U_{Gj} = \sqrt{2}\left(\frac{g_z \Delta\rho\ \sigma}{\rho_L^2}\right)^{1/4} \quad \text{and} \quad C_0 = 1.2 - 0.2\sqrt{\frac{\rho_G}{\rho_L}},$$

where now the correction for the void fraction used for bubbly flow is no longer present. The square root of the density ratio introduces the effect of pressure.

More generally, expressions forU_{Gj}, based on the terminal rise velocity of a single bubble in an infinite medium are given, for churn-turbulent or bubbly flow as:

$$U_{Gj} = (1.18 \text{ to } 1.53)\left(\frac{g_z \Delta\rho\ \sigma}{\rho_L^2}\right)^{1/4}. \tag{5.5.2}$$

For *very small bubbles* obeying Stokes' law:

$$U_{Gj} = \frac{g_z\,\Delta\rho\,d^2}{18\,\mu_L} < 1 - \varepsilon_G >^3,$$

where d is the bubble diameter. For the *general case*, Hibiki and Ishii (2003a, 2005) give much more complex expressions involving also the frictional pressure gradient.

Distribution coefficient C_0

Regarding the distribution coefficient in bubbly flow, Hibiki and Ishii (2003a, 2005) postulate an expression of the form

$$C_0 = C_\infty(\mathrm{Re}) - (C_\infty(\mathrm{Re}) - 1)\sqrt{\frac{\rho_G}{\rho_L}}, \tag{5.5.3}$$

where Re is the liquid Reynolds number, $\mathrm{Re} \equiv <j_L> D/\nu_L$, and C_∞ the asymptotic value of C_0. They state that for *laminar* flow the value of C_0 is $C_{\infty,l} = 2$, but is very sensitive to the average void fraction at low void fractions. For *turbulent* flows

$$C_{\infty,t} = 1.2\left(1 - e^{-22 D_{Sm}/D}\right),$$

where D_{Sm} is the Sauter mean diameter of the bubbles, which can be predicted by a complex relation given in their paper and D is, as usual, the pipe diameter. The authors propose a generalized expression taking into account the flow transition from laminar to turbulent,

$$C_\infty \equiv 2.0\, e^{-0.000584\ \mathrm{Re}} + 1.2\left(1 - e^{-22(D_{Sm}/D)}\right) \cdot \left(1 - e^{-0.000584\ \mathrm{Re}}\right).$$

For *annular flow,* Hibiki and Ishii (2003a, 2005) note that there is no local drift between the phases in the sense given to it in bubbly or churn flow; a *local* relative velocity between two phases cannot be defined. If some small liquid droplets are entrained in the gas core or small gas bubbles are entrained in the liquid film, the average local relative velocity should be approximately zero, $U_{Gj} \approx 0$. Annular flow can still, however, be included in the DF formulation. Hibiki and Ishii propose the following simplified expressions for the DF parameters for the case $\rho_L \gg \rho_G$; the more complex formulations for the general case can be found in their writings.

As noted above $U_{Gj} \approx 0$. Regarding the distribution coefficient C_0, we can extract it from Eq. (5.4.10) for the average drift velocity

$$\bar{U}_{Gj} = (C_0 - 1)\langle j \rangle + U_{Gj}.$$

We need to compute $\bar{U}_{Gj}$ first and then extract C_0 noting that $U_{Gj} \approx 0$. The derivation starts from a development similar to the one presented in Chap.4, Sect. 4.5 for stratified flow. The relative motions between phases are governed again by the interfacial geometry, gravity and interfacial and wall shears. Providing expressions for the latter, one can obtain, after a lengthy development, and several approximations, including the use of $\rho_L \gg \rho_G$ the following expression for the average drift velocity of the gas (Hibiki and Ishii 2003a, 2005; Ishii and Hibiki 2011, Chap. 14),

$$\bar{U}_{Gj} \approx \frac{\langle 1-\varepsilon_G \rangle}{\langle \varepsilon_G \rangle + 4\sqrt{\rho_G/\rho_L}} \left(\langle j \rangle + \sqrt{\frac{g_z \Delta\rho \, D \langle 1-\varepsilon_G \rangle}{0.015\, \rho_L}} \right)$$

that leads, according to Eq. (5.4.10) to:

$$C_0 = \frac{\bar{U}_{Gj} + \langle j \rangle + U_{Gj}}{\langle j \rangle} \approx \frac{\bar{U}_{Gj} + \langle j \rangle}{\langle j \rangle} \approx \frac{\langle 1-\varepsilon_G \rangle}{\langle \varepsilon_G \rangle + 4\sqrt{\rho_G/\rho_L}} \left(1 + \frac{\sqrt{\frac{g_z \Delta\rho \, D \langle 1-\varepsilon_G \rangle}{0.015\, \rho_L}}}{\langle j \rangle} \right) + 1.$$

Hibiki and Ishii (2003b) specialize the DF model parameters for the case of large pipes and Clark et al. (2014), following the same approach, for rod bundles. The book by Ishii and Hibiki (2011) treats numerous other particular application cases.

An interesting table summarizing the various proposals made for the DF model parameters (well over a dozen) is given in a paper by Bhagwat and Ghajar (2014). The authors reviewed several existing DF correlations and proposed a new one that is not based on flow patterns and pipe orientation and can predict the void fraction over a wide range of system pressures, pipe diameters and fluid properties. They introduced correction factors to extend the application of their correlation to non-circular pipes (rectangular and annular geometries), large-diameter pipes and very viscous liquids. Their correlation was verified against 8255 data points and they claim better results than from all the other correlations they examined for all ranges of the void fraction and fluid combinations considered. The distribution coefficient is given as:

$$C_0 = \frac{2 - (\rho_G/\rho_L)^2}{1 + (\mathrm{Re}_{tp}/1000)^2} + \frac{\left[\left(\sqrt{\left(1 + \frac{(\rho_G/\rho_L)^2 \cos\beta}{1+\cos\beta}\right)} \right)^{(1-\langle \varepsilon_G \rangle)} + C_{o,1} \right]^{2/5}}{1 + (1000/\mathrm{Re}_{tp})^2} \quad , \qquad (5.5.4)$$

where $C_{o,1}$ is defined in terms of the gas-to-liquid density ratio, the homogeneous void fraction, the two phase friction factor, the flow quality and pipe geometry. Re_{tp} is a Reynolds number calculated with the volumetric flux and the liquid properties. The interested reader is referred to the original paper for the numerous details. The inclination angle β is measured from the horizontal. The correlation for C_0 includes the void fraction on the right side making it implicit and requiring an iterative solution.

The average drift velocity is given by

$$U_{Gj} = (0.35\ \sin\beta + 0.45\ \cos\beta) \cdot \left(\frac{g\ \Delta\rho\ D_h}{\rho_L}\right)^{1/2} \langle 1 - \varepsilon_G \rangle^{0.5} C_2 C_3 C_4,$$

where D_h is the hydraulic diameter and the correction coefficients C are functions of the viscosity, the Laplace wavelength divided by the hydraulic diameter $\sqrt{\sigma/g\,\Delta\rho}/D_h$, and a variant of Froude number based on the volumetric flux of the gas,

$$\mathrm{Fr}_{sG} = \sqrt{\frac{\rho_G}{\Delta\rho}} \frac{U_{sG}}{\sqrt{gD_h \cos\beta}}.$$

5.5.1 The EPRI (1996) Chexal-Lellouche Correlation

A recent correlation for the drift-flux model parameters developed by Chexal et al. (1997) at the Electric Power Research Institute, EPRI, should have a wide range of applicability. This correlation was obtained without regard to the prevailing flow regime; any flow regime dependence is inherently taken into consideration. The correlation takes into account all orientations of the flow with respect to gravity: co-current upwards and downwards flows, horizontal co-current and countercurrent flows. Its data base includes data from rod bundles as well as from large-diameter pipes. The authors claim that the correlation is particularly suited to "difficult" situations such as low pressures, low mass fluxes and low steam qualities.

The distribution coefficient

The correlation for the parameter C_0 has the form

$$C_0 = \frac{L}{K_o + (1 - K_o)\langle \varepsilon_G \rangle^r}, \tag{5.5.5}$$

where the Chexal-Lellouche fluid parameter L is a weighted sum considering the inclination of the pipe:

$L = F_r L_{vert} + (1 - F_r) L_{horiz}$ with the orientation parameter $F_r = \left(1 - \frac{\theta}{90}\right)^{0.2}$.

In the flow orientation parameter, θ is the pipe orientation measured from the vertical axis. The Chexal-Lellouche fluid parameters L_{vert}*and* L_{horiz} take different forms for vertical and horizontal flows and according to the fluids. We give here only the formulas for *steam–water flows*:

For vertical flows: $L_{vert} = \frac{1-\exp\left(-C_p\langle \varepsilon_G \rangle\right)}{1-\exp(C_p)}$

For horizontal flows: $L_{horiz} = \frac{1-\exp\left(-C_p\langle \varepsilon_G \rangle\right)}{1-\exp(C_p)} \left[1 + \langle \varepsilon_G \rangle^{0.05} (1 - \langle \varepsilon_G \rangle)^2\right]$.

The coefficient C_p is function of pressure, $C_p = \frac{4p_{crit}^2}{p(p_{crit}-p)}$, p_{crit} being the thermodynamic critical pressure.

For co-current downflow, however, a limiting value of C_0 is provided as:

$$C_0 = \max\left\{\frac{L}{K_o + (1-K_o)\langle\varepsilon_G\rangle^r}, \frac{U_{Gj}^0(1-\langle\varepsilon_G\rangle)^2}{|\langle j_L\rangle| + |\langle j_G\rangle|}\right\},$$

where $U_{Gj}^0 = U_{Gj}/C_1$, with C_1 depending on the void fraction and other parameters in a complex way (Chexal et al. 1997).

K_o and r in Eq. (5.5.5) have a complex dependence on pressure and on Reynolds numbers calculated using the superficial gas or liquid velocities (positive or negative according to flow direction).

The U_{Gj} correlation has the general form (for all flow orientations and all fluids):

$$U_{Gj} = 1.41\left(\frac{g\,\Delta\rho\,\sigma}{\rho_L^2}\right)^{1/4}\langle 1-\varepsilon_G\rangle^{C_{1x}} C_2 C_3 C_4, \tag{5.5.6}$$

where C_{1x} is another coefficient with complex dependence and selection logic. The other three correction terms (C_2, C_3, C_4) to the basic formula for U_{Gj} are functions of superficial Reynolds numbers, pressure, and hydraulic diameter. The details of the extremely lengthy equations and selection logic of coefficients, and an extensive comparison with experimental data can be found in Chexal et al. (1997). The correlation is implicit as the void fraction appears in the DF model parameters and requires an iterative procedure to compute the coefficients and the void fraction. The correlation was designed for inclusion in system codes and would be impractical to use in hand calculations. The EPRI booklet (Chexal et al. 1997) provides, however, an embeddable software that performs this iteration as well as Excel spreadsheets that can be used to enter the input values and obtain the void

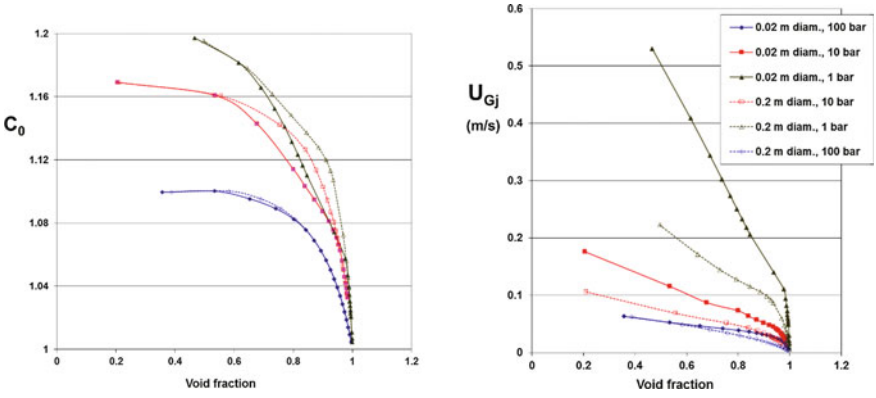

Fig. 5.10 Values of the DF parameters according to the Chexal et al. (1997) correlation plotted for three different pressures and two tube diameters

fraction. Values of the DF parameters, calculated using the EPRI software are plotted in Fig. 5.10 to get a feeling for their variation.

The EPRI group published two years later a small booklet regarding "pressure drop technology" (Chexal et al. 1999). Values of the void fraction were needed to correlate experimental pressure drop data and they have decided to introduce a correction for liquid entrainment in the Chexal-Lellouche correlation of the form:

$$\langle \varepsilon_G \rangle = \langle \varepsilon_G \rangle_{C-L} + E\left(\langle \varepsilon_G \rangle_{\text{hom}} - \langle \varepsilon_G \rangle_{C-L}\right), \tag{5.5.7}$$

where E is the liquid entrainment fraction varying between 0 and 1 (from no entrainment, to all liquid entrained in the gaseous core). This way, the corrected value of the void fraction has the Chexall-Lellouche value without entrainment (at low gas velocities and void fractions) and reaches asymptotically the homogeneous value when all the liquid is entrained (at the gas velocity). The authors claim that this procedure improves the predictions, but no comparisons are presented. The entrainment fraction is obtained from a correlation proposed by Ishii and Mishima (1982):

$$E = \tanh\left(7.25 \cdot 10^{-7} \text{We}^{1.25} \text{Re}_{LP}^{0.25}\right), \quad \text{We} \equiv \frac{\rho_G \langle j_G \rangle^2 D}{\sigma}\left(\frac{\Delta\rho}{\rho_G}\right)^{1/3},$$
$$\text{Re}_{LP} \equiv \frac{\rho_L \langle j_L \rangle D}{\mu_L},$$

where We is the entrainment Weber number.[4]

5.6 Comparisons of Various Correlations

A comparison of the performance of several DF model correlations by Bhagwat and Ghajar (2014) was already mentioned above. Earlier, Woldesemayat and Ghajar (2007) produced also a comparison of 68 void fraction correlations (not necessarily based on the DF model) for different flow patterns in horizontal and upward inclined pipes and concluded that most of the correlations are very restricted in terms of handling a wide variety of data sets. Their paper also lists the numerous, similar, but more limited in scope comparisons that were conducted in the past. Woldesemayat and Ghajar confirm that even for the same or similar fluid types, correlations developed from specific experimental data sets with fitted constants fail to adequately predict data sets from other tests or operating conditions, something that is not surprising. For horizontal flows, the only correlation that was able to give a fair result was that of Premoli et al. (1971)Premoli et al. .

[4]The correlation is expressed in the EPRI booklet in terms of other non-dimensional numbers; the Ishii and Mishima version is the one presented here.

Coddington and Macian (2002) compared the 13 best performing DF model correlations (selected from a broader comparison of correlations) using void fraction data from rod bundle, level swell and boil-off experiments performed at various (mainly nuclear-related) experimental facilities in Europe, Japan and the USA. The pressure and mass fluxes of the analysed experiments ranged from atmospheric to 150 bar and from 1 to 2000 kg $m^{-2}s^{-1}$. Their results are mainly concerned with the performance of the correlations when used in the so-called "system codes" (used in the nuclear industry). Comparisons with transient void fraction data were also made and showed that it is even possible to use a DF approach for the analysis of moderately rapid transients. A point that was confirmed by this work and should be keep in mind is that, according to Eq. (5.4.11) high, fixed values of the distribution coefficient preclude correlations from predicting high void fraction values (e.g. $C_0 = 1.2$ will limit $<\varepsilon_G>$ to less than $\beta/1.2$) that are, however, physically present under certain conditions. Somewhat surprisingly an old and not much published, very simple correlation (Dix 1971) for C_0, combined with a proposition for the drift velocity by Lahey and Moody (1977) predicted the (limited) data that Coddington and Macian used as well as the Chexall-Lellouche, much more sophisticated correlation that requires, rather extensive computation work to evaluate. According to Dix (1971) and Lahey and Moody (1977)

$$C_0 = \frac{\langle j_G \rangle}{\langle j \rangle}\left(1 + \left(\frac{\langle j \rangle}{\langle j_G \rangle} - 1\right)^{\left(\frac{\rho_G}{\rho_L}\right)^{0.1}}\right), \qquad U_{Gj} = \pm\, 2.9\left(\frac{g\,\Delta\rho\,\sigma}{\rho_L^2}\right)^{1/4},$$

where the sign of U_{Gj} is dictated by the flow orientation (+ for upwards).

For vertical flows, always according to Woldesemayat and Ghajar, the very simple drift flux correlation by Toshiba (Coddington and Macian 2002)

$$C_0 = 1.08, \quad U_{Gj} = 0.45,$$

also produced good results. Overall, Woldesemayat and Ghajar recommend six correlations for void fraction in horizontal and upward inclined pipes. These are the following correlations: the Toshiba correlation just mentioned; the simple "Rouhani I" (Rouhani and Axelsson 1970; Rouhani 1984), with $C_0 = 1 + 0.2\,(1 - x)$ and U_{Gj} given by Eq. (5.5.2) with the coefficient set to 1.18; the Dix correlation mentioned above; the Hughmark (1962); the Premoli et al. (1971) given above that was also the top-ranking one in a comparison reported by Hewitt (1985); and the Filimonov et al. (1957). The predictions were capturing about 80% of all data points correctly within a 15% error. The comparisons did not differentiate significantly the top-performing correlations over all aspects of the problem (fluids, pipe inclination, sets of experimental data used, etc.) and the interested reader should look carefully into the original paper for the numerous details provided. It was confirmed that the drift flux analysis method is a powerful tool in developing void fraction correlations as well as analysing experimental data.

5.7 Correlations for Horizontal or Inclined Pipes

Horizontal pipes are obviously of interest to the oil and gas industries. Large-diameter pipes are the main interest and the literature deals with *liquid holdup* rather than void fraction. The volume fraction of the liquid phase is the homogeneous liquid fraction λ defined as

$$\lambda \equiv \frac{\dot{Q}_L}{\dot{Q}} = \frac{\dot{Q}_L}{\dot{Q}_L + \dot{Q}_G} = \frac{\langle j_L \rangle}{\langle j_L \rangle + \langle j_G \rangle}.$$

The Gas-To-Oil ratio, GOR, is the ratio of the volumetric flow rates of the two phases,

$$\mathrm{GOR} \equiv \frac{\dot{Q}_G}{\dot{Q}_L}, \quad \mathrm{GOR} = \frac{1-\lambda}{\lambda}.$$

The GOR is often expressed in practical units of "standard cubic feet of gas per barrel of oil," scf/STB. A standard cubic foot is the volume of gas at conditions of 0 °C and 1 atmosphere and is equal to 0.02832 standard m^3. A barrel is equal to 0.15899 m^3. Thus 1 scf/STB = 0.178 m^3/m^3 (under standard temperature and pressure).

The classical work in this area, aiming at correlations applicable without particular knowledge of the flow regime, will be briefly reviewed here. After the period of the works cited here, the interest shifted to flow regime mechanistic modelling.

Chen and Spedding (1983) reviewed the methods available for predicting holdup in horizontal pipes. These can be classified in general categories according to the form of the equation used. Chen and Spedding conclude that there is a form that is most suitable for each family of flow patterns: For stratified and annular flows they recommend use of correlation forms proposed by Butterworth (1975), using property groupings reminiscent of the Lockhart–Martinelli (1949) X_{tt} factor:

$$\frac{\langle \varepsilon_L \rangle}{\langle \varepsilon_G \rangle} = K \left(\frac{\langle j_G \rangle}{\langle j_L \rangle} \right)^a \left(\frac{\rho_G}{\rho_L} \right)^b \left(\frac{\mu_G}{\mu_L} \right)^c, \tag{5.6.1}$$

where K, a, b, and c are empirical constants depending on the range of $<\varepsilon_L>/<\varepsilon_G>$ values, tabulated by Chen and Spedding (1983). A simpler form of Eq. (5.6.1) is

$$\frac{\langle \varepsilon_L \rangle}{\langle \varepsilon_G \rangle} = K \left(\frac{\langle j_G \rangle}{\langle j_L \rangle} \right)^a.$$

For slug flow, data are described best by a drift-flux model (or Armand 1946) type equation:

$$\frac{\langle \varepsilon_G \rangle}{\langle \varepsilon_L \rangle} = \frac{1}{0.2 + 1.2 \frac{\langle j_L \rangle}{\langle j_G \rangle}}.$$

The Chexal and Lellouche drift-flux correlation described in Sect. 5.5.1 is also applicable to horizontal flows.

5.7.1 Void Fraction Correlations for Inclined Pipes

Most of the published void fraction (or holdup) correlations and models, do not account explicitly for pipe inclination. Gregory (1975) has reviewed holdup correlations suitable for inclined pipes available up to 1975. Beggs and Brill (1973) conducted systematic investigations of liquid holdup and pressure drop in inclined pipes. The trends obtained in their measured values of the liquid holdup are sketched versus the angle of inclination from horizontal for various values of the *homogeneous volume flow fraction* λ in Fig. 5.11. One observes a large variation of the holdup with angle. For upward inclined pipes the holdup is always greater than or equal to that occurring in a horizontal pipe.

Beggs and Brill (1973) propose a method for estimating the liquid holdup in inclined pipes based on correction factors applied to the homogeneous liquid fraction λ:

$$\langle \varepsilon_L \rangle = A\, \lambda^a\, \mathrm{Fr}^b\, \Psi, \tag{5.6.2}$$

where Fr is a Froude number defined using the homogeneous mixture velocity, $u_{hom} = \langle j \rangle$

$$\mathrm{Fr} = \frac{u_{\mathrm{hom}}^2}{gD}$$

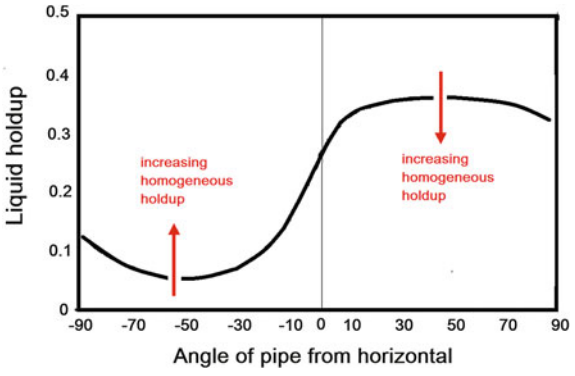

Fig. 5.11 Trends of the liquid holdup with pipe inclination according to Beggs and Brill (1973)

and the constants A, a, and b are given by expressions that vary according to the flow regime (given in the original paper). The data were segregated according to the flow regime using criteria developed by the authors. Correlations were then derived for each group of data. For consistency, one should be using the same flow regime determination criteria while using the correlations. The inclination factor Ψ corrects the holdup for the angle of inclination from the horizontal β and has the general form

$$\Psi = 1 + C(\sin\phi - \frac{1}{3}\sin^3\phi), \qquad \phi \equiv 1.8\beta.$$

The parameter C is again a function of flow regime and flow direction, it is also given in terms of a "liquid velocity number" Lv:

$$\mathrm{Lv} = U_{sL}\left(\frac{\rho_L}{g\sigma}\right)^{1/4}. \tag{5.6.3}$$

Certain comparisons of the Beggs and Brill correlation and recent data from large pipelines indicate considerable overpredictions of holdup. More recent data were correlated by Mukherjee and Brill (Mukherjee 1979) using linear regression analysis as follows:

$$\langle \varepsilon_L \rangle = \exp\left[\left(C_1 + C_2\sin\beta + C_3\sin^2\beta + C_4\mathrm{N}_L^2\right)\frac{\mathrm{Gv}^{C_5}}{\mathrm{Lv}^{C_6}}\right],$$

where Lv is given by Eq. (5.6.3) above, while the "gas velocity number" is

$$\mathrm{Gv} = U_{sG}\left(\frac{\rho_L}{g\sigma}\right)^{1/4}$$

and the "liquid viscosity number" $\mathrm{N_L}$ is given by

$$\mathrm{N_L} = \mu_L\left(\frac{1}{\rho_L\sigma^3}\right)^{1/4}.$$

The regression coefficients are given in tabular form by Mukherjee (1979). For consistency, the flow regimes should be determined using the Mukherjee and Brill methods also (Mukherjee 1979).

5.7.2 Mechanistic Models Based on Two-Fluid Formulation

In a way very similar to the one presented in Sect. 4.5.1 of Chap.4, one can write the momentum conservation equations for the two phases in stratified horizontal or inclined flow. If closure laws for the interfacial and wall shear are available, the equations can be solved to obtain the height of the liquid, i.e. the liquid holdup. An early example of this approach is the work of Modisette (1983). The main difficulty lies in formulating the proper expression for the interfacial shear.

References

Agostini G, Era A, Premoli A (1969) Density measurements of steam-water mixtures flowing in a tubular channel under adiabatic and heated conditions. CISE, Milan, Report CISE-R-29l

Andreussi P, Di Donfrancesco A, Messia M (1988) An impedance method for the measurement of liquid hold-up in two-phase flow. Int J Multiph Flow 14:777–785

Armand AA (1946) The resistance during the movement of a two-phase system in horizontal pipes. Izv VTI 1:16–23. Translation AERE No. 828

Bailey RV et al (1956) Transport of gases through liquid-gas mixture. Paper presented at the AIChE, New Orleans Meeting

Banerjee S, Lahey RT Jr (1981) Advances in two-phase flow instrumentation. In: Lewins J, Becker M (ed) Advances in nuclear science and technology, vol 13. Plenum Publishing Corporation, New York, pp 227–414

Banerjee S, Hussein E, Meneley DA (1979) Simulation of a neutron scattering method of measuring void fraction in two-phase flow. Nucl Eng Des 53:393–405

Beggs HD, Brill JP (1973) A study of two-phase flow in inclined pipes. J Petr Technol 725:607–617

Bhagwat SM, Ghajar AJ (2014) A flow pattern independent drift flux model based void fraction correlation for a wide range of gas–liquid two phase flow. Int J Multiph Flow 59:186–205

Butterworth D (1975) A comparison of some void-fraction relationships for gas-liquid flow. Int J Multiph Flow 1:845–850

Chen JJJ, Spedding PL (1983) An analysis of holdup in horizontal two-phase gas-liquid flow. Int J Multiph Flow 2:147–159

Chexal B, Merilo M, Maulbetsch J, Horowitz J, Harrison J, Westacott J, Peterson C, Kastner W, Schmidt H (1997) Void fraction technology for design and analysis. Electric Power Research Institute, Palo Alto, CA

Chexal B, Horowitz J, McCarthy G, Merilo M, Sursock JP, Harrison J, Peterson C, Shatford J, Hughes D, Ghiaasiaan M, Dhir V (1999) Two-phase pressure drop technology for design and analysis. Technical Report Aug 1999. Electric Power Research Institute Inc, Palo Alto, CA, USA

Clark C, Griffiths M, Chen SW, Hibiki T, Ishii M, Ozaki T, Kinoshita I, Yoshida Y (2014) Drift-flux correlation for rod bundle geometries. Int J Heat Fluid Flow 48:1–4

Coddington P, Macian R (2002) A study of the performance of void fraction correlations used in the context of drift-flux two-phase flow models. Nucl Eng Des 215(3):199–216

Delhaye J-M (1981) Two-phase flow instrumentation. In: Delhaye J-M, Giot M, Riethmuller ML (eds) Thermohydraulics of two-phase systems for industrial design and nuclear engineering. Hemisphere Publishing Corporation, Washington DC, USA

Delhaye J-M, Cognet G (ed) (1984) Measuring techniques in gas-liquid two-phase flows. Symposium, Nancy, France, July 5–8, 1983. Springer, Berlin

Dix GE (1971) Vapor void fractions for forced convection with subcooled boiling at low flow rates. Doctoral dissertation, University of California, Berkeley, CA, USA
Filimonov AI, Przhizhalovski MM, Dik EP, Petrova JN (1957) The driving head in pipes with a free interface in the pressure range from 17 to 180 atm. Teploenergetika 4:22–26
Gallaup J-P, Delhaye J-M (1976) Utilisation de sondes optiques miniatures en écoulement diphasique gaz-liquide. La Houille Blanche 1:17–30
Gregory GA (1975) Comparison of methods for the prediction of liquid holdup for upward gas-liquid flow in inclined Pipes. Can J Chem Eng 53:384
Harmathy TZ (1960) Velocity of large drops and bubbles in media of infinite or restricted extent. AIChE J 6(2):281–288
Hawighorst A (1984) Drop size measurement in a vertical gas-liquid flow. In: Delhaye J-M, Cognet G (eds) Measuring techniques in gas-liquid two-phase flows, IUTAM Symposium, Nancy, France, July 5–8, 1983. Springer, Berlin, pp 23–40
Hewitt GF (1978) Measurement of two-phase flow parameters. Academic Press, New York
Hewitt GF (1985) Pressure drop and void fraction. Notes for short course on two-phase flow and heat transfer, Zurich, Mar 18–22, 1985
Hewitt GF, Whalley PB (1980) Advanced optical instrumentation methods. Int J Multiph Flow 6 (1–2):139–156
Hibiki T, Ishii M (2003a) One-dimensional drift-flux model and constitutive equations for relative motion between phases in various two-phase flow regimes. Int J Heat Mass Transf 46 (25):4935–4948
Hibiki T, Ishii M (2003b) One-dimensional drift-flux model for two-phase flow in a large diameter pipe. Int J Heat Mass Transf 46:1773–1790
Hibiki T, Ishii M (2005) Erratum to: "One-dimensional drift-flux model and constitutive equations for relative motion between phases in various two-phase flow regimes". Int J Heat Mass Transf 48(6):1222–1223
Hughmark GA (1962) Holdup in gas liquid flow. Chem Eng Progr 58:62–65
Ishii M, Mishima K (1982) Liquid transfer and entrainment correlation for droplet-annular flow. In: 7th international heat-transfer conference, Munich, Sept 1982
Ishii M, Hibiki T (2011) Thermo-fluid dynamics of the-phase flow, 2nd edn. Springer, New York
Lahey RT, Moody FJ (1977) The thermal-hydraulics of a boiling water nuclear reactor. Am Nucl Soc
Lockhart RW, Martinelli RC (1949) Proposed correlation of data for isothermal two-phase, two-component flow in pipes. Chem Eng Prog 45(1):39–48
McFarlane DR (1966) An analytic study of the transient boiling of sodium in reactor coolant channels. ANL-7222, Argonne National Laboratory, Argonne, IL, USA
Martinelli RT, Nelson DB (1948) Prediction of pressure drop during forced-circulation boiling of water. Trans ASME 70(6):695–702
Milenkovic R (2005) Experimental investigation of bubbly Jets. ETH-Zurich Dissertation Nr 16206
Modisette JL (1983) Two-phase flow in pipelines-I: steady-state flow. J Energy 7(6):502–507
Mukherjee H (1979) An experimental study of inclined two-phase flow. PhD Dissertation, The University of Tulsa
Peterson DA, Tankin RS, Bankoff SG (1984) Holographic measurements of bubble size and velocity in a three-phase system. In: Delhaye J-M, Cognet G (eds) Measuring techniques in gas-liquid two-phase flows, IUTAM Symposium, Nancy, France, July 5–8, 1983. Springer, Berlin, p 1
Premoli A, Francesco D, Prina A (1971) A dimensionless correlation for determining the density of two-phase mixtures. Termotecnica 25:17–26
Rouhani SZ (1984) Personal communication
Rouhani SZ, Axelsson E (1970) Calculation of void volume fraction in the sub cooled and quality boiling regions. Int J Heat Mass Transf 13:383–393
Rousseau JC, Riegel B (1981) Super canon experiments. In: Transient two-phase flow. Proceedings of the second CSNI specialists meeting, Paris, 12–14 June 1978

Chapter 6
Pressure Drop—Empirical Methods

George Yadigaroglu

6.1 Introduction

The estimation of the pressure drop, as well as of the void fraction discussed in the previous chapter, is one of the main concerns in two-phase flow design and analysis. Seventy years after the pioneering work of Martinelli et al. (1944) and following a very large number of publications on the subject, there are still no completely satisfactory procedures and it seems that not much further progress is likely to be made. Indeed, we have probably reached the point where, in spite of the fact that the influence of the main parameters affecting the pressure gradient and the void fraction is well understood and can be modelled with sufficient accuracy, a number of secondary variables (e.g. flow entrance conditions) remain unquantifiable. The effect of these is small but contributes to the scatter of the data around the analytical predictions. Thus, precision of the order of 10–20% in the estimations should be considered good. One should recall that, even for the single-phase-flow, pressure gradient errors of that order of magnitude are not uncommon.

As already noted in Chap. 5, quite different methods are used in the oil-and-gas and in the thermal and nuclear engineering industries; the interest in the oil-and-gas industry is centred around different fluids and much larger-diameter and longer pipes. This chapter is again mainly devoted to the thermal/nuclear applications, but a separate section at the end reviews the main works in the oil-and-gas area.

We recall that the pressure gradient is the rate of change of the *static* pressure[1] with distance along a duct (i.e. the slope of the static pressure profile along the duct, *dp/dz*). In practice, it is measured as a *finite* pressure difference between two wall

[1]we recall that the *static* pressure is different from the *total* pressure, i.e. the pressure measured where the fluid is brought to rest.

G. Yadigaroglu (✉)
Emeritus of Nuclear Engineering, ETH-Zurich, Zurich, Switzerland
e-mail: yadi@ethz.ch

G. Yadigaroglu and G.F. Hewitt (eds.), *Introduction to Multiphase Flow*,
Zurich Lectures on Multiphase Flow, DOI 10.1007/978-3-319-58718-9_6

pressure taps spaced along the test section. These cannot be placed too closely, as the difference in the signal would be too small to measure accurately, and not too far so that a local-average gradient can be obtained. Details of pressure measurement procedures and equipment are given by Chexal et al. (1999). Pressure gradient measurements should be conducted for fully developed flow, though it should be noted that reaching fully developed flow under two-phase conditions takes a longer pipe length than for single phase flow.

In this chapter we are mainly concerned with two-phase pressure drop in straight, constant-area channels, except for a brief section at the end regarding flow singularities. For more complex situations, the reader is referred to the specialized literature, e.g. Hetsroni (1982).

6.2 The Pressure Gradient in Two-Phase Flow

The approach that will be followed here for calculating pressure drop is the traditional, empirical one, based on *mixture models*. Although the phenomenological or mechanistic approach discussed in another volume may be scientifically more satisfying, it should be reminded that there is still a large measure of empiricism in that approach also: the flow-pattern related mechanistic models depend themselves on empirical relationships, although these may be for more fundamental quantities such as wall friction, interfacial friction, etc. that may be difficult to estimate or measure, however. The empirical models are still widely used in industry, and are incorporated into the "system" codes used for nuclear power plant or pipeline analysis.

The methods used to provide the necessary corresponding closure laws (wall friction) in *two-fluid models* and codes will be discussed elsewhere. The closure laws needed to complete the *mixture* momentum conservation equation are expressions for the two-phase friction factor (determining the shear forces acting between the wall and the mixture), the subject of this chapter, and for the void fraction.

A large number of the available methods and correlations were developed for or using data from adiabatic tests. There are indeed not very important differences regarding the frictional pressure gradient between *adiabatic two-component systems* and *diabatic single-component systems* such as steam generators. It appears that the effects of bulk boiling on the frictional pressure gradient are minor; most of the increase in pressure drop can be explained in terms of the increased velocities in two-phase flow, rather than an increase of the wall friction per se due to the nucleation of bubbles at the wall, etc. This explains why, with few exceptions, most of the procedures and correlations do not make this distinction. In the case of subcooled boiling, however, the presence of bubbles at and near the wall has a dominant effect on pressure drop.

The gravity term obviously depends on the direction of the channel. The influence of *channel orientation* on the frictional and acceleration components is often, but not always, as we will see later, ignored.

We will start by repeating here the *mixture momentum conservation equation*, developed in Chap. 2, Eq. (2.5.4):

$$\frac{\partial}{\partial t}\dot{m} + \frac{1}{A}\frac{\partial}{\partial z}A\left(\rho_L\langle 1-\varepsilon\rangle\langle u_L\rangle_L^2 + \rho_G\langle\varepsilon\rangle\langle u_G\rangle_G^2\right) = -\frac{\partial p}{\partial z} + g\langle\rho\rangle\cos\theta - \frac{P_w\tau_w}{A} \tag{6.2.1}$$

We are not going to be concerned with the first term on the left side of Eq. (6.2.1). This term accounts for the rate of change of momentum within the infinitesimal control volume considered. It is present during transients only; it is not important, except for violent changes in flow rate. For *steady state situations*, Eq. (6.2.1) can be rearranged as follows:

$$-\frac{dp}{dz} = \frac{P_w\tau_w}{A} + \frac{1}{A}\frac{d}{dz}A\left(\rho_L\langle 1-\varepsilon\rangle\langle u_L\rangle_L^2 + \rho_G\langle\varepsilon\rangle\langle u_G\rangle_G^2\right) - g\langle\rho\rangle\cos\theta \tag{6.2.2}$$

where <ρ> denotes the two-phase density,

$$\langle\rho\rangle = \rho_L\langle 1-\varepsilon\rangle + \rho_G\langle\varepsilon\rangle \tag{6.2.3}$$

The three terms on the right side of Eq. (6.2.2) are usually identified as the partial, *frictional*, *accelerational* (or *acceleration*), and *gravitational* pressure gradients, respectively. Similar terms appear also in the momentum equation for one-dimensional *single-phase flow*. In this case, however, the calculation of the gravity head and of the acceleration term are straightforward. In fact, the acceleration term is often small or negligible in many single-phase flow situations, as the density does not change drastically. This is not the case in two-phase flow, but these two terms can be calculated if the void fraction (or the mixture density) are known. The frictional part of the pressure gradient will require some additional modelling.

The methods presented in the following section for calculating the three components of the pressure gradient are applicable in general, without *explicitly* accounting for the prevailing particular flow regime. Any such dependence is *implicit* in the correlations used; indeed, the same variables (the geometry, the mass flux, the pressure and the local quality) determine both the flow regime and the corresponding void fraction and pressure drop as already stated in the preceding chapters. Flow-regime specific models are also available but may be often avoided since they require, as an additional step, the determination of the flow regime first; these phenomenological models will be treated in another volume.

6.3 Gravitational Pressure Gradient

The gravitational pressure gradient, represented by the last term of Eq. (6.2.2), is calculated in a straightforward way provided that the two-phase density $<\rho>$ is known. The models available for calculating the average void fraction $<\varepsilon>$ needed for calculating $<\rho>$ were the object of Chap. 5.

In the case of *homogeneous flow*, the mixture density is given simply by

$$\langle\rho\rangle = \frac{1}{v} = \frac{1}{v_L + x v_{LG}} \tag{6.3.1}$$

as already noted in Chap. 5 and is readily available to use if the quality is known. If the flow is not homogeneous, the density and the gravitational gradient can be calculated using Eq. (6.2.3) for the density and an appropriate void fraction correlation.

6.4 Accelerational Pressure Gradient

The accelerational component of the pressure gradient is given by the second term on the right side of Eq. (6.2.2). This term is generated by the spatial acceleration of the flow because of changes in the average density. Such changes might be due to heat addition, to vaporization, or to flashing, (i.e. to vapour generation due to a reduction of the pressure level rather than heat addition).

In the case of *homogeneous flow*, and for a channel having a constant cross-section A, this term takes the simple form

$$-\left[\frac{dp}{dz}\right]_{ac} = \dot{m}^2 \frac{dv}{dz} \tag{6.4.1}$$

If the fluid properties remain approximately constant along the channel (the case of high-pressure systems, where the pressure drop is relatively small compared to the absolute system pressure), and we further assume thermal equilibrium between the phases, it can be easily shown that

$$-\left[\frac{dp}{dz}\right]_{ac} = \dot{m}\frac{v_{LG}\, q'}{A h_{LG}}, \quad v_{LG} \equiv v_G - v_L, \quad h_{LG} \equiv h_G - h_L \tag{6.4.2}$$

Thus the accelerational pressure gradient can be easily calculated in terms of the mass flux, the total local linear heat addition rate q', and the fluid properties.

With a *separated-flow model*, we find

$$-\left[\frac{dp}{dz}\right]_{ac} = \dot{m}^2 \frac{d}{dz}\left(\frac{(1-x)^2}{\langle 1-\varepsilon\rangle \rho_L} + \frac{x^2}{\langle\varepsilon\rangle \rho_G}\right) = \dot{m}\frac{dv'}{dz} \tag{6.4.3}$$

where v' is the notation for the "momentum specific volume," defined already by Eq. (2.5.6) in Chap. 2.

The integral of the accelerational gradient, i.e. the acceleration pressure drop from inlet to some point downstream, can be easily evaluated. Indeed, the expressions for the accelerational gradient, Eqs. (6.4.1) or (6.4.3), involve *exact* differentials and therefore only the inlet and exit values of the specific volumes v or v' are needed.

Since the exact *radial* velocity and void fraction *distributions* in the channel cross-section are not taken into account for the calculation of the accelerational gradient (see the discussion in Sect. 2.4.2 of Chap. 2), both Eqs. (6.4.1) and (6.4.3) are approximate. The separated flow model generally underestimates the acceleration effects, while the homogeneous model tends to overestimate them. In practice, the homogeneous model was often found to yield better results.

6.5 Frictional Pressure Gradient

As noted above, the calculation of the two-phase frictional pressure gradient requires some special modelling; this is the object of the following sections.

6.5.1 Parallel with Single-Phase Flow Situation

We start by recalling the situation in single-phase flow where the frictional pressure gradient is function of the fluid properties, the channel hydraulic diameter and wall roughness, and flow velocity:

$$-\left[\frac{dp}{dz}\right]_{fr,1ph} = \frac{4f}{D}\frac{\rho u^2}{2} = \frac{4f}{D}\frac{\dot{m}^2}{2\rho} \tag{6.5.1}$$

where u is the cross-sectional average or "bulk" velocity. The minus sign on the left side reminds us that the frictional pressure gradient is negative. The Reynolds number Re determines the flow regime as being either laminar or turbulent. The simplest, typical expressions for the Fannning friction factor f defined by Eq. (6.5.1) have the form

$$f = C\mathrm{Re}^{-m} \tag{6.5.2}$$

where C and m are constants (e.g. $C = 0.046$ and $m = 0.2$ for turbulent flow and $C = 16$, $m = 1$ for laminar flow), and

$$\mathrm{Re} = \frac{\rho u D}{\mu} = \frac{\dot{m} D}{\mu} \tag{6.5.3}$$

The situation is much more complex in two-phase flow: the flow regimes depend in a complex way on several system and flow parameters. The momentum exchanges between the phases and the properties of both phases influence the pressure gradient.

6.5.2 Two-Phase Flow Situation

The effects of wall shear in two-phase flow can be evaluated by an extension of the well-established methods used for single-phase flows, i.e. by the use of a friction factor and an appropriate mixture velocity and properties. This is the approach usually taken in connection with homogeneous flow models. Otherwise, the pressure gradient is usually obtained by computing a *reference pressure gradient* for a corresponding single-phase flow and correcting it with a *two-phase multiplier*, obtained from correlation of experimental data. The value of the two-phase multiplier can be much larger than one.

The influence of the *wall roughness* on two-phase pressure drop is probably flow-pattern specific. In the absence of better information, it is usual practice to account for the effects of wall roughness through its usual influence on the reference single-phase friction factor. Similarly, the *geometry of the cross-sectional area* is accounted for through use of the channel hydraulic diameter, as is done in single-phase flow.

6.5.3 The Homogeneous-Flow Model

For two-phase flows, the *logical* values of ρ and u in Eq. (6.5.1) are the two-phase, homogeneous mixture density $<\rho>_{hom}$ and velocity $<u>_{hom} = <j>$ and the frictional pressure gradient can be calculated as

$$\begin{aligned} -\left[\frac{dp}{dz}\right]_{fr,2p} &= \frac{4f}{D}\frac{\langle\rho\rangle_{\mathrm{hom}}\langle u\rangle_{\mathrm{hom}}^2}{2} = \frac{4f}{D}\frac{\dot{m}^2}{2\langle\rho\rangle_{\mathrm{hom}}} \\ \frac{1}{\langle\rho\rangle_{\mathrm{hom}}} &= \frac{1-x}{\rho_L} + \frac{x}{\rho_G}, \quad \langle u\rangle_{\mathrm{hom}} = \frac{\dot{m}}{\langle\rho\rangle_{\mathrm{hom}}} = \langle j\rangle \end{aligned} \tag{6.5.4}$$

Comparing Eqs. (6.5.1) and (6.5.4) we see that the two-phase effect enters the formulation as a density effect. The question is raised, however, as to how the value of the friction factor should be computed; this is the only remaining degree of freedom. Most of the industrial two-phase flows are likely to be turbulent and the friction factor is generally obtained by an equation of the type of Eq. (6.5.2); this requires definition of a mixture viscosity. There is no general agreement regarding this choice. Practically all possibilities have been tried for the two-phase viscosity μ:

$$\begin{array}{ll} \frac{1}{\mu} = \frac{x}{\mu_G} + \frac{1-x}{\mu_L} & \text{McAdams (1942)} \\ \mu = x\mu_G + (1-x)\mu_L & \text{Cicchitti (1960)} \\ \mu = \langle 1-\varepsilon \rangle \mu_L + \langle \varepsilon \rangle \mu_G & \text{Dukler (1964)} \\ \mu = \mu_L & \text{Owens (1961)} \end{array} \tag{6.5.5}$$

As the value of μ appears at a low power (usually m = 0.2 to 0.25 in Eq. (6.5.2) for the prevailing turbulent flows), the formulas listed above do not yield drastically different results. Wallis (1969) goes further and recommends the use of f = 0.005 as a reasonable average value for most cases.

More recently Beattie and Whalley (1982) proposed the following expression, which is based on theoretical considerations including the effect of flow patterns,

$$\mu = \mu_{\mathrm{L}}(1-\beta)(1+2.5\beta) + \mu_{\mathrm{G}}\beta$$

where β is the homogeneous void fraction. They claim that their simple method yields better results than most other available methods. The Owens choice seems also to be a simple, good one that also makes good physical sense: it is the liquid that is, most of the time, in contact with the wall.

Another advantage of the homogeneous model, beyond its inherent simplicity, is that as an analytic expression for the quality and consequently for $<\rho>$ is available, when the fluid properties can be considered constant along the channel, Eq. (6.5.4) can often be analytically integrated to yield the pressure profile along the channel.

6.5.4 *Two-Phase-Multiplier Methods for the Frictional Pressure Gradient*

It has been customary, following the seminal work of Martinelli (Martinelli et al. 1944; Lockhart and Martinelli 1949) to relate the two-phase frictional pressure gradient to some reference single-phase value through a two-phase multiplier, Φ^2.

The effects of hydraulic diameter and relative wall roughness are implicitly included in the reference single-phase pressure gradient, while those of the fluid properties and mass flux are only partly accounted for. The multiplier, which is mainly a function of quality and physical properties (density and viscosity) is

occasionally corrected for additional mass-flux and other effects, as we will see below.

Two distinct kinds of reference frictional gradients are in use. The first, distinguished in the literature by the subscripts g (or G) and f (or L), for gas and liquid, respectively, or alternatively by GP and LP (the notation used here and already introduced in Chap. 1, Sect. 1.10), are calculated assuming that *only one of the two phases is flowing alone* in the channel:

$$-\left[\frac{dp}{dz}\right]_{frLP} = \frac{4f_{LP}}{D}\frac{\dot{m}^2(1-x)^2}{2\rho_L}, \quad -\left[\frac{dp}{dz}\right]_{frGP} = \frac{4f_{GP}}{D}\frac{\dot{m}^2x^2}{2\rho_G} \tag{6.5.6}$$

where the friction factors are calculated on the basis of the following Reynolds numbers:

$$\mathrm{Re}_{LP} \equiv \frac{\dot{m}\,(1-x)D}{\mu_L} \quad \text{and} \quad \mathrm{Re}_{GP} \equiv \frac{\dot{m}\,xD}{\mu_G} \tag{6.5.7}$$

The second set of reference frictional pressure gradients, usually distinguished in the literature by the subscripts LO and GO (or occasionally by fo and go) is calculated assuming that the entire two-phase mass flow rate is flowing as *a single phase* in the channel:

$$-\left[\frac{dp}{dz}\right]_{frLO} = \frac{4f_{LO}}{D}\frac{\dot{m}^2}{2\rho_L}, \quad -\left[\frac{dp}{dz}\right]_{frGO} = \frac{4f_{GO}}{D}\frac{\dot{m}^2}{2\rho_G} \tag{6.5.8}$$

with the friction factors evaluated at the following Reynolds numbers:

$$\mathrm{Re}_{LO} = \frac{\dot{m}D}{\mu_L}, \quad \mathrm{Re}_{GO} = \frac{\dot{m}D}{\mu_G} \tag{6.5.9}$$

Obviously the frictional pressure gradient must be the same, no matter what the reference pressure gradient is. Thus, the two-phase frictional pressure gradient is given by the following expressions, which also define the various multipliers used:

$$\left[\frac{dp}{dz}\right]_{fr2ph} = \left[\frac{dp}{dz}\right]_{frLP}\Phi_{LP}^2 = \left[\frac{dp}{dz}\right]_{frGP}\Phi_{GP}^2 = \left[\frac{dp}{dz}\right]_{frLO}\Phi_{LO}^2 = \left[\frac{dp}{dz}\right]_{frGO}\Phi_{GO}^2$$

If the friction factors are given by Eq. (6.5.2) then

$$\frac{\left[\frac{dp}{dz}\right]_{fr\,LP}}{\left[\frac{dp}{dz}\right]_{fr\,LO}} = \frac{\Phi_{LO}^2}{\Phi_{LP}^2} = (1-x)^{2-m}, \quad \frac{\left[\frac{dp}{dz}\right]_{fr\,GP}}{\left[\frac{dp}{dz}\right]_{fr\,GO}} = \frac{\Phi_{GO}^2}{\Phi_{GP}^2} = x^{2-m} \tag{6.5.10}$$

Thus the two definitions of the multiplier can be used interchangeably. When x changes along the channel, the second definition offers computational advantages since the reference pressure gradient remains constant (except for changes in fluid properties). The definition of all these different but essentially equivalent multipliers can lead to confusion and the reader of the literature should be careful since the various contributors are not always using consistent notation *and* defining their approach carefully.

Note that for the simple *homogeneous flow model* with $\mu = \mu_{L,}$

$$\Phi_{LO}^2 = 1 + x\left(\frac{\rho_L}{\rho_G} - 1\right) \tag{6.5.11}$$

6.5.5 The Martinelli et al. Method

This approach (Martinelli et al. 1944) has formed the basis for most of the correlation work that followed. It is based on a physical model of the two phases flowing separately; this model is not really defensible, but the resulting method has been shown to work in practice well. The important step taken by Martinelli was to correlate the multiplier (and the void fraction) in terms of *only* the square root of the ratio of the two pressure gradients:

$$X \equiv \left[\frac{\left[\frac{dp}{dz}\right]_{fr\,LP}}{\left[\frac{dp}{dz}\right]_{fr\,GP}}\right]^{1/2} = \frac{\Phi_{GP}}{\Phi_{LP}} \tag{6.5.12}$$

The useful qualities of this parameter probably stem from the fact that it contains the relevant geometrical and fluid variables with the same exponents as in the single-phase classical pressure drop formula. Using the appropriate expressions for the reference pressure gradients, Eq. (6.5.6), for the friction factors, Eq. (6.5.2), and the definition of the quality,$x = \dot{m}_G/\dot{m}$, we can compute the general expression for X^2:

$$X^2 = \frac{C_L}{C_G}\left[\frac{1-x}{x}\right]^2 \frac{\rho_G}{\rho_L}\frac{\mathrm{Re}_{GP}^m}{\mathrm{Re}_{LP}^n} = \frac{C_L}{C_G}\frac{(1-x)^{2-n}}{x^{2-m}}\frac{\rho_G}{\rho_L}\frac{\mu_L^n}{\mu_G^m}(\pi D)^{n-m} \tag{6.5.13}$$

where m and n are the exponents of the Reynolds number in Eq. (6.5.2) for the gas and liquid friction factors, and C_G and C_L the coefficients the equations, respectively. Four different cases are considered according to the flow regime (turbulent of laminar) for each phase. For each case the values of C and m (or n) and the resulting definition of X are different. The corresponding values and the limiting values of the Reynolds numbers can be found in Lockhart and Martinelli (1949). For the most

common, *turbulent-turbulent* case we find the expression already introduced in Chap. 1, Sect. 1.10:

$$X_{tt} = \left[\frac{1-x}{x}\right]^{0.9}\left[\frac{\rho_G}{\rho_L}\right]^{0.5}\left[\frac{\mu_L}{\mu_G}\right]^{0.1} \tag{6.5.14}$$

As noted in Chap. 1, the Martinelli parameter X_{tt} has also found applications in other areas of two-phase flow and boiling heat transfer, for example, in forced-convection vaporization.

For a given liquid-vapour mixture of a single component at saturation conditions, X_{tt} is a function of local quality and pressure only. The figure in the Appendix to this chapter can be used to rapidly estimate the dimensionless property group contained in X_{tt} for various fluids, facilitating its computation.

The Lockhart-Martinelli correlation for the frictional multiplier

Lockhart and Martinelli (1949) correlated a variety of void fraction and pressure drop data for two-component isothermal mixtures flowing in horizontal pipes and arrived at values of $<\varepsilon>$ and Φ as functions of X that are still widely used. The values and plots of the multipliers and of the void fraction, as proposed by Lockhart and Martinelli separately for each combination of regimes, can be found in the original work and in most standard reference works. A simple expression approximating fairly well the Lockhart and Martinelli values for Φ^2 (for the turbulent-L/turbulent-G case) was proposed by McFarlane (1966):

$$\Phi^2_{LPtt} = 1 + \frac{20}{X_{tt}} + \frac{1}{X_{tt}^2} \tag{6.5.15}$$

The Φ^2_{LPtt} values are accurate to within 10–30% for X_{tt} between 0.01 and 1 and within a few percent for higher values.

Integral pressure drop correlations

At a given system pressure level (i.e. neglecting the variations of the properties along the channel with pressure), the total pressure drop from the bulk boiling boundary (point where $x = 0$) to the exit of the heated length ($x = x_e$) can be estimated by integration of the pressure gradient, if the variation of the quality along the channel is known. *When the variation of the quality is linear*, i.e. for a uniform heat input distribution and no significant flashing, we obtain

$$\frac{\Delta p_{fr2\varphi}}{\Delta p_{LO}} = \overline{\Phi^2_{LO}} = \frac{1}{x_e}\int_0^{x_e} \Phi^2_{LP}(1-x)^{2-m}dx$$

where Δp_{LO} is the pressure drop calculated assuming that the entire two-phase flow is flowing as liquid. This form of the equation is useful for practical applications (provided, as noted above, that the variation of the quality is linear or nearly linear).

The values of the integral can be calculated once and for all, since, for a given fluid, these are functions of the saturation pressure only. When the heat input distribution is not uniform and the variation of the properties must be accounted for, stepwise numerical integration of the momentum equation is necessary using some correlation for the local pressure gradient.

Thom (1964) has correlated high-pressure boiling-water data ($p > 17$ bar or 250 psia, $x = 0.1$ to 1.0). He has postulated that the velocity ratio S is a function of system pressure only (which is clearly an oversimplification); these values of S where then used to calculate the gravity and acceleration pressure drops using Eqs. (6.3.1) and (6.4.3). The frictional pressure drop was correlated in terms of an integral multiplier. Using Thom's notations, the pressure gradient equation, Eq. (6.2.2), integrated from the beginning of the boiling length to the point where $x = x_e$, assuming constant properties, is written in integral form as

$$\Delta p = g\rho_L L \cos\theta\, r_4 + \Delta p_{LO}\, r_3 - \frac{\dot{m}^2}{\rho_L} r_2 \tag{6.5.16}$$

For a constant-quality channel,

$$\Delta p = g\langle\rho\rangle L \cos\theta + \Delta p_{LO}\, r_5$$

where L is the boiling length. The coefficients r of his correlations are plotted in figures presented by Thom as functions of the exit quality and of the pressure and are also tabulated in the original work. The density $<\rho>$ in Eq. (6.5.16) must be calculated using Thom's S values. The graphs are convenient to use to rapidly obtain an estimate of the void fraction in a boiling channel without lengthy computations; they can be found in the Appendix to this chapter (unfortunately in the original British units).

6.5.6 The Friedel Correlation

Friedel (1979) assembled a large data bank containing 25,000 pressure drop points and obtained a correlation based on these as follows:

For horizontal and vertical upflow:

$$\Phi_{LO}^2 = A + 3.43\, x^{0.685}(1-x)^{0.24}\left(\frac{\rho_L}{\rho_G}\right)^{0.8}\left(\frac{\mu_G}{\mu_L}\right)^{0.22}\left(1-\frac{\mu_G}{\mu_L}\right)^{0.89} \mathrm{Fr}_L^{-0.047}\mathrm{We}_L^{-0.0334} \tag{6.5.17}$$

An improved correlation for vertical downflow (Friedel 1984) is given by:

$$\Phi_{LO}^2 = A + 5.7\,x^{0.7}(1-x)^{0.14}\left(\frac{\rho_L}{\rho_G}\right)^{0.85}\left(\frac{\mu_G}{\mu_L}\right)^{0.36}\left(1-\frac{\mu_G}{\mu_L}\right)^{0.2}\mathrm{Fr}_L^{-0.09}\mathrm{We}_L^{-0.007} \tag{6.5.18}$$

with

$$A = (1-x)^2 + x^2\left(\frac{\rho_L f_{GO}}{\rho_G f_{LO}}\right)$$

$$\mathrm{Fr}_L \equiv \frac{\dot{m}^2}{gD\rho_L^2}\ ,\ \mathrm{We}_L \equiv \frac{\dot{m}^2 D}{\rho_L \sigma}$$

with

$$\mathrm{Fr} \equiv \frac{\dot{m}^2}{gD\langle\rho\rangle_{\mathrm{hom}}^2},\quad \mathrm{We} \equiv \frac{\dot{m}^2 D}{\langle\rho\rangle_{\mathrm{hom}}\sigma},\quad \frac{1}{\langle\rho\rangle_{\mathrm{hom}}} = \frac{x}{\rho_G} + \frac{1-x}{\rho_L}$$

where $<\rho>_{\mathrm{hom}}$ in Fr and We is calculated with the homogeneous flow assumption. Inclusion of the surface tension via the Weber number into the correlation is apparently an improvement. One notes that the effect of the surface tension is, however, weak as the exponents of Fr and We are small.

More recent correlations for the frictional pressure gradient

Many frictional pressure drop correlations have been proposed. Baroczy (1965) developed a broadly based correlation using data for boiling water, water-air, and mercury-nitrogen flows. The correlation was tested satisfactorily with a variety of other data including some boiling liquid-metal data. His method may constitute an improvement over the Lockhart-Martinelli approach as it replaces X_{tt} by two separate correlating parameters: the quality, x, and a property index Γ,

$$\frac{1}{\Gamma^2} \equiv \frac{\rho_G}{\rho_L}\left[\frac{\mu_L}{\mu_G}\right]^{0.2} \tag{6.5.19}$$

However, Baroczy introduced also a correction to the multiplier value for mass flux having a very complex graphical form, making it difficult to use and conceptually "unattractive." The correlation produces, however, good results (Chexal et al. 1999).

Chisholm (1967) has shown that Eq. (6.5.15) for the frictional multiplier can be derived analytically, provided the exponent of the viscosity in the pressure gradient expression, (the m in Eq. (6.5.2)) is taken as zero. This gives reassurance regarding the use of an equation having that form for correlating frictional pressure drop data. Using the property index Γ proposed earlier by Baroczy (1965), Chisholm (1973) arrives at the following formulation for the local frictional pressure gradient

$$\Phi_{LO}^2 = 1 + (\Gamma^2 - 1)\left[B[x(1-x)]^{\frac{2-m}{2}} + x^{2-m}\right], \quad B = B(\Gamma, \dot{m}) \tag{6.5.20}$$

where m is the coefficient of the Reynolds number in the friction factor formula, Eq. (6.5.2); usually, $m = 0.2$. Chisholm (1973) recommends the following expressions for B (for smooth tubes) according to the mass flux and the property index:

Γ	$\dot{m}$ (kg/m^2 s)	B
$\Gamma < 9.5$	<500	4.8
	$500 < \dot{m} < 1900$	$2400/\dot{m}$
	>1900	$55/\dot{m}^{0.5}$
$9.5 < \Gamma < 28$	<600	$520/(\Gamma\dot{m}^{0.5})$
	>600	$21/\Gamma$
$\Gamma > 28$		$15\,000/(\Gamma^2\dot{m}^{0.5})$

Approach based on a two-phase friction factor

A new approach, not based on the use of the conventional reference pressure gradient and the two-phase multiplier, was more recently presented by Shannak (2008) who correlated directly a two-phase friction factor in the expression for the frictional gradient, defined as:

$$\left[\frac{dp}{dz}\right]_{fr\,2p} = \frac{f_{2p}}{D}\frac{\dot{m}^2}{2\langle\rho\rangle_{\text{hom}}}$$

(note that he uses the Weisbach friction factor which is four times the Fanning friction factor used usually in this volume; there is no factor 4 in the equation). Shannak defines a two-phase Reynolds number as the ratio of the sum of the "inertial forces" of each phase to that of the sum of the "viscous forces" of each phase (apparently using the volumetric fluxes or superficial velocities as "velocity of the phase"):

$$\text{Re}_{2p} \equiv \frac{\left(\rho_G\langle j_G\rangle^2 + \rho_L\langle j_L\rangle^2\right)D^2}{(\mu_G\langle j_G\rangle + \mu_L\langle j_L\rangle)D} = \frac{\dot{m}D\left(x^2 + (1-x)^2\frac{\rho_G}{\rho_L}\right)}{\mu_G x + \mu_L(1-x)\frac{\rho_G}{\rho_L}}$$

The two-phase friction factor is then correlated in terms of the two-phase Reynolds number as:

$$\frac{1}{\sqrt{f_{2p}}} = -2\log\left[\frac{1}{3.7065}\left(\frac{\varepsilon_r}{D}\right) - \frac{5.0452}{\text{Re}_{2p}}\log\left(\frac{1}{1.2857}\left(\frac{\varepsilon_r}{D}\right)^{1.1098} + \frac{5.8506}{\text{Re}_{2p}^{0.8981}}\right)\right] \tag{6.5.21}$$

where ε_r/D is the relative pipe roughness. The correlation was obtained with the author's relatively low-pressure (5–14 bar), moderate mass flux (200–1500 kg/m^{2}s), air-water data, but was tested against other experimental data from the literature (the 16000 experimental data points from Friedel (1979)) also against the most common methods (including the Friedel (1979), Lockhart and Martinelli (1949) and other correlations). The author's experiments were conducted in a horizontal test section 9.6 m in length and a vertical test section with a length of 5.9 m; he does not state how he evaluated the gravitational component of the pressure gradient for the vertical test section data. Shannak concludes that his correlation was the best-fitting one, followed by the Friedel (1979) correlation. The author also notes that the wall roughness becomes important at high mass fluxes.

6.5.7 The EPRI Chexal-Harrison Approach

The EPRI group that had produced the EPRI Chexal-Lellouche correlation for void fraction continued their work and produced a correlation for the two-phase pressure drop (Chexal et al. 1997), the Chexal-Harrison (1999) set of correlations. These are, however, mainly intended for use in system codes and therefore provide (for both vertical and horizontal flows) the mixture-wall shear but also the shear between each phase and the wall, as well as the interfacial shear (the last three clearly needed in the two-fluid formulation discussed in Chap. 2).

The wall-mixture frictional two-phase pressure gradient includes contributions from situations where the liquid or the gas on the wall "dominate" and has the general form:

$$\left(\frac{dp}{dz}\right)_{fr\,wall} = \left(\frac{dp}{dz}\right)_l \left[1 + \frac{f_{w\,LOs}}{f_{w\,LO}} \prod_{i=1-6} F_{l\,i}\right] F_l + \left(\frac{dp}{dz}\right)_g \left[1 + \frac{f_{w\,GOs}}{f_{w\,GO}} \prod_{i=1-6} F_{g\,i}\right] F_g \tag{6.5.22}$$

with a "mixed" definition of the reference pressure gradients

$$\left(\frac{dp}{dz}\right)_k = f_{w\,kO} \frac{\rho_k \langle j_k \rangle^2}{2D}, \quad k = L, G$$

The friction factors are computed assuming that the entire mixture flows as one phase (the "LO-GO" convention) while the term $f_{w\,LOs}/f_{w\,LO}$ is the ratio of wall friction factors with a smooth-wall and the real wall roughness, (a detail not considered in other correlations where simply the equivalent single-phase reference friction factor is used). The coefficients F_{ki}, $k = l,g$, appearing in the products in Eq. (6.5.22) are functions of non-dimensional flow parameters, flow orientation (horizontal-vertical), void fraction, and fluid properties. Finally, the weighting factors F_k, $k = l,g$

$$F_l = 1 - e^{(-C_{l10}\langle \varepsilon_L \rangle)}, \quad F_g = e^{(-C_{g10}\langle \varepsilon_L \rangle)}$$

provide the necessary weighting of the two phases in the sum of the two "dominant" terms of Eq. (6.5.22) with exponentially decaying functions of the liquid fraction. The coefficients C_{k10} depend on flow orientation. The method distinguishes between heated and unheated channels, something that no other correlation does. Great care was taken to provide smooth forms of the equations for use in codes that "do not like" discontinuities. Implemented in system codes, the (very complex) Chexal-Harrison approach produced results better than those from the traditional correlations for diabatic flows, as shown in Fig. 6.1.

The useful publication by EPRI (Chexal et al. 1999) contains also a lot of information on pressure drop, including discussion on measurement methods, comparisons of the traditional correlations discussed above, a long discussion of the single-phase friction factor, etc. It also includes the necessary software for the implementation of the methods proposed on a CD-ROM.

6.6 Comparisons of Available Correlations

In determining the total pressure drop, one should try to calculate with the greatest accuracy the dominant components. Gravity is dominant at low flow and low quality; friction dominates at high mass flux and high quality, while acceleration is important at high quality and low mass flux. Figure 6.2 shows the regions of dominance of the three components in the mass-flux vs quality plane. This is obviously a particular case and the figure may be quite different for other combinations of fluids and conditions.

An important fact to keep in mind when comparing frictional pressure gradient correlations is that their accuracy is obscured by the fact that a void fraction correlation must be used first to extract the frictional gradient from the total *measured* pressure gradient (by subtracting the gravity and acceleration components) and the results depend on the choice of the void fraction correlation used for this. In principle, to be consistent, one should be using the same void fraction correlation as the authors of the frictional-pressure-gradient correlation used, but it is often not done so.

Several comparisons of the accuracy of available (void fraction and) frictional pressure drop correlations have been published. Idsinga et al. (1977) assessed pressure drop correlations for steam-water systems using over 3000 adiabatic, as well as diabatic data points. Considering the total data bank, the four methods exhibiting minimum prediction error were the homogeneous flow models of Owens (1963) and of Cicchitti (1960)—see Sect. 6.5.3 on the Homogeneous Flow Model; the Thom (1964); and the Baroczy (1965) correlations. The authors also present a useful table listing the most successful correlations according to the quality, pressure, and mass flux range.

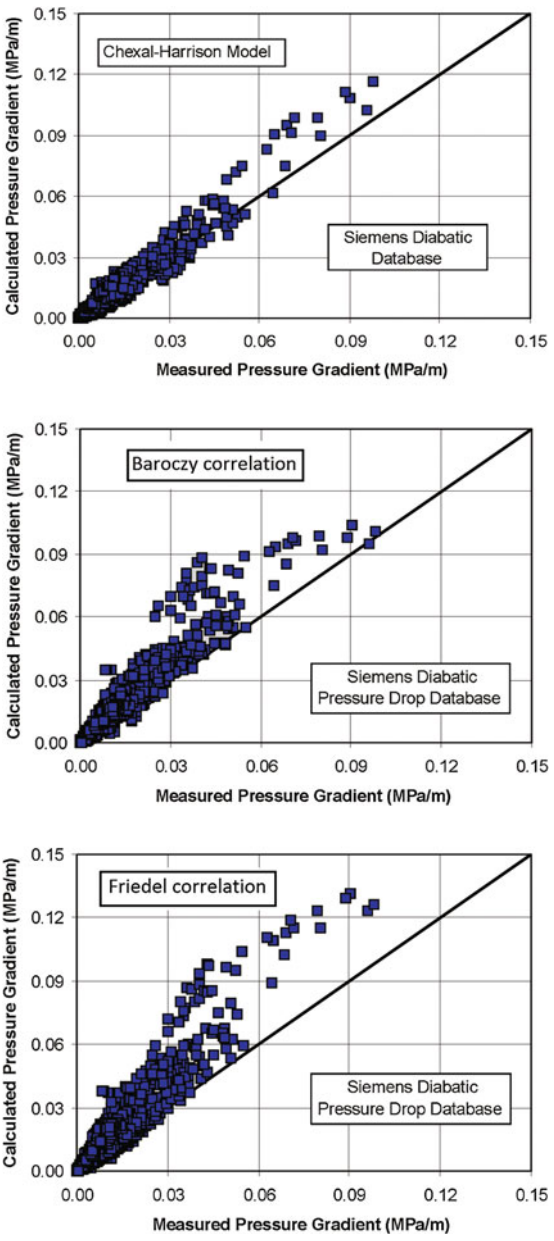

Fig. 6.1 Comparisons of the predictions of the Chexal-Harrison model with the predictions of the Baroczy (1965) and Friedel (1979) correlations made with a diabatic data set containing 862 points. The correlations were incorporated in system codes for these comparisons. The Baroczy-correlation graphical correction factors for the effect of the mass flux were replaced by tables. © and courtesy of EPRI

Vijayan et al. (2000) compared pressure drop and void fraction correlations using data from two-phase natural circulation loops; they recommend the Chexal et al. (1997) correlation discussed in Chap. 5 for the void fraction and found that the Lockhart-Martinelli correlation for void fraction discussed in this chapter gave the

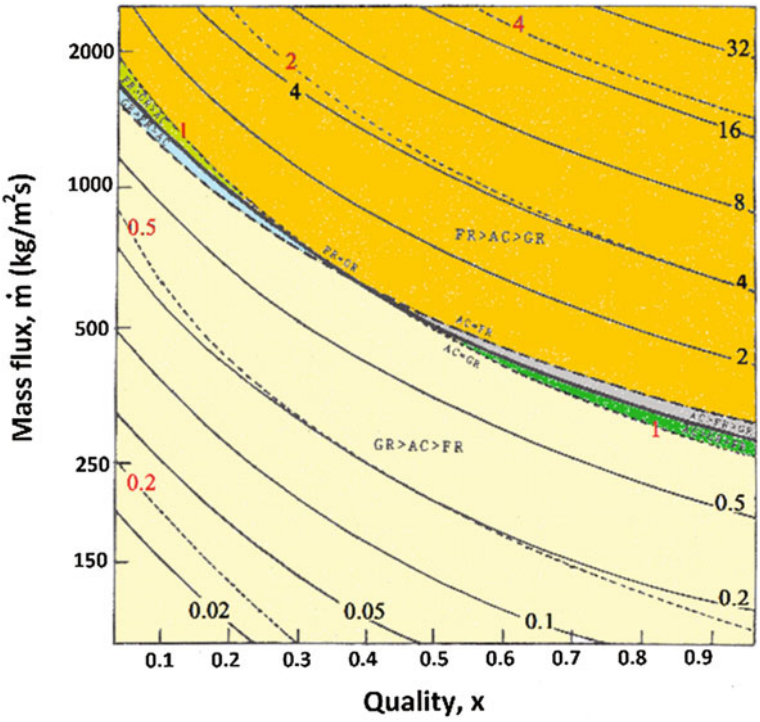

Fig. 6.2 Contour map in the $(\dot{m}, x)$ plane showing the regions of dominance of the three components of the total pressure gradient (FR denotes friction, GR gravity and AC acceleration). The continuous lines and the black numbers indicate the ratio FR/GR; the dotted lines and the red numbers the ratio AC/GR. Map produced for saturated water at 146 bar flowing in a 10 mm ID pipe. The heat input used to produce the various conditions plotted was 27 kW/m. The computations were performed with the homogeneous flow model

best results for the frictional pressure gradient in relation to their data base. One conclusion that the reader gets in reading their paper is that there is no consistent image regarding the "best correlation" for the frictional pressure gradient.

Beattie and Whalley (1982) discuss comparisons using an adiabatic data bank. Very good results were obtained using the Baroczy (1965), the Friedel (1979) (except for horizontal steam/water flows), and the Beattie and Whalley (1982) correlations. The Lockhart-Martinelli (1949) correlation gave also good results for non-steam/water flows.

In conclusion, it can be said, that correlations, such as the Chisholm (1973), the Friedel (1979), and the Beattie and Whalley (1982) correlations have been "tuned" with large enough data sets to insure an acceptable degree of accuracy in most situations. It is interesting to note that simple correlations, such as that of Beattie and Whalley, can yield good results. Some older correlations remain good over their respective ranges: the Lockhart-Martinelli correlation for non-steam/water

flows, the Thom correlation for high-pressure steam-water flows. The Baroczy (1965) correlation also yields generally good results.

Figure 6.1 shows the more recent comparisons of the Chexal-Harrison, Baroczy and Friedel models; additional comparisons can be found in the booklet by Chexal et al. (1999). Here the comparisons were systematically made using the Chexal-Lellouche (Lellouche et al. 1997) correlation for the void fraction. The Chexal-Harrison model that considers boiling seems to have some advantage over the other two correlations.

6.7 Pressure Drop Work for Large and Inclined Pipes Used in the Oil-and-Gas Industry

In Chap. 5 we had discussed the liquid holdup correlations of interest to the oil-and-gas industry. We will do the same now for the pressure drop in large pipes including inclined ones (pipelines). Practically all oil-well production involves two-phase flow in pipelines.

Most of the reliable and complete experimental information regarding two-phase flow in horizontal and inclined pipes has been obtained in the past with pipes of relatively modest diameter (up to a few inches, at most). Data from actual-size pipelines are relatively scarce and often proprietary and an important extrapolation of knowledge obtained with small diameters to large diameters must be made. It is only recently that some data from large-diameter pipeline testing facilities have become available but it is likely to be proprietary, given the commercial interests and the cost of producing such data.

Aggour and Al-Yousef (1996) made a comprehenive evaluation of pressure-drop data sets and correlations, including cases of three component flow (oil, water, gas). They concluded that the fairly old Beggs and Brill (1973) correlation provided the best pressure predictions. However, an older correlation (Hagedorn and Brown 1964) was better for water cuts (ratio of water produced to the volume of total liquids from an oil well) above 80% and another phenomenological model (Hasan and Kabir 1988) for gas/oil mixtures in vertical oil wells was better for high production rates. Ferguson and Spedding (1995) and Vijayan et al. (2000) provide additional comparisons and make recommendations for the selection of methods. The papers just quoted, as well as some other papers cited below provide a lot of additional detailed information that is beyond our scope here.

Most of the published void fraction (or holdup) and frictional pressure gradient correlations and models, do not account explicitly for pipe inclination. Gregory (1975) has reviewed holdup correlations suitable for inclined pipes available up to 1975. Behnia (1991) compared several correlations with vertical flow data and states that overall, the Beggs and Brill correlation produced the most accurate results. The same conclusion was reached by Aggour and Al-Yousef (1996) who made detailed comparisons with various data sets.

The Beggs and Brill (1973) correlation was derived specifically for flow in inclined pipes but it can be used for any inclination. It presents itself as a multiplier of a reference frictional gradient calculated assuming homogeneous flow. The homogenous friction factor f_{hom} for the reference gradient is estimated using the usual Moody chart and the following Reynolds number:

$$\mathrm{Re} \equiv \frac{\dot{m}D}{\mu_L \lambda + \mu_G(1-\lambda)}$$

The frictional pressure gradient takes the form

$$\left[\frac{dp}{dz}\right]_{fr} = \frac{4f_{\mathrm{hom}}}{D}\frac{\dot{m}\langle j\rangle}{2}e^s$$

where the exponent s of the multiplier e^s is given by

$$\frac{1}{s} = \frac{-0.0523 + 3.182\,\xi - 0.8725\,\xi^2 + 0.01853\,\xi^4}{\xi}$$

with $\xi = \ln y$ with $y = \frac{\lambda}{\langle \varepsilon_G(\beta)\rangle^2}$

where $\langle \varepsilon_G(\beta)\rangle$ is the void fraction in the pipe with an inclination angle β. Somewhere in the interval $1 < y < 1.2$, s, as given by the equation above, becomes unbounded and should be calculated from $s = \ln(2.2y - 1.2)$.Thus one must estimate first the liquid holdup, as presented in Sect. 5.6.1 of Chap. 5, and then use it for estimating the frictional pressure gradient.

6.7.1 Experimental Data

Extensive data on the frictional pressure gradient in inclined pipes are presented by Spedding et al. (1982, 2006), who also review previously available information. Spedding et al. (1982) conclude that the effect of inclination is greatest at low flow rates. This should not be surprising since at high flow rates the effects of gravity become relatively less pronounced. The data of the authors are presented as plots of the frictional velocity U^*

$$U^* \equiv \sqrt{\frac{\tau_w}{\rho_L}} = \sqrt{-\left.\frac{dp}{dz}\right|_{fr}\frac{D}{4\rho_L}}$$

versus the total volumetric flux <j>. The plots also include flow regime boundaries, as shown in Fig. 6.3 taken from their work. Examination of the two plots of Fig. 6.3 confirms the great differences due to an upward inclination of only 2.75°.

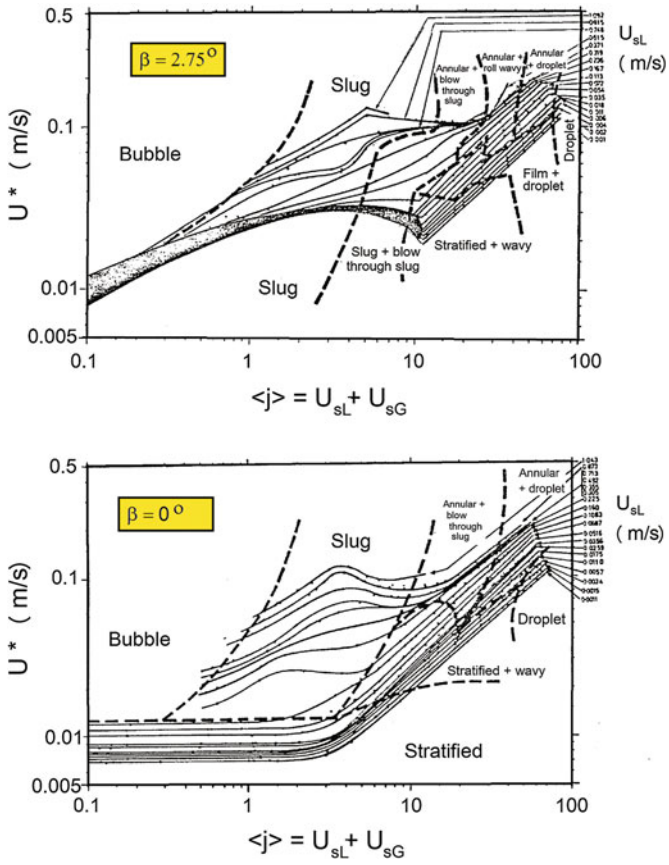

Fig. 6.3 Frictional velocity plotted against the total volumetric flux with the liquid volumetric flux as a parameter. Air-water in 45.5 mm tube. (Spedding et al. 1982). *Top* 2.75° upwards inclined pipe. *Bottom* horizontal pipe

The authors also conclude that the frictional velocity clearly depends on the flow regime in the pipe and that a correlation of the data for all flow regimes would necessarily be inaccurate. Minimal frictional velocities are encountered in the stratified regimes. The transition to large waves and to slug flow is accompanied by a large increase in wall friction. The frictional velocity in downward flow is higher than in the corresponding horizontal case.

The authors also note that negative frictional pressure losses were measured in upward flow situations with low liquid flow rates. Correlations never predict such negative values. The same observation was made earlier by Singh and Griffith (1970) who studied slug flow in inclined pipes and noticed that one could have liquid running down at the wall and still have net liquid flow up.

6.7.2 Pipeline Design

Two-phase flow problems encountered in power or nuclear engineering typically involve the calculation of pressure drop and void fraction for vertical or horizontal channels of *given* moderate dimensions (of the order of an inch) and for specified quality and total flow rate. In the case of pipelines the engineer often faces an optimization problem: the pipeline diameter capable of carrying a certain load under minimal pressure drop conditions must be found. The pipe diameters are now much larger (6–8 inches or 0.15 to 0.2 m for short pipelines, and up to 24–36 inches or 0.6 to 0.9 m for long-distance transport lines) and the pipeline often traverses hilly terrain where there is a continuous variation of the inclination (Gregory et al. 1975). The authors show that the total pressure drop calculated for a pipeline traversing hilly terrain, at very low gas-to-oil ratios (GOR), decreases monotonically with increasing pipe diameter, as expected. This is not the case, however, at higher GORs: they found a broad minimum around 5 inches and the pressure loss does not diminish much by increasing the diameter beyond this value.

According to the findings of Beggs and Brill (1973) presented above, for upward inclined pipes the holdup is always greater than or equal to that occurring in a horizontal pipe. Thus the liquid will have the tendency to accumulate in uphill portions of the pipelines increasing the gravitational pressure drop.

A number of additional phenomena must also be considered in pipeline design, including phase changes along the pipeline and the effects of dropping pressure on the gas properties. Such phenomena are beyond the scope of these notes but can easily be accounted for when a stepwise integration of the momentum equation along the pipe is performed.

6.7.3 Mechanistic Models Based on Two-Fluid Formulation

As we have said in the preceding chapter on void fraction, one can write the momentum conservation equations for the two phases in stratified horizontal or inclined flow (see Sect. 4.5.1 of Chap. 4). If closure laws for the interfacial and wall shear are available, the equations can be solved to obtain the void fraction (or, equivalently the height of the liquid in the pipe) and then compute the frictional pressure gradient. Examples of this approach are the works of Taitel and Dukler (1976), Modisette (1983), Spedding and Hand (1997) and others. Mechanistic models will be discussed in another volume as mentioned in the introduction.

6.8 Two-Phase Pressure Drop in Singularities

All practical two-phase flow systems or pipe arrangements include "point singularities" such as enlargements, contractions, bends, fitting, valves, instrumentation, etc. For single-phase flow, there are well-established engineering methods to deal with these local pressure losses. These are usually defined as shown in Fig. 6.4 for the example of a sudden expansion: the local pressure loss is obtained by extrapolation of the pressure gradients on both sides of the discontinuity.

Let us recall first that in single-phase flow, the total pressure drop at the discontinuity has a reversible part and a non-reversible one. The reversible part is due to the acceleration/deceleration of the flow (the acceleration term in the momentum equation) and can be positive or negative. The irreversible part is always positive (a loss) and is due to the transformation of mechanical energy into heat due to viscous dissipation. It is often represented by a loss factor K multiplying the kinetic energy term:

$$\Delta p_{local\ loss} = K\frac{\rho u^2}{2} = K\frac{\dot{m}^2}{2\rho}$$

Often the K coefficient is expressed as "number of equivalent diameters" N_{eq}, as if the pipe had become locally longer,

$$K = \frac{4fL_{eq}}{D} = 4fN_{eq}, \quad N_{eq} = \frac{L_{eq}}{D}$$

consistent with the formula for pressure drop in a straight pipe where the friction factor depends on the Reynolds number:

$$\Delta p_{fr} = \frac{4fL}{D}\frac{\rho u^2}{2}, \quad f = f(\mathrm{Re})$$

In two-phase flow, the reversible loss is in principle the acceleration/deceleration term of the momentum equation that we have discussed earlier, but the situation gets complicated as the configuration of the flow before and after the discontinuity may be different, and, e.g. the average void fraction may have changed or the two phases may have been accelerated in different ways. This is a complex situation that is not easily amenable to treatment. The simplest model, homogeneous flow, seems often to be performing adequately, it has at least the advantage of simplicity.

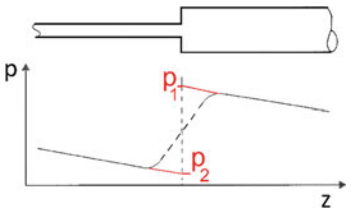

Fig. 6.4 Definition by extrapolation of the pressure loss ($p_1 - p_2$) at a singularity; example of a sudden expansion

The irreversible loss is often simply obtained by applying the homogeneous or another two-phase multiplier to the local reference single-phase pressure loss. Beattie (1973) reviews the subject and proposes definitions of the friction factor, of the Reynolds number and of the multiplier according to the type of singularity and the two-phase flow regime. The book by Chisholm (1983) also treats the subject and proposes two-phase multipliers. Ahmed et al. (2007), Harshe et al. (1976), Murakami and Shimizu (1973), Schmidt and Friedel (1997), Azzi et (1999) and Tapucu et al. (1989) provide additional information on pressure losses caused by singularities.

Appendix

Variation of Baroczy's property index with temperature for various fluids. Conversion:°F = 32 + °C·9/5

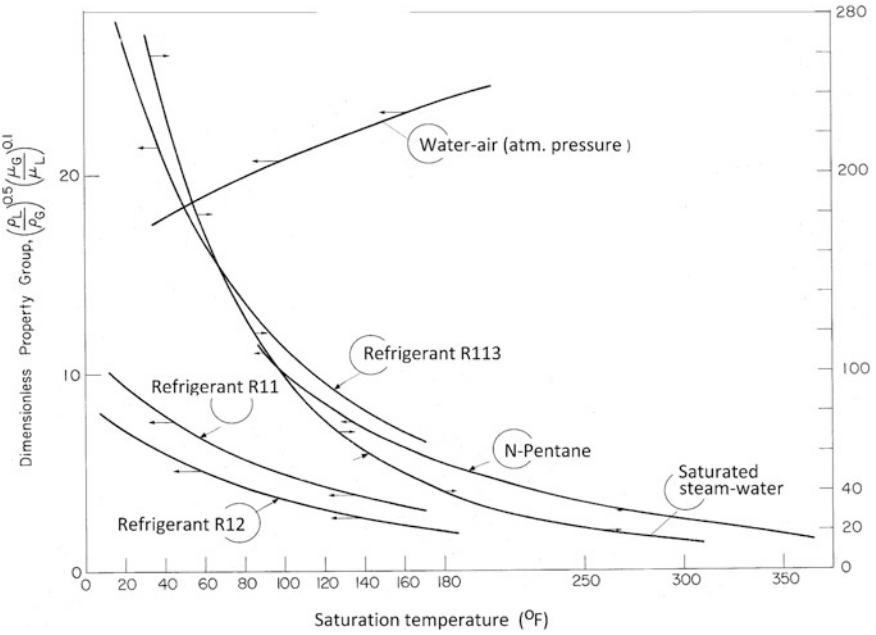

The Thom (1964) multipliers r_2 to r_5 for estimating the pressure drop in a boiling length Conversion bar to psia: 1 bar = 14.504 psia. Explanations in Sect. 6.5.4, Eq. (6.5.16) for diabatic boiling flow and following one for adiabatic flow

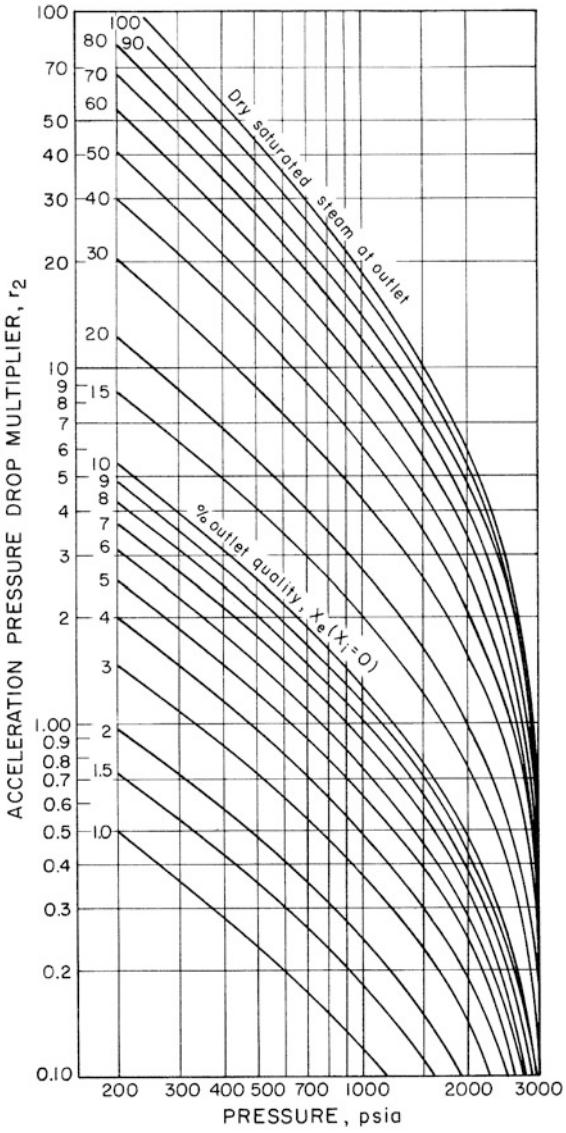
ACCELERATION PRESSURE DROP MULTIPLIER, r_2
PRESSURE, psia
Dry saturated steam at outlet
% outlet quality, $X_e (X_i = 0)$
100
80
70
60
50
40
30
20
10
9
8
7
6
5
4
3
2
1.5
1.0
0.9
0.8
0.7
0.6
0.5
0.4
0.3
0.2
0.10
200
300
400
500
700
1000
2000
3000

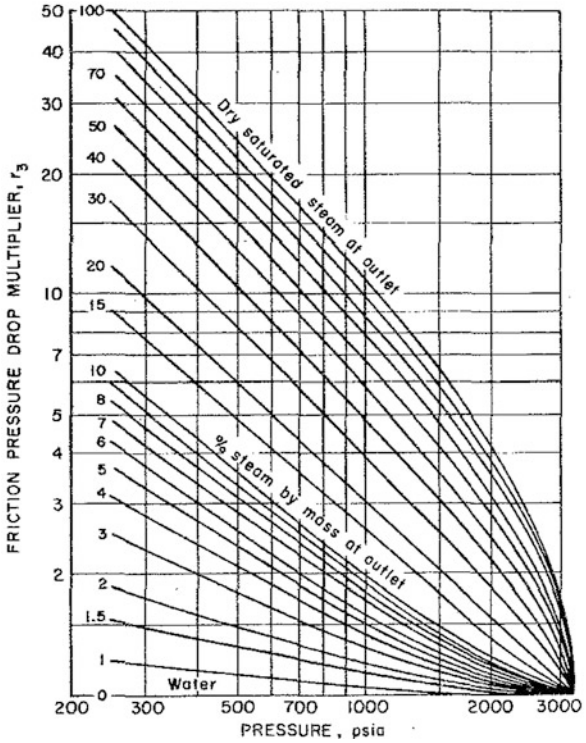
FRICTION PRESSURE DROP MULTIPLIER, r_3
50
40
30
20
10
7
5
4
3
2
100
70
50
40
30
20
15
10
8
7
6
5
4
3
2
1.5
1
0
Dry saturated steam at outlet
% steam by mass at outlet
Water
200
300
500
700
1000
2000
3000
PRESSURE, psia

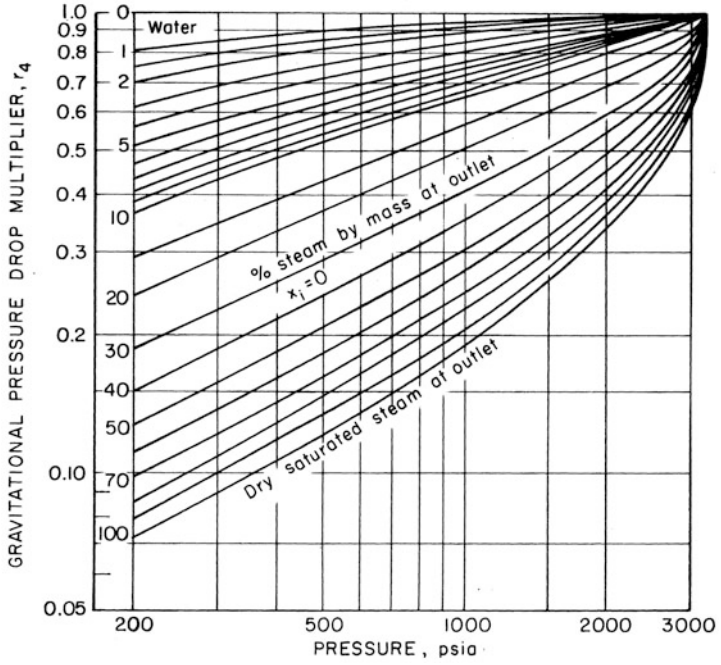
GRAVITATIONAL PRESSURE DROP MULTIPLIER, r_4
1.0
0.9
0.8
0.7
0.6
0.5
0.4
0.3
0.2
0.10
0.05
0
Water
1
2
5
10
20
30
40
50
70
100
% steam by mass at outlet
$x_i = 0$
Dry saturated steam at outlet
200
500
1000
2000
3000
PRESSURE, psia

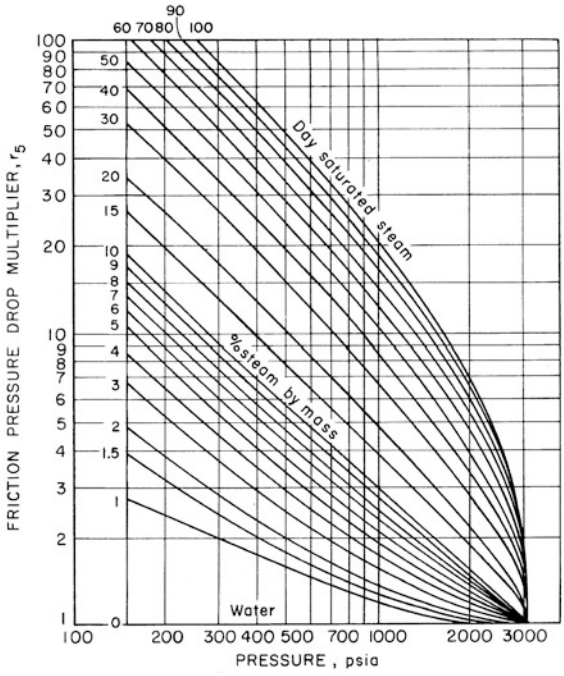

References

Aggour MA, Al-Yousef HY (1996) Vertical multiphase flow correlations for high production rates and large tubulars. SPE Prod Facil 11(01):41–48

Ahmed WH, Ching CY, Shoukri M (2007) Pressure recovery of two-phase flow across sudden expansions. Int J Multiphase Flow 33:575–594

Azzi A, Belaadi S, Friedel L (1999) Two-phase gas/liquid flow pressure loss in bends. Forsch Ingenieurwes 65(7):309–318

Baroczy CJ (1965) A systematic correlation for two-phase pressure drop. Chem Engng Prog Symp Series, *62*:232–249 (1966). Also NAA-SR-MEMO-11858

Beattie DHH, Whalley PB (1982) A simple two-phase frictional pressure drop calculation method. Int J Multiphase Flow 8:83–87

Beattie DR (1973) A note on the calculation of two-phase pressure losses. Nucl Eng Des 25 (3):395–402

Beggs HD, Brill JP (1973) A study of two-phase flow in inclined pipes. J Petr Technol 725:607–617

Behnia M (1991) Most accurate two-phase pressure-drop correlation identified. Oil Gas J (United States) 89(37): 91–95 (1991)

Chexal B, Merilo M, Maulbetsch J, Horowitz J, Harrison J, Westacott J, Peterson C, Kastner W, Schmidt H (1997) Void fraction technology for design and analysis. Electric Power Research Institute, Palo Alto

Chexal B, Horowitz J, McCarthy G, Merilo M, Sursock JP, Harrison J, Peterson C, Shatford J, Hughes D, Ghiaasiaan M, Dhir V (1999) Two-phase pressure drop technology for design and analysis. Technical Report, Electric Power Research Institute Inc., Palo Alto

Chisholm D (1967) A theoretical basis for the Lockhart-Martinelli correlation for two-phase flow. Int J Heat Mass Transf 10(12):1767–1778
Chisholm D (1983) Two-phase flow in pipelines and heat exchangers. George Godwin, London
Chisholm D (1973) Pressure gradients due to friction during the flow of evaporating two-phase mixtures in smooth tubes and channels. Int J Heat Mass Transf 16:347–358
Cicchitti A et al (1960) Two-phase cooling experiments – pressure drop, heat transfer and burnout measurements. Energia Nucleare 7:407–425
Ferguson ME, Spedding PL (1995) Measurement and prediction of pressure drop in two-phase flow. J Chem Technol Biotechnol 63(3):262–278
Friedel L (1979) Improved friction pressure drop correlations for horizontal and vertical two phase pipe flow. 3R Int 18(7):485–491
Friedel L (1984) Personal communication
Gregory GA (1975) Comparison of methods for the prediction of liquid holdup for upward gas-liquid flow in inclined pipes. Can J Chem Eng 53: 384
Gregory GA, Mandhane JM, Aziz K (1975) Some design considerations for two-phase flow in pipes. J Can Petr Technol 14(1):65–71
Hagedorn AR, Brown KE (1964) The effect of viscosity on two-phase vertical flow. J Petrol Tech 16:203–210
Harshe B, Hussian A, Weisman J (1976) Two-phase pressure drop across restrictions and other abrupt area changes. Cincinnati Univ, Ohio (USA), Department of Chemical and Nuclear Engineering report PB-251915 (1976 Apr 01), DOE Contract Number: AT(49–24)–0179
Hasan AR, Kabir CS (1988) A study of multiphase flow behavior in vertical wells. SPE Prod Eng 3(02):263–272
Hetsroni G (1982) Handbook of Multiphase Systems. Hemisphere, Washington
Idsinga W, Todreas N, Bowring R (1977) An assessment of two-phase pressure drop correlations for steam-water systems. Int J Multiph Flow 3:401–413
Lockhart RW, Martinelli RC (1949) Proposed correlation of data for isothermal two-phase, two-component flow in pipes. Chem Eng Prog 45(1):39–48
McFarlane DR (1966) An analytic study of the transient boiling of sodium in reactor coolant channels. ANL-7222, Argonne National Laboratory, Argonne, IL, USA
Martinelli RC, Boelter LK, Taylor TH, Thomsen EG, Morrin EH (1944) Isothermal pressure drop for two-phase two-component flow in a horizontal pipe. Trans ASME 66(2):139–151
Modisette JL (1983) Two-phase flow in pipelines-I: Steady-state flow. J Energy 7(6):502–507
Murakami M, Shimizu Y (1973) Studies on the hydraulic loss in pipe bends. Jpn Soc Mech Eng 16:981–992
Owens WS (1961) Two-phase pressure gradient. International Developments in Heat Transfer, Part II, ASME
Shannak BA (2008) Frictional pressure drop of gas liquid two-phase flow in pipes. Nucl Eng Des 38(12):3277–3284
Singh G, Griffith P (1970) Determination of the pressure drop optimum pipe size for a two-phase slug flow in an inclined pipe. J Eng Ind 92:717–726
Schmidt J, Friedel L (1997) Two-phase pressure drop across sudden contractions in duct areas. Int J Multiph Flow 23:283–299
Spedding PL, Chen JJJ, Nguyen VT (1982) Pressure drop in two-phase gas-liquid flow in inclined pipes. Int J Multiph Flow 8:407–431
Spedding PL, Hand NP (1997) Prediction in stratified gas-liquid co-current flow in horizontal pipelines. Int J Heat Mass Transf 40(8):1923–1935
Spedding PL, Bénard E, Donnelly GF (2006) Prediction of pressure drop in multiphase horizontal pipe flow. Int Comm Heat Mass Transf 33(9):1053–1062
Taitel Y, Dukler AE (1976) A model for predicting flow regime transitions i n horizontal and near horizontal gas-liquid flow. AIChE J 22:47–55
Tapucu A, Teyssedou A, Troche N, Merilo M (1989) Pressure losses caused by area changes in a single-channel flow under two-phase flow conditions. Int J Multiph Flow 15:51–64

Thom JRS (1964) Prediction of pressure drop during forced circulation boiling of water. Int J Heat Mass Transf 7:709–724

Vijayan PK, Patil AP, Pilkhwal DS, Saha D, Raj VV (2000) An assessment of pressure drop and void fraction correlations with data from two-phase natural circulation loops. Heat Mass Transf 36(6):541–548

Wallis GB (1969) One dimensional two phase flow. McGraw-Hill

Appendix A
Tutorial

A.1 Recall of the Single-Phase Flow Conservations Equations

The single-phase flow conservation equations will be given here to facilitate the introduction of the two-phase conservations equations in this volume.

A.1.1 The Conservation Equations for "Closed Systems"

In thermodynamics, a *system*, is a definite mass of material. We often refer to a *closed system* or an *isolated body* to emphasize that there is no exchange of mass between the closed system and its surroundings. Thus a closed system is a collection of mass within prescribed boundaries.

Conservation laws can be written for a closed system and constitute the basis for the solution of all thermodynamics, mechanics, and what engineers call "thermal-hydraulics" problems (combination of heat transfer and fluid mechanics or hydraulics). There are three fundamental conservation laws:

Conservation of mass
Newton's equation of motion, conservation of momentum
First law of thermodynamics, conservation of energy

The law of **conservation of mass** states that the mass within a closed system remains constant. The volume of the system may of course change, like in the example of a cylinder closed by a moving piston, or a balloon that is deformed. So we write

$$M = \text{constant}, \quad \text{or} \quad \frac{dM}{dt} = 0 \tag{A.1}$$

where M is the total mass in the system.

According to **Newton's law of motion**, or the law of *conservation of momentum*, the sum of all the external forces applied on an isolated body produces an acceleration, i.e. a rate of change of its momentum (the product of its mass M times the

G. Yadigaroglu and G.F. Hewitt (eds.), *Introduction to Multiphase Flow*,
Zurich Lectures on Multiphase Flow, DOI 10.1007/978-3-319-58718-9

velocity of its centre of mass U). Note that this is a vector equation, since both the forces and the velocity have a direction:

$$\sum \vec{F} = \frac{d}{dt}(M\vec{U}) \tag{A.2}$$

The **first law of thermodynamics** is a law ofconservation of energy and expresses the interplay between heat, work and internal energy of a system. It states that the heat added to a system, denoted here Q, minus the work done by the system W on its surroundings is equal to the change of its "total" internal energy $E°$ (*total* here means: the sum of the intrinsic internal energy of the system—essentially its heat content, plus its kinetic energy (related to its velocity), plus its potential energy (related to its elevation about a ground level). Considering small changes (denoted by the δ):

$$\delta Q - \delta W = dE^{\circ} \tag{A.3}$$

We have written $dE°$ instead of $\delta E°$ to indicate that the change in *total* internal energy depends only on the initial and final states of the system and is not dependent on the path followed; the internal energy is a *thermodynamic property* of the system.

In our work, that has to do mainly with the effects of heat addition or removal, we can often neglect the kinetic and potential energy contributions. (These, however, may be the dominant terms if we deal, e.g., with a gas turbine or compressor.)

A.1.2 Conservation Equations for a Control Volume

Since we will be dealing mostly with situations in which there is flow of a fluid *through* a system, we will transform the conservation laws into laws applicable to *control volumes* or *flow-through systems*. Acontrol volume is a well-defined volume in space, for example, the volume of a pipe between its two ends or the internal volume of a vessel. Figure A.1 shows a very simple control volume that will be, however, very useful for what we will be doing.

The transformation of the closure laws to equations applicable to flow systems can be accomplished using a form of the Leibnitz rule. For some *extensive* property of the system N such as the total mass, momentum of internal energy and its specific value n, i.e., the amount of the property per unit mass of the system:

$$\frac{dN}{dt} = \frac{\partial}{\partial t}\int_{cv} n\rho dV + \int_{cs} n\rho(\bar{u}\cdot d\bar{A}) \tag{A.4}$$

The first integral on the right side is the time rate of change of the contents of the control volume (cv); the second one is the sum of the fluxes entering the control

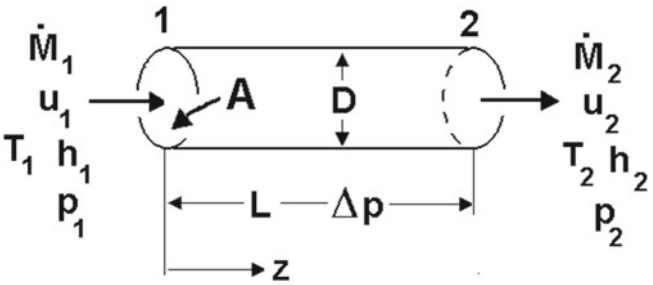

Fig. A.1 Typical "one dimensional" control volume, a "channel" of circular cross-section in this particular case. The cross sectional areas that define the two ends of the control volume (the two ends of the pipe) are marked 1 and 2. The coordinate (the length) along this pipe is denoted by z. This control volume has a constant cross-sectional or flow area A, a length L and a diameter D. The usual thermodynamic and flow variables involved are the pressure p, the cross-sectional-average fluid velocity u, the fluid temperature T and the corresponding enthalpy h. The pressure difference (or "pressure drop") across the two ends of the pipe is $\Delta p = p_2 - p_1$

surface (cs). We can use the Leibnitz rule that is a purely kinematic/mathematical equation and has nothing to do with the physical conservation laws, to transform the three conservation laws given for closed systems above to conservations laws for flow volumes. The conservation laws can be obtained using the Leibnitz rule and specializing the meaning of N and n:

Mass conservation	$N = M$	and	$n = 1$
Momentum conservation	$N = M\bar{u}$	and	$n = \rho\bar{u}/\rho = \bar{u}$
Energy conservation	$N = E^o$	and	$n = \rho e^o/\rho = e^o$

where e^o is the total internal specific energy of the fluid, i.e., its intrinsic internal energy, plus its kinetic and potential energies.

The conservation equations in integral form become:

$$\frac{\partial}{\partial t}\int_{cv} \rho dV + \int_{cs} \rho(\bar{u}\cdot d\bar{A}) = 0 \tag{A.5}$$

$$\frac{\partial}{\partial t}\int_{cv} \rho\bar{u} dV + \int_{cs} \rho\bar{u}(\bar{u}\cdot d\bar{A}) = \sum \bar{F} \tag{A.6}$$

$$\frac{\partial}{\partial t}\int_{cv} \rho e^o dV + \int_{cs} \rho e^o(\bar{u}\cdot d\bar{A}) = \dot{Q} - \dot{W} \tag{A.7}$$

We have accounted for the work of body forces due to a potential field (such as gravity) in the *total* internal energy changes of the system. $\dot{Q}$ and $\dot{W}$ are the *rates* of heat addition and work done by the system.

The rate of work done by the system on its surroundings can be broken now explicitly in its two parts: the part that corresponded in Eq. (A.3) to the work done by pressure forces on moving system boundaries and the work done by shear forces on moving boundaries, i.e., the "shaft" work. The first term is sometimes called the "flow work" and is due to the fact that matter entering into the control volume does work by "pushing the matter inside the control volume out of the way." The flow work in Eq. (A.7) involves streams crossing control volume boundaries, while the corresponding work term in Eq. (A.3) involved expansion or contraction of the system. The flow term can be written as

$$\dot{W}_{pr} = \int_{cs} p(\bar{u} \cdot d\bar{A})$$

We will not make the second term explicit but we will simply denote it by $\dot{W}_s$. In the absence of capillary, electrical, magnetic or nuclear forces, the total specific internal energy e^o can be combined with the p/ρ term to yield the total enthalpy h^o:

$$e^o + \frac{p}{\rho} = e + \frac{u^2}{2} - gz\cos\theta + \frac{p}{\rho} \equiv h^o \tag{A.8}$$

where h^o is the specific enthalpy defined as $h^o = e^o + p/\rho$, and $g\ z\ \cos\theta$ represents the potential energy due to the gravity field, θ being the angle between the acceleration of gravity and the positive flow direction, taken as the z–direction here (upwards). In many heat transfer applications, the potential and kinetic energy changes are negligible in comparison to the internal energy changes; thus $e^o \approx e$ and $h^o \approx h$, as we already noted above.

Using Eq. (A.8) and noting that

$$\int_{cs} \rho e^o(\bar{u} \cdot d\bar{A}) + W_{pr} = \int_{cs} \rho e^o(\bar{u} \cdot d\bar{A}) + \int_{cs} \rho \frac{p}{\rho}(\bar{u} \cdot d\bar{A}) = \int_{cs} \rho h^o(\bar{u} \cdot d\bar{A})$$

Equation (A.7) takes the form

$$\frac{\partial}{\partial t}\int_{cv} \rho e^o dV + \int_{cs} \rho h^o(\bar{u} \cdot d\bar{A}) = \dot{Q} - \dot{W}_s \tag{A.9}$$

If we wish to have an equation in terms of enthalpy only, we can replace in the first integral of Eq. (A.9) the internal energy (e^o which is now approximated as e) by $h - p/\rho$,

$$\frac{\partial}{\partial t}\int_{cv} \rho h^o dV + \int_{cs} \rho h^o(\bar{u} \cdot d\bar{A}) = \dot{Q} - \dot{W}_s + \frac{\partial}{\partial t}\int_{cv} p dV \tag{A.10}$$

When one applies Eqs. (A.9) or (A.10) to problems involving shaft work (turbomachinery), clearly the W_s term is the most important one. On the other hand, in heat transfer problems not involving any shaft work (e.g. a heat exchanger), the W term vanishes.

A.1.3 One-Dimensional, Differential form of the Equations

We will present here only the *one-dimensional* (1D) form of these laws that are usually sufficient for solving many basic problems of interest. *One dimensional* here means that the flow is predominantly in one dimension, like flow in a straight pipe (round or of any prismatic shape) and that we are using for our formulations cross-sectional average variables. In their 1D form, the conservation laws will be essentially applicable to control volumes that are channels or pipes with a fluid flowing inside, such as the one shown in Fig. A.1.

Without entering into the details, Eqs. (A.5), (A.6) and (A.10) can be written in differential form (applied to an infinitesimal control volume) and for one-dimensional flows as:

$$A\frac{\partial}{\partial t}\rho + \frac{\partial}{\partial z}(\dot{m}A) = 0 \tag{A.11}$$

$$\frac{\partial \dot{m}}{\partial t} + \frac{1}{A}\frac{\partial}{\partial z}\left[\frac{\dot{m}^2 A}{\rho}\right] = -\frac{\partial p}{\partial z} + g\rho\cos\theta - \frac{\tau_w P_w}{A} \tag{A.12}$$

$$\rho\frac{\partial h^0}{\partial t} + \dot{m}\frac{\partial h^0}{\partial z} = q''' + \frac{P_h}{A}q'' + \frac{\partial p}{\partial t} \tag{A.13}$$

where the external forces applicable to the momentum Eq. (A.12) are the pressure gradient, the force of gravity and the wall shear τ_w. P_w is the wetted perimeter, q''' a volumetric heat source, P_h the heated perimeter and q'' the heat flux from the wall. We have not included any shaft work.

The conservation of momentum equation leads to an equation for the pressure gradient in the channel. This equation can be integrated to yield the pressure drop.

At steady state, the energy conservation equation for a control volume where only heat exchange takes place takes the very simple and very useful form:

$$\Delta h = \frac{q}{\dot{M}}, \quad \text{or in differential form,} \quad dh = \frac{dq}{\dot{M}}$$

where q is the heat added to the control volume and Δh or dh is the change in enthalpy of the fluid.

A.1.4 Thermodynamic Variables

The density, the pressure, the specific heat, the enthalpy and the internal energy are all thermodynamic variables. In principle, any thermodynamic variable of a (simple) fluid is defined if we know two other variables. For example, we can get the specific enthalpy, if the pressure and the temperature of the fluid are given. The thermodynamic properties are tabulated in property tables. For water, we call these *steam tables.*

The equilibrium state, when water and steam co-exist, is called the *saturation state* (denoted by the subscript *sat*). As the pressure, for example, is increased, a mixture of water and steam at thermodynamic equilibrium follows the saturation line, i.e. there is a relationship between T_{sat} and p_{sat}. As a consequence, the properties of a saturated fluid depend only on *one* thermodynamic variable, for example, the density of *saturated* water depends either on its temperature or its pressure *only*.

A.2 On the Two Most Important Closure Relationships

Assume that we have a pipe heated, say electrically, at a given rate and cooled by the flow of a fluid traversing it, and we wish to know the temperature distribution along the heat transfer surface. If we could solve this problem analytically or numerically, this temperature distribution would be part of the solution. Such solutions are possible in simple cases, e.g. for laminar flow in a uniformly heated pipe. In the more complex turbulent-flow cases analytical solutions are not possible and it is only relatively recently that numerical simulation techniques (the simplest one being the RANS or Reynolds Average Navier-Stokes[1] solutions) have become widespread; these remain, however, relatively expensive for simple engineering applications. Another example would be to estimate the pressure drop in this pipe.

The engineering approach to such problems has been the following: one conducts experiments and measures the wall temperature distribution or the pressure drop. The data are then correlated to arrive at useful engineering closure laws: in this case the heat transfer coefficient for the heated pipe and the friction factor for the pressure drop.

More generally, we can say that we wish to establish the heat transfer and frictional pressure drop laws for a given pipe geometry, flow conditions, fluid, etc. For the heat transfer law, we would like to establish the relationship between the heat flux from the wall and the difference wall temperature minus bulk temperature (that we will define below). For the wall shear, its dependence on the flow conditions, namely the average fluid velocity.

[1]The RANS equations are time-averaged equations of motion for fluid flow (the Navier-Stokes equations) that consider the turbulence of the fluid in a relatively simple form.

Without entering into all details, and assuming for simplicity axisymmetric conditions, we could express the heat transfer and pressure drop or wall-shear τ_w laws as

$$q''(z) = q''\left(D, z, T_w(z), u(z,r), \rho, \mu, c_p, \lambda, \ldots\right)$$
$$\Delta p(z) = \Delta p(D, z, u(z,r), \rho, \mu, \varepsilon_r, \ldots) \quad \text{or} \quad \tau_w = \tau_w(D, z, u(z,r), \rho, \mu, \varepsilon_r, \ldots)$$

where D is a characteristic dimension of the pipe (typically its diameter), z the coordinate along the pipe, $u(z,r)$ the time-average velocity profile of the fluid at location z in terms of the radial coordinate r, $T_w(z)$ the heated wall temperature at location z, ρ and μ the density and viscosity of the fluid, respectively, c_p its specific heat capacity at constant pressure, λ its thermal conductivity, and ε_r the wall roughness of the pipe. We would have to provide the pipe inlet conditions:

$$u(z = 0, r) = u_0(r)$$
$$T(z = 0, r) = T_0(r)$$

The relation between the wall shear τ_w and the pressure drop is obtained from a simple force balance on the pipe:

$$A \cdot \Delta p = \pi D \cdot L \cdot \tau_w$$

or

$$\Delta p = \frac{\pi D \cdot L}{A} \cdot \tau_w = \frac{4L}{D} \cdot \tau_w \tag{A.14}$$

and in differential form

$$\frac{dp}{dz} = \frac{\pi D}{A}\tau_w = \frac{4L}{D}\tau_w$$

where we have considered only the frictional pressure drop.

If we could solve this problem, the solution would have provided the (time-average) temperature and velocity distributions in the fluid, $T(z,r)$ and $u(z,r)$ and from these also the velocity and temperature gradients at the heated wall that define the heat flux to the fluid and the wall shear:

$$q''(x, r_w) = -\lambda \left.\frac{dT}{dr}\right|_w$$
$$\tau_w(z) = -\mu \left.\frac{du}{dr}\right|_w$$

(where r_w is the radial position of the wall) according to the Fourier law of heat conduction and the Newton law of viscosity. In turbulent-flow solutions we would have also obtained the fluctuations of T and u at a given point, normally denoted T' and u'.

The engineering approach has been to try to obtain expressions for the heat transfer and wall shear laws in terms of non-dimensional numbers such as the Reynolds number Re, the Prandtl number Pr and the Nusselt number Nu. Since we do not wish to know (or cannot obtain) the details of the radial variable distributions, these expressions should be in terms of cross-sectional-average variables, namely u_b the *bulk* (or cross-sectional-average) *velocity* of the fluid and its *bulk temperature* T_b

$$u_b(z) = \int_A u(z, \mathbf{r}) dA$$
$$T_b(z) = \frac{1}{u_b(z)} \int_A T(z, \mathbf{r}) \cdot u(z, \mathbf{r}) dA$$

where $\mathbf{r}$ is a point in the cross section. For the simple case of axisymmetric flow:

$$u_b(z) = \int_r u(z, r) \cdot 2\pi r \cdot dr$$
$$T_b(z) = \frac{1}{u_b(z)} \int_r T(z, r) \cdot u(z, r) \cdot 2\pi r \cdot dr$$

We note that the bulk temperature is velocity weighted.

The wall shear is related to the kinetic energy of the fluid via the Fanning[2] *friction factor f:*

$$\tau_w = f \frac{\rho u_b^2}{2} \tag{A.15}$$

and the heat flux is related to the wall-to-bulk temperature difference via a *heat transfer coefficient α:*

$$\alpha = \frac{q''}{T_w - T_b} \tag{A.16}$$

[2]Unfortunately there are two alternative definitions of friction factors, the Fanning friction factor and the Weisbach friction factor. According to Eqs. (A.14) and (A.15): $\Delta p = \frac{4L}{D} \cdot \tau_w = \frac{4L}{D} \cdot f \frac{\rho u^2}{2}$. Certain authors prefer to incorporate the factor 4 into the friction factor writing $\Delta p = \frac{L}{D} \cdot f_W \frac{\rho u^2}{2}$, where $f_W = 4f$.

We try to obtain correlations of the data in the following forms for the heat transfer and shear stress laws, respectively:

$$\mathrm{Nu} = \mathrm{f}\ (\mathrm{Re}, \mathrm{Pr}, \ldots)$$
$$f = \mathrm{f}\ (\mathrm{Re}, \varepsilon_{r,} \ldots)$$

where the non-dimensional numbers are

$$\mathrm{Re} \equiv \frac{\rho u D}{\mu}, \quad \mathrm{Pr} \equiv \frac{c_p \mu}{\lambda}, \quad Nu \equiv \frac{\alpha D}{\lambda}$$

We note that the heat transfer coefficient has been included in the Nusselt number that represents also in a non-dimensional form the temperature gradient of the fluid at the wall:

$$Nu = \frac{\alpha D}{\lambda} = \frac{q^{''}/\lambda}{(T_w - T_b)/D}$$

The Reynolds number is a ratio between the inertial forces and the frictional forces:

$$\mathrm{Re} = \frac{\rho u D}{\mu} = \frac{\rho u^2}{\mu u/D}$$

while the Prandtl number scales the kinematic viscosity to the heat conductivity, or better said, the rate of diffusion of momentum to the rate of diffusion of heat

$$\mathrm{Pr} \equiv \frac{c_p \mu}{\lambda} = \frac{\mu}{\lambda/c_p} = \frac{\mu/\rho}{\lambda/\rho c_p} = \frac{\nu}{\kappa}$$

where ν is the kinematic viscosity, $\nu = \frac{\mu}{\rho}$and κ the thermal diffussivity, $\kappa = \frac{\lambda}{\rho c_p}$.

Most commonly used, simple, expressions for the heat transfer coefficient and the friction factor (for smooth pipes) in turbulent flow are:

$$\mathrm{Nu} = 0.023\ \mathrm{Re}_b^{0.8}\, Pr_b^{0.4}$$
$$f = \frac{0.046}{\mathrm{Re}^{0.2}}$$

The Nusselt-number correlation is valid in the range $0.5 < \mathrm{Pr} < 120$ and $\mathrm{Re} > 4000$. The subscript b in Re and Pr means that the properties of the fluid are to be evaluated at the bulk temperature. There are many more sophisticated—and more specialized to certain situations—correlations such as the two given above, but this are clearly beyond the scope of this Tutorial.

A.2.1 An Important Remark Regarding the Heat Transfer Coefficient

The definition of the heat transfer coefficient, Eq. (A.16) implies that there is proportionality between the heat flux and the wall-bulk temperature difference. Ignoring at this point that there are minor departures from linearity due to the variation of the physical properties with temperature, this is largely the case in convective, single-phase heat transfer. Thus the heat transfer coefficient becomes a very useful engineering quantity.

There are situations, however, where the heat transfer law is not linear. This is the case, e.g. in single-phase natural convection and in boiling heat transfer where the dependence between heat flux and wall-bulk temperature difference (in this case usually wall minus saturation temperature difference) could be of the form $q'' = (T_w - T_{sat})^n$ where the exponent n can take values say between 2 and 5. In such situations there is no advantage of using a heat transfer coefficient, that can still be defined, however, but will depend on $(T_w - T_{sat})$, losing most of its usefulness.

Appendix B
Common Nomenclature

The most often used common nomenclature is listed here. Other symbols or other meanings of the symbols may be defined locally in the various chapters.

Symbol Variable [SI units]

A	Cross-sectional flow area [m^2]
c_p	Specific heat at constant pressure [J/kg K]
D	Diameter or hydraulic diameter, $4A/P$ [m]
e	Internal specific energy [J/kg = m^2/s^2]
f	Friction factor
g	Acceleration of gravity [m/s^2]
h	Specific enthalpy [J/kg = m^2/s^2]
j	Volumetric flux [m^3/m^2s = m/s]
m	Mass [kg]
$\dot{M}$	Mass flow rate [kg/s]
$\dot{m}$	Mass flux [kg/m^2s]
P	Perimeter [m]
p	Pressure [Pa = N/m^2 = kg/s^2m]
$\dot{Q}$	Volumetric flow rate [m^3/s]
R, r	Radius [m]
S	Phase velocity ratio
t	Time [s]
U, u	Velocity [m/s]
v	Specific volume, $1/\rho$ [m^3/kg]
x	Flow quality
z	Axial (longitudinal) coordinate [m]
α	Heat transfer coefficient [W/m^2 s]
β	Homogeneous void fraction
Γ	Volumetric vapour generation rate [kg/m^3s]
Δ	Difference, for example, pressure difference Δp
δ	Thickness, film thickness [m]
ε	Void (presence) fraction
ε_k	Presence-fraction of phase k, void fraction

G. Yadigaroglu and G.F. Hewitt (eds.), *Introduction to Multiphase Flow*,
Zurich Lectures on Multiphase Flow, DOI 10.1007/978-3-319-58718-9

ε_r	Pipe roughness [m]
θ	Angle between z coordinate and gravity vector
κ	Thermal diffusivity [m^2/s]
λ	Thermal conductivity [W/m K]
μ	Viscosity [Ns/m^2 = kg/s m = Pa s]
ν	Kinematic viscosity [m^2/s]
ρ	Density [kg/m^3]
σ	Surface tension [$N/m = kg/m^2s^2$]
τ	Shear stress [$N/m^2 = kg/s^2m$]

Subscripts

eq	Equilibirum
f	Liquid (also L or *l*)
G, g	Gas
hom	Homogeneous
i	Interface
k	Phase (G or g and L or f or *l*)
L or *l*	Liquid (also f)
s	Superficial (velocity)
sat	Saturated
w	Wall
z	Along z-coordinate

Operators

$< f >$	Cross-sectional average of variable f
$< f_k >_k$	Phase-cross-sectional-average of phase variable f_k

Appendix C
Most Useful Conversion Factors Between British and Si Units

British units are often found in older thermal-hydraulics papers. A few useful conversion factors are listed below.

The usual basic British units are the foot (ft), the inch (in), the pound-mass (lbm), the pound-force (lbf), the hour (hr), the British Thermal Unit (BTU or Btu) and the degrees Fahrenheit (°F, the equivalent of the degree Celsius) and Rankine (R, absolute scale, the equivalent of the Kelvin).

(continued)

Length	1 ft = 12 in = 12 × 25.4 mm = 0.3048 m
Area	1 ft^2 = 144 in^2 = $(0.3048)^2$ m^2 = 0.092 903 m^2
Mass	1 kg = 2.2046 lbm (pound-mass)
Density	1000 kg/m^3 = 62.43 lbm/ft^3 (the density of water)
Mass flow rate	1000'000 lbm/hr = 126.0 kg/s
Mass flux	1000'000 lbm/hr ft^2 = 1360 kg/m^2s
Volume	1 USG (US gallon) = 0.13368 ft^3 = 3.7853 Litre
Volumetric flow rate	The USG/min = $63.0915 \cdot 10^{-6}$ m^3/s
Pressure	1 bar = 14.504 psi (lbf/in^2)
Temperature	1 K = 1.8 R (degree Rankine)
	T[°F] = 1.8 · *T[°C] + 32
Energy	1 kWh = 3413 Btu (British thermal unit)
	1 Btu = 1054.8 J
Power	1 Btu/hr = 0.29301 W
Enthalpy	1 Btu/lbm = 2326 J/kg
Specific heat	1 Btu/lbm °F = 1 kcal/kg °C (by definition)
	1 Btu/lbm °F = 4186 J/kg °C
Heat flux	1 Btu/hr ft^2 = 3.1546 W/m^2
Heat transfer coefficient	1 Btu/hr ft^2 °F = 5.6783 W/m^2 °C
Thermal conductivity	1 Btu/hr ft °F = 1.7307 W/m °C
Viscosity	1 lbm/hr ft = $4.1338 \cdot 10^{-4}$ N s $/m^2$
Kinematic viscosity	1 ft^2/hr = $25.806 \cdot 10^{-6}$ m^2/s
Surface tension	1 lbf/ft = 14.59 N/m

(continued)

G. Yadigaroglu and G.F. Hewitt (eds.), *Introduction to Multiphase Flow*,
Zurich Lectures on Multiphase Flow, DOI 10.1007/978-3-319-58718-9

(continued)

Length	1 ft = 12 in = 12 × 25.4 mm = 0.3048 m
Area	1 ft^2= 144 in ^{2} = (0.3048) ^{2} m ^{2} = 0.092 903 m^2
Mass	1 kg = 2.2046 lbm (pound-mass)
Density	1000 kg/m^3 = 62.43 lbm/ft^3 (the density of water)
Mass flow rate	1000'000 lbm/hr = 126.0 kg/s
Mass flux	1000'000 lbm/hr ft^2 = 1360 kg/m^2s
Volume	1 USG (US gallon) = 0.13368 ft^3 = 3.7853 Litre
Volumetric flow rate	The USG/min = 63.0915 · 10 $^{-6}$ m^3 /s
Pressure	1 bar = 14.504 psi (lbf/in^2)
Temperature	1 K = 1.8 R (degree Rankine)
	T [° F] = 1.8 · * T [° C] + 32
Energy	1 kWh = 3413 Btu (British thermal unit)
	1 Btu = 1054.8 J
Power	1 Btu/hr = 0.29301 W
Enthalpy	1 Btu/lbm = 2326 J/kg
Specific heat	1 Btu/lbm °F = 1 kcal/kg °C (by definition)
	1 Btu/lbm °F = 4186 J/kg °C
Heat flux	1 Btu/hr ft^2 = 3.1546 W/m^2
Heat transfer coefficient	1 Btu/hr ft^2 °F = 5.6783 W/m^2 °C
Thermal conductivity	1 Btu/hr ft °F = 1.7307 W/m °C
Viscosity	1 lbm/hr ft = $4.1338 \cdot 10^{-4}$ N s $/m^2$
Kinematic viscosity	1 ft^2/hr = $25.806 \cdot 10^{-6}$ m^2/s
Surface tension	1 lbf/ft = 14.59 N/m

Index

G. Yadigaroglu and G.F. Hewitt (eds.), *Introduction to Multiphase Flow*,
Zurich Lectures on Multiphase Flow, DOI 10.1007/978-3-319-58718-9